MESON WIDTH DIFFERENCES AND ASYMMETRIES

CALCULATIONS OF HIGHER ORDER CONTRIBUTIONS TO NEUTRAL B-MESON MIXING

ZUR ERLANGUNG DES AKADEMISCHEN GRADES EINES

Doktors der Naturwissenschaften (Dr. rer. nat.)

VON DER KIT-FAKULTÄT FÜR PHYSIK DES
KARLSRUHER INSTITUTS FÜR TECHNOLOGIE (KIT)
GENEHMIGTE
Dissertation

VON

M.Sc. Marvin Gerlach

Tag der mündlichen Prüfung:	22.04.2022
Referent:	Prof. Dr. Matthias Steinhauser
Korreferent:	Prof. Dr. Ulrich Nierste

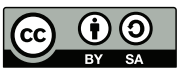

ABSTRACT

Experiments are ahead in the race for determining the features of neutral B-mesons. Recent measurements at the LHCb experiment have pushed the uncertainties of the decay width difference $\Delta\Gamma$ in the B_s-$\overline{B}_s$ system to about 6%, whereas the uncertainty of the theory prediction is about a factor of four larger. First results for $\Delta\Gamma$ and the parameter a_{fs}, quantifying the violation of the CP symmetry in B_s and B_d mixing, were already obtained in the Standard Model of particle physics several decades ago. In this thesis we improve on earlier predictions and provide the first next-to-next-to-leading order prediction which stabilizes the dependence on the renormalization scale and reduces uncertainties. The necessary calculations demand attention toward perturbative and non-perturbative aspects of meson physics. Focusing on the former, we carefully construct effective field theories where we complement the physical operators with properly chosen evanescent operators. Furthermore, efficient tools are necessary to compute the thousands of Feynman diagrams.

ZUSAMMENFASSUNG

Experimente liegen vorne im Rennen zur Bestimmung der Eigenschaften neutraler B-Mesonen. Neueste Messungen am LHCb Experiment haben die Messunsicherheit der Zerfallsbreitendifferenz $\Delta\Gamma$ des B_s-$\overline{B}_s$-Systems auf 6% verringert, wohingegen die Unsicherheit der Theorievorhersage ungefähr viermal so groß ist. Erste Ergebnisse für $\Delta\Gamma$ und den Parameter a_{fs}, der die Brechung der CP-Symmetrie in B_s- und B_d-Mischungen quantifizert, wurden bereits vor einigen Jahrzehnten im Standardmodell der Teilchenphysik errechnet. In dieser Dissertation werden an frühere Theorievorhersagen angeknüpft und die erste Vorhersage zur Ordnung α_s^2 vorgestellt, die sowohl die Renormierungsskalenabhängigkeit als auch die entsprechende Unsicherheit reduziert. Die dafür notwendigen Berechnungen erfordern die Behandlung perturbativer sowie nichtperturbativer Aspekte der Mesonphysik. Der Fokus liegt hier auf ersterem, was die Konstruktion effektiver Feldtheorien beinhaltet, in denen physikalische Operatoren durch sorgfältig gewählte evaneszente Operatoren ergänzt werden. Zudem werden effiziente Werkzeuge benötigt, die die Berechnung der tausenden notwendigen Feynman-Diagramme ermöglichen.

Nicht der *Besitz* von Wissen, von unumstößlichen Wahrheiten macht den Wissenschaftler, sondern das rücksichtslos kritische, das unablässige *Suchen* nach Wahrheit.

— **Karl Popper**, *Logik der Forschung*

CONTENTS

ACRONYMS

1PI	One-Particle Irreducible
1PR	One-Particle Reducible
ADM	Anomalous Dimension Matrix
C	Charge Conjugation
CKM	Cabibbo-Kobayashi-Maskawa
CMM	Chetyrkin-Misiak-Münz
CP	Charge Conjugation and Parity Transformation
CPV	Charge-Parity Violation
CPT	Charge, Parity and Time Reversal
DRED	Dimensional Reduction
EFT	Effective Field Theory
FCNC	Flavor Changing Neutral Current
GIM	Glashow-Iliopoulos-Maiani
HPL	Harmonic Polylogarithm
HQE	Heavy Quark Expansion
HV	't Hooft-Veltman
IBP	Integration-by-Parts
IR	Infrared
LO	Leading Order
LSZ	Lehmann-Symanzik-Zimmermann
MPL	Multiple Polylogarithm
$\overline{\text{MS}}$	Modified Minimal Subtraction
NDR	Naive Dimensional Regularization
NLO	Next-to-Leading Order
NNLO	Next-to-Next-to-Leading Order
N^3LO	Next-to-Next-to-Next-to-Leading Order
OPE	Operator Product Expansion
OS	On-Shell
PS	Potential Subtracted
QCD	Quantum Chromodynamics

QED	Quantum Electrodynamics
QFT	Quantum Field Theory
RGE	Renormalization Group Equation
SM	Standard Model of Particle Physics
UV	Ultraviolet

1 INTRODUCTION

Already in ancient Greece the question arose what the boundaries of existence are. To the smaller end of this question, already Demokrit introduced in the 5th century BCE a theory of atoms as smallest "uncuttable" particles. This hypothesis remained valid until around 1900 smaller particles were discovered: The electron and the nucleus. These building blocks of the atom opened the imagination of ever smaller particles which form the matter of our visible world.

A breakthrough in the further history was accomplished in the 1920s by Paul Dirac [1] who formulated a theory which combined quantum mechanics with Albert Einstein's special relativity [2]. Based on Dirac's work, Richard Feynman [3–5], Sin-Itiro Tomonaga [6] and Julian Schwinger [7, 8] formulated a fully covariant theory of *Quantum Electrodynamics* (QED). Their work inspired further developments, leading finally to the formulation of the *Standard Model of Particle Physics* (SM) [9–11] in the 1960s. The following decades were a mere success story for the SM since vast developments of particle accelerators and detector techniques showed continuous agreement with the theoretical predictions.

However, the SM alone is not sufficient to explain all observations from experiment and astronomy. The first problem is due to Einstein's theory of general relativity [12] which is not described by the SM. Although several observations are in accordance with general relativity (e.g. [13–15]), every approach of formulating it as a Quantum Field Theory (QFT) leads to a non-renormalizable theory which contradicts its fundamental claim.

Another question arises from the particle content of the observed universe. To explain the imbalance of matter and antimatter, Andrei Sakharov determined three necessary criteria to be fulfilled in the early universe [16]:

- Violation of baryon number conservation,
- Violation of C (Charge Conjugation) and CP (Charge Conjugation and Parity Transformation) symmetries,
- Violation of thermodynamic equilibrium.

Concerning the second point, the SM does indeed allow for such an asymmetry. The first experimental discovery of Charge-Parity Violation (CPV) was made in the experiment of Cronin and Fitch in 1964 where CP changing kaon decays into pions were observed [17]. Although many subsequent experiments found CPV in different particle interactions, the overall measured quantitative size of CPV is not sufficient to fulfill Sakharov's condition. Moreover, the electroweak phase transition in the SM is not strong enough to fulfill the third condition (see e.g. ref. [18]).

Furthermore, among others, precision measurements of $b \to sl\bar{l}$ processes [19] and of the magnetic moment of the muon [20] observe a significant discrepancy to SM predictions.

In this dissertation we focus on the physics of neutral B_s- and B_d-mesons. The SM predicts a certain gap between the masses (ΔM) and the decay widths ($\Delta\Gamma$) of their respective mass eigenstates. Additionally, a certain CP asymmetry a_{fs} quantifying CPV in the time evolution is predicted for the mixing of neutral B-mesons. Every deviation between the SM and measurement opens further the idea for physics beyond the SM.

In the following chapter we explain the quantum mechanical details of neutral B-mixing. We use the definitions and conventions of refs. [21–23].

1.1 QUANTUM MECHANICS OF NEUTRAL B-MESONS

The four neutral B-mesons are characterized by their valence quarks. They read

$$B_s \equiv (\bar{b}s)\,, \qquad \overline{B}_s \equiv (b\bar{s})\,, \qquad B_d \equiv (\bar{b}d) \qquad \text{and} \qquad \overline{B}_d \equiv (b\bar{d})\,. \tag{1.1}$$

In the following we do not differentiate between B_s and B_d. The time evolution of these mesons in terms of flavor eigenstates can be described quantum mechanically as

$$\begin{pmatrix} |B(t)\rangle \\ |\overline{B}(t)\rangle \end{pmatrix} = e^{-iHt} \begin{pmatrix} |B(0)\rangle \\ |\overline{B}(0)\rangle \end{pmatrix}. \tag{1.2}$$

This equation is used to describe the mixing and decay properties of $B/\overline{B}$ using an effective Hamiltonian operator H which is given by

$$H = M - i\frac{\Gamma}{2}\,. \tag{1.3}$$

The first term describes the time evolution of stable $B/\overline{B}$ particles in the rest frame using the *mass matrix* M. It is hermitian and the diagonal elements are equal due to the combined Charge, Parity and Time Reversal (CPT) invariance. It is called the *dispersive* part of eq. (1.3).

The second term accounts for the decay law which can be derived within the Wigner-Weisskopf approximation [24, 25]. It consists of the two-particle generalization of the *decay width* Γ and is called *absorptive* part of eq. (1.3). For Γ also the hermiticity and CPT arguments apply.

Thus, the effective Hamiltonian operator can be written as

$$H = \begin{pmatrix} M_{11} - i\frac{\Gamma_{11}}{2} & M_{12} - i\frac{\Gamma_{12}}{2} \\ M_{12}^* - i\frac{\Gamma_{12}^*}{2} & M_{11} - i\frac{\Gamma_{11}}{2} \end{pmatrix}, \tag{1.4}$$

where we have used

$$M_{22} = M_{11}\,, \quad M_{21} = M_{12}^*\,, \quad \Gamma_{22} = \Gamma_{11} \quad \text{and} \quad \Gamma_{21} = \Gamma_{12}^*\,. \tag{1.5}$$

Since H has off-diagonal elements we can diagonalize it with the matrix Q:

$$H = Q \cdot \begin{pmatrix} E_1 & 0 \\ 0 & E_2 \end{pmatrix} \cdot Q^{-1} . \tag{1.6}$$

The eigenvalues of H are given by

$$\begin{aligned} E_{1,2} &= M_{11} - i\frac{\Gamma_{11}}{2} \mp \sqrt{|M_{12}|^2 - \frac{i}{2}\Gamma_{12}^* M_{12} - \frac{i}{2}\Gamma_{12} M_{12}^* - \frac{|\Gamma_{12}|^2}{4}} \\ &\equiv M_{L,H} - i\frac{\Gamma_{L,H}}{2} , \end{aligned} \tag{1.7}$$

where the indices L and H denote the eigenvalues of the corresponding light and heavy states.

The matrix Q can be parametrized as

$$Q^{-1} = \begin{pmatrix} p & q \\ p & -q \end{pmatrix} , \qquad Q = \frac{1}{2pq}\begin{pmatrix} q & q \\ p & -p \end{pmatrix} , \qquad p, q \in \mathbb{C} . \tag{1.8}$$

After diagonalizing eq. (1.2), we obtain the mass eigenstates of the neutral B-meson system which are given by

$$\begin{aligned} |B_L\rangle &= p\,|B\rangle + q\,|\overline{B}\rangle , \\ |B_H\rangle &= p\,|B\rangle - q\,|\overline{B}\rangle . \end{aligned} \tag{1.9}$$

Unitarity demands that $|p|^2 + |q|^2 = 1$. Additionally, we observe that the states $|B_{L,H}\rangle$ are not orthogonal since the Hamiltonian operator of eq. (1.3) is not hermitian. Nevertheless, observables can be stated according to the operators M and Γ which are manifestly hermitian.

So far, everything stated applies to a general system of (anti-)particles which mix into each other due to quantum effects. A special property we did not yet mentioned is the CP symmetrization. For the flavor eigenstates of neutral B-mesons, we can specify the action of applying a CP transformation as

$$CP\,|B\rangle = -|\overline{B}\rangle , \quad CP\,|\overline{B}\rangle = -|B\rangle . \tag{1.10}$$

We can thus define two eigenstates:

$$\begin{aligned} |B_1\rangle &= \frac{1}{\sqrt{2}}\left(|B\rangle + |\overline{B}\rangle\right) \qquad (\text{CP odd}) , \\ |B_2\rangle &= \frac{1}{\sqrt{2}}\left(|B\rangle - |\overline{B}\rangle\right) \qquad (\text{CP even}) . \end{aligned} \tag{1.11}$$

For the case that CP is a symmetry of the physical system, eq. (1.11) would be equal to eq. (1.9), and it would hold $p = -q = 1/\sqrt{2}$. However, since CP symmetry is broken this is not the case.

Important quantities which characterize neutral B systems are the masses and the decay widths of the heavy and the light states. Especially interesting for oscillation

sensitive experiments are the differences of these observables ΔM and $\Delta\Gamma$. For B-mesons they can be approximated by using

$$\begin{aligned} M_{12} &= |M_{12}|e^{i\phi_M}\,, \\ \Gamma_{12} &= |\Gamma_{12}|e^{i\phi_\Gamma}\,. \end{aligned} \tag{1.12}$$

In the SM, the ratio Γ_{12}/M_{12} is numerically suppressed by $\mathcal{O}(10^{-3})$ for B-mesons. From eq. (1.7) we obtain

$$\Delta M \equiv M_H - M_L = 2|M_{12}| + \mathcal{O}\left(\frac{|\Gamma_{12}|^2}{|M_{12}|^2}\right), \tag{1.13}$$

$$\Delta\Gamma \equiv \Gamma_L - \Gamma_H = -2|\Gamma_{12}|\cos(\phi_\Gamma - \phi_M) + \mathcal{O}\left(\frac{|\Gamma_{12}|^2}{|M_{12}|^2}\right). \tag{1.14}$$

The ratio thus reads

$$\frac{\Delta\Gamma}{\Delta M} = -\,\mathrm{Re}\left(\frac{\Gamma_{12}}{M_{12}}\right). \tag{1.15}$$

The phases ϕ_M and ϕ_Γ in eq. (1.12) are unphysical. Relevant is instead the difference between them:

$$\phi_{12} \equiv \arg\left(-\frac{M_{12}}{\Gamma_{12}}\right) = \pi + \phi_M - \phi_\Gamma\,. \tag{1.16}$$

Alternatively, one can define the observable,

$$a_{\mathrm{fs}} \equiv \frac{|\Gamma_{12}|}{|M_{12}|}\sin(\phi_{12}) = \mathrm{Im}\left(\frac{\Gamma_{12}}{M_{12}}\right), \tag{1.17}$$

which is a CP asymmetry in flavor specific decays. To see why it carries this name, let us examine the ratio of the coefficients of eq. (1.9):

$$\begin{aligned} \frac{q}{p} &= -\frac{\sqrt{\left(M_{12} - \frac{i\Gamma_{12}}{2}\right)\left(M_{12}^* - \frac{i\Gamma_{12}^*}{2}\right)}}{M_{12}^* - \frac{i\Gamma_{12}^*}{2}} \\ &= e^{-i\phi_M}\left(-1 + \frac{a_{\mathrm{fs}}}{2}\right) + \mathcal{O}\left(\frac{|\Gamma_{12}|^2}{|M_{12}|^2}\right). \end{aligned} \tag{1.18}$$

In the case of no CP violation one would get $q/p = -e^{-i\phi_M}$. Thus, a_{fs} quantifies the CP asymmetry as it expresses the deviation of the physical states from the CP eigenstates.

The asymmetry parameter a_{fs} can be experimentally accessed from decays into final states $f/\overline{f}$ for which the processes $\overline{B} \to f$ and $B \to \overline{f}$ are forbidden and no direct CPV occurs, i.e.

$$|\,\langle f|B(t)\rangle\,| = |\,\langle \overline{f}|\overline{B}(t)\rangle\,|\,. \tag{1.19}$$

With the considerations of refs. [23, 26], it follows

$$a_{\mathrm{fs}} = \frac{\Gamma\left(\overline{B}(t) \to f\right) - \Gamma\left(B(t) \to \overline{f}\right)}{\Gamma\left(\overline{B}(t) \to f\right) + \Gamma\left(B(t) \to \overline{f}\right)}, \tag{1.20}$$

where $\Gamma(i \to f)$ is the partial decay width of the regarded process.

Returning to the time evolution, we get for the physical states

$$\begin{aligned} |B_L(t)\rangle &= e^{-iM_L t - \frac{\Gamma_L}{2}t} |B_L(0)\rangle \,, \\ |B_H(t)\rangle &= e^{-iM_H t - \frac{\Gamma_H}{2}t} |B_H(0)\rangle \,, \end{aligned} \tag{1.21}$$

and for the flavor eigenstates of eq. (1.2)

$$\begin{aligned} |B(t)\rangle &= g_+(t)\,|B(0)\rangle \;+\; \frac{q}{p} g_-(t)\,|\overline{B}(0)\rangle \,, \\ |\overline{B}(t)\rangle &= \frac{p}{q} g_-(t)\,|B(0)\rangle \;+\; g_+(t)\,|\overline{B}(0)\rangle \,, \end{aligned} \tag{1.22}$$

with

$$g_\pm(t) = \frac{1}{2}\left(e^{-iM_L t - \frac{\Gamma_L}{2}t} \pm e^{-iM_H t - \frac{\Gamma_H}{2}t}\right) . \tag{1.23}$$

In the following we focus on the individual observables ΔM, $\Delta\Gamma$ and a_{fs} and how they can be predicted by the SM. From eqs. (1.13), (1.14) and (1.17) we see that these quantities can solely be computed from the complex off-diagonal elements of the mass and width matrices, M_{12} and Γ_{12}. Hence, we will take a closer look at their definitions in quantum field theory.

1.2 M_{12}

The transition between flavor eigenstates of a B-$\overline{B}$ system is described in QFT by the *self-energy matrix element* Σ. It is given by

$$-i(2\pi)^4 \delta^{(4)}(p_i - p_j)\Sigma_{ij} \;=\; \frac{\langle B_i|\,\mathcal{S}\,|B_j\rangle}{2M_B} \,, \tag{1.24}$$

where $|B_{i/j}\rangle$ are either $|B\rangle$ or $|\overline{B}\rangle$, with all states defined in the Heisenberg picture and in momentum space. The normalization factor $(2M_B)^{-1}$ with the average B-meson mass M_B is convention. Since the meson flavor eigenstates mix during propagation, Σ is a 2×2 matrix. Also, momentum conservation between initial and final state is implied in eq. (1.24) due to the Dirac δ-function.

We can define the *transfer matrix* $\mathcal{T}$ as the non-trivial part of the $\mathcal{S}$-matrix:

$$\mathcal{S} \;=\; \mathbb{1} + i\mathcal{T} \;=\; e^{-i\int \mathrm{d}^4x\; \mathcal{H}^{\text{SM}}} \,, \tag{1.25}$$

where $\mathcal{H}^{\text{SM}}$ is the *Hamiltonian density operator* (or shorthand "*Hamiltonian*") of the Standard Model.

According to ref. [22], the effective Hamiltonian of eq. (1.3) is given by the self-energy:

$$\Sigma \;\equiv\; H \;=\; M - i\frac{\Gamma}{2} \,. \tag{1.26}$$

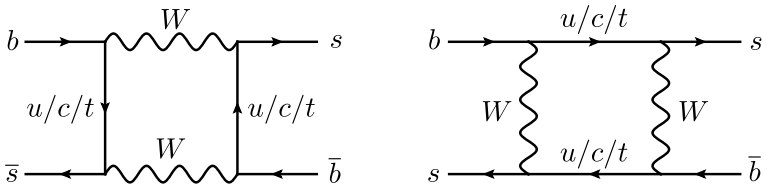

Figure 1.1: In the SM the oscillations of the flavor eigenstates of $B_s/\overline{B}_s$ and $B_d/\overline{B}_d$ are dominated by two W-exchanges. The diagrams for $B_d/\overline{B}_d$ look similar with $s \leftrightarrow d$ exchanged.

By recalling eq. (1.4) we get

$$M_{12} \;=\; \frac{\Sigma_{12} + \Sigma_{21}^*}{2} \;\equiv\; \mathrm{Disp}(\Sigma_{12})\,. \tag{1.27}$$

What we previously called "dispersive" part now reveals to be connected to the real part of the self-energy. M_{12} is sensitive to heavy virtual particles which can or cannot go on-shell in the loop diagrams. This includes particles like W, Z, the top-quark and the Higgs boson.

In the SM the leading contributions to Σ_{12} are given by box diagrams with virtual W-boson exchange, as shown in fig. 1.1. Loop diagrams are the only source of these so-called *Flavor Changing Neutral Currents* (FCNCs) in the SM. Besides the fact that no tree-level graph exists, they are additionally suppressed due to the *Glashow-Iliopoulos-Maiani* (GIM) mechanism [27]. This suppression is of phenomenological importance for the building and constraining new physics models.

The relevant SM interactions for this process are given by the weak interaction Hamiltonian responsible for charged currents:

$$\mathcal{H}^W \;=\; -\frac{g_W}{\sqrt{2}}\left(V_{ij}\overline{u}_i\gamma^\mu P_L d_j W_\mu^+ \;+\; V_{ij}^*\overline{d}_i\gamma^\mu P_L u_j W_\mu^-\right)\,. \tag{1.28}$$

Here, the W gauge field couples only to left-handed quark fields and right-handed anti-quark fields, as indicated by the chiral projection operator:

$$P_{R/L} = \frac{1 \pm \gamma_5}{2}\,. \tag{1.29}$$

The left-handed up-type quark flavor u_i and the down-type d_i interact proportionally to the corresponding entries of the *Cabibbo-Kobayashi-Maskawa* (CKM) matrix V [28, 29]. Its numerical scaling can be approximated using the *Wolfenstein parameterization* [30]. It reads

$$\begin{aligned} V \;&=\; \begin{pmatrix} V_{ud} & V_{us} & V_{ub} \\ V_{cd} & V_{cs} & V_{cb} \\ V_{td} & V_{ts} & V_{tb} \end{pmatrix} \\ &=\; \begin{pmatrix} 1-\frac{\lambda}{2} & \lambda & \lambda^3 A(\rho - i\eta) \\ -\lambda & 1-\frac{\lambda}{2} & \lambda^2 A \\ \lambda^3 A(1-\rho-i\eta) & -\lambda^2 A & 1 \end{pmatrix} \;+\; \mathcal{O}\left(\lambda^4\right)\,, \end{aligned} \tag{1.30}$$

where $\rho, \eta, \lambda = \mathcal{O}(0.1)$ are treated as small expansion parameters and $A = \mathcal{O}(1)$ [31].

Since V is unitary we can state six equations describing triangles in the complex space. They are called *unitarity triangles*:

$$\begin{aligned} V_{ui}^* V_{uj} + V_{ci}^* V_{cj} + V_{ti}^* V_{tj} &= 0\,, \\ V_{kd}^* V_{ld} + V_{ks}^* V_{ls} + V_{kb}^* V_{lb} &= 0\,, \end{aligned} \tag{1.31}$$

with $i, j \in \{d, s, b\}$ and $k, l \in \{u, c, t\}$.

Regarding the off-diagonal elements of the self-energy matrix, the CKM matrix elements factorize as

$$\begin{aligned} \Sigma_{12} &= \sum_{i,j} (V_{is}^* V_{jb})^2 \, \mathcal{M}_{ij}(\overline{B} \to B)\,, \\ \Sigma_{21} &= \sum_{i,j} (V_{is} V_{jb}^*)^2 \, \mathcal{M}_{ij}(B \to \overline{B})\,. \end{aligned} \tag{1.32}$$

After the CP-violating CKM matrix elements are removed, the remainder of the amplitude is CP invariant. Hence, the terms of eq. (1.32) are connected according to

$$\mathcal{M}_{ij}(\overline{B} \to B) = \mathcal{M}_{ij}(B \to \overline{B}) \equiv \mathcal{M}_{ij}\,. \tag{1.33}$$

Thus, eq. (1.27) simplifies to

$$M_{12} = \sum_{i,j} (V_{is}^* V_{jb})^2 \, \mathrm{Re}\big(\mathcal{M}_{ij}\big)\,. \tag{1.34}$$

The CKM matrix elements allow for another simplification of M_{12}. From fig. 1.1 one can see that M_{12} can in general be parametrized as

$$\begin{aligned} M_{12} &= \lambda_u^2 M_{12}^{uu} + 2\lambda_u\lambda_c M_{12}^{uc} + 2\lambda_u\lambda_t M_{12}^{ut} \\ &\quad + \lambda_c^2 M_{12}^{cc} + 2\lambda_c\lambda_t M_{12}^{ct} + \lambda_t^2 M_{12}^{tt} \\ &\overset{(1.31)}{=} \lambda_c^2 \left(M_{12}^{uu} - 2M_{12}^{uc} + M_{12}^{cc}\right) \\ &\quad + 2\lambda_c\lambda_t \left(M_{12}^{uu} - M_{12}^{uc} - M_{12}^{ut} + M_{12}^{ct}\right) \\ &\quad + \lambda_t^2 \left(M_{12}^{uu} - 2M_{12}^{ut} + M_{12}^{tt}\right)\,. \end{aligned} \tag{1.35}$$

We use the abbreviation $\lambda_q \equiv V_{qs}^* V_{qb}$ for B_s-mesons. For B_d, V_{qs}^* is replaced by V_{qd}^*.

From eq. (1.35) it is apparent that M_{12} vanishes if all quarks would carry the same mass. This follows directly from the GIM mechanism. Hence, the mass dependence plays a crucial role in the determination of M_{12}.

Until now, we consider processes with many scales involved, including quark and gauge boson masses, as well as Λ_{QCD}. Taking all of them into account would lead to large logarithms which spoil the scaling behavior of the perturbative expansion. The common way to avoid these difficulties is the utilization of approximate methods like *Operator Product Expansion* (OPE) [32–35]. It allows the separation of scales

which are divided by several orders of magnitude. We can expand eq. (1.24) by introducing an effective Hamiltonian $\mathcal{H}^{\text{eff}}$ according to

$$\begin{aligned}\langle B|\, e^{-i\int \mathrm{d}^4x\ \mathcal{H}^{\text{SM}}}\,|\overline{B}\rangle \ &\overset{!}{=}\ \langle B|\, e^{-i\int \mathrm{d}^4x\ \mathcal{H}^{\text{eff}}}\,|\overline{B}\rangle \ +\ \mathcal{O}\left(\frac{m_{\text{light}}}{m_{\text{heavy}}}\right)\\ &=\ -i\int \mathrm{d}^4x\ \langle B|\,\mathcal{H}^{\text{eff}}(x)\,|\overline{B}\rangle\\ &\quad -\frac{1}{2}\int \mathrm{d}^4x\int \mathrm{d}^4y\ \langle B|\,\mathbf{T}\mathcal{H}^{\text{eff}}(x)\mathcal{H}^{\text{eff}}(y)\,|\overline{B}\rangle\\ &\quad +\ \dots\,.\end{aligned} \tag{1.36}$$

This equation holds to a fixed order in the expansion of small scale ratios, denoted for simplification by "$m_{\text{light}}/m_{\text{heavy}}$". In our case we have $m_{\text{heavy}} \sim m_W, m_Z, m_t, m_H$ and the remaining scales being treated as m_{light}. The effective Hamiltonian can then be written as

$$\mathcal{H}^{\text{eff}} \ \equiv\ \mathcal{H}^{\Delta B=2} \ +\ \mathcal{H}^{\Delta B=1} \ +\ \mathcal{H}^{\text{QCD},(5)}\,. \tag{1.37}$$

The first two terms describe an *Effective Field Theory* (EFT) of flavor changing interactions. They include operators which change the *beauty* quantum number (denoted by B) by $\Delta B = 2$ and $\Delta B = 1$, respectively. These two theories are discussed in more detail in chapters 2 and 3.

To account for effects from the strong force, which are the dominant corrections in meson physics, we include the *Quantum Chromodynamics* (QCD) Hamiltonian $\mathcal{H}^{\text{QCD},(5)}$ with five active quark flavors.

Overall, $\mathcal{H}^{\text{eff}}$ describes only the dynamics of light particles, whereas the heavy particles are *integrated out* of the theory. Their remaining effect consists of higher dimensional effective operators and corresponding proportionality factors, called *Wilson coefficients*.

Coming back to the description of M_{12}, the Leading Order (LO) contribution is given by the $\Delta B = 2$ Hamiltonian:

$$\mathcal{H}^{\Delta B=2} \ \approx\ \frac{G_F^2}{16\pi^2} m_W^2 \lambda_t^2\ C_Q\ Q^{\Delta B=2} \ +\ \text{h.c.}\,, \tag{1.38}$$

where G_F is Fermi's constant. The effective operator

$$Q^{\Delta B=2} \ =\ 4\left(\overline{b}_i\gamma^\mu P_L s_i\right)\left(\overline{b}_j\gamma_\mu P_L s_j\right) \tag{1.39}$$

stems from the diagrams of fig. 1.2 in the full theory[1]. As mentioned before, the quark mass dependence plays a crucial role in the calculation of M_{12}. The GIM suppression has the least effect in diagrams involving two virtual top-quarks. Therefore, they are the dominant contributions to M_{12}.

Additionally, since M_{12} includes only contributions from virtual particles it would be sensitive to heavy particles beyond the Standard Model [36] as well.

1 As *full theory* we denote the theory from which an effective theory is derived. The former may be an effective theory as well.

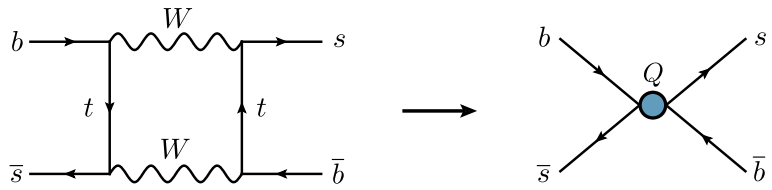

Figure 1.2: If heavy particles are integrated out of the theory, mainly single operator insertions of an effective $\Delta B = 2$ theory contribute to M_{12}. The leading effects stem from box diagrams with two top quarks. The same holds for $B_d/\overline{B}_d$.

Keeping only the leading effects, eq. (1.36) leads to

$$M_{12} \;=\; \frac{G_F^2}{32\pi^2} m_W^2 \lambda_t^2 C_Q \left\langle B\right| Q^{\Delta B=2} \left|\overline{B}\right\rangle \,. \tag{1.40}$$

The hadronic matrix element $\left\langle B\right| Q^{\Delta B=2} \left|\overline{B}\right\rangle$ cannot be computed in perturbation theory. The contributing hadronization effects take place at energies below Λ_{QCD}, i.e. the fundamental scale of QCD. At these energies, the perturbative description of α_s is ill-defined and cannot be used anymore. Therefore, one has to turn to non-perturbative methods such as *lattice gauge theory* [37–41] or *sum rules* [42–46] which allow a numerical determination of such quantities.

In the literature, the matrix element is conventionally defined as [47]

$$\left\langle B\right| Q^{\Delta B=2} \left|\overline{B}\right\rangle \;\equiv\; \frac{8}{3} M_B^2 f_B^2 B_Q \,, \tag{1.41}$$

where f_B is the decay constant of the B-$\overline{B}$ system. B_Q is called *bag parameter*.

The Wilson coefficient C_Q in eq. (1.40) contains information about the short range effects of the $B \leftrightarrow \overline{B}$ transition. It can hence be computed using perturbative tools. At leading order in α_s, it is given by

$$C_Q(\mu = m_W) \;=\; S_0(x_t) \;\equiv\; \frac{4x_t - 11x_t^2 + x_t^3}{4(1-x_t)^2} - \frac{3x_t^3 \ln(x_t)}{2(1-x_t)^3} \,. \tag{1.42}$$

The function $S_0(x_t)$ is called *Inami-Lim function* with $x_t = m_t^2/m_W^2$ [48]. At the time of writing, C_Q is known to next-to-leading order in α_s [49].

As it can be seen from eq. (1.36), also the dispersive part of two $\Delta B = 1$ insertions contributes, a priori, to M_{12}. However, the $\Delta B = 1$ contributions are substantially smaller than the $\Delta B = 2$ ones due to the dominance of the top-quark mass.

In the next section we put the main focus on these $\Delta B = 1$ terms in the context of Γ_{12}.

1.3 Γ_{12}

Similar to the definition of M_{12}, we can formulate Γ_{12} according to eq. (1.4):

$$-\frac{\Gamma_{12}}{2} \;=\; -i\frac{\Sigma_{12} - \Sigma_{21}^*}{2} \;\equiv\; \text{Abs}(\Sigma_{12}) \,. \tag{1.43}$$

By using the parameterization as in eq. (1.32), we see that the absorptive part of the self-energy is connected to its imaginary part:

$$-\frac{\Gamma_{12}}{2} = \sum_{i,j} (V_{is} V_{jb}^*)^2 \, \mathrm{Im}(\mathcal{M}_{ij}) \, . \tag{1.44}$$

According to Cutkosky's cutting rules, the imaginary part of a Feynman amplitude is defined as the sum of all possible cuts through loop propagators in such a way that the remaining graph is separated [50]. These cut propagators are then put on-shell. Thus, only virtual particles in loop diagrams contribute to Γ_{12} which are allowed by the kinematics to go on-shell. Recalling eq. (1.36) we see that the single $\Delta B = 2$ insertion therefore cannot contribute. The leading contributions are two $\Delta B = 1$ insertions:

$$\Gamma_{12} = \frac{1}{2M_B} \mathrm{Abs}\left(i \int \mathrm{d}^4 x \, \langle B | \, \mathbf{T} \mathcal{H}^{\Delta B=1}(x) \mathcal{H}^{\Delta B=1}(0) \, | \overline{B} \rangle \right) . \tag{1.45}$$

In order to get a predictable observable, this expression is simplified to a local operator matrix element. Otherwise, the evaluation of the hadronic matrix element would be not feasible with current non-perturbative techniques. Thus, a second OPE is needed, for which we choose $\Lambda / m_b \approx 0.05$ as a small parameter with Λ being a hadronic scale of the order of Λ_{QCD}. The precise value of Λ is determined by non-perturbative calculations. This expansion is known as *Heavy Quark Expansion* (HQE) [51–56]. In this approximation Γ_{12} can be written as

$$\Gamma_{12} = \frac{\Lambda^3}{m_b^3} \Gamma_{12}^{(3)} + \frac{\Lambda^4}{m_b^4} \Gamma_{12}^{(4)} + \mathcal{O}\left(\frac{\Lambda^5}{m_b^5} \right) . \tag{1.46}$$

Similar to M_{12}, the expression for Γ_{12} simplifies to single $\Delta B = 2$ operator insertions:

$$\Gamma_{12} \propto \sum_i C_i \, \langle B | \, \mathcal{H}_i^{\Delta B=2} \, | \overline{B} \rangle \, , \tag{1.47}$$

where the Wilson coefficients C_i are functions of $\Delta B = 1$ parameters, and hence depend only indirectly on the fundamental theory. This enables the investigation of changes in the $\Delta B = 1$ contributions due to new physics effects and the impact on Γ_{12}. To evaluate Γ_{12} it is necessary to compute contributions of $\Delta B = 1$ and $\Delta B = 2$. Afterwards, both results are connected by a matching calculation. This procedure is similar to the first operator product expansion in which the degrees of freedom of W, Z, H and t were integrated out.

The terms of eq. (1.46) individually receive QCD corrections which must be taken into account for high precision predictions of Γ_{12}. The leading term $\Gamma_{12}^{(3)}$ includes four-quark operators of dimension-6 and chromomagnetic dimension-5 operators, whereas $\Gamma_{12}^{(4)}$ includes further power suppressed operators of various dimensions. The results for $\Gamma_{12}^{(3)}$ and $\Gamma_{12}^{(4)}$ to leading order in α_s are known for several decades [57–63]. In contrast to $\Gamma_{12}^{(3)}$, no further orders are known for $\Gamma_{12}^{(4)}$.

According to the various CKM matrix contributions, Γ_{12} can be decomposed as

$$\begin{aligned} \Gamma_{12} &= -\lambda_u^2 \Gamma_{12}^{uu} - 2\lambda_u \lambda_c \Gamma_{12}^{uc} - \lambda_c^2 \Gamma_{12}^{cc} \\ &\overset{(1.31)}{=} -\lambda_t^2 \left[\Gamma_{12}^{cc} + 2\frac{\lambda_u}{\lambda_t} \left(\Gamma_{12}^{cc} - \Gamma_{12}^{uc} \right) + \frac{\lambda_u^2}{\lambda_t^2} \left(\Gamma_{12}^{uu} - 2\Gamma_{12}^{uc} + \Gamma_{12}^{cc} \right) \right] . \end{aligned} \tag{1.48}$$

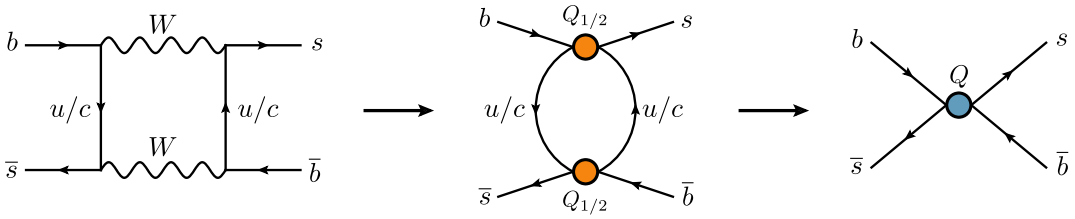

Figure 1.3: After the first OPE the B-$\overline{B}$ mixing is described by two effective interactions in the $\Delta B = 1$ theory. We expand then in Λ/m_b and project the absorptive part of the corresponding matrix elements on local $\Delta B = 2$ operator insertions. The diagram with two c-quarks contributes solely to Γ_{12}^{cc}, the one with two u-quarks to Γ_{12}^{uu} and the mixed variant to Γ_{12}^{uc}.

We see that the GIM mechanism enhances the contribution of Γ_{12}^{cc} which stems primarily from diagrams with two virtual charm quarks. Also, the relative scaling of the terms in eq. (1.48) is influenced by the factor λ_u/λ_t which scales as $\lambda^2 \approx 0.05$ according to the Wolfenstein parameterization. The procedure to compute Γ_{12} is illustrated in fig. 1.3.

From eq. (1.48) one can see that a_{fs}, being the imaginary part of Γ_{12}/M_{12}, receives no contributions from the $(\lambda_u/\lambda_t)^0$ term of Γ_{12} since the prefactor λ_t^2 cancels in the ratio. Therefore, a_{fs} is GIM suppressed and sensitive to the mass of the c-quark m_c. This renders a_{fs} numerically small which gives a strong constraint on the CP violating effects of new physics in neutral B-meson mixing.

The computation of Γ_{12} to higher orders in α_s is the main topic of this dissertation.

Part I

EFFECTIVE THEORY FRAMEWORK OF B-MESON MIXING

2

ΔB=1 THEORY

In this chapter we focus on the effective interactions that lead to a beauty-flavor change of $\Delta B = 1$, as well as the implications and difficulties of their formulation.

2.1 EFFECTIVE FIELD THEORIES

In the SM the most significant contribution to processes which change the beauty flavor quantum number by $\Delta B = 1$ comes from a virtual W-boson exchange. For example, the transition $b\bar{s} \to c\bar{c}$ is depicted in the following Feynman diagram:

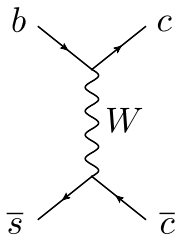

The corresponding tree-level matrix element with the Hamiltonian of eq. (1.28) in the Feynman-'t Hooft gauge is given by

$$\begin{aligned} i\mathcal{M}_{\text{SM}} &= i\frac{g_W^2}{2} V_{cb}V_{cs}^* \frac{1}{q^2 - m_W^2} \left(\bar{s}\gamma^\mu P_L c\right)\left(\bar{c}\gamma_\mu P_L b\right) \\ &= -i\frac{g_W^2}{2m_W^2} V_{cb}V_{cs}^* \left(\bar{s}\gamma^\mu P_L c\right)\left(\bar{c}\gamma_\mu P_L b\right) + \mathcal{O}\left(\frac{q^2}{m_W^2}\right) . \end{aligned} \tag{2.1}$$

We use $m_W \gg \sqrt{q^2}$ to simplify the matrix element, where q is the exchanged momentum between the two quark lines. The leading term of this approximation describes a local interaction which does not depend on the kinematics of the external particles.

Let us repeat this calculation with an effective local interaction which is described by the Hamiltonian:

$$\mathcal{H}^{\Delta B=1} = \frac{4G_F}{\sqrt{2}} V_{cb}V_{cs}^* \left(C_1 Q_1 + C_2 Q_2\right) + \text{h.c.}, \tag{2.2}$$

with

$$Q_1 = \left(\bar{s}_i\gamma^\mu P_L c_j\right)\left(\bar{c}_j\gamma_\mu P_L b_i\right) , \quad Q_2 = \left(\bar{s}_i\gamma^\mu P_L c_i\right)\left(\bar{c}_j\gamma_\mu P_L b_j\right) . \tag{2.3}$$

QED	$\alpha\left(\overline{m}_b(\overline{m}_b)\right)$	≈ 0.0074
QCD	$\alpha_s^{(5)}\left(\overline{m}_b(\overline{m}_b)\right)$	≈ 0.2245
Weak theory	$\alpha_W \frac{\overline{m}_b^2(\overline{m}_b)}{m_W^2}$	≈ 0.0001

Table 2.1: This table provides an overview of the relative size of effects expected for higher order corrections at the scale $\overline{m}_b(\overline{m}_b)$. For the QED fine structure constant α, only the one-loop corrections are taken into account. For the running of α_s we use the five-loop corrections from `RunDec` [64]. The size of the weak coupling constant $\alpha_W = 0.0339$ is estimated from eq. (2.6). The used input parameters are given in table 7.1.

The indices i and j denote the color indices of the quark fields. This theory is supposed to describe the physics of energies below m_W. This requirement is expressed in terms of $\mathcal{S}$ matrix elements,

$$\langle f|\, e^{-i\int \mathrm{d}^4x \mathcal{H}^{\text{full}}}\, |i\rangle \;\stackrel{!}{=}\; \langle f|\, e^{-i\int \mathrm{d}^4x \mathcal{H}^{\text{eff}}}\, |i\rangle \;+\; \mathcal{O}\left(\frac{\Lambda^3}{m_W^3}\right). \tag{2.4}$$

Instead of truncating eq. (2.4) the higher order terms could also be included in $\mathcal{H}^{\text{eff}}$. This leads to a population with infinitely many operators and Wilson coefficients. This OPE provides a powerful tool to resum large logarithms of the type $\ln(m_b^2/m_W^2)$, and it simplifies computations, additionally. However, the effective theory is constructed in such a way that it is only valid in a certain energy range.

The matrix element for the $b\bar{s} \to c\bar{c}$ process in the effective theory of eq. (2.2) is given by

$$\begin{aligned} i\mathcal{M}_{\text{eff}} &= -i\frac{4G_F}{\sqrt{2}} V_{cb}V_{cs}^* C_2 \left(\bar{s}\gamma^\mu P_L c\right)\left(\bar{c}\gamma_\mu P_L b\right) \\ &= -i\frac{g_W^2}{2m_W^2} V_{cb}V_{cs}^* C_2 \left(\bar{s}\gamma^\mu P_L c\right)\left(\bar{c}\gamma_\mu P_L b\right), \end{aligned} \tag{2.5}$$

where we use

$$G_F = \frac{\sqrt{2}g_W^2}{8m_W^2}. \tag{2.6}$$

The comparison of eqs. (2.1) and (2.5), together with the requirement of eq. (2.4), gives:

$$C_1 = 0, \qquad C_2 = 1. \tag{2.7}$$

This equality holds at leading order in Λ/m_W. To obtain more accurate predictions for the process $b\bar{s} \to c\bar{c}$, one could include higher-order corrections from the Standard Model. A naive numerical comparison of the coupling constants gives an approximate relative size of the expected corrections. The comparison is shown in table 2.1. Hence, it is sufficient to focus solely on QCD corrections before other corrections have to be considered.

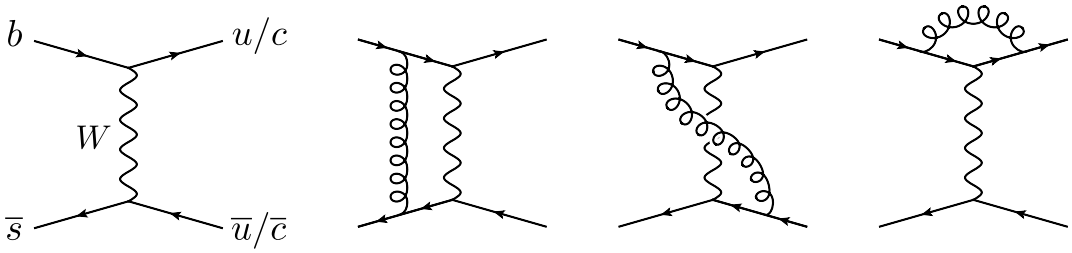

Figure 2.1: SM contributions to the Wilson coefficients of current-current operators are shown at LO and NLO in QCD.

In general, renormalization of effective field theories leads to a mixing of the effective operators. Denoting the renormalization matrix for the operators $\vec{Q}$ by $\widetilde{Z}$, we have

$$\mathcal{M}_{\text{ren}} \;=\; C_i \langle Q_i \rangle \;=\; C_i \widetilde{Z}^{-1}_{ij} \langle Q_j \rangle^0 \,. \tag{2.8}$$

Thus, in order to renormalize the theory properly a closed set of operators has to be considered. This means that the operator basis includes all operators which are allowed by the symmetries of the theory and occur due to quantum corrections. Nevertheless, one has some freedom in the choice of the basis because the effective Hamiltonian which satisfies eq. (2.4) is not unique. In the following we discuss two different operator bases for the $\Delta B = 1$ theory. The first basis was used in previous calculations of Γ_{12}. In this work we use the second one due to its advantageous properties.

2.2 TRADITIONAL BASIS

For the calculation of Γ_{12} in refs. [47, 63, 65–71], the operator basis of ref. [72] was used for the $\Delta B = 1$ effective Hamiltonian, which is given by

$$\begin{aligned}\mathcal{H}^{\Delta B=1} \;=\; \frac{4G_F}{\sqrt{2}} \Bigg[& V_{cb}V_{cs}^* \left(C_1^{cc} Q_1^{cc} + C_2^{cc} Q_2^{cc}\right) + V_{cb}V_{us}^* \left(C_1^{cu} Q_1^{cu} + C_2^{cu} Q_2^{cu}\right) \\ & + V_{ub}V_{cs}^* \left(C_1^{uc} Q_1^{uc} + C_2^{uc} Q_2^{uc}\right) + V_{ub}V_{us}^* \left(C_1^{uu} Q_1^{uu} + C_2^{uu} Q_2^{uu}\right) \\ & - V_{tb}V_{ts}^* \left(\sum_{i=3}^{6} C_i Q_i + C_8 Q_8 \right) + \sum_i C_{E_i} E_i \Bigg] \;+\; \text{h.c.}\,.\end{aligned} \tag{2.9}$$

The operators of eq. (2.9) are separated into three classes. The class of *current-current operators* involves

$$\begin{aligned} Q_1^{cc} &= \left(\bar{s}_i \gamma^\mu P_L c_j\right)\left(\bar{c}_j \gamma_\mu P_L b_i\right) , & Q_2^{cc} &= \left(\bar{s}_i \gamma^\mu P_L c_i\right)\left(\bar{c}_j \gamma_\mu P_L b_j\right) , \\ Q_1^{cu} &= \left(\bar{s}_i \gamma^\mu P_L u_j\right)\left(\bar{c}_j \gamma_\mu P_L b_i\right) , & Q_2^{cu} &= \left(\bar{s}_i \gamma^\mu P_L u_i\right)\left(\bar{c}_j \gamma_\mu P_L b_j\right) , \\ Q_1^{uc} &= \left(\bar{s}_i \gamma^\mu P_L c_j\right)\left(\bar{u}_j \gamma_\mu P_L b_i\right) , & Q_2^{uc} &= \left(\bar{s}_i \gamma^\mu P_L c_i\right)\left(\bar{u}_j \gamma_\mu P_L b_j\right) , \\ Q_1^{uu} &= \left(\bar{s}_i \gamma^\mu P_L u_j\right)\left(\bar{u}_j \gamma_\mu P_L b_i\right) , & Q_2^{uu} &= \left(\bar{s}_i \gamma^\mu P_L u_i\right)\left(\bar{u}_j \gamma_\mu P_L b_j\right) . \end{aligned} \tag{2.10}$$

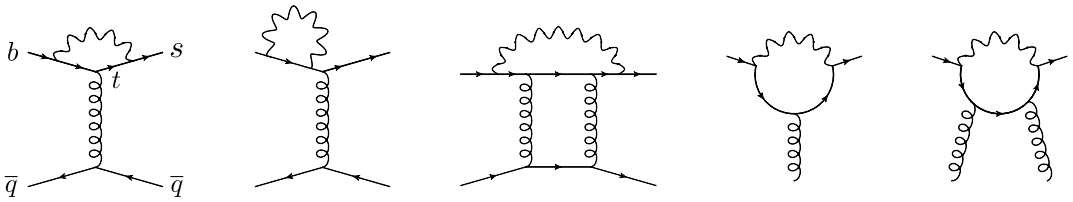

Figure 2.2: SM equivalent of penguin diagrams have a spectator fermion line which is connected by gluons. Since QCD is flavor-blind, the spectator quark can be any quark flavor. The two diagrams on the right contribute to the chromomagnetic dimension-5 operator Q_8.

These operators stem from SM diagrams with the combination of two charged currents mediated by a W boson (hence the name) as shown in fig. 2.1. For the corresponding Wilson coefficients we have

$$\begin{aligned} C_1 &\equiv C_1^{cc} = C_1^{cu} = C_1^{uc} = C_1^{uu}\,, \\ C_2 &\equiv C_2^{cc} = C_2^{cu} = C_2^{uc} = C_2^{uu}\,, \end{aligned} \tag{2.11}$$

which must be treated differently for the renormalization.

The second operator class is called *penguin operators*. They are given by

$$\begin{aligned} Q_3 &= (\bar{s}_i\gamma^\mu P_L b_i)\sum_q \left(\bar{q}_j\gamma_\mu P_L q_j\right)\,, \\ Q_4 &= (\bar{s}_i\gamma^\mu P_L b_j)\sum_q \left(\bar{q}_j\gamma_\mu P_L q_i\right)\,, \\ Q_5 &= (\bar{s}_i\gamma^\mu P_L b_i)\sum_q \left(\bar{q}_j\gamma_\mu P_R q_j\right)\,, \\ Q_6 &= (\bar{s}_i\gamma^\mu P_L b_j)\sum_q \left(\bar{q}_j\gamma_\mu P_R q_i\right)\,, \\ Q_8 &= \frac{g_s}{16\pi^2} m_b \bar{s}\sigma^{\mu\nu} P_R T^a b G^a_{\mu\nu}\,, \end{aligned} \tag{2.12}$$

with $\sigma^{\mu\nu} = i[\gamma^\mu, \gamma^\nu]/2$ and the $\mathrm{SU}_c(3)$ group generators T^a. We also use the QCD field strength tensor (see e.g. ref. [73])

$$G^a_{\mu\nu} = \partial_\mu G^a_\nu - \partial_\nu G^a_\mu + g_s f^{abc} G^b_\mu G^c_\nu\,, \tag{2.13}$$

with f^{abc} being the structure constants and g_s the strong coupling constant. The sum over q iterates through all five active quark flavors. These operators are related in the SM to diagrams shown in fig. 2.2.

The *chromomagnetic moment operator* Q_8 plays a special role since it is a dimension-5 operator, in contrast to the remaining operators which are dimension-6. Thus, Q_8 has to be taken into account for the renormalization of Q_{1-6}. On the contrary, no other operator is needed to renormalize the contributions of Q_8 [21].

The last operator class are the so-called *evanescent operators*. They are the topic of section 2.4.

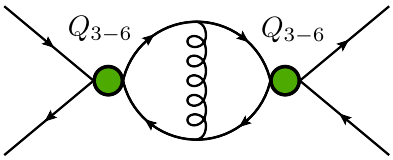

Figure 2.3: Diagrams with two penguin insertions lead to ill-defined traces with γ_5 in the traditional basis. This problem arises first at $\mathcal{O}(\alpha_s)$ which was not yet the subject in the literature. In the full theory equivalent of this diagram, such objects are absent. Therefore, they can be prevented by a different choice of the operator basis.

2.3 CMM BASIS

The operator basis introduced in section 2.2 has a practical disadvantage: Diagrams with two penguin operator insertions, as for example fig. 2.3, give rise to the Dirac structure

$$\mathrm{Tr}_d(\gamma_5\gamma^\mu\gamma^\nu\gamma^\rho\gamma^\sigma)\ . \tag{2.14}$$

In $d = 4$ space-time dimensions this trace can be evaluated using the *Levi-Civita symbol*:

$$\mathrm{Tr}_4(\gamma_5\gamma^\mu\gamma^\nu\gamma^\rho\gamma^\sigma) \ = \ -4i\epsilon^{\mu\nu\rho\sigma}\,. \tag{2.15}$$

In calculations employing the *dimensional regularization* scheme, the Dirac matrices are formally defined as infinite dimensional [74]. Hence, the combinatorically motivated $\epsilon^{\mu\nu\rho\sigma}$ is ill-defined in $d = 4 - 2\epsilon$.

From the full-theory equivalent of the two penguin insertion diagram, it is evident that no such trace can appear. Since only the weak interactions are sensitive to the chirality of the interacting particles, additional corrections from chirality-blind theories, such as QCD, do not lead to new appearances of traces with γ_5.

Thus, the appearance of eq. (2.14) is a spurious artifact of the chosen basis of eq. (2.9). To circumvent this issue, a different basis has been proposed in ref. [75]. We refer to it as the "CMM" basis according to its inventors *K. Chetyrkin*, *M. Misiak* and *M. Münz*. The effective Hamiltonian has the same structure as eq. (2.9), except for the operators which we denote by P_i to distinguish them from the traditional basis. They read

$$\begin{aligned}
P_1^{cc} &= (\bar{s}\gamma^\mu P_L T^a c)\,(\bar{c}\gamma_\mu P_L T^a b)\ , \quad P_2^{cc} = (\bar{s}\gamma^\mu P_L c)\,(\bar{c}\gamma_\mu P_L b)\ ,\\
P_1^{cu} &= (\bar{s}\gamma^\mu P_L T^a u)\,(\bar{c}\gamma_\mu P_L T^a b)\ , \quad P_2^{cu} = (\bar{s}\gamma^\mu P_L u)\,(\bar{c}\gamma_\mu P_L b)\ ,\\
P_1^{uc} &= (\bar{s}\gamma^\mu P_L T^a c)\,(\bar{u}\gamma_\mu P_L T^a b)\ , \quad P_2^{uc} = (\bar{s}\gamma^\mu P_L c)\,(\bar{u}\gamma_\mu P_L b)\ ,\\
P_1^{uu} &= (\bar{s}\gamma^\mu P_L T^a u)\,(\bar{u}\gamma_\mu P_L T^a b)\ , \quad P_2^{uu} = (\bar{s}\gamma^\mu P_L u)\,(\bar{u}\gamma_\mu P_L b)\ ,\\
P_3 &= (\bar{s}\gamma^\mu P_L b)\sum_q (\bar{q}\gamma_\mu q)\ ,\\
P_4 &= (\bar{s}\gamma^\mu P_L T^a b)\sum_q (\bar{q}\gamma_\mu T^a q)\ ,\\
P_5 &= (\bar{s}\gamma^{\mu_1}\gamma^{\mu_2}\gamma^{\mu_3} P_L b)\sum_q (\bar{q}\gamma_{\mu_1}\gamma_{\mu_2}\gamma_{\mu_3} q)\ ,
\end{aligned} \tag{2.16}$$

Wilson coefficient	$\mathcal{O}(\alpha_s^0)$	$\mathcal{O}(\alpha_s^1)$	$\mathcal{O}(\alpha_s^2)$
$C_1(\overline{m}_b)$	-0.6367	0.2986	0.0455
$C_2(\overline{m}_b)$	1.0389	-0.0322	0.0026
$C_3(\overline{m}_b)$	-0.0078	0.0023	-0.0005
$C_4(\overline{m}_b)$	-0.0898	-0.0013	0.0042
$C_5(\overline{m}_b)$	0.0007	-0.0004	5×10^{-5}
$C_6(\overline{m}_b)$	0.0016	-0.0005	8×10^{-6}
$C_8(\overline{m}_b)$	-0.1580	-0.0104	0.0057

Table 2.2: This table illustrates the numerical sizes for Wilson coefficients of the CMM basis with the results of refs. [75–79]. The coefficients are evaluated at the $\overline{\text{MS}}$ mass $\overline{m}_b \equiv \overline{m}_b(\overline{m}_b)$, using $\alpha_s^{(5)}(\overline{m}_b) = 0.2245$. The numeric input is given in table 7.1.

$$
\begin{aligned}
P_6 &= (\bar{s}\gamma^{\mu_1}\gamma^{\mu_2}\gamma^{\mu_3} P_L T^a b) \sum_q \left(\bar{q}\gamma_{\mu_1}\gamma_{\mu_2}\gamma_{\mu_3} T^a q\right) , \\
P_8 &= \frac{g_s}{16\pi^2} m_b \bar{s}\sigma^{\mu\nu} P_R T^a b G^a_{\mu\nu} .
\end{aligned}
$$

Compared to eq. (2.12), one can see that no γ_5-dependence is present in the spectator fermion line of the penguin operators. This allows for a straightforward evaluation of diagrams as in fig. 2.3. The Wilson coefficients to these operators are currently known at Next-to-Next-to-Leading Order (NNLO) in QCD [76–79].

From the numerical values of the Wilson coefficients, as shown in table 2.2, one can see a clear enhancement of the current-current in comparison to the penguin operators. The numerical differences is the reason to treat penguin contributions in the literature as higher order. This observation holds in the traditional basis as well. Note that the relatively large value of C_8 is misleading since every contribution of P_8 comes with an additional factor of α_s.

2.4 DIMENSIONAL REGULARIZATION AND EVANESCENT OPERATORS

For schemes in which the dimension is used as the regularization parameter, there are multiple variants to extend four-dimensional quantities. For example, in the original *'t Hooft-Veltman* (HV) scheme [80] Dirac matrices are split into four- and $(d-4)$-dimensional parts, where the latter is defined with infinite dimensions. Another frequently used modification is *Dimensional Reduction* (DRED) [81] in which only momenta and coordinates are defined in d dimensions. Tensor structures are kept four-dimensional in this scheme.

In this work we use the *Naive Dimensional Regularization* (NDR) scheme (e.g. as used in ref. [82]) which prescribes the "naive" usage of an anti-commuting γ_5:

$$\{\gamma^\mu, \gamma_5\} = 0 . \tag{2.17}$$

Figure 2.4: To reduce the Dirac matrix structures of physical operators at higher orders (i), an evanescent operator (ii) is introduced.

In NDR the spinor space is four-dimensional and the following relations hold:

$$\begin{aligned} g_\mu{}^\mu &= d\,, & \{\gamma^\mu,\gamma^\nu\} &= 2g^{\mu\nu}\,,\\ \gamma_\mu\gamma^\mu &= d\,, & \mathrm{Tr}_d(\mathbb{1}) &= 4\,. \end{aligned} \tag{2.18}$$

Additional care must be taken if γ_5 occurs in calculations of higher order. As stated in the literature [83–87], the usage of eq. (2.17) leads to inconsistencies in d dimensions if traces such as eq. (2.14) appear. Thus, NDR is only consistent if traces with an odd number of γ_5 do not contribute, or else the anti-commutation property must be dropped. Furthermore, four-dimensional relations like the Chisholm identity [88],

$$\gamma^\mu\gamma^\nu\gamma^\rho \overset{d=4}{=} g^{\mu\nu}\gamma^\rho - g^{\mu\rho}\gamma^\nu + g^{\nu\rho}\gamma^\mu + i\epsilon^{\alpha\mu\nu\rho}\gamma_\alpha\gamma_5\,, \tag{2.19}$$

cannot be used in NDR.

For all schemes an additional set of auxiliary operators has to be included to resolve common problems that appear at higher loop orders in dimensional regularization. This class of *evanescent operators* is the subject of several publications [74, 89, 90]. Their usage and computational necessity was stressed for the first time in ref. [82]. Their appearance is unique to dimensional regularization as they describe objects that vanish in the limit $d \to 4$.

An example where these operators may appear is given by the matrix element describing higher order corrections to an insertion of P_2, as shown in fig. 2.4:

$$\langle P_2\rangle^{\text{1-loop}} = a\,(\bar{s}\gamma^{\mu_1}\gamma^{\mu_2}\gamma^{\mu_3}P_L c)\,(\bar{c}\gamma_{\mu_1}\gamma_{\mu_2}\gamma_{\mu_3}P_L b) + \dots\,, \tag{2.20}$$

with s, b and c describing spinors. The coefficient a contains the remainder of the amplitude.

In four space-time dimensions we are able to reduce any string of Dirac matrices between spinors to a combination of 16 *bilinear covariants*:

$$\{\mathbb{1},\ \gamma^\mu,\ \sigma^{\mu\nu},\ \gamma_5,\ \gamma_5\gamma^\mu\}\,. \tag{2.21}$$

Equation (2.20) can hence be simplified to

$$\begin{aligned} (\bar{s}\gamma^{\mu_1}\gamma^{\mu_2}\gamma^{\mu_3}P_L c)\,(\bar{c}\gamma_{\mu_1}\gamma_{\mu_2}\gamma_{\mu_3}P_L b) &\overset{d=4}{=} 16\,(\bar{s}\gamma^\mu P_L c)\,(\bar{c}\gamma_\mu P_L b)\\ &= 16\,\langle P_2\rangle^{\text{tree}}\,. \end{aligned} \tag{2.22}$$

Since in $d = 4 - 2\epsilon$ the γ-matrices are infinite dimensional, the same also holds for the basis of bilinear covariants. Therefore, eq. (2.20) cannot be further reduced,

and we formally have to treat it as an additional operator of our d-dimensional Hamiltonian. This has the disadvantage that the operator basis is redundant in the limit $d \to 4$. Alternatively, one could start with the $d = 4$ operator basis and add an evanescent operator of the type:

$$E_2 = (\bar{s}\gamma^{\mu_1}\gamma^{\mu_2}\gamma^{\mu_3}P_L c)\left(\bar{c}\gamma_{\mu_1}\gamma_{\mu_2}\gamma_{\mu_3}P_L b\right) - 16\,(\bar{s}\gamma^{\mu}P_L c)\left(\bar{c}\gamma_{\mu}P_L b\right) . \tag{2.23}$$

Thus, the operator insertion of eq. (2.20) reduces to

$$\langle P_2\rangle^{\text{1-loop}} = a\left(16\,\langle P_2\rangle^{\text{tree}} + \langle E_2\rangle^{\text{tree}}\right) + \dots . \tag{2.24}$$

The comparison to eq. (2.22) implies

$$\langle E_2\rangle^{\text{tree}} = \mathcal{O}(\epsilon_{\text{UV}}) , \tag{2.25}$$

which we want to hold for renormalized matrix elements of evanescent operators to all orders in perturbation theory.

The definition of eq. (2.23) is by far not unique. With the restriction of eq. (2.25), one could as well add arbitrary $\mathcal{O}(\epsilon)$ terms without changing the physical outcome. Hence, the definition of the evanescent operators implies a specific renormalization scheme. Intermediate (non-physical) results from different schemes are not comparable without a proper scheme change [90].

Equation (2.25) introduces a dimensional parameter to regularize Ultraviolet (UV) divergences which is denoted by ϵ_{UV}. In general, also physical Infrared (IR) divergences appear which must be separated from UV poles in computations of the renormalization constants. However, in physical quantities where IR divergences are absent, the matrix elements of evanescent operators vanish again in the limit $\epsilon \to 0$.

As we have seen, the need for evanescent operators is tied to computations of higher loop order. Therefore, the operator basis has to grow accordingly with the given problem. This implies that also the renormalization of the physical operators has to be adjusted to the choice of evanescent operators. The renormalization conditions for Wilson coefficients in an extended definition of the Modified Minimal Subtraction ($\overline{\text{MS}}$) scheme are [91]:

- Renormalized amplitudes proportional to Wilson coefficients of physical operators have no UV poles, i.e. they start at $\mathcal{O}\left(\epsilon_{\text{UV}}^0\right)$. Renormalization constants which render these terms finite must contain only terms proportional to $1/\epsilon^n$ with $n \in \{1, \dots, l\}$, where l is the loop order.
- Renormalized amplitudes proportional to Wilson coefficients of evanescent operators are $\mathcal{O}(\epsilon_{\text{UV}})$. According renormalization constants must contain only terms proportional to $1/\epsilon^n$ with $n \in \{0, \dots, l-1\}$.

Unlike the regular $\overline{\text{MS}}$ scheme, the renormalization constants of evanescent operators include additional finite terms to fulfill eq. (2.25). More details are given in section 2.5.

In the CMM basis, we have to include the following evanescent operators for calculations up to $\mathcal{O}(\alpha_s)$ [75]:

$$\begin{aligned}
E_1^{q_1q_2,(1)} &= (\bar{s}\gamma^{\mu_1}\gamma^{\mu_2}\gamma^{\mu_3}P_L T^a q_2)\,(\overline{q_1}\gamma_{\mu_1}\gamma_{\mu_2}\gamma_{\mu_3}P_L T^a b) - 16P_1^{q_1q_2}\,,\\
E_2^{q_1q_2,(1)} &= (\bar{s}\gamma^{\mu_1}\gamma^{\mu_2}\gamma^{\mu_3}P_L q_2)\,(\overline{q_1}\gamma_{\mu_1}\gamma_{\mu_2}\gamma_{\mu_3}P_L b) - 16P_2^{q_1q_2}\,,\\
E_3^{(1)} &= (\bar{s}\gamma^{\mu_1}\gamma^{\mu_2}\gamma^{\mu_3}\gamma^{\mu_4}\gamma^{\mu_5}P_L b)\sum_q (\bar{q}\gamma_{\mu_1}\gamma_{\mu_2}\gamma_{\mu_3}\gamma_{\mu_4}\gamma_{\mu_5}P_L q)\\
&\quad - 20P_5 + 64P_3\,,\\
E_4^{(1)} &= (\bar{s}\gamma^{\mu_1}\gamma^{\mu_2}\gamma^{\mu_3}\gamma^{\mu_4}\gamma^{\mu_5}P_L T^a b)\sum_q (\bar{q}\gamma_{\mu_1}\gamma_{\mu_2}\gamma_{\mu_3}\gamma_{\mu_4}\gamma_{\mu_5}P_L T^a q)\\
&\quad - 20P_6 + 64P_4\,,
\end{aligned} \tag{2.26}$$

with $q_1, q_2 \in \{u, c\}$. If we want to compute contributions up to $\mathcal{O}(\alpha_s^2)$ additional evanescent operators are needed:

$$\begin{aligned}
E_1^{q_1q_2,(2)} &= (\bar{s}\gamma^{\mu_1}\gamma^{\mu_2}\gamma^{\mu_3}\gamma^{\mu_4}\gamma^{\mu_5}P_L T^a q_2)\,(\overline{q_1}\gamma_{\mu_1}\gamma_{\mu_2}\gamma_{\mu_3}\gamma_{\mu_4}\gamma_{\mu_5}P_L T^a b)\\
&\quad - 20E_1^{q_1q_2,(1)} - 256P_1^{q_1q_2}\,,\\
E_2^{q_1q_2,(2)} &= (\bar{s}\gamma^{\mu_1}\gamma^{\mu_2}\gamma^{\mu_3}\gamma^{\mu_4}\gamma^{\mu_5}P_L q_2)\,(\overline{q_1}\gamma_{\mu_1}\gamma_{\mu_2}\gamma_{\mu_3}\gamma_{\mu_4}\gamma_{\mu_5}P_L b)\\
&\quad - 20E_2^{q_1q_2,(1)} - 256P_2^{q_1q_2}\,,\\
E_3^{(2)} &= (\bar{s}\gamma^{\mu_1}\gamma^{\mu_2}\gamma^{\mu_3}\gamma^{\mu_4}\gamma^{\mu_5}\gamma^{\mu_6}\gamma^{\mu_7}P_L b)\\
&\quad \times\sum_q (\bar{q}\gamma_{\mu_1}\gamma_{\mu_2}\gamma_{\mu_3}\gamma_{\mu_4}\gamma_{\mu_5}\gamma_{\mu_6}\gamma_{\mu_7}P_L q) - 336P_5 + 1280P_3\,,\\
E_4^{(2)} &= (\bar{s}\gamma^{\mu_1}\gamma^{\mu_2}\gamma^{\mu_3}\gamma^{\mu_4}\gamma^{\mu_5}\gamma^{\mu_6}\gamma^{\mu_7}P_L T^a b)\\
&\quad \times\sum_q (\bar{q}\gamma_{\mu_1}\gamma_{\mu_2}\gamma_{\mu_3}\gamma_{\mu_4}\gamma_{\mu_5}\gamma_{\mu_6}\gamma_{\mu_7}P_L T^a q) - 336P_6 + 1280P_4\,.
\end{aligned} \tag{2.27}$$

Since each operator set is only necessary at a fixed order in perturbation theory, we denote eq. (2.26) as *first* and eq. (2.27) as *second generation* evanescent operators.

In the literature, there are different definitions of the evanescent operators in the traditional basis. However, their knowledge is necessary to transform results from the traditional to the CMM basis. In the context of computing Γ_{12}, two different sets were used. Both are given by a reduction prescription for Dirac matrix chains.

Reference [65] uses the basis of [92]. According to ref. [77] this leads to the following definition of evanescent operators:

$$\begin{aligned}
E_1^{q_1q_2} &= (\bar{s}_i\gamma^{\mu_1}\gamma^{\mu_2}\gamma^{\mu_3}P_L(q_2)_j)\,((\bar{q}_1)_j\gamma_{\mu_1}\gamma_{\mu_2}\gamma_{\mu_3}P_L b_i) - (16-4\epsilon)Q_1^{q_1q_2}\,,\\
E_2^{q_1q_2} &= (\bar{s}_i\gamma^{\mu_1}\gamma^{\mu_2}\gamma^{\mu_3}P_L(q_2)_i)\,((\bar{q}_1)_j\gamma_{\mu_1}\gamma_{\mu_2}\gamma_{\mu_3}P_L b_j) - (16-4\epsilon)Q_2^{q_1q_2}\,,\\
E_3 &= (\bar{s}_i\gamma^{\mu_1}\gamma^{\mu_2}\gamma^{\mu_3}P_L b_i)\sum_q \left(\bar{q}_j\gamma_{\mu_1}\gamma_{\mu_2}\gamma_{\mu_3}P_L q_j\right) - (16-4\epsilon)Q_3\,,\\
E_4 &= (\bar{s}_i\gamma^{\mu_1}\gamma^{\mu_2}\gamma^{\mu_3}P_L b_j)\sum_q \left(\bar{q}_j\gamma_{\mu_1}\gamma_{\mu_2}\gamma_{\mu_3}P_L q_i\right) - (16-4\epsilon)Q_4\,,\\
E_5 &= (\bar{s}_i\gamma^{\mu_1}\gamma^{\mu_2}\gamma^{\mu_3}P_L b_i)\sum_q \left(\bar{q}_j\gamma_{\mu_1}\gamma_{\mu_2}\gamma_{\mu_3}P_R q_j\right) - (4+4\epsilon)Q_5\,,\\
E_6 &= (\bar{s}_i\gamma^{\mu_1}\gamma^{\mu_2}\gamma^{\mu_3}P_L b_j)\sum_q \left(\bar{q}_j\gamma_{\mu_1}\gamma_{\mu_2}\gamma_{\mu_3}P_R q_i\right) - (4+4\epsilon)Q_6\,.
\end{aligned} \tag{2.28}$$

The other basis used in the literature [68, 69] is defined with an implicit change of the operators analogous to the current-current ones:

$$\begin{aligned} E_1'^{q_1q_2} &= \left(\bar{s}_i\gamma^{\mu_1}\gamma^{\mu_2}\gamma^{\mu_3}P_L(q_2)_j\right)\left((\bar{q}_1)_j\gamma_{\mu_1}\gamma_{\mu_2}\gamma_{\mu_3}P_Lb_i\right) \\ &\quad -(16-4\epsilon-4\epsilon^2)Q_1^{q_1q_2}\,, \\ E_2'^{q_1q_2} &= \left(\bar{s}_i\gamma^{\mu_1}\gamma^{\mu_2}\gamma^{\mu_3}P_L(q_2)_i\right)\left((\bar{q}_1)_j\gamma_{\mu_1}\gamma_{\mu_2}\gamma_{\mu_3}P_Lb_j\right) \\ &\quad -(16-4\epsilon-4\epsilon^2)Q_2^{q_1q_2}\,, \end{aligned} \tag{2.29}$$

with the remaining operators equal to eq. (2.28).

Since both bases use different evanescent operators also the used renormalization schemes change. Thus, a comparison of results stemming from either basis needs a proper transformation. However, the difference between them is $\mathcal{O}(\epsilon^2)$, leading to different results at NNLO. Since in [65] only Next-to-Leading Order (NLO) contributions were computed, the same transformation rules can be used for both results.

2.5 RENORMALIZATION

With renormalization, it is possible to render formally UV-divergent quantities UV-finite in quantum field theory. As we have seen in section 2.4, evanescent operators require a special treatment such that $\mathcal{O}(\epsilon)$ terms do not contribute in four space-time dimensions. In this section we will analyze the renormalization of the effective $\Delta B = 1$ field theory in more detail. The definitions and notation follow refs. [21, 73] except for the gauge definition.

Renormalization can be understood as identifying the parameters and fields of the Lagrangian as *bare*. To get access to the physical parameters one has to shift the bare ones by intrinsically divergent values.

The QCD Lagrangian is given by

$$\begin{aligned} \mathcal{L}^{\text{QCD}} &= \overline{\psi}\left(i\not{D}-m\right)\psi - \frac{1}{4}G^a_{\mu\nu}G^{a,\mu\nu} - \frac{1}{2(1-\xi)}\left(\partial^\mu G^a_\mu\right)^2 \\ &\quad + \left(\partial^\mu\overline{c}^a\right)\left(\delta^{ab}\partial_\mu + g_s f^{abc}G^b_\mu\right)c^c\,, \end{aligned} \tag{2.30}$$

where D_μ denotes the covariant derivative which is given by

$$D_\mu = \partial_\mu - ig_sG^a_\mu T^a\,. \tag{2.31}$$

In eq. (2.30), we include the Fadeev-Popov ghost field c and gauge fixing parameter ξ in the so-called R_ξ gauge with $\xi = 0$ corresponding to the Feynman-'t Hooft gauge. For the renormalization procedure the Lagrangian is expressed in terms of

$$\begin{aligned} \psi^0 &= \sqrt{Z_2}\psi\,, & m_i^0 &= Z_{m_i}m_i\,, \\ g_s^0 &= \mu^\epsilon Z_{g_s}g_s = \mu^\epsilon\sqrt{Z_{\alpha_s}}g_s\,, & (1-\xi^0) &= Z_3(1-\xi)\,, \\ G^{a,0}_\mu &= \sqrt{Z_3}G^a_\mu\,, & c^{a,0} &= \sqrt{\widetilde{Z}_3}c^a\,, \end{aligned} \tag{2.32}$$

where μ is called *renormalization scale* or *'t Hooft mass*. The renormalization constants Z_i are given by an expansion in α_s and depend on the chosen renormalization scheme. The structure is hence

$$Z_i \;=\; \sum_{j=0}^{\infty} \sum_{k=-\infty}^{j} \left(\frac{\alpha_s}{4\pi}\right)^j \frac{1}{\epsilon^k} Z_i^{(j,k)} \,. \tag{2.33}$$

In the $\overline{\text{MS}}$ scheme, the Z_i are defined such that they remove only poles of the type

$$\frac{1}{\widetilde{\epsilon}} \;\equiv\; \frac{1}{\epsilon} - \gamma_E + \ln(4\pi)\,, \tag{2.34}$$

in which γ_E is the *Euler–Mascheroni constant*. We therefore have $Z_i^{(j,k\leq 0)} = \delta_{j,0}$.

In effective field theories where the effective operators mix under renormalization, additional renormalization constants are needed to obtain finite quantities. In the following we exemplify this mixing for a sample set of operators $\{\mathcal{O}_i\}$ of the form $(\overline{\psi}\Gamma\psi)(\overline{\phi}\Gamma'\phi)$. The bare amplitude of the process $\psi\overline{\psi} \to \phi\overline{\phi}$ is given by

$$\mathcal{A} \;=\; C_i^0 \,\langle \mathcal{O}_i^0(\psi^0, \phi^0)\rangle \,. \tag{2.35}$$

With the renormalization of the fields and parameters of eq. (2.32) alone, this amplitude will in general remain UV divergent. We have two possibilities to include the additional renormalization. One way is to renormalize the Green's functions themselves. The renormalized amplitude is then given by

$$\mathcal{A} \;=\; C_i \,\langle \mathcal{O}_i(\psi,\phi)\rangle \;=\; Z_{2,\psi} Z_{2,\phi} C_i \widetilde{Z}_{ij}^{-1} \,\langle \mathcal{O}_j^0(\psi,\phi)\rangle \,. \tag{2.36}$$

The *renormalization matrix* $\widetilde{Z}_{ij}$ takes into account that effective operators are not distinct at higher order corrections. Therefore, the whole set of operators is necessary for renormalization. Here we use the fact that the operator basis is closed under renormalization, i.e. the operators in the sums of eqs. (2.35) and (2.36) are sufficient to obtain a UV-finite amplitude.

Another way to renormalize eq. (2.35) is through the Wilson coefficients. Similarly, we get

$$\mathcal{A} \;=\; Z_{2,\psi} Z_{2,\phi} C_j Z_{ji} \,\langle \mathcal{O}_i^0(\psi,\phi)\rangle \,. \tag{2.37}$$

Both ways are equivalent in describing the poles occurring in higher order computations. Since they must lead to the same finite results, we can summarize our finding as

$$C_i^0 \;=\; C_j Z_{ji}\,, \quad \mathcal{O}_i^0 \;=\; \widetilde{Z}_{ij}\mathcal{O}_j \qquad \text{with} \quad Z \;=\; \widetilde{Z}^{-1}\,. \tag{2.38}$$

To account for both evanescent (E_i) and physical operators (Q_i), the matrix $\widetilde{Z}$ can be written as

$$\begin{pmatrix} \vec{Q}^0 \\ \vec{E}^0 \end{pmatrix} = \begin{pmatrix} \widetilde{Z}_{QQ} & \widetilde{Z}_{QE} \\ \widetilde{Z}_{EQ} & \widetilde{Z}_{EE} \end{pmatrix} \begin{pmatrix} \vec{Q} \\ \vec{E} \end{pmatrix} . \tag{2.39}$$

As stated in section 2.4, the evanescent operators are needed to close the renormalization of the physical operators. For the adjusted $\overline{\text{MS}}$ renormalization conditions, we parameterize the renormalization matrices as

$$\begin{aligned}
\widetilde{Z}_{QQ} &= \mathbb{1} + \sum_{j=1}^{l} \sum_{k=1}^{j} \left(\frac{\alpha_s}{4\pi}\right)^j \frac{1}{\epsilon^k} \widetilde{Z}_{QQ}^{(j,k)} , \\
\widetilde{Z}_{QE} &= \sum_{j=1}^{l} \sum_{k=1}^{j} \left(\frac{\alpha_s}{4\pi}\right)^j \frac{1}{\epsilon^k} \widetilde{Z}_{QE}^{(j,k)} , \\
\widetilde{Z}_{EQ} &= \sum_{j=1}^{l} \sum_{k=0}^{j-1} \left(\frac{\alpha_s}{4\pi}\right)^j \frac{1}{\epsilon^k} \widetilde{Z}_{EQ}^{(j,k)} , \\
\widetilde{Z}_{EE} &= \mathbb{1} + \sum_{j=1}^{l} \sum_{k=1}^{j} \left(\frac{\alpha_s}{4\pi}\right)^j \frac{1}{\epsilon^k} \widetilde{Z}_{EE}^{(j,k)} .
\end{aligned} \tag{2.40}$$

In order to renormalize the physical operators at l-loop order, we have to include l generations of evanescent operators. To render evanescent operator insertions to be $\mathcal{O}(\epsilon)$, we need a finite renormalization proportional to the physical operators and other evanescent operators. Therefore, the matrix $\widetilde{Z}$ is only sufficient for a fixed order in l and must be extended accordingly when higher order corrections are taken into account. Remarkable is that $\widetilde{Z}_{EQ}$ and $\widetilde{Z}_{EE}$ are not sufficient to renormalize *all* evanescent operators to order l. This follows from the fact that for the renormalization of a certain generation, evanescent operators of a higher generation are needed.

To illustrate the statements above, we consider a physical operator insertion at one-loop order, as shown in fig. 2.4i:

$$\langle Q \rangle^{\text{1-loop}} = a_i \langle Q_i \rangle^{\text{tree}} + b_i \langle E_i^{(1)} \rangle^{\text{tree}} , \tag{2.41}$$

where the coefficients a_i and b_i contain UV-poles and finite contributions. Obviously, renormalization constants $\widetilde{Z}_{QE}$ which are proportional to the first generation evanescent operators are needed to obtain a UV-finite result. Turning to the insertion of an evanescent operator at NLO, we have

$$\langle E^{(1)} \rangle^{\text{1-loop}} = c_i \langle Q_i \rangle^{\text{tree}} + d_i \langle E_i^{(1)} \rangle^{\text{tree}} + e_i \langle E_i^{(2)} \rangle^{\text{tree}} . \tag{2.42}$$

To renormalize this quantity, we have to extend our Lagrangian by second generation evanescent operators. In turn, to compute the regarded process to full extent, we now have to consider $\langle E^{(2)} \rangle^{\text{1-loop}}$ as well. Hence, we have to formally include an infinite amount of evanescent operators. This is a direct consequence of the infinite-dimensional Dirac matrices in d dimensions.

Nevertheless, it is possible to formulate a closed renormalization group which is only valid up to a specific order in perturbation theory. Thus, matrix elements are only computable for insertions of n^{th} generation evanescent operators up to $\mathcal{O}(\alpha_s^i)$, with $n + i \leq l$. The upper bound l is the number of the highest generation which has to be taken into account at least at LO. Physical operators are treated in this context as zeroth generation.

Therefore, to compute an operator insertion to e.g. $\mathcal{O}(\alpha_s^2)$, we have to take evanescent operators of first and second generation into account. But only the matrix elements $\langle Q\rangle^{\text{tree}}$, $\langle Q\rangle^{\text{1-loop}}$, $\langle Q\rangle^{\text{2-loop}}$, $\langle E^{(1)}\rangle^{\text{tree}}$, $\langle E^{(1)}\rangle^{\text{1-loop}}$ and $\langle E^{(2)}\rangle^{\text{tree}}$ can be renormalized.

The renormalization matrix for the CMM basis is shown in appendix A.

2.6 BASIS TRANSFORMATION

Since the operator bases of sections 2.2 and 2.3 describe the same SM processes, it is possible to transform them into each other. We follow here the description of refs. [77, 93] for the NNLO basis transformation. In the following, objects defined in different bases are distinguished by primes.

In a first step, we describe a shift of the physical operators by a linear combination of evanescent ones, i.e.

$$\vec{Q}' \;=\; \vec{Q} + W\vec{E}\,, \qquad \vec{E}' \;=\; \vec{E}\,. \tag{2.43}$$

Then, the evanescent operators are shifted by a term which is proportional to the physical operators with the matrix U. To render this sum evanescent again, the physical term is multiplied by ϵ. Afterwards, a linear transformation of both operator classes using the matrices R and M is applied. Ref. [77] finds

$$\begin{aligned} \vec{Q}'' \;&=\; R\vec{Q}' \;=\; R\left(\vec{Q} + W\vec{E}\right)\,, \\ \vec{E}'' \;&=\; M\left(\vec{E}' + \epsilon U\vec{Q}'\right) \;=\; M\left[(\mathbb{1} + \epsilon UW)\vec{E} + \epsilon U\vec{Q}\right]\,. \end{aligned} \tag{2.44}$$

According to ref. [77] this transformation leads to a finite renormalization of physical operators in the new basis. At NLO the transition between Wilson coefficients is given by

$$\vec{C}''(\mu) \;=\; \left[\mathbb{1} + \frac{\alpha_s(\mu)}{4\pi} Z_{QQ}^{''(1,0)}\right]^T \left(R^{-1}\right)^T \vec{C}(\mu)\,, \tag{2.45}$$

with

$$Z_{QQ}^{''(1,0)} \;=\; R\left[WZ_{EQ}^{(1,0)} - \left(Z_{QE}^{(1,1)} + WZ_{EE}^{(1,1)} - \frac{1}{2}\gamma_0 W\right) U\right] R^{-1}\,, \tag{2.46}$$

whereγ_0 is the LO term of the Anomalous Dimension Matrix (ADM) in the unprimed basis.

For the change from the CMM to the traditional basis of eqs. (2.9) and (2.28), the finite renormalization matrix is given by

$$Z_{QQ}^{''(1,0)} \;=\; \begin{pmatrix} -\frac{7}{3} & -1 & 0 & 0 & 0 & 0 \\ -2 & \frac{2}{3} & 0 & 0 & 0 & 0 \\ 0 & 0 & \frac{178}{27} & -\frac{34}{9} & -\frac{164}{27} & \frac{20}{9} \\ 0 & 0 & 1-\frac{n_f}{9} & \frac{n_f}{3}-\frac{25}{3} & -\frac{n_f}{9}-2 & \frac{n_f}{3}+6 \\ 0 & 0 & -\frac{160}{27} & \frac{16}{9} & \frac{146}{27} & -\frac{2}{9} \\ 0 & 0 & \frac{n_f}{9}-2 & 6-\frac{n_f}{3} & \frac{n_f}{9}+3 & -\frac{n_f}{3}-\frac{11}{3} \end{pmatrix}\,, \tag{2.47}$$

where $n_f = 5$ is the number of active flavors. In eq. (2.47) we use the fact that only two Wilson coefficients of the current-current operators are distinct.

Together with the rotation matrix

$$R = \begin{pmatrix} 2 & \frac{1}{3} & 0 & 0 & 0 & 0 \\ 0 & 1 & 0 & 0 & 0 & 0 \\ 0 & 0 & -\frac{1}{3} & 0 & \frac{1}{12} & 0 \\ 0 & 0 & -\frac{1}{9} & -\frac{2}{3} & \frac{1}{36} & \frac{1}{6} \\ 0 & 0 & \frac{4}{3} & 0 & -\frac{1}{12} & 0 \\ 0 & 0 & \frac{4}{9} & \frac{8}{3} & -\frac{1}{36} & -\frac{1}{6} \end{pmatrix}, \tag{2.48}$$

we can write the CMM Wilson coefficients to up to $\mathcal{O}(\alpha_s)$ as

$$\begin{aligned}
C_{P_1} &= 2C_{Q_1} + \left(\frac{\alpha_s}{4\pi}\right)\left(\frac{14C_{Q_1}}{3} + 4C_{Q_2}\right), \\
C_{P_2} &= \frac{C_{Q_1}}{3} + C_{Q_2} + \left(\frac{\alpha_s}{4\pi}\right)\frac{16C_{Q_1}}{9}, \\
C_{P_3} &= -\frac{C_{Q_3}}{3} - \frac{C_{Q_4}}{9} + \frac{4C_{Q_5}}{3} + \frac{4C_{Q_6}}{9} \\
&\quad + \left(\frac{\alpha_s}{4\pi}\right)\left(\frac{80C_{Q_3}}{9} - \frac{16C_{Q_4}}{27} - \frac{80C_{Q_5}}{9} - \frac{64C_{Q_6}}{27}\right), \\
C_{P_4} &= -\frac{2C_{Q_4}}{3} + \frac{8C_{Q_6}}{3} + \left(\frac{\alpha_s}{4\pi}\right)\left(-\frac{76C_{Q_3}}{9} - \frac{194C_{Q_4}}{9}\right. \\
&\quad \left. + \frac{16C_{Q_5}}{9} + \frac{124C_{Q_6}}{9} - \frac{2C_{Q_4}n_f}{3} + \frac{2C_{Q_6}n_f}{3}\right), \\
C_{P_5} &= \frac{C_{Q_3}}{12} + \frac{C_{Q_4}}{36} - \frac{C_{Q_5}}{12} - \frac{C_{Q_6}}{36} \\
&\quad + \left(\frac{\alpha_s}{4\pi}\right)\left(-\frac{8C_{Q_3}}{9} + \frac{4C_{Q_4}}{27} + \frac{8C_{Q_5}}{9} + \frac{4C_{Q_6}}{27}\right), \\
C_{P_6} &= \frac{C_{Q_4}}{6} - \frac{C_{Q_6}}{6} + \left(\frac{\alpha_s}{4\pi}\right)\left(C_{Q_3} + \frac{43C_{Q_4}}{18} - \frac{C_{Q_5}}{3} - \frac{29C_{Q_6}}{18}\right).
\end{aligned} \tag{2.49}$$

In order to compare NNLO results of refs. [68, 69], $\mathcal{O}(\epsilon^2)$ terms of evanescent operators have to be taken into account as well. It turns out that the evanescent operators of eqs. (2.28) and (2.29) alone are not sufficient for a full calculation at NNLO. Together with the formulae of ref. [93] we can only state $\mathcal{O}(\alpha_s^2)$ corrections to current-current coefficients which are proportional to the number of active flavors n_f:

$$\begin{aligned}
C_{P_1} &= 2C_{Q_1} + \left(\frac{\alpha_s}{4\pi}\right)\left(\frac{14C_{Q_1}}{3} + 4C_{Q_2}\right) \\
&\quad + \left(\frac{\alpha_s}{4\pi}\right)^2\left[n_f\left(\frac{35C_{Q_1}}{27} + \frac{10C_{Q_2}}{9}\right) + \text{non-}n_f\right], \\
C_{P_2} &= \frac{C_{Q_1}}{3} + C_{Q_2} + \left(\frac{\alpha_s}{4\pi}\right)\frac{16C_{Q_1}}{9} \\
&\quad + \left(\frac{\alpha_s}{4\pi}\right)^2\left[n_f\frac{40C_{Q_1}}{81} + \text{non-}n_f\right].
\end{aligned} \tag{2.50}$$

Nevertheless, this partial transformation is sufficient to compare the NNLO results of refs. [68, 69] which include only n_f dependent terms.

3

ΔB=2 THEORY

In the previous chapter we discussed interactions in the effective $\Delta B = 1$ theory. The only missing piece in the Hamiltonian of eq. (1.37) are the $\Delta B = 2$ interactions. With them, we have everything at hand to compute Γ_{12} in the matching between both theories.

3.1 OPERATOR BASIS

Similar to $\Delta B = 1$ there are several approaches to define a $\Delta B = 2$ operator basis. For lattice computations the so-called *supersymmetric basis* of refs. [94–96] has been established [40]. It includes five dimension-6 operators of which three are not present in the SM.

Furthermore, bases like in refs. [97–100] focus more on SM phenomenology and the application for higher order calculations. This includes the definition and proper treatment of evanescent operators.

We have already seen in section 1.2 that to describe the leading effects of M_{12} only a single effective $\Delta B = 2$ operator Q is needed. For the purpose of computing Γ_{12}, we start with six operators in the leading order of the Λ/m_b expansion: [100]

$$\begin{aligned}
Q &= 4\,(\bar{s}_i\gamma^\mu P_L b_i)\,(\bar{s}_j\gamma_\mu P_L b_j)\,, \\
\widetilde{Q} &= 4\,(\bar{s}_i\gamma^\mu P_L b_j)\,(\bar{s}_j\gamma_\mu P_L b_i)\,, \\
Q_S &= 4\,(\bar{s}_i P_R b_i)\,(\bar{s}_j P_R b_j)\,, \\
\widetilde{Q}_S &= 4\,(\bar{s}_i P_R b_j)\,(\bar{s}_j P_R b_i)\,, \\
Q_T &= 4\,(\bar{s}_i\sigma^{\mu\nu} P_R b_i)\,(\bar{s}_j\sigma_{\mu\nu} P_R b_j)\,, \\
\widetilde{Q}_T &= 4\,(\bar{s}_i\sigma^{\mu\nu} P_R b_j)\,(\bar{s}_j\sigma_{\mu\nu} P_R b_i)\,.
\end{aligned} \tag{3.1}$$

This basis is redundant in four dimensions since some operators are related according to the so-called *Fierz symmetry* [101]. This symmetry makes use of the finiteness of the bilinear covariant basis in $d = 4$ to find relations between spinor tensor structures with Dirac matrices. A simple way to find these identities is described in appendix B.

In $d = 4$ we find

$$\widetilde{Q} = Q\,, \tag{3.2a}$$

$$Q_T = -4Q_S - 8\widetilde{Q}_S\,, \tag{3.2b}$$

$$\widetilde{Q}_T = -4\widetilde{Q}_S - 8Q_S\,. \tag{3.2c}$$

In addition to the remaining three operators, we extend the effective Hamiltonian to include also terms of the next-to-leading order in Λ/m_b. The d-dimensional $\Delta B = 2$ Hamiltonian is then given by

$$\mathcal{H}^{\Delta B=2} = \frac{G_F^2 m_b^2}{12\pi^2}\left[C_Q Q + C_{Q_S} Q_S + C_{\widetilde{Q}_S}\widetilde{Q}_S + \sum_i C_{E_i} E_i\right] + \mathcal{H}^{\Delta B=2}_{1/m_b} + \text{h.c.}\,. \tag{3.3}$$

This definition is different from the one in eq. (1.38), where no Λ/m_b expansion is applied. The operators of the eq. (3.3) is what we need to express the HQE of Γ_{12} as shown in eq. (1.47).

The Hamiltonian $\mathcal{H}^{\Delta B=2}_{1/m_b}$ includes 10 physical operators which are given by [63]

$$R_0 = \frac{1}{2}Q + Q_S + \widetilde{Q}_S\,, \tag{3.4a}$$
$$\widetilde{R}_0 = \frac{1}{2}\widetilde{Q} + Q_S + \widetilde{Q}_S\,, \tag{3.4b}$$
$$R_1 = 4\frac{m_s}{m_b}\left(\bar{s}_i P_R b_i\right)\left(\bar{s}_j P_L b_j\right)\,, \tag{3.4c}$$
$$\widetilde{R}_1 = 4\frac{m_s}{m_b}\left(\bar{s}_i P_R b_j\right)\left(\bar{s}_j P_L b_i\right)\,, \tag{3.4d}$$
$$R_2 = \frac{4}{m_b^2}\left(\bar{s}_i \overleftarrow{D}^\rho \gamma^\mu P_L D_\rho b_i\right)\left(\bar{s}_j \gamma_\mu P_L b_j\right)\,, \tag{3.4e}$$
$$\widetilde{R}_2 = \frac{4}{m_b^2}\left(\bar{s}_i \overleftarrow{D}^\rho \gamma^\mu P_L D_\rho b_j\right)\left(\bar{s}_j \gamma_\mu P_L b_i\right)\,, \tag{3.4f}$$
$$R_3 = \frac{4}{m_b^2}\left(\bar{s}_i \overleftarrow{D}^\rho P_R D_\rho b_i\right)\left(\bar{s}_j P_R b_j\right)\,, \tag{3.4g}$$
$$\widetilde{R}_3 = \frac{4}{m_b^2}\left(\bar{s}_i \overleftarrow{D}^\rho P_R D_\rho b_j\right)\left(\bar{s}_j P_R b_i\right)\,, \tag{3.4h}$$
$$R_4 = \frac{4}{m_b}\left(\bar{s}_i i\overleftarrow{D}^\rho P_R b_i\right)\left(\bar{s}_j \gamma_\mu P_L b_j\right)\,, \tag{3.4i}$$
$$\widetilde{R}_4 = \frac{4}{m_b}\left(\bar{s}_i i\overleftarrow{D}^\rho P_R b_j\right)\left(\bar{s}_j \gamma_\mu P_L b_i\right)\,. \tag{3.4j}$$

The covariant derivative D^μ is defined in eq. (2.31). Note that all operators of eq. (3.4) are sensitive to the kinematics of the s-quark.

It is again possible to find linear relations between different operators using equations of motions, Fierz identities and by dropping terms of higher order in the Λ/m_b expansion. This results in

$$\widetilde{R}_0 = R_0\,, \tag{3.5a}$$
$$\widetilde{R}_2 = -R_2\,, \tag{3.5b}$$
$$\widetilde{R}_3 = R_3 + \frac{R_2}{2}\,, \tag{3.5c}$$
$$R_4 = \frac{R_0}{2} - \widetilde{R}_1 + \frac{R_2}{2}\,, \tag{3.5d}$$
$$\widetilde{R}_4 = \frac{R_0}{2} - R_1 - \frac{R_2}{2}\,. \tag{3.5e}$$

In the literature these relations are used to remove $\widetilde{R}_0, R_4$ and $\widetilde{R}_4$ from the operator basis. All others are kept and used for the matching of $\Delta B = 1$ contributions.

From eq. (3.4) we see that a linear combination of Q, Q_S and $\widetilde{Q}_S$ is suppressed by Λ/m_b. The proof and the technical implications are presented in appendix C and section 3.5. Another important aspect of the effective $\Delta B = 2$ theory is the treatment of evanescent terms which is the topic of the next section.

3.2 EVANESCENT OPERATORS

In section 2.4 we included a new class of operators to the effective $\Delta B = 1$ theory to resolve emerging difficulties when extending the effective operator basis to d dimensions. Also, for the $\Delta B = 2$ theory we have to introduce evanescent operators to get a well-defined regularization and renormalization procedure. We have seen in eq. (3.2) that four-dimensional Fierz identities can be used to reduce the number of physical operators in the Hamiltonian. In dimensional regularization these relations receive $\mathcal{O}(\epsilon)$ corrections which must not be neglected. We define the first generation of evanescent operators as

$$E_1^{(1)} = \widetilde{Q} - Q\,, \tag{3.6a}$$

$$E_2^{(1)} = 4\left(\bar{s}_i\gamma^{\mu_1}\gamma^{\mu_2}\gamma^{\mu_3}P_L b_j\right)\left(\bar{s}_j\gamma_{\mu_1}\gamma_{\mu_2}\gamma_{\mu_3}P_L b_i\right) - (16 + e_{2,1}^{(1)}\epsilon + e_{2,2}^{(1)}\epsilon^2)\widetilde{Q}\,, \tag{3.6b}$$

$$E_3^{(1)} = 4\left(\bar{s}_i\gamma^{\mu_1}\gamma^{\mu_2}\gamma^{\mu_3}P_L b_i\right)\left(\bar{s}_j\gamma_{\mu_1}\gamma_{\mu_2}\gamma_{\mu_3}P_L b_j\right) - (16 + e_{3,1}^{(1)}\epsilon + e_{3,2}^{(1)}\epsilon^2)Q\,, \tag{3.6c}$$

$$E_4^{(1)} = 4\left(\bar{s}_i\gamma^{\mu_1}\gamma^{\mu_2}P_R b_j\right)\left(\bar{s}_j\gamma_{\mu_1}\gamma_{\mu_2}P_R b_i\right) - (-8 + e_{4,2,1}^{(1)}\epsilon + e_{4,2,2}^{(1)}\epsilon^2)Q_S - (e_{4,1,1}^{(1)}\epsilon + e_{4,1,2}^{(1)}\epsilon^2)\widetilde{Q}_S\,, \tag{3.6d}$$

$$E_5^{(1)} = 4\left(\bar{s}_i\gamma^{\mu_1}\gamma^{\mu_2}P_R b_i\right)\left(\bar{s}_j\gamma_{\mu_1}\gamma_{\mu_2}P_R b_j\right) - (-8 + e_{5,1,1}^{(1)}\epsilon + e_{5,1,2}^{(1)}\epsilon^2)\widetilde{Q}_S - (e_{5,2,1}^{(1)}\epsilon + e_{5,2,2}^{(1)}\epsilon^2)Q_S\,. \tag{3.6e}$$

Equation (3.6) is necessary to renormalize the physical operators at $\mathcal{O}(\alpha_s)$. The leading order matrix elements of these operators can be used to relate spinor tensor structures with up to three Dirac matrices to the reduced four-dimensional equivalent. Such terms arise from physical operator contributions at one-loop order. Additionally, the operator $E_1^{(1)}$ expresses the Fierz symmetry between Q and $\tilde{Q}$ which holds in four dimensions.

The parameters $e_x^{(i)}$ of eq. (3.6) denote alternative evanescent contributions of order ϵ and beyond. They express the arbitrariness in the choice of the evanescent operators. Physical observables must not dependent on them [90]. The latter condition would provide a consistency check for phenomenological results. In our case the $e_x^{(i)}$ are kept unspecified throughout the calculation. This dependence is expected to cancel in the lattice-continuum matching if the matrix elements are calculated in lattice QCD. Hence, this check is beyond the scope of this work.

According to refs. [49, 65, 68, 90] a certain numerical choice for the $e_x^{(i)}$ parameters preserves Fierz symmetry in d dimensions. It is given by

$$\begin{aligned}
e^{(1)}_{2,1} &= e^{(1)}_{3,1} = -4\,,\\
e^{(1)}_{2,2} &= e^{(1)}_{3,2} = -4\,,\\
e^{(1)}_{4,2,1} &= e^{(1)}_{5,1,1} = 8\,,\\
e^{(1)}_{4,1,1} &= e^{(1)}_{5,2,1} = 0\,,\\
e^{(1)}_{4,1,2} &= e^{(1)}_{5,2,2} = 4\,,\\
e^{(1)}_{4,2,2} &= e^{(1)}_{5,1,2} = 0\,.
\end{aligned} \tag{3.7}$$

As we see in chapter 4, three more generations are needed for the calculation of Γ_{12} in addition to the evanescent operators of eq. (3.6). For the renormalization of the physical operators at two-loops and for the first generation at one-loop we introduce the following:

$$\begin{aligned}
E^{(2)}_1 &= 4\left(\bar{s}_i\gamma^{\mu_1}\dots\gamma^{\mu_5}P_L b_j\right)\left(\bar{s}_j\gamma_{\mu_1}\dots\gamma_{\mu_5}P_L b_i\right)\\
&\quad -(256+e^{(2)}_{1,1}\epsilon+e^{(2)}_{1,2}\epsilon^2)\widetilde{Q}\,,
\end{aligned} \tag{3.8a}$$

$$\begin{aligned}
E^{(2)}_2 &= 4\left(\bar{s}_i\gamma^{\mu_1}\dots\gamma^{\mu_5}P_L b_i\right)\left(\bar{s}_j\gamma_{\mu_1}\dots\gamma_{\mu_5}P_L b_j\right)\\
&\quad -(256+e^{(2)}_{2,1}\epsilon+e^{(2)}_{2,2}\epsilon^2)Q\,,
\end{aligned} \tag{3.8b}$$

$$\begin{aligned}
E^{(2)}_3 &= 4\left(\bar{s}_i\gamma^{\mu_1}\dots\gamma^{\mu_4}P_R b_i\right)\left(\bar{s}_j\gamma_{\mu_1}\dots\gamma_{\mu_4}P_R b_j\right)\\
&\quad -(128+e^{(2)}_{3,1,1}\epsilon+e^{(2)}_{3,1,2}\epsilon^2)\widetilde{Q}_S-(128+e^{(2)}_{3,2,1}\epsilon+e^{(2)}_{3,2,2}\epsilon^2)Q_S\,,
\end{aligned} \tag{3.8c}$$

$$\begin{aligned}
E^{(2)}_4 &= 4\left(\bar{s}_i\gamma^{\mu_1}\dots\gamma^{\mu_4}P_R b_j\right)\left(\bar{s}_j\gamma_{\mu_1}\dots\gamma_{\mu_4}P_R b_i\right)\\
&\quad -(128+e^{(2)}_{4,1,1}\epsilon+e^{(2)}_{4,1,2}\epsilon^2)\widetilde{Q}_S-(128+e^{(2)}_{4,2,1}\epsilon+e^{(2)}_{4,2,2}\epsilon^2)Q_S\,.
\end{aligned} \tag{3.8d}$$

For the renormalization of the first generation evanescent operators at two-loops and for the second generation at one-loop we also need a third generation. It is given by

$$\begin{aligned}
E^{(3)}_1 &= 4\left(\bar{s}_i\gamma^{\mu_1}\dots\gamma^{\mu_7}P_L b_j\right)\left(\bar{s}_j\gamma_{\mu_1}\dots\gamma_{\mu_7}P_L b_i\right)\\
&\quad -(4096+e^{(3)}_{1,1}\epsilon+e^{(3)}_{1,2}\epsilon^2)\widetilde{Q}\,,
\end{aligned} \tag{3.9a}$$

$$\begin{aligned}
E^{(3)}_2 &= 4\left(\bar{s}_i\gamma^{\mu_1}\dots\gamma^{\mu_7}P_L b_i\right)\left(\bar{s}_j\gamma_{\mu_1}\dots\gamma_{\mu_7}P_L b_j\right)\\
&\quad -(4096+e^{(3)}_{2,1}\epsilon+e^{(3)}_{2,2}\epsilon^2)Q\,,
\end{aligned} \tag{3.9b}$$

$$\begin{aligned}
E^{(3)}_3 &= 4\left(\bar{s}_i\gamma^{\mu_1}\dots\gamma^{\mu_6}P_R b_i\right)\left(\bar{s}_j\gamma_{\mu_1}\dots\gamma_{\mu_6}P_R b_j\right)\\
&\quad -(2048+e^{(3)}_{3,1,1}\epsilon+e^{(3)}_{3,1,2}\epsilon^2)\widetilde{Q}_S-(2048+e^{(3)}_{3,2,1}\epsilon+e^{(3)}_{3,2,2}\epsilon^2)Q_S\,,
\end{aligned} \tag{3.9c}$$

$$\begin{aligned}
E^{(3)}_4 &= 4\left(\bar{s}_i\gamma^{\mu_1}\dots\gamma^{\mu_6}P_R b_j\right)\left(\bar{s}_j\gamma_{\mu_1}\dots\gamma_{\mu_6}P_R b_i\right)\\
&\quad -(2048+e^{(3)}_{4,1,1}\epsilon+e^{(3)}_{4,1,2}\epsilon^2)\widetilde{Q}_S-(2048+e^{(3)}_{4,2,1}\epsilon+e^{(3)}_{4,2,2}\epsilon^2)Q_S\,.
\end{aligned} \tag{3.9d}$$

Finally, the fourth generation with up to nine Dirac matrices in one bilinear factor is given by

$$\begin{aligned}
E^{(4)}_1 &= 4\left(\bar{s}_i\gamma^{\mu_1}\dots\gamma^{\mu_9}P_L b_j\right)\left(\bar{s}_j\gamma_{\mu_1}\dots\gamma_{\mu_9}P_L b_i\right)\\
&\quad -(65536+e^{(4)}_{1,1}\epsilon+e^{(4)}_{1,2}\epsilon^2)\widetilde{Q}\,,
\end{aligned} \tag{3.10a}$$

$$
\begin{aligned}
E_2^{(4)} &= 4\,(\bar{s}_i\gamma^{\mu_1}\dots\gamma^{\mu_9}P_L b_i)\,(\bar{s}_j\gamma_{\mu_1}\dots\gamma_{\mu_9}P_L b_j) \\
&\quad - (65536 + e_{2,1}^{(4)}\epsilon + e_{2,2}^{(4)}\epsilon^2)Q\,,
\end{aligned} \tag{3.10b}
$$

$$
\begin{aligned}
E_3^{(4)} &= 4\,(\bar{s}_i\gamma^{\mu_1}\dots\gamma^{\mu_8}P_R b_i)\,(\bar{s}_j\gamma_{\mu_1}\dots\gamma_{\mu_8}P_R b_j) \\
&\quad - (32768 + e_{3,1,1}^{(4)}\epsilon + e_{3,1,2}^{(4)}\epsilon^2)\widetilde{Q}_S - (32768 + e_{3,2,1}^{(4)}\epsilon + e_{3,2,2}^{(4)}\epsilon^2)Q_S\,,
\end{aligned} \tag{3.10c}
$$

$$
\begin{aligned}
E_4^{(4)} &= 4\,(\bar{s}_i\gamma^{\mu_1}\dots\gamma^{\mu_8}P_R b_j)\,(\bar{s}_j\gamma_{\mu_1}\dots\gamma_{\mu_8}P_R b_i) \\
&\quad - (32768 + e_{4,1,1}^{(4)}\epsilon + e_{4,1,2}^{(4)}\epsilon^2)\widetilde{Q}_S - (32768 + e_{4,2,1}^{(4)}\epsilon + e_{4,2,2}^{(4)}\epsilon^2)Q_S\,.
\end{aligned} \tag{3.10d}
$$

In the next section we compute the renormalization constants of this operator basis at the leading power in Λ/m_b.

3.3 RENORMALIZATION

For the determination of the renormalization constants of effective operators, respective matrix elements with QCD corrections have to be considered. For the $\Delta B = 2$ theory this involves the computation of the process $\bar{s}b \to \bar{b}s$.

Since renormalization constants in $\overline{\text{MS}}$ do not depend on the masses or momenta of the interacting particles, we can simplify the calculation by setting $q_b = q_s = 0$. Thus, only tadpole integrals occur which can be directly evaluated with usage of the program `MATAD` [102].

Unfortunately, the resulting matrix elements do not only involve ultraviolet but also infrared divergences. This problem can be resolved if we introduce a mass for every quark. For simplicity this mass is chosen to be equal among different flavors. This unphysical kinematics regulates the IR divergences, whereas the UV behavior is not effected. Thus, all occurrences of ϵ can be interpreted as ϵ_{UV}. Therefore, the renormalization condition for evanescent operators, as stated in section 2.5, can be applied without restriction.

Additionally, QCD renormalization constants have to be inserted to render the matrix elements finite. We employ in the following the parameterization of eq. (2.33). The renormalization matrix for the Wilson coefficients is defined as

$$
\begin{pmatrix} \vec{C}_Q^{\,0} \\ \vec{C}_E^{\,0} \end{pmatrix} = \begin{pmatrix} \vec{C}_Q & \vec{C}_E \end{pmatrix} \begin{pmatrix} Z_{QQ} & Z_{QE} \\ Z_{EQ} & Z_{EE} \end{pmatrix}, \tag{3.11}
$$

with the parameterization equivalent to eq. (2.40).

Schematically, we compute the one-loop corrections to a physical operator insertion and express it in terms of tree-level matrix elements. Up to NLO in QCD we obtain

$$\begin{aligned}\langle Q_i\rangle^{\text{NLO}} &= C_i^0 \langle Q_i(\psi^0)\rangle^{\text{tree}} \\ &+ \left(\frac{\alpha_s}{4\pi}\right)\left(a_{ij}^{(1,0)} + \frac{a_{ij}^{(1,1)}}{\epsilon}\right) C_i^0 \langle Q_j(\psi^0)\rangle^{\text{tree}} \\ &+ \left(\frac{\alpha_s}{4\pi}\right)\left(b_{ij}^{(1,0)} + \frac{b_{ij}^{(1,1)}}{\epsilon}\right) C_i^0 \langle E_j(\psi^0)\rangle^{\text{tree}} ,\end{aligned} \tag{3.12}$$

where the sum over i and j is implied. In general, the coefficients a and b are mass dependent. Since the tree-level contribution does not include any masses, Z_m becomes relevant first at NNLO. The argument ψ^0 implicates that the quark fields are unrenormalized.

Similarly, we can write the evanescent operator insertions as

$$\begin{aligned}\langle E_i\rangle^{\text{NLO}} &= C_{E_i}^0 \langle E_i(\psi^0)\rangle^{\text{tree}} \\ &+ \left(\frac{\alpha_s}{4\pi}\right)\left(c_{ij}^{(1,0)} + \frac{c_{ij}^{(1,1)}}{\epsilon}\right) C_{E_i}^0 \langle Q_j(\psi^0)\rangle^{\text{tree}} \\ &+ \left(\frac{\alpha_s}{4\pi}\right)\left(d_{ij}^{(1,0)} + \frac{d_{ij}^{(1,1)}}{\epsilon}\right) C_{E_i}^0 \langle E_j(\psi^0)\rangle^{\text{tree}} .\end{aligned} \tag{3.13}$$

In the $\overline{\text{MS}}$ scheme we demand that all $\mathcal{O}\left(\epsilon_{\text{UV}}^{-1}\right)$ terms are removed by the renormalization constants. Combining both eqs. (3.12) and (3.13) leads to an overall pole structure of

$$\begin{aligned}&\left(\frac{\alpha_s}{4\pi\epsilon}\right)\Big[\left(a_{ji}^{(1,1)}C_j + 2Z_2^{(1,1)}C_i + Z_{Q_jQ_i}^{(1,1)}C_j + Z_{E_jQ_i}^{(1,1)}C_{E_j} + c_{ji}^{(1,1)}C_{E_j}\right)\langle Q_i\rangle^{\text{tree}} \\ &+ \left(d_{ji}^{(1,1)}C_{E_j} + 2Z_2^{(1,1)}C_{E_i} + Z_{E_jE_i}^{(1,1)}C_{E_j} + Z_{Q_jE_i}^{(1,1)}C_j + b_{ji}^{(1,1)}C_j\right)\langle E_i\rangle^{\text{tree}}\Big] .\end{aligned} \tag{3.14}$$

Since evanescent operators are formally defined as $\mathcal{O}(\epsilon)$, we always have $c_{ji}^{(1,1)} = 0$. Comparing the coefficients of eq. (3.14) leads to

$$\begin{aligned} Z_{Q_iQ_j}^{(1,1)} &= -2Z_2^{(1,1)}\delta_{ij} - a_{ij}^{(1,1)} , \\ Z_{E_iQ_j}^{(1,1)} &= 0 , \\ Z_{Q_iE_j}^{(1,1)} &= -b_{ij}^{(1,1)} , \\ Z_{E_iE_j}^{(1,1)} &= -2Z_2^{(1,1)}\delta_{ij} - d_{ij}^{(1,1)} . \end{aligned} \tag{3.15}$$

Our renormalization condition for evanescent operators further demands that finite terms of eqs. (3.12) and (3.13) proportional to C_E vanish in the limit $\epsilon \to 0$. They are given by

$$\left(\frac{\alpha_s}{4\pi}\right)\left[\left(Z_{E_jQ_i}^{(1,0)}C_{E_j} + c_{ji}^{(1,0)}C_{E_j}\right)\langle Q_i\rangle^{\text{tree}} + \left(d_{ji}^{(1,0)}C_{E_j}\right)\langle E_i\rangle^{\text{tree}}\right] . \tag{3.16}$$

The second term vanishes for $d \to 4$ due to $\langle E \rangle^{\text{tree}} = \mathcal{O}(\epsilon_{\text{UV}})$. Applying the renormalization condition to the first term gives

$$Z^{(1,0)}_{E_i Q_j} = -c^{(1,0)}_{ij} \,. \tag{3.17}$$

Our renormalization scheme is chosen such that all renormalization constants are independent of the chosen kinematics for the underlying process. For the terms containing poles this condition is evident from standard $\overline{\text{MS}}$. However, it is not easy to see that eq. (3.17) also fulfills this requirement. This becomes clear, if we look at the general structure of an evanescent matrix element. Schematically,

$$\langle E \rangle = \langle \widetilde{E} \rangle + c\,\epsilon\,\langle Q \rangle \,. \tag{3.18}$$

Every evanescent matrix element can be written as a sum of a matrix element $\langle \widetilde{E} \rangle$ which vanishes in $d = 4$ due to its connection to four-dimensional identities (such as Fierz identities), and a term which is proportional to a physical operator matrix element $\langle Q \rangle$. The proportionality factor c is UV-finite. The one-loop corrections of such an operator are given by

$$\begin{aligned} \langle E \rangle^{\text{1-loop}} &= \langle \widetilde{E} \rangle^{\text{1-loop}} + c\,\epsilon\,\langle Q \rangle^{\text{1-loop}} \\ &= \langle \widetilde{E} \rangle^{\text{1-loop}} + c\,\epsilon \left(a^{(0)} + \frac{a^{(1)}}{\epsilon} \right) \langle Q \rangle^{\text{tree}} \\ &\quad + c\,\epsilon \left(b^{(0)} + \frac{b^{(0)}}{\epsilon} \right) \langle E' \rangle^{\text{tree}} \,, \end{aligned} \tag{3.19}$$

where E' denotes further evanescent operators. Their tree-level matrix element arises from the one-loop corrections to Q.

Thus,

$$\langle E \rangle^{\text{1-loop}} = \langle \widetilde{E} \rangle^{\text{1-loop}} + c\,a^{(1)}\,\langle Q \rangle^{\text{tree}} + \mathcal{O}(\epsilon) \,. \tag{3.20}$$

The one-loop matrix element contains only poles from the evanescent terms $\langle \widetilde{E} \rangle^{\text{1-loop}}$. The finite terms proportional to physical matrix elements, $c\,a^{(1)}$, stem from $\mathcal{O}(\epsilon)$ terms of the evanescent operator definition multiplied by $\mathcal{O}(\epsilon^{-1})$ terms from the one-loop correction. Since these terms do not depend on the kinematics of the external particles, the same applies to the counterterm which removes them.

Our physical $\Delta B = 2$ operators are Q, Q_S and $\widetilde{Q}_S$. Regarding the first order in the Λ/m_b expansion, we see that we could replace one of them by R_0, as defined in eq. (3.4a). The Λ/m_b suppression of R_0 is of kinematic nature and follows from equations of motions and Fierz identities, as shown in appendix C. Therefore, it cannot be neglected in the basis and must be also part of the renormalization if only two operators out of Q, Q_S and $\widetilde{Q}_S$ are used to describe the leading Λ/m_b effects.

Following the renormalization procedure as described, we compute the renormalization matrix of the Wilson coefficients. The renormalization of the effective operators follows from eq. (2.38). Our choice for the physical operator basis is

$$Q \equiv \{Q, Q_S, \widetilde{Q}_S\} \,. \tag{3.21}$$

Since we are interested in the matching of NNLO amplitudes, evanescent operators of *at least* second generation have to be included, because structures with 5×5 γ-matrices appear. According to the discussion in chapter 4, we take evanescent operators up to fourth generation into account for the matching of $\Delta B = 1$ and $\Delta B = 2$. This allows us to compute the renormalization of first and second generation evanescent operators up to NNLO, and of third generation to NLO. In the corresponding matrix elements, we encounter terms with up to $9 \otimes 9$ γ-matrices. Thus, we have

$$\begin{aligned} E \equiv \{&E_1^{(1)}, E_2^{(1)}, E_3^{(1)}, E_4^{(1)}, E_5^{(1)}, E_1^{(2)}, E_2^{(2)}, E_3^{(2)}, E_4^{(2)}, \\ &E_1^{(3)}, E_2^{(3)}, E_3^{(3)}, E_4^{(3)}, E_1^{(4)}, E_2^{(4)}, E_3^{(4)}, E_4^{(4)}\}\,. \end{aligned} \tag{3.22}$$

Note that in general the evanescent structure of our chosen basis is sufficient to renormalize physical operator insertions with up to four-loop QCD corrections.

At one-loop order we obtain for the renormalization mixing of physical Wilson coefficients:

$$Z_{QQ}^{(1,1)} = \begin{pmatrix} 2 & 0 & 0 \\ 0 & -\frac{14}{3} & \frac{2}{3} \\ 0 & \frac{8}{3} & \frac{16}{3} \end{pmatrix}. \tag{3.23}$$

All results are given in the ancillary files of this thesis with exact n_c dependence, where n_c denotes the number of colors. For illustration purposes we present the results for $n_c = 3$. Equation (3.23) agrees with the matrix found in ref. [65]. The structure of the matrix shows that Q does not mix with the other physical operators at one-loop order.

The renormalization matrix which mixes evanescent into physical coefficients is given by

$$Z_{QE}^{(1,1)} = \begin{pmatrix} 3 & \frac{1}{2} & -\frac{1}{6} & 0 & 0 & 0 & 0 & 0 & 0 & 0 & 0 & 0 & 0 & 0 & 0 & 0 \\ 0 & 0 & 0 & -\frac{1}{2} & \frac{1}{6} & 0 & 0 & 0 & 0 & 0 & 0 & 0 & 0 & 0 & 0 & 0 \\ 0 & 0 & 0 & -\frac{7}{12} & -\frac{1}{4} & 0 & 0 & 0 & 0 & 0 & 0 & 0 & 0 & 0 & 0 & 0 \end{pmatrix}. \tag{3.24}$$

One can see that only the first generation of evanescent operators is needed for the renormalization of the physical operators at $\mathcal{O}(\alpha_s)$.

The finite renormalization, which is responsible for removing contributions of evanescent Wilson coefficients in physical matrix elements, is split into three columns:

$$Z_{EQ}^{(1,0)} = (Z_{EQ}^{(1,0),1}, Z_{EQ}^{(1,0),2}, Z_{EQ}^{(1,0),3})\,. \tag{3.25}$$

They read

$$Z_{EQ}^{(1,0),1} = \begin{pmatrix} \frac{1}{12}e_{(2,1)}^{(1)} + \frac{5}{12}e_{(3,1)}^{(1)} + 2 \\ -\frac{65}{3}e_{(2,1)}^{(1)} - 5e_{(3,1)}^{(1)} + \frac{7}{12}e_{(1,1)}^{(2)} + \frac{1}{4}e_{(2,1)}^{(2)} + 48 \\ -13e_{(2,1)}^{(1)} + \frac{7}{3}e_{(3,1)}^{(1)} + \frac{1}{2}e_{(1,1)}^{(2)} - \frac{1}{6}e_{(2,1)}^{(2)} - 48 \\ 0 \\ 0 \\ -\frac{1888}{3}e_{(2,1)}^{(1)} + 96e_{(3,1)}^{(1)} + \frac{35}{3}e_{(1,1)}^{(2)} - 9e_{(2,1)}^{(2)} + \frac{7}{12}e_{(1,1)}^{(3)} + \frac{1}{4}e_{(2,1)}^{(3)} + 3840 \\ -288e_{(2,1)}^{(1)} + \frac{1568}{3}e_{(3,1)}^{(1)} + 3e_{(1,1)}^{(2)} - \frac{73}{3}e_{(2,1)}^{(2)} + \frac{1}{2}e_{(1,1)}^{(3)} - \frac{1}{6}e_{(2,1)}^{(3)} - 3840 \\ 0 \\ 0 \\ -\frac{39424}{3}e_{(2,1)}^{(1)} + 2560e_{(3,1)}^{(1)} - 672e_{(1,1)}^{(2)} + 224e_{(2,1)}^{(2)} + \frac{179}{3}e_{(1,1)}^{(3)} - 25e_{(2,1)}^{(3)} + \frac{7}{12}e_{(1,1)}^{(4)} + \frac{1}{4}e_{(2,1)}^{(4)} + 258048 \\ -5632e_{(2,1)}^{(1)} + \frac{34304}{3}e_{(3,1)}^{(1)} - 224e_{(1,1)}^{(2)} + 672e_{(2,1)}^{(2)} + 19e_{(1,1)}^{(3)} - \frac{217}{3}e_{(2,1)}^{(3)} + \frac{1}{2}e_{(1,1)}^{(4)} - \frac{1}{6}e_{(2,1)}^{(4)} - 258048 \\ 0 \\ 0 \\ * \\ * \\ * \\ * \end{pmatrix}, \tag{3.26}$$

$$Z_{EQ}^{(1,0),2} = \begin{pmatrix} 0 \\ 0 \\ 0 \\ -\frac{8}{3}e_{(4,1,1)}^{(1)} - \frac{52}{3}e_{(4,2,1)}^{(1)} - \frac{2}{3}e_{(5,2,1)}^{(1)} - \frac{1}{4}e_{(3,2,1)}^{(2)} - \frac{7}{12}e_{(4,2,1)}^{(2)} - \frac{88}{3} \\ -\frac{44}{3}e_{(4,2,1)}^{(1)} - \frac{8}{3}e_{(5,1,1)}^{(1)} + \frac{26}{3}e_{(5,2,1)}^{(1)} + \frac{1}{6}e_{(3,2,1)}^{(2)} - \frac{1}{2}e_{(4,2,1)}^{(2)} + \frac{152}{3} \\ 0 \\ 0 \\ \frac{608}{3}e_{(4,2,1)}^{(1)} - \frac{544}{3}e_{(5,2,1)}^{(1)} - \frac{8}{3}e_{(3,1,1)}^{(2)} - \frac{8}{3}e_{(3,2,1)}^{(2)} - 2e_{(4,2,1)}^{(2)} - \frac{1}{6}e_{(3,2,1)}^{(3)} + \frac{1}{2}e_{(4,2,1)}^{(3)} - \frac{5248}{3} \\ \frac{992}{3}e_{(4,2,1)}^{(1)} - \frac{160}{3}e_{(5,2,1)}^{(1)} - 4e_{(3,2,1)}^{(2)} - \frac{8}{3}e_{(4,1,1)}^{(2)} + \frac{10}{3}e_{(4,2,1)}^{(2)} + \frac{1}{4}e_{(3,2,1)}^{(3)} + \frac{7}{12}e_{(4,2,1)}^{(3)} + \frac{2432}{3} \\ 0 \\ 0 \\ \frac{7424}{3}e_{(4,2,1)}^{(1)} - \frac{1792}{3}e_{(5,2,1)}^{(1)} + 720e_{(3,2,1)}^{(2)} - 240e_{(4,2,1)}^{(2)} - \frac{8}{3}e_{(3,1,1)}^{(3)} - \frac{116}{3}e_{(3,2,1)}^{(3)} + 10e_{(4,2,1)}^{(3)} - \frac{1}{6}e_{(3,2,1)}^{(4)} + \frac{1}{2}e_{(4,2,1)}^{(4)} - \frac{203776}{3} \\ \frac{8960}{3}e_{(4,2,1)}^{(1)} - \frac{256}{3}e_{(5,2,1)}^{(1)} + 240e_{(3,2,1)}^{(2)} - 720e_{(4,2,1)}^{(2)} - 16e_{(3,2,1)}^{(3)} - \frac{8}{3}e_{(4,1,1)}^{(3)} + \frac{118}{3}e_{(4,2,1)}^{(3)} + \frac{1}{4}e_{(3,2,1)}^{(4)} + \frac{7}{12}e_{(4,2,1)}^{(4)} + \frac{195584}{3} \\ * \\ * \\ * \\ * \end{pmatrix}, \tag{3.27}$$

$$Z_{EQ}^{(1,0),3} = \begin{pmatrix} 0 \\ 0 \\ 0 \\ -\frac{82}{3}e^{(1)}_{(4,1,1)} - \frac{2}{3}e^{(1)}_{(4,2,1)} - \frac{2}{3}e^{(1)}_{(5,1,1)} - \frac{1}{4}e^{(2)}_{(3,1,1)} - \frac{7}{12}e^{(2)}_{(4,1,1)} - \frac{376}{3} \\ -\frac{44}{3}e^{(1)}_{(4,1,1)} - \frac{4}{3}e^{(1)}_{(5,1,1)} - \frac{2}{3}e^{(1)}_{(5,2,1)} + \frac{1}{6}e^{(2)}_{(3,1,1)} - \frac{1}{2}e^{(2)}_{(4,1,1)} - \frac{136}{3} \\ 0 \\ 0 \\ \frac{608}{3}e^{(1)}_{(4,1,1)} - \frac{544}{3}e^{(1)}_{(5,1,1)} - \frac{38}{3}e^{(2)}_{(3,1,1)} - \frac{2}{3}e^{(2)}_{(3,2,1)} - 2e^{(2)}_{(4,1,1)} - \frac{1}{6}e^{(3)}_{(3,1,1)} + \frac{1}{2}e^{(3)}_{(4,1,1)} - \frac{640}{3} \\ \frac{992}{3}e^{(1)}_{(4,1,1)} - \frac{160}{3}e^{(1)}_{(5,1,1)} - 4e^{(2)}_{(3,1,1)} - \frac{20}{3}e^{(2)}_{(4,1,1)} - \frac{2}{3}e^{(2)}_{(4,2,1)} + \frac{1}{4}e^{(3)}_{(3,1,1)} + \frac{7}{12}e^{(3)}_{(4,1,1)} + \frac{7040}{3} \\ 0 \\ 0 \\ \frac{7424}{3}e^{(1)}_{(4,1,1)} - \frac{1792}{3}e^{(1)}_{(5,1,1)} + 720e^{(2)}_{(3,1,1)} - 240e^{(2)}_{(4,1,1)} - \frac{146}{3}e^{(3)}_{(3,1,1)} - \frac{2}{3}e^{(3)}_{(3,2,1)} + 10e^{(3)}_{(4,1,1)} - \frac{1}{6}e^{(4)}_{(3,1,1)} + \frac{1}{2}e^{(4)}_{(4,1,1)} - \frac{166912}{3} \\ \frac{8960}{3}e^{(1)}_{(4,1,1)} - \frac{256}{3}e^{(1)}_{(5,1,1)} + 240e^{(2)}_{(3,1,1)} - 720e^{(2)}_{(4,1,1)} - 16e^{(3)}_{(3,1,1)} + \frac{88}{3}e^{(3)}_{(4,1,1)} - \frac{2}{3}e^{(3)}_{(4,2,1)} + \frac{1}{4}e^{(4)}_{(3,1,1)} + \frac{7}{12}e^{(4)}_{(4,1,1)} + \frac{232448}{3} \\ * \\ * \\ * \\ * \end{pmatrix}. \tag{3.28}$$

The unknown dependence on the NLO contributions of the fourth generation evanescent terms are denoted by an asterisk "$*$". They are not relevant for the calculations of this thesis.

Furthermore, at NLO we have a 17×17 sub-matrix to renormalize evanescent operators among themselves. It is given by

$$Z_{EE}^{(1,1)} = \begin{pmatrix} -4 & \frac{1}{12} & \frac{5}{12} & 0 & 0 & 0 & 0 & 0 & 0 & 0 & 0 & 0 & 0 & 0 & 0 & 0 & 0 \\ 0 & -\frac{59}{3} & -5 & 0 & 0 & \frac{7}{12} & \frac{1}{4} & 0 & 0 & 0 & 0 & 0 & 0 & 0 & 0 & 0 & 0 \\ 0 & -13 & \frac{13}{3} & 0 & 0 & \frac{1}{2} & -\frac{1}{6} & 0 & 0 & 0 & 0 & 0 & 0 & 0 & 0 & 0 & 0 \\ 0 & 0 & 0 & -22 & -\frac{2}{3} & 0 & 0 & -\frac{1}{4} & -\frac{7}{12} & 0 & 0 & 0 & 0 & 0 & 0 & 0 & 0 \\ 0 & 0 & 0 & -\frac{44}{3} & 4 & 0 & 0 & \frac{1}{6} & -\frac{1}{2} & 0 & 0 & 0 & 0 & 0 & 0 & 0 & 0 \\ 0 & -\frac{1888}{3} & 96 & 0 & 0 & \frac{41}{3} & -9 & 0 & 0 & \frac{7}{12} & \frac{1}{4} & 0 & 0 & 0 & 0 & 0 & 0 \\ 0 & -288 & \frac{1568}{3} & 0 & 0 & 3 & -\frac{67}{3} & 0 & 0 & \frac{1}{2} & -\frac{1}{6} & 0 & 0 & 0 & 0 & 0 & 0 \\ 0 & 0 & 0 & \frac{608}{3} & -\frac{544}{3} & 0 & 0 & -\frac{22}{3} & -2 & 0 & 0 & -\frac{1}{6} & \frac{1}{2} & 0 & 0 & 0 & 0 \\ 0 & 0 & 0 & \frac{992}{3} & -\frac{160}{3} & 0 & 0 & -4 & -\frac{4}{3} & 0 & 0 & \frac{1}{4} & \frac{7}{12} & 0 & 0 & 0 & 0 \\ 0 & -\frac{39424}{3} & 2560 & 0 & 0 & -672 & 224 & 0 & 0 & \frac{185}{3} & -25 & 0 & 0 & \frac{7}{12} & \frac{1}{4} & 0 & 0 \\ 0 & -5632 & \frac{34304}{3} & 0 & 0 & -224 & 672 & 0 & 0 & 19 & -\frac{211}{3} & 0 & 0 & \frac{1}{2} & -\frac{1}{6} & 0 & 0 \\ 0 & 0 & 0 & \frac{7424}{3} & -\frac{1792}{3} & 0 & 0 & 720 & -240 & 0 & 0 & -\frac{130}{3} & 10 & 0 & 0 & -\frac{1}{6} & \frac{1}{2} \\ 0 & 0 & 0 & \frac{8960}{3} & -\frac{256}{3} & 0 & 0 & 240 & -720 & 0 & 0 & -16 & \frac{104}{3} & 0 & 0 & \frac{1}{4} & \frac{7}{12} \\ * & * & * & * & * & * & * & * & * & * & * & * & * & * & * & * & * \\ * & * & * & * & * & * & * & * & * & * & * & * & * & * & * & * & * \\ * & * & * & * & * & * & * & * & * & * & * & * & * & * & * & * & * \\ * & * & * & * & * & * & * & * & * & * & * & * & * & * & * & * & * \end{pmatrix}. \tag{3.29}$$

The unknown NLO contributions of $E^{(4)}$ also lead here to no further specification of the last rows.

For the order $\mathcal{O}(\alpha_s^2)$, we depict only the parts of the renormalization matrix which are necessary to renormalize physical operators. At this order the factors $e_x^{(i)}$ are present in the ϵ^{-1} terms of Z_{QQ}, which is given by

$$Z_{QQ}^{(2,2)} = \begin{pmatrix} \frac{2n_f}{3} - 9 & 0 & 0 \\ 0 & \frac{337}{9} - \frac{14n_f}{9} & \frac{2n_f}{9} - \frac{31}{9} \\ 0 & \frac{8n_f}{9} - \frac{124}{9} & \frac{16n_f}{9} - \frac{128}{9} \end{pmatrix}, \tag{3.30}$$

$$Z_{QQ}^{(2,1),1} = \begin{pmatrix} \frac{1}{6}n_f e_{2,1}^{(1)} - \frac{1}{18}n_f e_{3,1}^{(1)} - \frac{167}{24}e_{2,1}^{(1)} + \frac{7}{72}e_{3,1}^{(1)} + \frac{5}{48}e_{1,1}^{(2)} + \frac{11}{144}e_{2,1}^{(2)} + \frac{5n_f}{9} + \frac{119}{12} \\ 0 \\ 0 \end{pmatrix}, \tag{3.31}$$

$$Z_{QQ}^{(2,1),2} = \begin{pmatrix} 0 \\ -\frac{1}{6}n_f e_{4,2,1}^{(1)} + \frac{1}{18}n_f e_{5,2,1}^{(1)} + \frac{4}{3}e_{4,1,1}^{(1)} + \frac{17}{3}e_{4,2,1}^{(1)} - \frac{4}{9}e_{5,1,1}^{(1)} - \frac{1}{9}e_{5,2,1}^{(1)} + \frac{11}{144}e_{3,2,1}^{(2)} + \frac{5}{48}e_{4,2,1}^{(2)} + \frac{58n_f}{27} - \frac{259}{9} \\ -\frac{7}{36}n_f e_{4,2,1}^{(1)} - \frac{1}{12}n_f e_{5,2,1}^{(1)} + \frac{14}{9}e_{4,1,1}^{(1)} + \frac{469}{72}e_{4,2,1}^{(1)} + \frac{2}{3}e_{5,1,1}^{(1)} - \frac{13}{24}e_{5,2,1}^{(1)} + \frac{5}{96}e_{3,2,1}^{(2)} + \frac{67}{288}e_{4,2,1}^{(2)} + \frac{23n_f}{27} + \frac{409}{18} \end{pmatrix}, \tag{3.32}$$

$$Z_{QQ}^{(2,1),3} = \begin{pmatrix} 0 \\ -\frac{1}{6}n_f e_{4,1,1}^{(1)} + \frac{1}{18}n_f e_{5,1,1}^{(1)} + \frac{32}{3}e_{4,1,1}^{(1)} + \frac{1}{3}e_{4,2,1}^{(1)} - \frac{16}{9}e_{5,1,1}^{(1)} - \frac{1}{9}e_{5,2,1}^{(1)} + \frac{11}{144}e_{3,1,1}^{(2)} + \frac{5}{48}e_{4,1,1}^{(2)} - \frac{10n_f}{27} + \frac{335}{9} \\ -\frac{7}{36}n_f e_{4,1,1}^{(1)} - \frac{1}{12}n_f e_{5,1,1}^{(1)} + \frac{889}{72}e_{4,1,1}^{(1)} + \frac{7}{18}e_{4,2,1}^{(1)} + \frac{47}{24}e_{5,1,1}^{(1)} + \frac{1}{6}e_{5,2,1}^{(1)} + \frac{5}{96}e_{3,1,1}^{(2)} + \frac{67}{288}e_{4,1,1}^{(2)} - \frac{65n_f}{27} + \frac{1393}{18} \end{pmatrix}, \tag{3.33}$$

with the splitting of individual columns as in eq. (3.25).

The two-loop contribution to the mixing of evanescent to physical operators is given by

$$Z_{QE}^{(2,2)} = \begin{pmatrix} n_f - \frac{39}{2} & \frac{n_f}{6} - \frac{143}{24} & -\frac{n_f}{18} - \frac{17}{72} & 0 & 0 & \frac{5}{48} & \frac{11}{144} & 0 & 0 & 0 & 0 & 0 & 0 & 0 & 0 & 0 \\ 0 & 0 & 0 & 8 - \frac{n_f}{6} & \frac{n_f}{18} - \frac{8}{9} & 0 & 0 & \frac{11}{144} & \frac{5}{48} & 0 & 0 & 0 & 0 & 0 & 0 & 0 \\ 0 & 0 & 0 & \frac{665}{72} - \frac{7n_f}{36} & \frac{5}{8} - \frac{n_f}{12} & 0 & 0 & \frac{5}{96} & \frac{67}{288} & 0 & 0 & 0 & 0 & 0 & 0 & 0 \end{pmatrix}. \tag{3.34}$$

The only non-vanishing entries of $Z_{QE}^{(2,1)}$ are given by

$$\begin{aligned} Z_{Q,E_1^{(1)}}^{(2,1)} &= \frac{1}{6}e_{2,1}^{(1)}n_f + \frac{5n_f}{6} - \frac{131}{24}e_{2,1}^{(1)} + \frac{1}{2}e_{3,1}^{(1)} + \frac{5}{48}e_{1,1}^{(2)} + \frac{83}{8}, \\ Z_{Q,E_2^{(1)}}^{(2,1)} &= -\frac{n_f}{36} - \frac{7}{24}e_{2,1}^{(1)} + \frac{1}{12}e_{3,1}^{(1)} + \frac{133}{24}, \\ Z_{Q,E_3^{(1)}}^{(2,1)} &= \frac{n_f}{108} - \frac{1}{8}e_{2,1}^{(1)} - \frac{1}{36}e_{3,1}^{(1)} + \frac{71}{72}, \\ Z_{Q,E_1^{(2)}}^{(2,1)} &= -\frac{35}{384}, \end{aligned}$$

$$
\begin{aligned}
Z^{(2,1)}_{Q,E_2^{(2)}} &= -\frac{77}{1152}\,,\\
Z^{(2,1)}_{Q_S,E_4^{(1)}} &= \frac{n_f}{36} - \frac{7}{24}e^{(1)}_{4,1,1} - \frac{1}{4}e^{(1)}_{4,2,1} + \frac{7}{72}e^{(1)}_{5,1,1} + \frac{1}{12}e^{(1)}_{5,2,1} - \frac{79}{12}\,,\\
Z^{(2,1)}_{Q_S,E_5^{(1)}} &= -\frac{n_f}{108} - \frac{1}{8}e^{(1)}_{4,1,1} + \frac{1}{12}e^{(1)}_{4,2,1} + \frac{1}{24}e^{(1)}_{5,1,1} - \frac{1}{36}e^{(1)}_{5,2,1} - \frac{41}{36}\,,\\
Z^{(2,1)}_{Q_S,E_3^{(2)}} &= -\frac{77}{1152}\,,\\
Z^{(2,1)}_{Q_S,E_4^{(2)}} &= -\frac{35}{384}\,,\\
Z^{(2,1)}_{\widetilde{Q}_S,E_4^{(1)}} &= \frac{7n_f}{216} - \frac{49}{144}e^{(1)}_{4,1,1} - \frac{7}{24}e^{(1)}_{4,2,1} - \frac{7}{48}e^{(1)}_{5,1,1} - \frac{1}{8}e^{(1)}_{5,2,1} - \frac{1271}{144}\,,\\
Z^{(2,1)}_{\widetilde{Q}_S,E_5^{(1)}} &= \frac{n_f}{72} - \frac{7}{48}e^{(1)}_{4,1,1} + \frac{7}{72}e^{(1)}_{4,2,1} - \frac{1}{16}e^{(1)}_{5,1,1} + \frac{1}{24}e^{(1)}_{5,2,1} - \frac{11}{16}\,,\\
Z^{(2,1)}_{\widetilde{Q}_S,E_3^{(2)}} &= -\frac{5}{48}\,,\\
Z^{(2,1)}_{\widetilde{Q}_S,E_4^{(2)}} &= -\frac{1}{36}\,.
\end{aligned}
\tag{3.35}
$$

We observe that the dependence on the QCD gauge parameter ξ drops out of the final renormalization matrix. This is expected from the fact that a ξ-dependence of Z would also imply a ξ-dependence of the ADM. The latter is used for the running of hadronic matrix elements down to the matching scale. Hence, the $\Delta B = 2$ matching coefficients would also be ξ-dependent. Since physical quantities are gauge independent, and neither the CMM Wilson coefficients nor the lattice results depend on ξ, this dependence is expected to drop out in Z_{QQ} as well.

Alternatively to the physical operator basis of eq. (3.21), one could also choose e.g.

$$
Q' \equiv \{Q, \widetilde{Q}_S, R_0\} \tag{3.36}
$$

as described in ref. [47]. For illustration, we state only the sub-matrix for the one-loop renormalization among physical operators. It is given by

$$
Z^{(1,1)}_{Q'Q'} = \begin{pmatrix} 2 & 0 & 0 \\ -\frac{4}{3} & \frac{8}{3} & \frac{8}{3} \\ 2 & 8 & -2 \end{pmatrix}. \tag{3.37}
$$

Without R_0 in the basis (3.36) no solution of eq. (3.14) can be constructed.

The complete 20×20 matrix can be found in the ancillary files of this thesis.

In the next chapter we use the renormalization matrices to relate the Wilson coefficients at different renormalization scales.

3.4 RENORMALIZATION GROUP OF EFFECTIVE INTERACTIONS

Since the bare Wilson coefficients do not depend on the renormalization scale μ in the Hamiltonian, we can formulate the equation

$$\begin{aligned} 0 &= \mu\frac{\mathrm{d}}{\mathrm{d}\mu}\vec{C}^0 = \mu\frac{\mathrm{d}}{\mathrm{d}\mu}\left(\vec{C}Z\right) \\ \Rightarrow \quad \mu\frac{\mathrm{d}}{\mathrm{d}\mu}\vec{C} &= -\vec{C}\left(\mu\frac{\mathrm{d}}{\mathrm{d}\mu}Z\right)Z^{-1} \\ &= -\vec{C}\,\beta(\alpha_s,\epsilon)\left(\frac{\mathrm{d}}{\mathrm{d}\alpha_s}Z\right)Z^{-1} \\ &\equiv \vec{C}\gamma\,, \end{aligned} \tag{3.38}$$

The matrix γ is called *Anomalous Dimension Matrix* (ADM) and eq. (3.38) is known as *Renormalization Group Equation* (RGE). We further introduce the QCD *β-function* which is defined as

$$\beta(\alpha_s,\epsilon) \equiv \mu\frac{\mathrm{d}}{\mathrm{d}\mu}\alpha_s\,, \tag{3.39}$$

with the parameterization

$$\beta(\alpha_s,\epsilon) = -2\alpha_s\left[\epsilon + \left(\frac{\alpha_s}{4\pi}\right)\beta_0 + \left(\frac{\alpha_s}{4\pi}\right)^2\beta_1 + \mathcal{O}\left(\alpha_s^3\right)\right]. \tag{3.40}$$

This function is currently known up five-loop order [103–105]. However, only the two-loop results are needed for the purposes of this thesis. They are given by [104]

$$\begin{aligned} \beta_0 &= \frac{11}{3}C_A - \frac{4}{3}T_F n_f\,, \\ \beta_1 &= \frac{34}{3}C_A^2 - \frac{20}{3}C_A T_F n_f - 4C_F T_F n_f\,, \end{aligned} \tag{3.41}$$

with the Casimir operators $C_A = n_c$, $C_F = (n_c^2-1)/(2n_c)$ and the color trace normalization $T_F = 1/2$.

Alternatively, the μ-dependence of the effective operators $\vec{\mathcal{O}}$ can be expressed by another ADM $\widetilde{\gamma}$. With the renormalization matrix defined in eq. (2.38), we obtain

$$\begin{aligned} 0 &= \mu\frac{\mathrm{d}}{\mathrm{d}\mu}\left(\vec{C}\vec{\mathcal{O}}\right) = \mu\frac{\mathrm{d}}{\mathrm{d}\mu}\left(\vec{C}^0\vec{\mathcal{O}}^0\right) = \vec{C}^0\mu\frac{\mathrm{d}}{\mathrm{d}\mu}\left(Z^{-1}\vec{\mathcal{O}}\right) \\ \Rightarrow \quad \mu\frac{\mathrm{d}}{\mathrm{d}\mu}\vec{\mathcal{O}} &= -\beta(\alpha_s,\epsilon)Z\left(\frac{\mathrm{d}}{\mathrm{d}\alpha_s}Z^{-1}\right)\vec{\mathcal{O}} \\ &= \beta(\alpha_s,\epsilon)\left(\frac{\mathrm{d}}{\mathrm{d}\alpha_s}Z\right)Z^{-1}\vec{\mathcal{O}} \\ &\equiv \widetilde{\gamma}\vec{\mathcal{O}}\,, \end{aligned} \tag{3.42}$$

In eq. (3.42) we use the following matrix identity:

$$\begin{aligned} 0 &= \frac{\mathrm{d}}{\mathrm{d}x}\mathbb{1} = \frac{\mathrm{d}}{\mathrm{d}x}\left(A^{-1}A\right) = \left(\frac{\mathrm{d}}{\mathrm{d}x}A^{-1}\right)A + A^{-1}\left(\frac{\mathrm{d}}{\mathrm{d}x}A\right) \\ \Rightarrow \quad \frac{\mathrm{d}}{\mathrm{d}x}A^{-1} &= -A^{-1}\left(\frac{\mathrm{d}}{\mathrm{d}x}A\right)A^{-1}\,, \end{aligned} \tag{3.43}$$

which holds for any invertible matrix A.

The following relation between the two ADMs can be found by comparing eqs. (3.38) and (3.42):

$$\widetilde{\gamma} \;=\; -\gamma\,. \tag{3.44}$$

In the full theory side of a matching calculation, logarithms such as $\ln(M/\mu)$ appear from loop corrections, where M is the mass of a heavy particle. To get a better perturbative convergence, a reasonable choice for the renormalization scale is obviously $\mu \approx M$. On the effective field theory side, where M is integrated out, the typical energy scales are of order m and corresponding logarithms $\ln(m/\mu)$ occur. The former choice $\mu \approx M$ leads to numerically enhanced terms with $\ln(m/M)$, which lead to large corrections in the perturbative expansion.

This problem can be solved by using RGE techniques. Since they describe the μ dependence of a quantity, they can be used to relate quantities at different scales. In general, we can describe the so-called *running* with a transition operator U. For the Wilson coefficients we get

$$\vec{C}(\mu_1) \;=\; \vec{C}(\mu_2) U(\mu_1,\mu_2)\,. \tag{3.45}$$

The structure of U can be derived from the ADM in eq. (3.38). We use the following parameterization:

$$\gamma \;=\; \sum_{i=0}^{\infty} \left(\frac{\alpha_s}{4\pi}\right)^{(i+1)} \gamma_i\,. \tag{3.46}$$

Equation (3.38) can be solved perturbatively as

$$\begin{aligned}
\vec{C}(\mu_1) \;&= \vec{C}(\mu_2) \exp\left[\int_{\mu_2}^{\mu_1} \frac{\mathrm{d}\mu}{\mu}\,\gamma\right] \\
&= \vec{C}(\mu_2) \exp\left[\int_{\alpha_s(\mu_2)}^{\alpha_s(\mu_1)} \mathrm{d}\alpha_s\,\frac{\gamma}{\beta(\alpha_s,0)}\right] \\
&= \vec{C}(\mu_2) \exp\left[\int_{\alpha_s(\mu_2)}^{\alpha_s(\mu_1)} \mathrm{d}\alpha_s \left(-\frac{\gamma_0}{2\beta_0\alpha_s} - \frac{\beta_0\gamma_1-\beta_1\gamma_0}{8\pi\beta_0^2} + \mathcal{O}(\alpha_s)\right)\right] \\
&= \vec{C}(\mu_2) \exp\left[-\frac{\gamma_0}{2\beta_0}\ln\left(\frac{\alpha_s(\mu_1)}{\alpha_s(\mu_2)}\right)\right. \\
&\quad \left. -\frac{\beta_0\gamma_1-\beta_1\gamma_0}{8\pi\beta_0^2}(\alpha_s(\mu_1)-\alpha_s(\mu_2)) + \mathcal{O}(\alpha_s^2)\right]\,,
\end{aligned} \tag{3.47}$$

where we set $\epsilon \to 0$ since all quantities are finite. It turns out that the large logarithms which appear when relating results at two different scales are automatically summed by the RGE running. Equation (3.47) enhances the Wilson coefficients to be defined in RGE *improved perturbation theory*.

If the scales μ_1 and μ_2 of eq. (3.47) are of the same order, the result can be expressed in terms of α_s at a single scale. The running of α_s is defined by solving eq. (3.39). We get

$$\begin{aligned} \ln\left(\frac{\mu_1}{\mu_2}\right) &= \int_{\alpha_s(\mu_2)}^{\alpha_s(\mu_1)} \mathrm{d}\alpha_s \, \frac{1}{\beta(\alpha_s,0)} \\ \Rightarrow \alpha_s(\mu_1) &= \alpha_s(\mu_2) - \frac{\alpha_s^2(\mu_2)}{2\pi}\beta_0 \ln\left(\frac{\mu_1}{\mu_2}\right) \\ &\quad + \frac{\alpha_s^3(\mu_2)}{8\pi^2}\left[2\beta_0^2 \ln^2\left(\frac{\mu_1}{\mu_2}\right) - \beta_1 \ln\left(\frac{\mu_1}{\mu_2}\right)\right] + \mathcal{O}(\alpha_s^4)\,. \end{aligned} \tag{3.48}$$

If μ_1 and μ_2 are not of the same order, we would again get large logarithms.

Inserting eq. (3.48) into eq. (3.47) and expanding the exponent, results in

$$\begin{aligned} \vec{C}(\mu_1) &= \vec{C}(\mu_2)\Bigg\{1 + \left(\frac{\alpha_s(\mu_2)}{4\pi}\right)\gamma_0 \ln\left(\frac{\mu_1}{\mu_2}\right) \\ &\quad + \left(\frac{\alpha_s(\mu_2)}{4\pi}\right)^2\left[\gamma_1 \ln\left(\frac{\mu_1}{\mu_2}\right) + \left(\frac{\gamma_0^2}{2} - \gamma_0\beta_0\right)\ln^2\left(\frac{\mu_1}{\mu_2}\right)\right] \\ &\quad + \mathcal{O}(\alpha_s^3)\Bigg\}\,. \end{aligned} \tag{3.49}$$

Starting at $\mathcal{O}(\alpha_s^3)$ also commutation relations have to be considered between the γ_i [106].

The ADM can be represented in the following way:

$$\gamma = \begin{pmatrix} \gamma_{QQ} & \gamma_{QE} \\ \gamma_{EQ} & \gamma_{EE} \end{pmatrix}. \tag{3.50}$$

The sub-matrices γ_{EQ} and γ_{EE} describe the mixing into and of evanescent Wilson coefficients. They can be ignored since physical quantities must not depend on them.

In the basis of physical operators Q, Q_S and $\widetilde{Q}_S$, we find

$$\gamma_{0,QQ} = \begin{pmatrix} 4 & 0 & 0 \\ 0 & -\frac{28}{3} & \frac{4}{3} \\ 0 & \frac{16}{3} & \frac{32}{3} \end{pmatrix}, \tag{3.51}$$

which agrees with ref. [65]. The ADM sub-matrix which mixes evanescent Wilson coefficients into physical ones reads

$$\gamma_{0,QE} = \begin{pmatrix} 6 & 1 & -\frac{1}{3} & 0 & 0 & 0 & 0 & 0 & 0 & 0 & 0 & 0 & 0 & 0 & 0 & 0 \\ 0 & 0 & 0 & -1 & \frac{1}{3} & 0 & 0 & 0 & 0 & 0 & 0 & 0 & 0 & 0 & 0 & 0 \\ 0 & 0 & 0 & -\frac{7}{6} & -\frac{1}{2} & 0 & 0 & 0 & 0 & 0 & 0 & 0 & 0 & 0 & 0 & 0 \end{pmatrix}. \tag{3.52}$$

At two-loops, the ADM is given by

$$\gamma_{1,QQ} = \left(\gamma_{1,QQ}^{(1)}, \gamma_{1,QQ}^{(2)}, \gamma_{1,QQ}^{(3)}\right), \tag{3.53}$$

with

$$\gamma^{(1)}_{1,QQ} = \begin{pmatrix} \frac{2}{3}n_f e^{(1)}_{2,1} - \frac{2}{9}n_f e^{(1)}_{3,1} - 11e^{(1)}_{2,1} + \frac{11}{3}e^{(1)}_{3,1} + \frac{20n_f}{9} - \frac{109}{3} \\ 0 \\ 0 \end{pmatrix}, \tag{3.54}$$

$$\gamma^{(2)}_{1,QQ} = \begin{pmatrix} 0 \\ -\frac{2}{3}n_f e^{(1)}_{4,2,1} + \frac{2}{9}n_f e^{(1)}_{5,2,1} + \frac{8}{3}e^{(1)}_{4,1,1} + \frac{92}{9}e^{(1)}_{4,2,1} - \frac{8}{9}e^{(1)}_{5,1,1} - 4e^{(1)}_{5,2,1} + \frac{232n_f}{27} - \frac{484}{3} \\ -\frac{7}{9}n_f e^{(1)}_{4,2,1} - \frac{1}{3}n_f e^{(1)}_{5,2,1} + \frac{28}{9}e^{(1)}_{4,1,1} - \frac{3}{2}e^{(1)}_{4,2,1} + \frac{4}{3}e^{(1)}_{5,1,1} + \frac{25}{18}e^{(1)}_{5,2,1} + \frac{92n_f}{27} + 82 \end{pmatrix}, \tag{3.55}$$

$$\gamma^{(3)}_{1,QQ} = \begin{pmatrix} 0 \\ -\frac{2}{3}n_f e^{(1)}_{4,1,1} + \frac{2}{9}n_f e^{(1)}_{5,1,1} + \frac{182}{9}e^{(1)}_{4,1,1} + \frac{2}{3}e^{(1)}_{4,2,1} - \frac{22}{3}e^{(1)}_{5,1,1} - \frac{2}{9}e^{(1)}_{5,2,1} - \frac{40n_f}{27} + \frac{116}{3} \\ -\frac{7}{9}n_f e^{(1)}_{4,1,1} - \frac{1}{3}n_f e^{(1)}_{5,1,1} + \frac{61}{6}e^{(1)}_{4,1,1} + \frac{7}{9}e^{(1)}_{4,2,1} + \frac{115}{18}e^{(1)}_{5,1,1} + \frac{1}{3}e^{(1)}_{5,2,1} - \frac{260n_f}{27} + \frac{422}{3} \end{pmatrix}. \tag{3.56}$$

For $\gamma_{1,QE}$ only few entries are non-zero. They are given by

$$\begin{aligned}
\gamma_{1,QE^{(1)}_1} &= \frac{2}{3}e^{(1)}_{2,1}n_f + \frac{10n_f}{3} - \frac{131}{6}e^{(1)}_{2,1} + 2e^{(1)}_{3,1} + \frac{5}{12}e^2_{1,1} + \frac{83}{2}, \\
\gamma_{1,QE^{(1)}_2} &= -\frac{n_f}{9} - \frac{7}{6}e^{(1)}_{2,1} + \frac{1}{3}e^{(1)}_{3,1} + \frac{133}{6}, \\
\gamma_{1,QE^{(1)}_3} &= \frac{n_f}{27} - \frac{1}{2}e^{(1)}_{2,1} - \frac{1}{9}e^{(1)}_{3,1} + \frac{71}{18}, \\
\gamma_{1,QE^{(2)}_1} &= -\frac{35}{96}, \\
\gamma_{1,QE^{(2)}_2} &= -\frac{77}{288}, \\
\gamma_{1,Q_S E^{(1)}_4} &= \frac{n_f}{9} - \frac{7}{6}e^{(1)}_{4,1,1} - e^{(1)}_{4,2,1} + \frac{7}{18}e^{(1)}_{5,1,1} + \frac{1}{3}e^{(1)}_{5,2,1} - \frac{79}{3}, \\
\gamma_{1,Q_S E^{(1)}_5} &= -\frac{n_f}{27} - \frac{1}{2}e^{(1)}_{4,1,1} + \frac{1}{3}e^{(1)}_{4,2,1} + \frac{1}{6}e^{(1)}_{5,1,1} - \frac{1}{9}e^{(1)}_{5,2,1} - \frac{41}{9}, \\
\gamma_{1,Q_S E^{(2)}_3} &= -\frac{77}{288}, \\
\gamma_{1,Q_S E^{(2)}_4} &= -\frac{35}{96}, \\
\gamma_{1,\tilde{Q}_S E^{(1)}_4} &= \frac{7n_f}{54} - \frac{49}{36}e^{(1)}_{4,1,1} - \frac{7}{6}e^{(1)}_{4,2,1} - \frac{7}{12}e^{(1)}_{5,1,1} - \frac{1}{2}e^{(1)}_{5,2,1} - \frac{1271}{36}, \\
\gamma_{1,\tilde{Q}_S E^{(1)}_5} &= \frac{n_f}{18} - \frac{7}{12}e^{(1)}_{4,1,1} + \frac{7}{18}e^{(1)}_{4,2,1} - \frac{1}{4}e^{(1)}_{5,1,1} + \frac{1}{6}e^{(1)}_{5,2,1} - \frac{11}{4}, \\
\gamma_{1,\tilde{Q}_S E^{(2)}_3} &= -\frac{5}{12}, \\
\gamma_{1,\tilde{Q}_S E^{(2)}_4} &= -\frac{1}{9}.
\end{aligned} \tag{3.57}$$

The transition operator U of eq. (3.45) can be computed by inserting this ADM into eq. (3.47). The alternative approach is to define the transition operator for effective operators:

$$\langle \mathcal{O} \rangle (\mu_1) \;=\; \widetilde{U}(\mu_1, \mu_2) \langle \mathcal{O} \rangle (\mu_2) \,. \tag{3.58}$$

The matrices U and $\widetilde{U}$ are related by

$$\widetilde{U}(\mu_1, \mu_2) \;=\; U^{-1}(\mu_1, \mu_2) \,. \tag{3.59}$$

The running of the three physical operators at $\mu_1 \sim \mu_2$ is given by

$$\begin{aligned} C_Q(\mu_1) \;=\; & C_Q(\mu_2) \Bigg\{ 1 - 4 \left(\frac{\alpha_s(\mu_2)}{4\pi} \right) \ln\left(\frac{\mu_1}{\mu_2} \right) \\ & + \left(\frac{\alpha_s(\mu_2)}{4\pi} \right)^2 \Bigg[\ln\left(\frac{\mu_1}{\mu_2} \right) \left(-\frac{2}{3} n_f e^{(1)}_{2,1} + \frac{2}{9} n_f e^{(1)}_{3,1} \right. \\ & \left. + 11 e^{(1)}_{2,1} - \frac{11}{3} e^{(1)}_{3,1} - \frac{20 n_f}{9} + \frac{109}{3} \right) \\ & + \left(52 - \frac{8 n_f}{3} \right) \ln^2\left(\frac{\mu_1}{\mu_2} \right) \Bigg] \Bigg\} , \end{aligned} \tag{3.60}$$

$$\begin{aligned} C_{Q_S}(\mu_1) \;=\; & C_{Q_S}(\mu_2) \Bigg\{ 1 + \frac{28}{3} \left(\frac{\alpha_s(\mu_2)}{4\pi} \right) \ln\left(\frac{\mu_1}{\mu_2} \right) \\ & + \left(\frac{\alpha_s(\mu_2)}{4\pi} \right)^2 \Bigg[\ln\left(\frac{\mu_1}{\mu_2} \right) \left(\frac{2}{3} n_f e^{(1)}_{4,2,1} - \frac{2}{9} n_f e^{(1)}_{5,2,1} \right. \\ & \left. - \frac{8}{3} e^{(1)}_{4,1,1} - \frac{92}{9} e^{(1)}_{4,2,1} + \frac{8}{9} e^{(1)}_{5,1,1} + 4 e^{(1)}_{5,2,1} - \frac{232 n_f}{27} + \frac{484}{3} \right) \\ & + \left(\frac{56 n_f}{9} - \frac{500}{9} \right) \ln^2\left(\frac{\mu_1}{\mu_2} \right) \Bigg] \Bigg\} \\ & + C_{\widetilde{Q}_S}(\mu_2) \Bigg\{ -\frac{4}{3} \left(\frac{\alpha_s(\mu_2)}{4\pi} \right) \ln\left(\frac{\mu_1}{\mu_2} \right) \\ & + \left(\frac{\alpha_s(\mu_2)}{4\pi} \right)^2 \Bigg[\ln\left(\frac{\mu_1}{\mu_2} \right) \left(\frac{2}{3} n_f e^{(1)}_{4,1,1} - \frac{2}{9} n_f e^{(1)}_{5,1,1} \right. \\ & \left. - \frac{182}{9} e^{(1)}_{4,1,1} - \frac{2}{3} e^{(1)}_{4,2,1} + \frac{22}{3} e^{(1)}_{5,1,1} + \frac{2}{9} e^{(1)}_{5,2,1} + \frac{40 n_f}{27} - \frac{116}{3} \right) \\ & + \left(\frac{140}{9} - \frac{8 n_f}{9} \right) \ln^2\left(\frac{\mu_1}{\mu_2} \right) \Bigg] \Bigg\} , \end{aligned} \tag{3.61}$$

$$\begin{aligned} C_{\widetilde{Q}_S}(\mu_1) \;=\; & C_{Q_S}(\mu_2) \Bigg\{ -\frac{16}{3} \left(\frac{\alpha_s(\mu_2)}{4\pi} \right) \ln\left(\frac{\mu_1}{\mu_2} \right) \\ & + \left(\frac{\alpha_s(\mu_2)}{4\pi} \right)^2 \Bigg[\ln\left(\frac{\mu_1}{\mu_2} \right) \left(\frac{7}{9} n_f e^{(1)}_{4,2,1} + \frac{1}{3} n_f e^{(1)}_{5,2,1} \right. \end{aligned}$$

$$
\begin{aligned}
&-\frac{28}{9}e^{(1)}_{4,1,1}+\frac{3}{2}e^{(1)}_{4,2,1}-\frac{4}{3}e^{(1)}_{5,1,1}-\frac{25}{18}e^{(1)}_{5,2,1}-\frac{92n_f}{27}-82\Bigg)\\
&+\left(\frac{560}{9}-\frac{32n_f}{9}\right)\ln^2\left(\frac{\mu_1}{\mu_2}\right)\Bigg]\Bigg\}\\
&+C_{\widetilde{Q}_S}(\mu_2)\Bigg\{1-\frac{32}{3}\left(\frac{\alpha_s(\mu_2)}{4\pi}\right)\ln\left(\frac{\mu_1}{\mu_2}\right)\\
&+\left(\frac{\alpha_s(\mu_2)}{4\pi}\right)^2\Bigg[\ln\left(\frac{\mu_1}{\mu_2}\right)\left(\frac{7}{9}n_f e^{(1)}_{4,1,1}+\frac{1}{3}n_f e^{(1)}_{5,1,1}\right.\\
&\left.-\frac{61}{6}e^{(1)}_{4,1,1}-\frac{7}{9}e^{(1)}_{4,2,1}-\frac{115}{18}e^{(1)}_{5,1,1}-\frac{1}{3}e^{(1)}_{5,2,1}+\frac{260n_f}{27}-\frac{422}{3}\right)\\
&+\left(\frac{1600}{9}-\frac{64n_f}{9}\right)\ln^2\left(\frac{\mu_1}{\mu_2}\right)\Bigg]\Bigg\}.
\end{aligned}
\tag{3.62}
$$

Although the evanescent operators are absent in the running, their definition affects the RGE-evolved coefficients through the $e^{(i)}_x$.

We observe that Wilson coefficients of evanescent operators do not mix into physical ones. This is a direct consequence of the renormalization scheme that we specified in section 2.4. To be more precise, the evanescent Wilson coefficients of the first two generations do not mix into physical coefficients at two-loop order. Since we only compute one-loop QCD corrections to the third generation operators, we see no mixing from $C_{E^{(3)}_i}$ at $\mathcal{O}(\alpha_s)$.

3.5 POWER SUPPRESSION OF R_0

In appendix C we show that the structure of R_0, as defined in eq. (3.4a), is twofold:

$$
R_0 = R_0^{\text{phys}} + E_{R_0}\,, \tag{3.63}
$$

where R_0^{phys} is the physical, $1/m_b$-suppressed operator. The evanescent operator E_{R_0} cannot be further specified and is given as a leading term in the $1/m_b$ expansion.

The non-specification of E_{R_0} is an issue if poles proportional to $\langle R_0\rangle$ appear. This becomes important in this section, where we analyze the power suppression of R_0 up to NNLO in α_s.

It is shown in ref. [65] that the matrix element of R_0, as it is stated in eq. (3.4a), is not $\mathcal{O}(\Lambda/m_b)$ at higher orders in α_s. To resolve this problem, ref. [47] introduces correction factors α_i according to

$$
\langle R_0\rangle \;=\; \frac{\alpha_Q}{2}\langle Q\rangle + \alpha_{Q_S}\langle Q_S\rangle + \alpha_{\widetilde{Q}_S}\langle \widetilde{Q}_S\rangle \;=\; \mathcal{O}\left(\frac{\Lambda}{m_b}\right). \tag{3.64}
$$

The α_i are perturbative objects and are defined in such a way that they restore the correct Λ/m_b scaling behavior of $\langle R_0\rangle$ at each order in α_s. Formally, eq. (3.64) can be obtained by introducing the α_i in the definition of R_0 as in ref. [47]. Alternatively, one could account for these corrections as finite renormalization factors and making

them thus part of the renormalization scheme. Since both approaches are equivalent, we simply define the matrix element $\langle R_0 \rangle$ by means of eq. (3.64).

The correction factors α_i are known to $\mathcal{O}(\alpha_s)$ and $\mathcal{O}(n_f \alpha_s^2)$ [47, 65, 68]. For our calculation of Γ_{12} the knowledge of the full $\mathcal{O}(\alpha_s^2)$ corrections is required. Thus, we can recover the correct scaling when removing one of the physical $\Delta B = 2$ operator matrix elements in favor of the suppressed $\langle R_0 \rangle$.

We can write the correction factors as

$$\alpha_i \;=\; \alpha_i^{(0)} + \left(\frac{\alpha_s}{4\pi}\right) \alpha_i^{(1)} + \left(\frac{\alpha_s}{4\pi}\right)^2 \alpha_i^{(2)} \,, \tag{3.65}$$

with the leading order result from appendix C,

$$\alpha_Q^{(0)} \;=\; \alpha_{Q_S}^{(0)} \;=\; \alpha_{\tilde{Q}_S}^{(0)} \;=\; 1 \,. \tag{3.66}$$

The tree-level relation of eq. (3.64) can always be used to remove one physical tree-level matrix element. Hence, one α_i can be chosen freely. We define

$$\alpha_{Q_S} \;\equiv\; 1 \,. \tag{3.67}$$

The further focus of this section is the computation of $\langle R_0 \rangle$ up to $\mathcal{O}(\alpha_s^2)$.

3.5.1 *One-Loop Corrections to α_Q and $\alpha_{\tilde{Q}_S}$*

To compute $\langle R_0 \rangle$ we consider the process $b\bar{s} \to \bar{b}s$. Furthermore, it is important to consider external on-shell particles, because the suppression of R_0 is only given in physical processes in which the HQE is valid. Since we are only interested in the leading order in the Λ/m_b expansion, the s-quark mass can be neglected, whereas for the b-quark we have $q_b^2 = m_b^2$. Hence, the simplest choice is $q_s = 0$ and $q \equiv q_b = (m_b, \vec{0})$.

The matrix elements of the B_s mixing process are infrared divergent at $\mathcal{O}(\alpha_s)$ and beyond. Due to the unknown structure of E_{R_0} in eq. (3.63), a computation in dimensional regularization where IR- and UV-poles are expressed in terms of the same regulator would lead to ambiguous results. Hence, we introduce a small gluon mass as an alternative IR regulator. The gluon propagator is then given by

$$iG_{\mu\nu}^{ab}(p) \;=\; \frac{i\delta_{ab}}{p^2 - m_g^2} \left(-g_{\mu\nu} + \xi \frac{p_\mu p_\nu}{p^2 - m_g^2} \right) . \tag{3.68}$$

Here we use a general R_ξ gauge, where Feynman-'t Hooft gauge is indicated by $\xi = 0$ and Lorenz gauge by $\xi = 1$. The Fadeev-Popov ghosts are kept massless. The mass m_g serves just as an ad hoc regulator in Feynman integrals. The Hamiltonian itself formally does not describe a massive gluon. Thus, we circumvent the problem of broken gauge symmetry, which becomes manifest in the three gauge boson coupling. Nevertheless, this ancillary mass receives a counterterm contribution as we will see later.

The NLO matrix element of R_0 is composed of tree-level and one-loop operator insertions:

$$\langle R_0 \rangle^{\text{NLO}} \equiv \langle R_0 \rangle^{\text{tree}} + \langle R_0 \rangle^{\text{1-loop}} . \tag{3.69}$$

The fermion fields are bare quantities in this relation. Thus, the tree-level amplitude is given by

$$\begin{aligned} \langle R_0 \rangle^{\text{tree}} &= Z_{2,s} Z_{2,b} \left(\frac{1}{2} \langle Q \rangle^{\text{tree}} + \langle Q_S \rangle^{\text{tree}} + \langle \widetilde{Q}_S \rangle^{\text{tree}} \right) \\ &= Z_{2,s} Z_{2,b} \sum_i \left(\frac{1}{2} Z_{Qi} + Z_{Q_S i} + Z_{\widetilde{Q}_S i} \right) \langle \mathcal{O}_i^0 \rangle^{\text{tree}} . \end{aligned} \tag{3.70}$$

The coefficients Z_{ij} are the renormalization constants of the effective operators, presented in section 3.3. Thus, evanescent operators of the first generation have to be considered in eq. (3.70) as well.

One can see that the $\mathcal{O}(\alpha_s^0)$ part of eq. (3.64) holds also for bare operator matrix elements:

$$\frac{1}{2} \langle Q^0 \rangle^{\text{tree}} + \langle Q_S^0 \rangle^{\text{tree}} + \langle \widetilde{Q}_S^0 \rangle^{\text{tree}} = \mathcal{O}\left(\frac{\Lambda}{m_b} \right) . \tag{3.71}$$

This can be used for one-loop corrections if they are expressed in terms of bare operator matrix elements. Schematically, the one-loop order result for $\langle R_0 \rangle$ is then given by

$$\begin{aligned} \langle R_0 \rangle^{\text{1-loop}} &= Z_{2,s} Z_{2,b} \left(\frac{1}{2} \langle Q \rangle^{\text{1-loop}} + \langle Q_S \rangle^{\text{1-loop}} + \langle \widetilde{Q}_S \rangle^{\text{1-loop}} \right) \\ &= \left(\frac{\alpha_s}{4\pi} \right) \left(a \langle Q^0 \rangle^{\text{tree}} + b \langle Q_S^0 \rangle^{\text{tree}} + c \langle \widetilde{Q}_S^0 \rangle^{\text{tree}} \right) \\ &\quad + \mathcal{O}(\epsilon) \\ &= \left(\frac{\alpha_s}{4\pi} \right) \left[\left(a - \frac{b}{2} \right) \langle Q^0 \rangle^{\text{tree}} + (c - b) \langle \widetilde{Q}_S^0 \rangle^{\text{tree}} \right] \\ &\quad + \mathcal{O}(\epsilon) . \end{aligned} \tag{3.72}$$

The coefficients a, b and c are $\mathcal{O}(\epsilon^0)$.

We renormalize the quark field in the $\overline{\text{MS}}$ scheme in which Z_2 is currently known to five-loop accuracy [107–109]. For our purposes we need

$$Z_2 = 1 + \left(\frac{\alpha_s}{4\pi\epsilon} \right) Z_2^{(1,1)} + \left(\frac{\alpha_s}{4\pi} \right)^2 \left(\frac{Z_2^{(2,1)}}{\epsilon} + \frac{Z_2^{(2,2)}}{\epsilon^2} \right) + \mathcal{O}(\alpha_s^3) , \tag{3.73}$$

with

$$\begin{aligned} Z_2^{(1,1)} &= C_F (\xi - 1) , \\ Z_2^{(2,1)} &= C_F \Big[+ \frac{3}{4} C_F - \frac{25}{8} C_A - (1 - \xi) C_A - \frac{1}{8} (1 - \xi)^2 C_A \\ &\quad + T_F n_f \Big] , \\ Z_2^{(2,2)} &= C_F \Big[\frac{3}{4} (1 - \xi) C_A + \frac{1}{2} (1 - \xi)^2 C_F + \frac{1}{4} (1 - \xi)^2 C_A \Big] . \end{aligned} \tag{3.74}$$

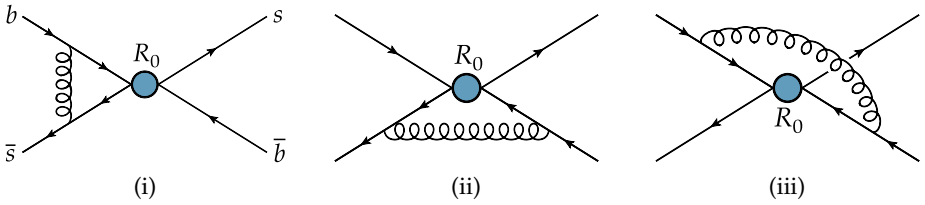

Figure 3.1: These sample Feynman diagrams contribute to $\langle R_0 \rangle^{\text{1-loop}}$.

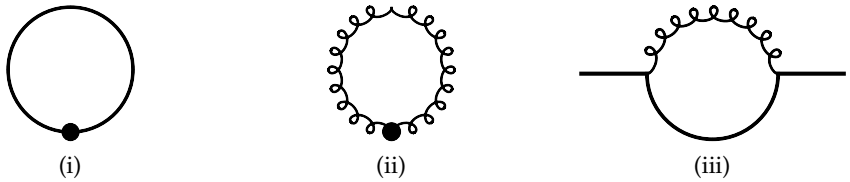

Figure 3.2: Only three master integrals remain after the reduction of $\langle R_0 \rangle^{\text{1-loop}}$. Solid lines denote denominators with the mass m_b, curly lines are associated with m_g.

The calculation of $\langle R_0 \rangle^{\text{1-loop}}$ includes the evaluation of diagrams as shown in fig. 3.1. For this we employ the setup described in chapter 5. In the following we focus only on the master integrals.

With the momenta of the s-quarks set to zero, only two-point On-Shell (OS) integrals with $q^2 = m_b^2$ occur. The one-loop problem reduces to three master integrals which are shown in fig. 3.2. The result for the massive tadpole integrals (i) and (ii) can be directly taken from e.g. [110]. The on-shell integral with two masses needs further analysis.

The integral of fig. 3.2iii has the following analytic form:

$$I = \int \frac{\mathrm{d}^d k}{\left(m_b^2 - (k+q)^2\right)\left(m_g^2 - k^2\right)} \,. \tag{3.75}$$

This integral can be solved with exact mass- and ϵ-dependence in terms of Gaußian hypergeometric functions. Nevertheless, the computation can be vastly simplified if we expand the result in the limit $m_g \ll m_b$. This scaling is allowed because we recover our original (infrared divergent) result in the limit $m_g \to 0$.

The expansion we apply is called *asymptotic expansion* and describes a formally non-convergent series. The advantage is that the expansion to a fixed order has a better convergence towards a limit point than a fixed order Laurent expansion. Thus, truncating the series at a certain order leads to a comparable scaling behavior as the original function with smaller deviations in comparison to a truncated Laurent series. For the purposes of Feynman integrals this expansion leads to additional logarithmic and fractional power scaling.

In eq. (3.75) we have $q^2 = m_b^2 \gg m_g^2$, which provides the possibility of a *threshold expansion* [111, 112]. We follow here ref. [113] which gives a comprehensive overview about asymptotic expansions in Feynman integrals. The procedure up to two-loop order is first applied in ref. [114], where also eq. (3.75) is considered as an example.

The easiest way to apply a threshold expansion is via the *method of regions*. It is defined as a splitting of integrals in different regions in which the loop momenta follow a certain scaling. After expanding the integrand accordingly, all separated integration regions are extended over the full momentum space. The final expansion is the sum of all these contributions. In eq. (3.75) we can find two regions, where the scaling $k \sim m_b$ is called *hard*, and $k \sim m_g$ is called *soft*.

The integral of the hard region is given by

$$I^{(h)} = \int \frac{\mathrm{d}^d k}{(m_b^2 - (k+q)^2)} \mathcal{T}_{m_g^2} \frac{1}{(m_g^2 - k^2)} . \tag{3.76}$$

The operator $\mathcal{T}_x$ describes a Laurent expansion in the limit $x \to 0$. To the quadratic term in m_g we get

$$\begin{aligned} I^{(h)} &= \int \frac{\mathrm{d}^d k}{(m_b^2 - (k+q)^2)(-k^2)} \\ &\quad - m_g^2 \int \frac{\mathrm{d}^d k}{(m_b^2 - (k+q)^2)(-k^2)^2} + \mathcal{O}\left(m_g^4\right) . \end{aligned} \tag{3.77}$$

The remaining integrals of eq. (3.77) can be directly solved as [110]

$$\begin{aligned} \frac{1}{\mathcal{N}} I^{(h)} &= \frac{1}{\epsilon} + 2 + \ln\left(\frac{\mu^2}{m_b^2}\right) - \frac{z_g}{2}\left[\frac{1}{\epsilon} - 2 + \ln\left(\frac{\mu^2}{m_b^2}\right)\right] \\ &\quad + \mathcal{O}(\epsilon) + \mathcal{O}\left(m_g^4\right) , \end{aligned} \tag{3.78}$$

with the normalization factor $\mathcal{N} = i\pi^{d/2}\mu^{-\epsilon}e^{-\epsilon\gamma_E}$ and the abbreviation $z_g \equiv m_g^2/m_b^2$.

Similarly, the soft region can be expressed as

$$\begin{aligned} I^{(s)} &= \int \frac{\mathrm{d}^d k}{(m_g^2 - k^2)} \mathcal{T}_{k^2} \frac{1}{(-k^2 - 2k\cdot q)} \\ &= \int \frac{\mathrm{d}^d k}{(m_g^2 - k^2)(-2k\cdot q)} - \int \frac{\mathrm{d}^d k\ (-k^2)}{(m_g^2 - k^2)(-2k\cdot q)^2} + \mathcal{O}\left(m_g^3\right) . \end{aligned} \tag{3.79}$$

The second term can be simplified by partial fraction decomposition. We make the following replacement in the numerator:

$$-k^2 = (m_g^2 - k^2) - m_g^2 . \tag{3.80}$$

The first term on the right-hand side cancels the mass-dependent denominator factor, leading to a scaleless integral which vanishes in dimensional regularization. Thus, the numerator of eq. (3.79) is simply replaced by $-m_g^2$.

The remaining integrals give the following result:

$$\frac{1}{\mathcal{N}} I^{(s)} = -\pi\sqrt{z_g} + \frac{z_g}{2}\left[\frac{1}{\epsilon} + \ln\left(\frac{\mu^2}{m_b^2}\right) - \ln(z_g)\right] + \mathcal{O}(\epsilon) + \mathcal{O}\left(m_g^3\right) . \tag{3.81}$$

By combining eqs. (3.78) and (3.81) we obtain

$$\frac{1}{\mathcal{N}} I \approx \frac{1}{\epsilon} + 2 + \ln\left(\frac{\mu^2}{m_b^2}\right) - \pi\sqrt{z_g} + z_g - \frac{z_g}{2}\ln(z_g) + \mathcal{O}(\epsilon) + \mathcal{O}\left(m_g^3\right), \tag{3.82}$$

which is in agreement with ref. [114]. The poles proportional to z_g, which appear in the individual regions, vanish in the sum. This is a basic feature of the asymptotic expansion, as it introduces new, spurious poles which only cancel in the sum of all regions.

In the Integration-by-Parts (IBP) reduction additional spurious infrared divergences may occur. For example, the integral I appears with a spurious factor of $1/m_g^2$ in $\langle R_0 \rangle^{\text{NLO}}$. Hence, it is necessary to compute also higher powers in z_g. After inserting the correct results for the master integrals, these inverse powers of z_g disappear.

With these master integrals we can finally evaluate $\langle R_0 \rangle^{\text{NLO}}$. By comparing the coefficients of the tree-level matrix elements $\langle Q^0 \rangle^{\text{tree}}$ and $\langle \tilde{Q}_S^0 \rangle^{\text{tree}}$, it is indeed possible to specify the NLO correction factors in such a way that the finite contributions of these matrix elements vanish. We get

$$\begin{aligned}
\alpha_Q^{\text{1-loop}} &= \frac{1}{2}e_{2,1}^{(1)} - \frac{1}{6}e_{3,1}^{(1)} + \frac{13}{12}e_{4,2,1}^{(1)} + \frac{1}{12}e_{5,2,1}^{(1)} + 4\ln\left(\frac{\mu^2}{m_b^2}\right) + \frac{4}{3}, \\
\alpha_{\tilde{Q}_S}^{\text{1-loop}} &= -\frac{13}{12}e_{4,1,1}^{(1)} + \frac{13}{12}e_{4,2,1}^{(1)} - \frac{1}{12}e_{5,1,1}^{(1)} + \frac{1}{12}e_{5,2,1}^{(1)} + 8\ln\left(\frac{\mu^2}{m_b^2}\right).
\end{aligned} \tag{3.83}$$

With the replacements of eq. (3.7), we get

$$\alpha_Q^{\text{1-loop}} = 4\ln\left(\frac{\mu^2}{m_b^2}\right) + \frac{26}{3}, \qquad \alpha_{\tilde{Q}_S}^{\text{1-loop}} = 8\ln\left(\frac{\mu^2}{m_b^2}\right) + 8, \tag{3.84}$$

which agrees with ref. [65] with full n_c-dependence. For $n_c = 3$, eq. (3.84) is also in accordance with ref. [47].

We observe that the individual coefficients a, b and c of eq. (3.72) contain additional IR poles of the form $\ln(\mu/m_g)$. These poles cancel when applying the relation of eq. (3.71). Additionally, to reduce terms with multiple Dirac matrices, leading order matrix elements of evanescent operators are introduced. Thus, terms of the form

$$\langle E \rangle^{\text{tree}} \ln(z_g) \tag{3.85}$$

remain which diverge for $z_g \to 0$. Since we have a clear splitting between IR- and UV-poles, it is possible to take the limit $\epsilon \to 0$ first. We then get an UV-safe quantity which is furthermore IR-safe.

Alternatively, using dimensional regularization for the calculation of $\langle R_0 \rangle^{\text{1-loop}}$ leads to terms of the form

$$\frac{\langle E \rangle^{\text{tree}}}{\epsilon_{\text{IR}}}, \tag{3.86}$$

which are formally finite for $\epsilon_{\text{IR}} = \epsilon_{\text{UV}} \equiv \epsilon$ and cannot be removed by the α_i. Furthermore, if the definition of $\langle E \rangle$ is changed by a $\mathcal{O}(\epsilon)$ term, the α_i differ from eq. (3.83).

3.5.2 *Two-Loop Corrections to α_Q and $\alpha_{\widetilde{Q}_S}$*

The determination of α_Q and $\alpha_{\widetilde{Q}_S}$ at NNLO ensures the correct power suppression of $\langle R_0 \rangle$ to $\mathcal{O}(\alpha_s^2)$. At this order we have to evaluate the renormalized amplitude

$$\langle R_0 \rangle^{\text{NNLO}} = \langle R_0 \rangle^{\text{tree}} + \langle R_0 \rangle^{\text{1-loop}} + \langle R_0 \rangle^{\text{2-loop}} . \tag{3.87}$$

The results for $\langle R_0 \rangle^{\text{1-loop}}$ have to be inserted up to $\mathcal{O}(\epsilon)$, since in combination with the renormalization constants, these terms contribute to $\mathcal{O}(\alpha_s^2 \epsilon^0)$. Furthermore, in $\langle R_0 \rangle^{\text{tree}}$ evanescent operators up to the second generation are needed for the renormalization.

In addition to the quark field, the renormalization of the b-quark mass must be taken into account. According to the Lehmann-Symanzik-Zimmermann (LSZ) theorem [115], the mass of the external b-field is identified as the OS mass, i.e. $q_b^2 = (m_b^{\text{OS}})^2$. This complies with the on-shell condition of the considered process. The corresponding renormalization constant is currently known to four-loop accuracy [116] and to three-loop with a second quark mass [117]. To order $\mathcal{O}(\alpha_s)$ it is given by

$$\begin{aligned} Z_{m_b}^{\text{OS}} &= 1 + \left(\frac{\alpha_s}{4\pi}\right) C_F \left\{ -\frac{3}{\epsilon} - 3\ln\left(\frac{\mu^2}{m_b^2}\right) - 4 \right. \\ &\quad \left. + \frac{\epsilon}{4}\left[-6\ln^2\left(\frac{\mu^2}{m_b^2}\right) - 16\ln\left(\frac{\mu^2}{m_b^2}\right) - \pi^2 - 32 \right] \right\} \\ &\quad + \mathcal{O}(\epsilon^2) + \mathcal{O}(\alpha_s^2) , \end{aligned} \tag{3.88}$$

where we use the notation $m_b \equiv m_b^{\text{OS}}$. This renormalization constant would in general be different when a massive gluon is considered. We explicitly checked that the α_i do not change with this altered $Z_{m_b}^{\text{OS}}$.

It turns out that a counterterm for the auxiliary gluon mass has to be introduced to remove all occurring poles. The gluon field- and mass-renormalization constants, Z_3, and Z_{m_g}, are defined in such way that the Green's function of the gluon self-energy is finite to all orders in perturbation theory. It is expected that Z_3 is the same as in regular QCD since the gluon mass is introduced as an ad-hoc IR regulator which does not affect the UV poles.

Including one-loop corrections, the renormalized gluon propagator is given by

$$iG_{\mu\nu} = \frac{1}{Z_3}\left(iG^0_{\mu\nu} + iG^0_{\mu\rho}\, i\Pi^{\rho\sigma}\, iG^0_{\sigma\nu} \right), \tag{3.89}$$

where we drop the color indices for simplicity.

The self-energy function $\Pi_{\mu\nu}$ can be separated into transversal (Π_T) and longitudinal (Π_L) parts:

$$i\Pi_{\mu\nu} \equiv i\delta_{ab}\left(\frac{\alpha_s}{4\pi}\right)\left[\left(g_{\mu\nu} - \frac{p_\mu p_\nu}{p^2} \right)\Pi_T(p^2) + \frac{p_\mu p_\nu}{p^2}\Pi_L(p^2) \right] . \tag{3.90}$$

For the bare gluon propagator, this splitting can also be applied as

$$\begin{aligned} iG^0_{\mu\nu} &= \frac{i\delta_{ab}}{p^2\left[p^2-(m_g^0)^2\right]}\left(-g_{\mu\nu}p^2+p_\mu p_\nu\right) \\ &\quad+\frac{i\delta_{ab}}{p^2\left[p^2-(m_g^0)^2\right]^2}\left[(m_g^0)^2+\left(\xi^0-1\right)p^2\right]p_\mu p_\nu\,, \end{aligned} \tag{3.91}$$

which is not transversal in Lorenz gauge ($\xi = 1$) due to the gluon mass. Similarly, the renormalized gluon propagator is separated according to

$$iG^{\mu\nu} \equiv i\left(g^{\mu\nu}-\frac{p^\mu p^\nu}{p^2}\right)G_T^{\mu\nu}(p^2)+i\frac{p^\mu p^\nu}{p^2}G_L^{\mu\nu}(p^2)\,. \tag{3.92}$$

The parameters ξ and m_g are renormalized with

$$\begin{aligned} (\xi^0-1) &= Z_3(\xi-1) = \left(1+\frac{\alpha_s}{4\pi}Z_3^{(1)}\right)(\xi-1)\,, \\ m_g^0 &= Z_{m_g}m_g = \left(1+\frac{\alpha_s}{4\pi}Z_{m_g}^{(1)}\right)m_g\,. \end{aligned} \tag{3.93}$$

The transversal and longitudinal parts, G_T and G_L, are renormalized independently. Up to $\mathcal{O}(\alpha_s)$ the transversal part is given by

$$\begin{aligned} iG_T(p^2) &= -\frac{i\delta_{ab}}{p^2-m_g^2} \\ &\quad-\left(\frac{\alpha_s}{4\pi}\right)\frac{i\delta_{ab}}{(p^2-m_g^2)^2}\left[Z_3^{(1)}(m_g^2-p^2)+2Z_{m_g}^{(1)}m_g^2+\Pi_T(p^2)\right], \end{aligned} \tag{3.94}$$

which in the limit $p^2 \gg m_g^2$ simplifies to

$$\begin{aligned} iG_T(p^2) &= -\frac{i\delta_{ab}}{p^4}\left(p^2+m_g^2\right) \\ &\quad+\left(\frac{\alpha_s}{4\pi}\right)\frac{i\delta_{ab}}{p^6}\Bigg\{p^4Z_3^{(1)}-p^2\Big(\Pi_T(p^2)\Big)_{m_g\to0} \\ &\quad+m_g^2\Bigg[p^2Z_3^{(1)}-2p^2Z_{m_g}^{(1)}-p^2\left(\frac{\mathrm{d}}{\mathrm{d}m_g^2}\Pi_T(p^2)\right)_{m_g\to0} \\ &\quad-2\Big(\Pi_T(p^2)\Big)_{m_g\to0}\Bigg]\Bigg\}+\mathcal{O}\left(m_g^4\right) \end{aligned} \tag{3.95}$$

Similarly, the longitudinal part is given in Feynman-'t Hooft gauge ($\xi = 0$) by

$$\begin{aligned} iG_L(p^2) &= \frac{i\delta_{ab}}{p^2-m_g^2}-\left(\frac{\alpha_s}{4\pi}\right)\frac{i\delta_{ab}}{(p^2-m_g^2)^2}\left[m_g^2(Z_3^{(1)}+2Z_{m_g}^{(1)})+\Pi_L(p^2)\right] \\ &\overset{p^2\gg m_g^2}{=} -\frac{i\delta_{ab}}{p^4}\left(p^2+m_g^2\right)-\left(\frac{\alpha_s}{4\pi}\right)\frac{i\delta_{ab}}{p^6}\Bigg\{p^2\Big(\Pi_L(p^2)\Big)_{m_g\to0} \\ &\quad+m_g^2\Bigg[p^2Z_3^{(1)}+2p^2Z_{m_g}^{(1)}+p^2\left(\frac{\mathrm{d}}{\mathrm{d}m_g^2}\Pi_L(p^2)\right)_{m_g\to0} \\ &\quad+2\Big(\Pi_L(p^2)\Big)_{m_g\to0}\Bigg]\Bigg\}+\mathcal{O}\left(m_g^4\right) \end{aligned} \tag{3.96}$$

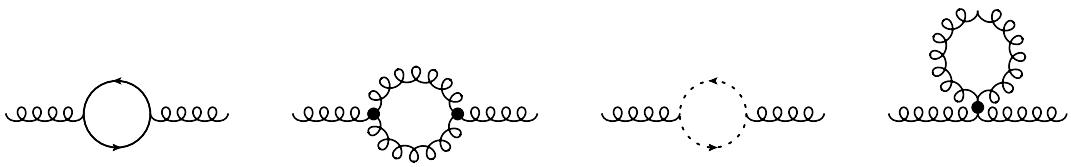

Figure 3.3: These diagrams contribute to the mass and field renormalization of the gluon at one-loop order. Note that the diagram with the four-gluon interaction does not vanish due to $m_g \neq 0$.

The limit $p^2 \gg m_g^2$ is allowed because the Green's function $G_{\mu\nu}$ is off-shell, and all renormalization constants in the $\overline{\text{MS}}$ scheme do not depend on the chosen kinematics of external particles.

The one-loop order contributions to $\Pi_{\mu\nu}$ are shown in fig. 3.3. For $p^2 \gg m_g^2$ the diagrams are evaluated using the large momentum expansion which is done with the program `exp` [118, 119]. The resulting Feynman integrals are either massive tadpoles or massless propagator-like integrals. Both can be evaluated in a highly automated way using the programs `MATAD` [102] and `MINCER` [120], respectively.

From the requirement that in eqs. (3.95) and (3.96) all divergences cancel, the renormalization constants in Feynman-'t Hooft gauge take the form

$$Z_3^{(1)} = \frac{1}{\epsilon}\left(\frac{5}{3}C_A - \frac{4}{3}n_f T_R\right), \tag{3.97}$$

$$Z_{m_g}^{(1)} = \frac{1}{\epsilon}\left(-\frac{19}{12}C_A + \frac{2}{3}n_f T_R\right). \tag{3.98}$$

The gluon field renormalization is in accordance with the $\overline{\text{MS}}$ result [109].

For the two-loop computation of $\langle R_0 \rangle^{\text{NNLO}}$, in total 1554 diagrams have to be evaluated. Sample diagrams are shown in fig. 6.9. As before, we use the computational setup described in chapter 5.

The topology reduction with `tapir` [121] leads to 91 independent Feynman graph topologies. Due to our special kinematics with $p_s = 0$, 1126 symbolic Feynman integral families appear after applying partial fraction decomposition. The integrated symbolic topology minimization of `tapir` reduces this number to 221 independent integral families.

After applying an IBP reduction with `FIRE` [122] the results are expressed as 25 master integrals. Two of them will appear in the matching calculation of Γ_{12} as shown in fig. 6.15. The remaining 23 are presented in fig. 3.4.

The integrals of figs. 3.4i, 3.4ii, 3.4v, 3.4vi and 3.4xiv are straightforward to compute since they are products of one-loop integrals. For the computation of the remaining master integrals a strategy similar to in the one-loop calculation is pursued. To apply a threshold expansion with $q^2 = m_b^2 \gg m_g^2$, we first have to identify all non-vanishing regions of loop momenta scaling. For this task we use the program `asy.m` [123]. For every input integral it returns a list of vectors which contain the scaling behavior of the propagators in the corresponding region. By applying shifts in the loop momenta, it is then possible to identify the individual regions in the momentum space representation of the integral.

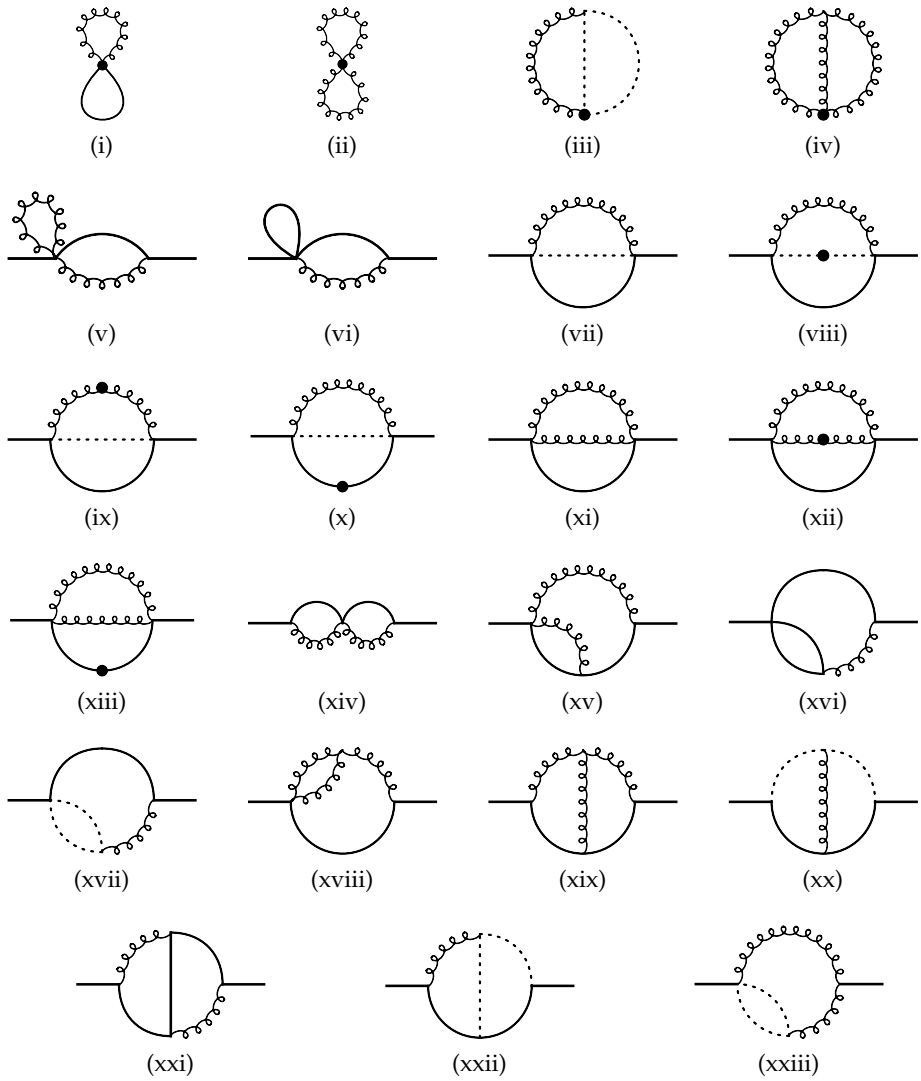

Figure 3.4: We show the master integrals which emerge after the IBP reduction of $\langle R_0 \rangle$ at NNLO. Solid lines denote propagators with mass m_b, curly lines with m_g and dashed lines are massless. A dot on a line means that the according propagator is squared.

Hence, each region introduces a new integral family. The expanded master integrals of fig. 3.4 can then be further reduced by an additional IBP reduction. This leads to simpler master integrals, partially without graph representation. These are either known, single scale, on-shell integrals [124], or can be evaluated straightforwardly using Feynman parameterization and the program `HyperInt` [125], or other common multi-loop techniques such as Mellin-Barnes representation (see e.g. ref. [110]). The evaluation with the former is explained in appendix D.5.

The α_i are again constrained by the fact that the finite part of $\langle R_0 \rangle^{\text{NNLO}}$ vanishes at leading order in the Λ/m_b expansion. We find that the individual NNLO matrix elements of Q, Q_S and $\widetilde{Q}_S$ are individually UV-finite in Feynman-'t Hooft gauge. Their IR-divergences are regulated by $\ln(z_g)$ terms which cancel in the combined $\langle R_0 \rangle^{\text{NNLO}}$. The results for the α_i as well as for $\langle Q \rangle^{\text{NNLO}}$, $\langle Q_S \rangle^{\text{NNLO}}$ and $\langle \widetilde{Q}_S \rangle^{\text{NNLO}}$ are given in the ancillary files of this thesis.

For the correction factors we find

$$
\begin{aligned}
\alpha_Q^{(2)} &= (n_l + n_h)\Big(-\frac{1}{36}e_{2,1}^{(1)} + \frac{1}{6}e_{2,2}^{(1)} + \frac{1}{108}e_{3,1}^{(1)} - \frac{1}{18}e_{3,2}^{(1)} - \frac{13}{216}e_{4,2,1}^{(1)} \\
&\quad + \frac{13}{36}e_{4,2,2}^{(1)} - \frac{1}{216}e_{5,2,1}^{(1)} + \frac{1}{36}e_{5,2,2}^{(1)} - \frac{4L^2}{3} - \frac{52L}{9} - \frac{8\pi^2}{9} - \frac{22}{3}\Big) \\
&\quad + n_h\Big(\frac{8\pi^2}{3} - 8\Big) + \frac{17\pi^2}{3} + \frac{1183}{24} + \frac{16}{3}\pi^2\ln(2) \\
&\quad + 2Le_{2,1}^{(1)} - \frac{2}{3}Le_{3,1}^{(1)} + 9Le_{4,2,1}^{(1)} + \frac{7}{3}Le_{5,2,1}^{(1)} - \frac{1}{24}(e_{2,1}^{(1)})^2 \\
&\quad + \frac{169}{144}(e_{4,2,1}^{(1)})^2 + \frac{1}{144}(e_{5,2,1}^{(1)})^2 + \frac{125}{24}e_{2,1}^{(1)} - \frac{167}{24}e_{2,2}^{(1)} - \frac{5}{24}e_{2,1}^{(1)}e_{3,1}^{(1)} \\
&\quad + \frac{55}{72}e_{3,1}^{(1)} + \frac{7}{72}e_{3,2}^{(1)} - \frac{26}{9}e_{4,1,2}^{(1)} + \frac{13}{24}e_{2,1}^{(1)}e_{4,2,1}^{(1)} - \frac{13}{72}e_{3,1}^{(1)}e_{4,2,1}^{(1)} \\
&\quad + \frac{809}{48}e_{4,2,1}^{(1)} - \frac{877}{72}e_{4,2,2}^{(1)} - \frac{2}{9}e_{5,1,2}^{(1)} + \frac{1}{24}e_{2,1}^{(1)}e_{5,2,1}^{(1)} - \frac{1}{72}e_{3,1}^{(1)}e_{5,2,1}^{(1)} \\
&\quad + \frac{13}{72}e_{4,2,1}^{(1)}e_{5,2,1}^{(1)} + \frac{31}{16}e_{5,2,1}^{(1)} + \frac{47}{72}e_{5,2,2}^{(1)} - \frac{35}{384}e_{1,1}^{(2)} + \frac{5}{48}e_{1,2}^{(2)} \\
&\quad - \frac{77e_{2,1}^{(2)}}{1152} + \frac{11}{144}e_{2,2}^{(2)} + \frac{197e_{3,2,1}^{(2)}}{1152} - \frac{37}{288}e_{3,2,2}^{(2)} + \frac{137e_{4,2,1}^{(2)}}{1152} \\
&\quad - \frac{97}{288}e_{4,2,2}^{(2)} - 8\zeta(3) + \frac{58L^2}{3} + \frac{83L}{2},
\end{aligned}
\tag{3.99}
$$

$$
\begin{aligned}
\alpha^{(2)}_{\bar{Q}_S} &= (n_l+n_h)\Big(\frac{13}{216}e^{(1)}_{4,1,1}-\frac{13}{36}e^{(1)}_{4,1,2}-\frac{13}{216}e^{(1)}_{4,2,1}+\frac{13}{36}e^{(1)}_{4,2,2}+\frac{1}{216}e^{(1)}_{5,1,1}\\
&\quad-\frac{1}{36}e^{(1)}_{5,1,2}-\frac{1}{216}e^{(1)}_{5,2,1}+\frac{1}{36}e^{(1)}_{5,2,2}-\frac{8L^2}{3}-\frac{104L}{9}-\frac{16\pi^2}{9}-\frac{374}{27}\Big)\\
&\quad+n_h\Big(\frac{16\pi^2}{3}-16\Big)+\frac{320\pi^2}{27}+\frac{871}{9}+\frac{32}{3}\pi^2\ln(2)\\
&\quad-\frac{14}{3}Le^{(1)}_{4,1,1}+\frac{40}{3}Le^{(1)}_{4,2,1}-2Le^{(1)}_{5,1,1}+\frac{8}{3}Le^{(1)}_{5,2,1}+\frac{169}{144}(e^{(1)}_{4,2,1})^2\\
&\quad+\frac{1}{144}(e^{(1)}_{5,2,1})^2-\frac{2219}{144}e^{(1)}_{4,1,1}+\frac{161}{8}e^{(1)}_{4,1,2}-\frac{169}{144}e^{(1)}_{4,1,1}e^{(1)}_{4,2,1}\\
&\quad+\frac{2219}{144}e^{(1)}_{4,2,1}-\frac{275}{24}e^{(1)}_{4,2,2}-\frac{13}{144}e^{(1)}_{4,2,1}e^{(1)}_{5,1,1}-\frac{263}{144}e^{(1)}_{5,1,1}\\
&\quad-\frac{1}{24}e^{(1)}_{5,1,2}-\frac{13}{144}e^{(1)}_{4,1,1}e^{(1)}_{5,2,1}+\frac{13}{72}e^{(1)}_{4,2,1}e^{(1)}_{5,2,1}-\frac{1}{144}e^{(1)}_{5,1,1}e^{(1)}_{5,2,1}\\
&\quad+\frac{263}{144}e^{(1)}_{5,2,1}+\frac{17}{24}e^{(1)}_{5,2,2}-\frac{197e^{(2)}_{3,1,1}}{1152}+\frac{37}{288}e^{(2)}_{3,1,2}+\frac{197e^{(2)}_{3,2,1}}{1152}\\
&\quad-\frac{37}{288}e^{(2)}_{3,2,2}-\frac{137e^{(2)}_{4,1,1}}{1152}+\frac{97}{288}e^{(2)}_{4,1,2}+\frac{137e^{(2)}_{4,2,1}}{1152}-\frac{97}{288}e^{(2)}_{4,2,2}\\
&\quad-16\zeta(3)+\frac{188L^2}{3}+\frac{388L}{3}\,,
\end{aligned}
\tag{3.100}
$$

with $L=\ln(\mu^2/m_b^2)$ and $\zeta(z)$ being the Riemann zeta function which is given by

$$
\zeta(z) \;=\; \sum_{n=1}^{\infty}\frac{1}{z^n}\,, \tag{3.101}
$$

with the function value

$$
\zeta(3) \;\approx\; 1.20206\,. \tag{3.102}
$$

The symbol n_h gives the number of quarks with the mass m_b. The number of massless flavors is denoted by n_l.

An arbitrary choice for the evanescent coefficients which is in accordance with the literature is given by

$$
\begin{aligned}
e^{(1)}_{2,1} &= -4\,, & e^{(1)}_{2,2} &= -4\,, & e^{(1)}_{3,1} &= -4\,, & e^{(1)}_{3,2} &= -4\,,\\
e^{(1)}_{4,2,1} &= 8\,, & e^{(1)}_{4,2,2} &= 0\,, & e^{(1)}_{4,1,1} &= 0\,, & e^{(1)}_{4,1,2} &= 4\,,\\
e^{(1)}_{5,2,1} &= 0\,, & e^{(1)}_{5,2,2} &= 4\,, & e^{(1)}_{5,1,1} &= 8\,, & e^{(1)}_{5,1,2} &= 0\,,\\
e^{(2)}_{1,1} &= 0\,, & e^{(2)}_{1,2} &= -\frac{52}{5}\,, & e^{(2)}_{2,1} &= 0\,, & e^{(2)}_{2,2} &= 4\,,\\
e^{(2)}_{3,2,1} &= 0\,, & e^{(2)}_{3,2,2} &= 266\,, & e^{(2)}_{3,1,1} &= 0\,, & e^{(2)}_{3,1,2} &= 284\,,\\
e^{(2)}_{4,2,1} &= 0\,, & e^{(2)}_{4,2,2} &= -88\,, & e^{(2)}_{4,1,1} &= 0\,, & e^{(2)}_{4,1,2} &= \frac{932}{5}\,.
\end{aligned}
\tag{3.103}
$$

With eq. (3.103) the correction factors read

$$
\begin{aligned}
\alpha^{(2)}_{Q} &= (n_l+n_h)\left(-\frac{4L^2}{3}-\frac{52L}{9}-\frac{8\pi^2}{9}-\frac{218}{27}\right)+n_h\left(\frac{8\pi^2}{3}-8\right)\\
&\quad+\frac{58L^2}{3}+\frac{649L}{6}+\frac{17\pi^2}{3}+\frac{11183}{48}+\frac{16}{3}\pi^2\ln(2)-8\zeta(3)\,,
\end{aligned}
\tag{3.104}
$$

$$\begin{aligned}\alpha_{\tilde{Q}_S}^{(2)} &= (n_l + n_h)\left(-\frac{8L^2}{3} - \frac{104L}{9} - \frac{16\pi^2}{9} - \frac{422}{27}\right) + n_h\left(\frac{16\pi^2}{3} - 16\right) \\ &\quad + \frac{188L^2}{3} + 220L + \frac{320\pi^2}{27} + \frac{326047}{720} + \frac{32}{3}\pi^2\ln(2) - 16\zeta(3)\,.\end{aligned} \tag{3.105}$$

Equations (3.104) and (3.105) are in accordance with ref. [68] where only terms proportional to n_h and n_l are given at NNLO, but additionally with a non-vanishing c-quark mass dependence. Thus, the results are complementary.

4

MATCHING CALCULATION

The effective field theories of chapters 2 and 3 contain effective couplings which describe interactions only correctly at certain energies. The renormalization constants which are defined in section 2.5 not only render our theory UV-finite over this valid energy range, but also introduce a renormalization scale μ. As we have seen, the latter can be chosen such that the occurring logarithms do not lead to large corrections in the perturbative series. Therefore, μ is usually set to the typical energy scale of the problem at hand. In the EFT picture it can hence take values of the range in which the theory leads to useful predictions. In perturbative QCD, for example, μ can be formally used in the range $(\Lambda_{\text{QCD}}, E_P]$ since we treat QCD as a UV-complete theory. No matter if the upper bound is actually the Planck energy E_P or not, QCD has become the empirically established theory of the experimentally accessible subset of this energy range. It is therefore treated as our "full theory" for interactions of particles depending on their color charges.

The basic requirement on an EFT is that it predicts the same results as the full theory in the limit where both are valid. The procedure to connect the different theories is called *matching*. Relevant for this work is the connection of the $\Delta B = 1$ theory to the SM. The scale μ_0 at which both theories agree is denoted as *matching scale*. Renormalized, amputated Green's functions with same external states are then computed in both theories and one demands that they agree at μ_0:

$$\left\langle f\right| \mathcal{S}^{\text{SM}} \left|i\right\rangle^{\text{ren}} \Big|_{\mu=\mu_0} \stackrel{!}{=} \left\langle f\right| \mathcal{S}^{\Delta B=1} \left|i\right\rangle^{\text{ren}} \left(1 + \mathcal{O}\left(1/m_W^2\right)\right) \Big|_{\mu=\mu_0} . \tag{4.1}$$

The resulting Wilson coefficients $C_i(\mu_0)$ are then extended to the whole valid energy regime through RGE techniques.

The HQE, as described in section 1.3, is an operator product expansion that marks the transition from one EFT to another. Thus, for the computation of Γ_{12} the following matching calculation at the scale μ_1 is applied:

$$\begin{aligned} \Gamma_{12} &= \frac{1}{2M_B} \text{Abs}\left(i \int \mathrm{d}^4 x \ \left\langle B\right| \mathbf{T} \mathcal{H}^{\Delta B=1}(x) \mathcal{H}^{\Delta B=1}(0) \left|\overline{B}\right\rangle \right) \Big|_{\mu=\mu_1} \\ &\stackrel{!}{=} \left\langle B\right| \mathcal{H}^{\Delta B=2}(0) \left|\overline{B}\right\rangle \Big|_{\mu=\mu_1} , \end{aligned} \tag{4.2}$$

where the Wilson coefficients of the $\Delta B = 2$ Hamiltonian are replaced by Γ_{12}-specific matching coefficients H_i. Using the operators of eq. (3.3), we obtain

$$\Gamma_{12} = \frac{G_F m_b^2}{24\pi M_B} \sum_i H_i(\mu_1) \left\langle B\right| \mathcal{O}_i^{\Delta B=2} \left|\overline{B}\right\rangle (\mu_1) + \Gamma_{1/m_b} . \tag{4.3}$$

The matching coefficients H_i include the leading effects in the Λ/m_b expansion, whereas the higher orders are denoted by Γ_{1/m_b}. With the RGE running of section 3.4, the resulting $\Delta B = 2$ operator matrix elements can be expressed at a different scale μ_2. This scale can later be chosen as the point where the hadronic matrix elements are evaluated by non-perturbative calculations. In the end, the $\Delta B = 2$ matching coefficients have the following structure:

$$H_i \equiv H_i\big(C_j(\mu_0,\mu_1),\mu_1,\mu_2\big), \tag{4.4}$$

where C_j denotes the $\Delta B = 1$ Wilson coefficients.

A look at eq. (4.2) reveals that it involves the bound states $|B\rangle$ and $|\overline{B}\rangle$, which cannot be fully described as local quark field operators in perturbation theory. It is anyway possible to access H_i if the final states are replaced, in first approximation, by their valence quark fields, i.e. $|B_s\rangle \to |\bar{b}s\rangle$, $|\overline{B}_s\rangle \to |b\bar{s}\rangle$ and $|B_d\rangle \to |\bar{b}d\rangle$, $|\overline{B}_d\rangle \to |b\bar{d}\rangle$. The matching equation simplifies to a comparison of local matrix elements describing the process $b\bar{s} \to \bar{b}s$ or $b\bar{d} \to \bar{b}d$

$$\frac{1}{2M_B}\mathrm{Abs}\left(i\mathcal{M}^{\Delta B=1}_{\mathrm{ren}}\right)\Big|_{\mu=\mu_1} \overset{!}{=} i\mathcal{M}^{\Delta B=2}_{\mathrm{ren}}\Big|_{\mu=\mu_1}. \tag{4.5}$$

Both sides entail quark field renormalizations which cancel in the direct comparison. It is nevertheless beneficial to work with UV-finite quantities, because the corresponding regulator can then be set to zero before the actual matching. This simplifies in general the whole procedure as evanescent operators are no concern.

Since in this work we focus solely on the matching of leading terms of the Λ/m_b expansion, the momenta of the external s-quarks (or respective d-quark) can be chosen as $q_{s/d} = 0$. Furthermore, the physical process is sensitive to the b-quark mass, but the matching coefficients do not depend on the three-momentum of the b. Thus, together with the on-shell condition $q_b^2 = m_b^2$, the easiest choice is $q_b = (m_b, \vec{0})^T$.

Note that the matrix elements of eq. (4.5) are IR divergent. As described in section 3.5, one possibility to regularize the divergences is to include a small gluon mass m_g into our Feynman integrals. This has the advantage of a simplified matching calculation as the limit $\epsilon \to 0$ can be taken after the renormalization. Since both sides of eq. (4.5) have by construction the same low energy behavior, the gluon mass dependence drops out, and H_i becomes independent of the chosen IR-regulator. The disadvantages of this approach are the appearance of more involved Feynman integrals since we introduce an additional scale. Also, the implications of the gauge breaking that come with a gluon mass may effect the UV-renormalization procedure, as discussed in section 3.5.2.

Another approach is pursued in refs. [91, 126] where both IR and UV divergences are regulated dimensionally. Hence, the matching must be performed in d dimensions. Due to the presence of IR poles, this implies that evanescent parts of the matrix elements contribute to the finite result. Thus, Wilson coefficients of evanescent operators have to be considered on both sides of eq. (4.5), and coefficients of physical operators are extended to include terms of higher order in ϵ. In the following we describe this approach in more detail.

At leading order there are no IR divergences and the two sides of eq. (4.5) are schematically given by

$$\begin{aligned}\frac{1}{2M_B}\text{Abs}\left(i\mathcal{M}^{\text{LO},\Delta B=1}\right) &= \left(a^{(0,0)}+a^{(0,1)}\epsilon\right)\langle Q\rangle^{\text{tree}} \\ &\quad+\left(b^{(0,0)}+b^{(0,1)}\epsilon\right)\langle E\rangle^{\text{tree}}+\mathcal{O}(\epsilon^2)\,, \end{aligned} \tag{4.6}$$

$$\frac{i}{2M_B}\mathcal{M}^{\text{LO},\Delta B=2} = H_Q^{(0)}\langle Q\rangle^{\text{tree}}+H_E^{(0)}\langle E\rangle^{\text{tree}}+\mathcal{O}(\epsilon^2)\,, \tag{4.7}$$

where we used the following parameterization for the $\Delta B=2$ Wilson coefficients:

$$H_i = 2M_B\left(H_i^{(0)}+\frac{\alpha_s}{4\pi}H_i^{(1)}\right)+\mathcal{O}(\alpha_s^2)\,. \tag{4.8}$$

The terms $\langle Q\rangle^{\text{tree}}$ and $\langle E\rangle^{\text{tree}}$ indicate tree-level matrix elements of physical and evanescent $\Delta B=2$ operators, and the coefficients a and b are finite. Comparing the coefficients of the matrix elements in eqs. (4.6) and (4.7) gives for the $\Delta B=2$ Wilson coefficients

$$H_Q^{(0)} = a^{(0,0)}+a^{(0,1)}\epsilon+\mathcal{O}(\epsilon^2)\,, \qquad H_E^{(0)} = b^{(0,0)}+b^{(0,1)}\epsilon+\mathcal{O}(\epsilon^2)\,. \tag{4.9}$$

Including $\mathcal{O}(\alpha_s)$ effects, the UV-renormalized matrix elements on the $\Delta B=1$ side read

$$\begin{aligned}\frac{1}{2M_B}\text{Abs}\left(i\mathcal{M}^{\text{NLO},\Delta B=1}\right)\Big|_{\alpha_s} &= \frac{\alpha_s}{4\pi}\left[\left(\frac{a^{(1,-1)}}{\epsilon}+a^{(1,0)}\right)\langle Q\rangle^{\text{tree}}\right. \\ &\quad\left.+\left(\frac{b^{(1,-1)}}{\epsilon}+b^{(1,0)}\right)\langle E\rangle^{\text{tree}}\right] \\ &\quad+\mathcal{O}(\epsilon)\,, \end{aligned} \tag{4.10}$$

where only $\mathcal{O}(\alpha_s)$ terms are considered. The coefficients $a^{(1,-1)}$ and $b^{(1,-1)}$ describe the IR poles which appear at this order for the first time. Similarly, for the $\Delta B=2$ matrix element we obtain

$$\begin{aligned}\frac{i}{2M_B}\mathcal{M}^{\text{NLO},\Delta B=2}\Big|_{\alpha_s} &= \frac{\alpha_s}{4\pi}\left[H_Q^{(1)}\langle Q\rangle^{\text{tree}}+H_E^{(1)}\langle E\rangle^{\text{tree}}\right. \\ &\quad+\left(\frac{c^{(1,-1)}}{\epsilon}+c^{(1,0)}\right)H_Q^{(0)}\langle Q\rangle^{\text{tree}} \\ &\quad+\left(\frac{d^{(1,-1)}}{\epsilon}+d^{(1,0)}\right)H_Q^{(0)}\langle E\rangle^{\text{tree}} \\ &\quad+e^{(1,0)}H_E^{(0)}\langle Q\rangle^{\text{tree}} \\ &\quad\left.+\left(\frac{f^{(1,-1)}}{\epsilon}+f^{(1,0)}\right)H_E^{(0)}\langle E\rangle^{\text{tree}}\right]+\mathcal{O}(\epsilon)\,. \end{aligned} \tag{4.11}$$

The first two terms stem from the LO amplitude, whereas in the remainder are one-loop corrections of physical and evanescent operators. Except for the mixing

of the evanescent into physical matrix elements (denoted by the prefactor e), the one-loop terms are IR divergent.

In order to determine $H_Q^{(1)}$ we have to compare the coefficients of $\langle Q \rangle^{\text{tree}}$ in both eqs. (4.10) and (4.11). We obtain

$$H_Q^{(1)} = \frac{a^{(1,-1)} - c^{(1,-1)} H_Q^{(0)}}{\epsilon} + a^{(1,0)} - c^{(1,0)} H_Q^{(0)} - e^{(1,0)} H_E^{(0)} , \tag{4.12}$$

which is IR-save if the following holds:

$$a^{(1,-1)} = c^{(1,-1)} H_Q^{(0)} + \mathcal{O}(\epsilon) . \tag{4.13}$$

From the contributions of $H_Q^{(0)}$ and $H_E^{(0)}$ to eq. (4.12), it is clear that the LO coefficients $b^{(0,0)}$ and $a^{(0,1)}$ become relevant due to eq. (4.9). Although the knowledge of $H_E^{(0)}$ is apparently needed for $H_Q^{(1)}$, physical results must not depend on the chosen evanescent operators. Thus, their contribution is an artifact of the chosen IR regularization. Since our renormalization condition requires $\langle E \rangle = \mathcal{O}(\epsilon_{\text{UV}})$, the multiplication with a dimensionally regularized IR pole makes this object finite. In the end, IR artifacts in eq. (4.12) are canceled by $H_E^{(0)}$ and the $\mathcal{O}(\epsilon)$ terms of $H_Q^{(0)}$. The same applies to the $\Delta B = 1$ side, where evanescent contributions are included in $a^{(1,0)}$ of eq. (4.10). Thus, the dependence on the Wilson coefficients of the evanescent $\Delta B = 1$ operators should cancel in this procedure, contributing only to H_E but not to H_Q.

Compared to using a gluon mass as IR regulator, a drawback of the d-dimensional matching procedure is that at $\mathcal{O}(\alpha_s^2)$ it requires the knowledge of renormalized terms up to $\mathcal{O}(\epsilon^2)$ at LO and up to $\mathcal{O}(\epsilon)$ at NLO. Nevertheless, the calculation of the Feynman integrals is substantially simplified in comparison to the case with $m_g \neq 0$.

For the matching we choose the physical operator basis of Q, Q_S and $\widetilde{Q}_S$ and the evanescent operators of eqs. (3.6) and (3.8) to (3.10). Anticipating the discussion in section 5.2, the fourth generation of evanescent operators are necessary since on the $\Delta B = 1$ side, structures with up to $9 \otimes 9$ Dirac matrices occur. Although these operators do not contribute to the matching calculation of the physical operators, they are needed for the reduction of Dirac matrix chains.

The matching of eq. (4.5) is performed up to $\mathcal{O}(\alpha_s^2)$. Additionally, a single Next-to-Next-to-Next-to-Leading Order (N^{3}LO) contribution is regarded which is $\mathcal{O}(\alpha_s^3)$. It consists of two-loop corrections to the double insertion of the chromomagnetic operator P_8. Since every occurrence of P_8 is proportional to α_s, it is possible to rescale the according Wilson coefficient by

$$C_8 \to \widetilde{C}_8 = \left(\frac{\alpha_s}{4\pi}\right)^{-1} C_8 . \tag{4.14}$$

Hence, with $\widetilde{C}_8$ both sides of the matching include a maximum order of α_s^2. The correct contribution is recovered if we return afterwards to the usual definition of C_8.

As a final result of the matching, we obtain

$$\begin{aligned}\Gamma_{12} \;=\; & \frac{G_F m_b^2}{24\pi M_B}\Big[H\,\langle Q\rangle^{\text{NNLO}}(\mu_2) + H_S\,\langle Q_S\rangle^{\text{NNLO}}(\mu_2) + \widetilde{H}_S\,\langle \widetilde{Q}_S\rangle^{\text{NNLO}}(\mu_2) \\ & + \sum_i H_{E_i}(\mu_1)\,\langle E_i\rangle^{\text{NNLO}}(\mu_2)\Big] \;+\; \Gamma_{1/m_b}\,.\end{aligned} \tag{4.15}$$

Since all UV and IR poles are absent at this point, we are allowed to put all regulators to zero. Thus, the matrix elements of the evanescent operators vanish.

Equation (4.15) can be further simplified if we account for the power scaling of the $\mathcal{O}(\Lambda/m_b)$-operator R_0. With the results of section 3.5 we get

$$\begin{aligned}\Gamma_{12} \;=\; & \frac{G_F m_b^2}{24\pi M_B}\Bigg[\left(H - \frac{\alpha_Q}{2}H_S\right)\langle Q\rangle^{\text{NNLO}}(\mu_2) \\ & + \left(\widetilde{H}_S - \alpha_{\widetilde{Q}_S}H_S\right)\langle \widetilde{Q}_S\rangle^{\text{NNLO}}(\mu_2)\Bigg] \;+\; \mathcal{O}\left(\frac{\Lambda}{m_b}\right).\end{aligned} \tag{4.16}$$

According to ref. [47] using the basis $\{Q\,,\widetilde{Q}_S\,,R_0\}$ has a positive effect on the Λ/m_b expansion since the numerical size of Γ_{1/m_b} is reduced in comparison to the previously used basis $\{Q\,,Q_S\,,R_0\}$ [65]. Also, the uncertainties from the bag parameters are decreased in the ratio $\Delta\Gamma/\Delta M$.

Part II

CALCULATION OF $\Delta\Gamma$ AND a_{FS}

5

TECHNICALITIES

In this chapter we focus on the technical aspects of the calculation of Γ_{12}. We start with a detailed summary of the evaluation of Feynman diagrams which contribute to Γ_{12}. We then turn to the topic of tensor reduction and how it is employed in our setup. Finally, we present the renormalization constants which are additionally needed to render Γ_{12} UV-finite.

5.1 DETAILS ABOUT THE CALCULATION OF Γ_{12}

For the calculation we use the program toolchain as described in appendix D.1. The overall amount of computed one-, two- and three-loop Feynman diagrams is $\mathcal{O}(140,000)$, as it is described in chapter 6 in more detail. All diagrams are generated with the use of `qgraf` [127] of which we also employ the implemented filter options to remove unwanted diagrams. Other diagrams such as the one shown in fig. 5.1 are not straightforward to select solely with `qgraf`. For this we employ the diagram filter functionality of `tapir` [121] with the option `external_self_energy_bridge_mixing`.

After all diagrams are generated, we use `tapir` to analyze their topological structure. As described in appendix D.2 this is done by generating the according Nickel index of every diagram. After comparison these indices, the set of unique topologies are used to generate according "topology files" which are used in our setup to express scalar integral expressions in terms of integral families. For the $\Delta B = 1$ computation without taking any other mass except for m_b into account, we get 12 one-loop topologies, 260 at two-loop and 141 at three-loop order. The number for the two-loop topologies is increased due to the fact that penguin operators introduce a large variety of possible topological structures, whereas current-current operators only have a restricted variety. The contributions with two insertions of the latter are the only considered three-loop diagrams in this work. On the $\Delta B = 2$ side, we have three one-loop and 15 two-loop topologies.

The overall amount of 413 integral families for $\Delta B = 1$ is further reduced to 77 if we employ the algebraic minimization routines of `tapir`. Similarly, for $\Delta B = 2$ the number of integral families reduces from 18 to 9. With the specification of the integral families, we create the input files for `FIRE` [122].

Returning to the individual diagrams, we use `tapir` to insert the according Feynman rules to create `FORM` [128] readable expressions. The respective momenta of the lines in the diagram are then mapped on the corresponding topology using the program `exp` [118, 119]. With our `calc` setup we express the amplitude, as the sum of all diagrams, in terms of the previously defined integral families. The individual integral members are then reduced to master integrals using an IBP reduction procedure with `FIRE` which is described in appendix D.4. Only three

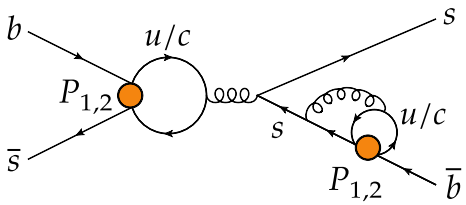

Figure 5.1: A sample three-loop diagram which is easy to separate from other diagrams with corrections to external legs, using a diagram filter which is implemented in `tapir`.

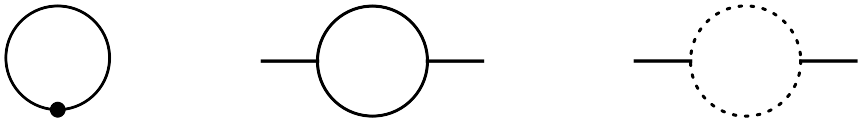

Figure 5.2: At one-loop order three master integrals emerge after the IBP reduction. Solid lines denote denominators with a mass m_b, dashed lines are massless.

master integrals occur at one-loop order, as shown in fig. 5.2. At two-loop order, we obtain the 14 master integrals of fig. 5.3 which are known in the literature for several years [124]. The three-loop amplitude leads to 27 master integrals which are computed by ref. [129] using either the program `HyperInt` [125] or `MINCER` [120]. They are depicted in fig. 5.4. In appendix D.5 the procedure of computing master integrals with `HyperInt` is further discussed.

5.2 TENSOR REDUCTION

A topic that has not yet been covered concerns the tensor structure of Feynman diagrams. In this section we present a straightforward way to handle tensor structures in Lorentz- and color space without computing tensor integrals for interactions with external fermions.

A matrix element of the process $b\bar{s} \to \bar{b}s$ can in general be written as

$$\mathcal{M} \;=\; \sum_{m,n} X^{(m,n)}\, \Sigma^{(m)}_{i_1 i_2 i_3 i_4}\, \Gamma^{(n)}_{s_1 s_2 s_3 s_4}\, \bar{s}^{i_1}_{s_1}\, b^{i_2}_{s_2}\, \bar{s}^{i_3}_{s_3}\, b^{i_4}_{s_4}\,. \tag{5.1}$$

Each term has a distinct splitting of color indices i_n and spinor indices s_n. The coefficients X are scalar expressions with respect to the spinor- and color space. Thus, all Lorentz- and color indices in X are contracted which also holds before evaluating the loop integrals. The goal of a *tensor reduction* is to find the these coefficients X.

The Lorentz structure can take only a limited set of possible forms. They read

$$\Gamma^{(n)}_{s_1 s_2 s_3 s_4} \;=\; \left(P_R B^{(n)}\right)_{s_1 s_2} \left(P_R B^{(n)}\right)_{s_3 s_4} \;\equiv\; \left(P_R B^{(n)}\right) \otimes \left(P_R B^{(n)}\right) \tag{5.2}$$

with

$$B^{(n)} \;\in\; \left\{\mathbb{1},\; \gamma^{\mu_1},\; \gamma^{\mu_1}\gamma^{\mu_2},\; \gamma^{\mu_1}\gamma^{\mu_2}\gamma^{\mu_3}, \ldots\right\}. \tag{5.3}$$

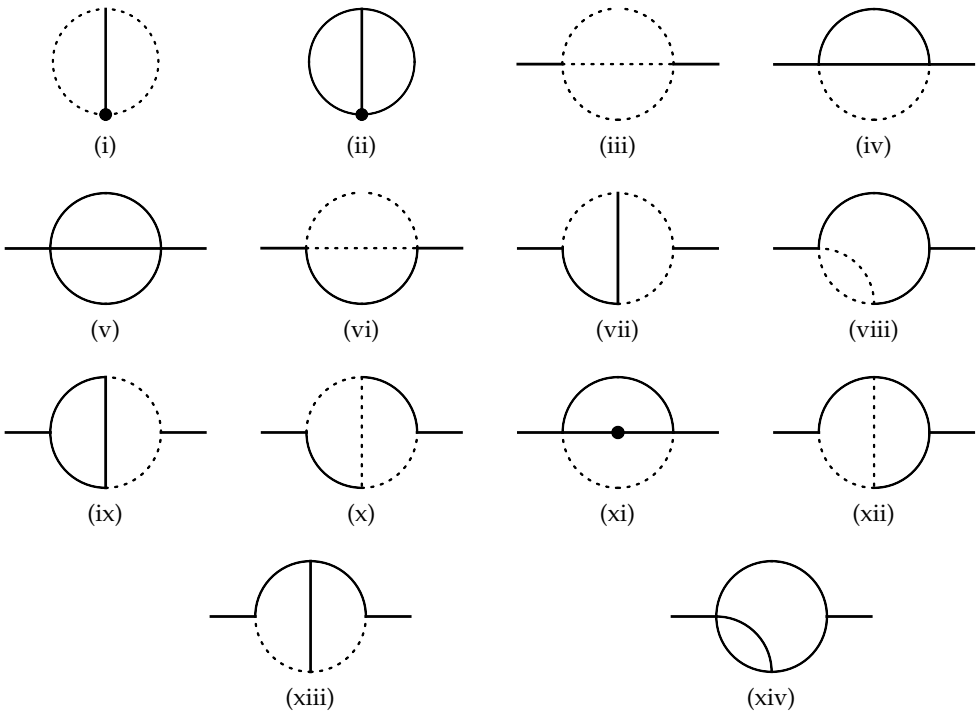

Figure 5.3: These two-loop master integrals arise from the $\Delta B = 1$ and $\Delta B = 2$ calculation of Γ_{12}. Hence, real and imaginary part must be determined. A dot on a line denotes an additional power of the respective denominator.

In four space-time dimensions, this set is reduced to a finite subset to all orders in perturbation theory due to relations such as Fierz identities. This reduction is not possible for $d = 4 - 2\epsilon$. However, at a fixed order in perturbation theory eq. (5.3) is also finite, but with an increased cardinality.

The number of possible color structures is always finite in dimensional regularization. In our case it can only be the following:

$$\Sigma^{(m)} \in \left\{ \delta_{i_1 i_2}\delta_{i_3 i_4},\ \delta_{i_1 i_4}\delta_{i_2 i_3} \right\}. \tag{5.4}$$

The coefficients X can be extracted from eq. (5.1) by defining a projection operator $\mathbf{P}$ as

$$X^{(m,n)} = \mathbf{P}^{(m,n)} \mathcal{M}. \tag{5.5}$$

Since color space and Lorentz space are independent, the corresponding projectors factorize:

$$\mathbf{P}^{(m,n)} = \mathbf{C}^{(m)} \mathbf{L}^{(n)}. \tag{5.6}$$

For the color projector we can make the following ansatz:

$$\mathbf{C}^{(m)} = \sum_i c^{(m,i)} \Sigma^{(i)}. \tag{5.7}$$

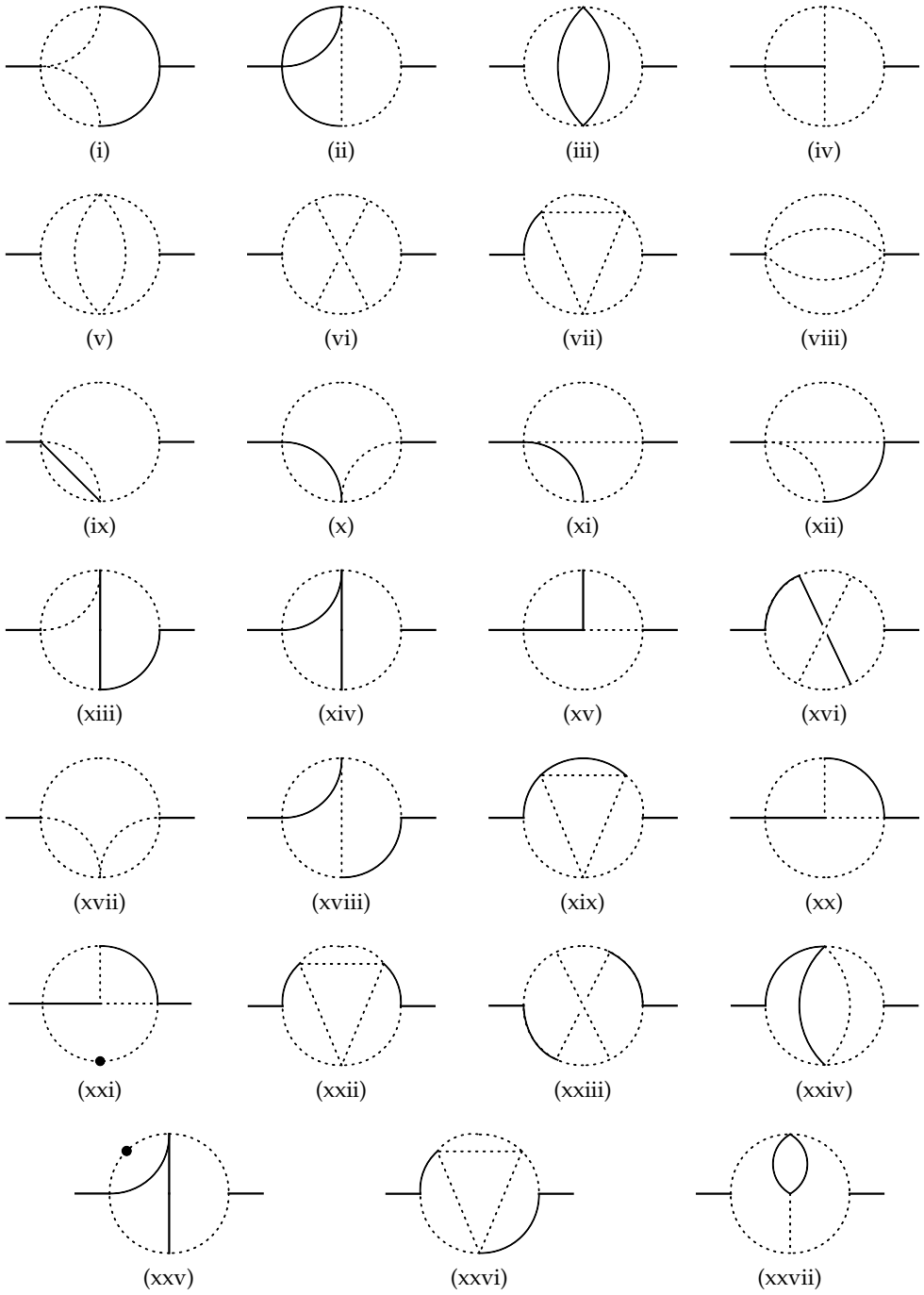

Figure 5.4: At three-loop order, the depicted master integrals emerge. All of them are evaluated with `HyperInt`. Although only the imaginary part contributes to Γ_{12}, the real parts are calculated as well.

The coefficients c are determined by the condition

$$\begin{aligned} X_C^{(m)} &\stackrel{!}{=} \mathbf{C}^{(m)} \mathcal{M}_\mathcal{C} \\ &= \mathbf{C}^{(m)} \left(\sum_i X_C^{(i)} \Sigma^{(i)} \right) \\ &\stackrel{(5.7)}{=} \sum_{i,j} X_C^{(i)} c^{(m,j)} \Sigma^{(j)} \Sigma^{(i)} \,. \end{aligned} \tag{5.8}$$

Thus,

$$\begin{aligned} \delta_{ij} &\stackrel{!}{=} c^{(i,k)} \Sigma^{(k)} \Sigma^{(j)} \;\equiv\; c^{(i,k)} \mathbb{G}_{kj} \left(\{\Sigma^{(m)}\} \right) \\ \Rightarrow \qquad c^{(i,j)} &= \mathbb{G}^{-1}_{ij} \left(\{\Sigma^{(m)}\} \right) , \end{aligned} \tag{5.9}$$

where $\mathbb{G}$ denotes the *Gram matrix* of the vector space spanned by $\{\Sigma^{(m)}\}$. The scalar product of the latter is a simple multiplication with same color indices in both basis vectors $\Sigma^{(m)}$. For the basis of eq. (5.4) we get

$$c^{(i,j)} \;=\; \begin{pmatrix} \left(\Sigma^{(1)}\right)^2 & \Sigma^{(1)}\Sigma^{(2)} \\ \Sigma^{(1)}\Sigma^{(2)} & \left(\Sigma^{(2)}\right)^2 \end{pmatrix}^{-1}_{ij} \;=\; \frac{1}{n_c^2 - 1} \begin{pmatrix} 1 & -\frac{1}{n_c} \\ -\frac{1}{n_c} & 1 \end{pmatrix}_{ij} . \tag{5.10}$$

In principle one could also construct the projector from a different set of basis vectors $\{v_i\}$. For this purpose, the Gram matrix is extended to two vector spaces:

$$\mathbb{G}_{ij}(\{a_k\}, \{b_k\}) \;=\; \langle a_i | b_j \rangle \,, \tag{5.11}$$

where $\langle \cdot | \cdot \rangle$ describes the scalar product.

The constraints on the new basis are (see e.g. ref. [130]):

- $\det\left[\mathbb{G}(\{v_i\})\right] \neq 0$,
- $\operatorname{rank}\left[\mathbb{G}(\{v_i\})\right] \geq \operatorname{rank}\left[\mathbb{G}(\{\Sigma_i\})\right]$.

A non-vanishing Gram determinant is equivalent to linear independence of the vectors v_i and to the matrix having a full rank. The same must also hold for the vectors $\{\Sigma_i\}$ on which we want to project. The matrix $\mathbb{G}$ is invertible if the ranks are equal in the second condition.

Thus, using a higher dimensional vector space to build the projector is possible as well. If the rank of the new basis is larger, the matrix spanned by $c^{(i,j)}$ is

$$c \;\in\; \mathbb{C}^{\operatorname{rank}[\mathbb{G}(\{\Sigma_i\})] \times \operatorname{rank}[\mathbb{G}(\{v_i\})]} \,, \tag{5.12}$$

and for the Gram matrix follows:

$$\operatorname{rank}(c) \;=\; \operatorname{rank}\Big[\mathbb{G}\left(\{\Sigma_i\}, \{v_i\}\right)\Big] \;=\; \operatorname{rank}\Big[\mathbb{G}\left(\{\Sigma_i\}\right)\Big] \,. \tag{5.13}$$

Also, the inverse of eq. (5.9) is replaced by the Moore-Penrose inverse [131, 132]:

$$\mathbb{G}^{-1}\left(\{\Sigma_i\}, \{v_i\}\right) \;\equiv\; \Big[\mathbb{G}^*\left(\{\Sigma_i\}, \{v_i\}\right) \mathbb{G}\left(\{\Sigma_i\}, \{v_i\}\right)\Big]^{-1} \mathbb{G}^*\left(\{\Sigma_i\}, \{v_i\}\right) \,, \tag{5.14}$$

which is the definition of a left-inverse, i.e.

$$\mathbb{G}^{-1}\left(\{\Sigma_i\},\{v_i\}\right)\mathbb{G}\left(\{\Sigma_i\},\{v_i\}\right) \;=\; \mathbb{1}_{\text{rank}[\mathbb{G}(\{\Sigma_i\})]}\,. \tag{5.15}$$

A similar procedure can be applied for the Lorentz-projector. First, we have to define how the projector $\mathbf{L}$ of eq. (5.6) acts on a matrix element:

$$\begin{aligned}\mathbf{L}^{(n)}\mathcal{M}_L \;&=\; \mathbf{L}^{(n)}\left(\sum_i X_L^{(i)} B^{(i)}\otimes B^{(i)}\right)\\ &\equiv\; \sum_{i,j} l^{(n,j)} X_L^{(i)} \text{Tr}_d\left(L_1^{(n)}B^{(i)}\right)\text{Tr}_d\left(L_2^{(n)}B^{(i)}\right)\,,\end{aligned} \tag{5.16}$$

where the traces are taken in the four-dimensional spinor space with d-dimensional Dirac matrices. Equation (5.16) also defines the scalar product of this space. With this definition, traces with γ_5 can arise in chiral interactions. This can be circumvented if an additional chiral projector is included in L:

$$P_{\text{R/L}} \;=\; \frac{\mathbb{1}\pm\gamma_5}{2}\,. \tag{5.17}$$

After projecting the left- or right-handed chirality by commuting all occurrences of γ_5 together, all remaining γ_5 in the traces of the Lorentz projector can be dropped. Thus, we can adjust eq. (5.16) according to

$$\widetilde{\mathbf{L}}^{(n)}\mathcal{M}_L \;\equiv\; \sum_{i,j} l^{(n,j)} X_L^{(i)} \text{Tr}_d\left(L_1^{(n)}B^{(i)}\Big|_{\gamma_5\to 0}\right)\text{Tr}_d\left(L_2^{(n)}B^{(i)}\Big|_{\gamma_5\to 0}\right)\,. \tag{5.18}$$

The chirality is not particularly relevant for our case since every basis vector of eqs. (5.2) and (5.3) renders the s-quark left-handed and its chirality does not change due to our treatment of $m_s = 0$. Thus, the chirality is neglected in the following.

An ansatz for $L_{1/2}^{(n)}$ is again given by the already known basis vectors:

$$L_1^{(n)}\otimes L_2^{(n)} \;\equiv\; B^{(n)}\otimes B^{(n)}\,. \tag{5.19}$$

As before, the coefficients $l^{(n,i)}$ are determined from the requirement

$$\begin{aligned}X_L^{(n)} \;&\overset{!}{=}\; \widetilde{\mathbf{L}}^{(n)}\mathcal{M}_L\\ &\overset{(5.19)}{=}\; \sum_{i,j} X_L^{(i)} l^{(n,j)} \underbrace{\text{Tr}_d\left(B^{(j)}B^{(i)}\Big|_{\gamma_5\to 0}\right)\text{Tr}_d\left(B^{(j)}B^{(i)}\Big|_{\gamma_5\to 0}\right)}_{\equiv\,\mathbb{G}_{ji}}\,,\end{aligned} \tag{5.20}$$

where we use the abbreviation $\mathbb{G}_{ji}\equiv\mathbb{G}_{ji}\left(\{B^{(i)}\otimes B^{(i)}\}\right)$. The projector coefficients are again given by the inverse of the Gram matrix:

$$l^{(i,j)} \;=\mathbb{G}_{ij}^{-1}\,. \tag{5.21}$$

A simple example of the Lorentz projector method is shown by means of the integral

$$I \;=\; \int \frac{\mathrm{d}^d k}{(2\pi)^d}\,\frac{\not{k}}{k^2(k-p)^2}\,, \tag{5.22}$$

where p is an external momentum. For the basis of possible Lorentz structures we make the ansatz

$$B^{(n)} \in \left\{\mathbb{1},\ \not{p}\right\}. \tag{5.23}$$

Since there is only a single spinor line, the Gram matrix is given by

$$\mathbb{G} = \begin{pmatrix} \mathrm{Tr}_d(\mathbb{1}) & \mathrm{Tr}_d(\not{p}) \\ \mathrm{Tr}_d(\not{p}) & \mathrm{Tr}_d(\not{p}\not{p}) \end{pmatrix} = \begin{pmatrix} 4 & 0 \\ 0 & 4p^2 \end{pmatrix}. \tag{5.24}$$

For the projector coefficients, it follows

$$l^{(i,j)} = \mathbb{G}^{-1}_{ij} = \begin{pmatrix} \frac{1}{4} & 0 \\ 0 & \frac{1}{4p^2} \end{pmatrix}_{ij}. \tag{5.25}$$

Thus, the Lorentz-projector has the form

$$L_{\mathbb{1}} = \frac{\mathbb{1}}{4}, \qquad L_{\not{p}} = \frac{\not{p}}{4p^2}. \tag{5.26}$$

One can see that the basis vectors do not have to be of the same mass dimension. If we apply the constructed projector on eq. (5.22), we obtain

$$\begin{aligned} I &= \mathbb{1} \cdot \mathrm{Tr}_d(L_{\mathbb{1}} I) \ + \ \not{p} \cdot \mathrm{Tr}_d\big(L_{\not{p}} I\big) \\ &= \frac{\not{p}}{p^2} \int \frac{\mathrm{d}^d k}{(2\pi)^d} \frac{k\cdot p}{k^2 (k-p)^2}. \end{aligned} \tag{5.27}$$

For the integral I the basis $\{\not{p}\}$ would already be sufficient. However, we see from the discussion below eq. (5.10) that projectors with a larger vector basis are always applicable to problems with a smaller subset.

For the calculation of Γ_{12} we have in addition the external b-quark momentum q. Thus, from the integrals a $\not{q}$ can appear in the chain of Dirac matrices which usually drops out by using the Dirac equation. Because the latter cannot be applied at this step, $\not{q}$ must also be considered in the projection. Hence, the basis of eqs. (5.2) and (5.3) cannot be used, and we have to define an alternative which is given by

$$\begin{aligned} B_1^{(n)} \otimes B_2^{(n)} \in \Big\{ & \mathbb{1}\otimes\mathbb{1},\ \mathbb{1}\otimes\not{q},\ \not{q}\otimes\mathbb{1},\ \not{q}\otimes\not{q}, \\ & \gamma^{\mu_1}\otimes\gamma_{\mu_1},\ \gamma^{\mu_1}\otimes\gamma_{\mu_1}\not{q},\ \gamma^{\mu_1}\not{q}\otimes\gamma_{\mu_1},\ \gamma^{\mu_1}\not{q}\otimes\gamma_{\mu_1}\not{q}, \\ & \gamma^{\mu_1}\gamma^{\mu_2}\otimes\gamma_{\mu_1}\gamma_{\mu_2},\ \gamma^{\mu_1}\gamma^{\mu_2}\otimes\gamma_{\mu_1}\gamma_{\mu_2}\not{q},\ \gamma^{\mu_1}\gamma^{\mu_2}\not{q}\otimes\gamma_{\mu_1}\gamma_{\mu_2}, \\ & \gamma^{\mu_1}\gamma^{\mu_2}\not{q}\otimes\gamma_{\mu_1}\gamma_{\mu_2}\not{q},\ \dots \Big\}, \end{aligned} \tag{5.28}$$

In order to fix the basis, it is important to know the longest string of occurring Dirac matrices. For our problem we find diagrams shown in fig. 5.5 to have the largest string simultaneously in both spinor lines. In principle, diagrams with a single fermion line with more Dirac matrices are possible, as shown in fig. 5.5iii. In that case, the Lorentz indices inside a single chain are contracted and can be reduced. For example, fig. 5.5iii reduces to $3\otimes 3$ matrices. Thus, diagrams with

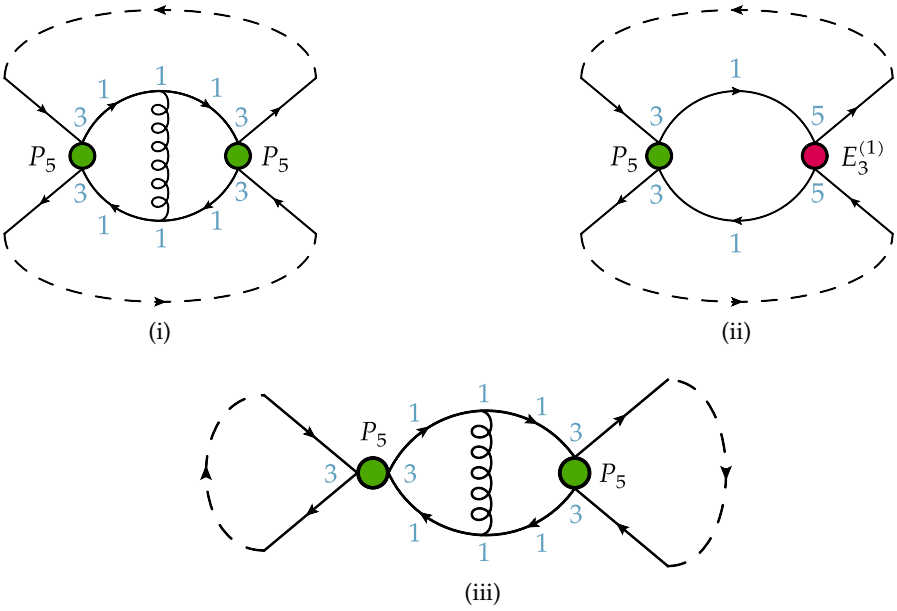

Figure 5.5: Diagrams (i) and (ii) lead to an overall maximum of $9 \otimes 9$ Dirac matrices in the two fermion lines if the traces are closed according to the dashed lines. The penguin operator P_5 introduces three Dirac matrices per line, the fermion propagators and gluon interaction vertices another one, respectively. In (ii) the evanescent operator $E_3^{(1)}$ includes five matrices which leads to $9 \otimes 9$ already at LO. In diagram (iii) Dirac chains with $3 \otimes 15$ matrices occur.

equally distributed Dirac matrices in both fermion lines are considered for the limiting case.

The diagram in figs. 5.5i and 5.5ii lead to a maximum of $9 \otimes 9$ matrices. For possible future applications, we implement the possibility to project on up to $10 \otimes 10$ matrices. The cardinality of the basis thus becomes[1] 43. Projecting only on up $9 \otimes 9$ matrices would involve a basis with 39 vectors. The computation of the Gram matrix as in eq. (5.20) includes the evaluation of terms of the form

$$\mathrm{Tr}_d(\gamma^{\mu_1}\gamma^{\mu_2}\dots\gamma^{\mu_{20}})\,\mathrm{Tr}_d(\gamma_{\mu_1}\gamma_{\mu_2}\dots\gamma_{\mu_{20}})\ , \tag{5.29}$$

which is challenging even for a specialized computer algebra system like `FORM` [128].

For our calculation, one frequently encounters structures like eq. (5.29) with a maximum of 18×18 matrices when applying the projection operator. To circumvent an expensive recalculation of these traces every time, we build a lookup table of `FORM` `id`-statements which replaces the traces by a previously evaluated quantity. `id`-statements have the advantage that the property of traces to be symmetric under cyclic permutation can be used for the identification. We can also benefit from the pattern-matching of `FORM`. After evaluating all Feynman diagrams of chapter 6, our lookup table includes $\mathcal{O}(380,000)$ entries and has a size of $\mathcal{O}(400)$ MB.

1 The 11 strings of $\mathbb{1} \otimes \mathbb{1}, \dots, \gamma_{\mu_1-\mu_{10}} \otimes \gamma^{\mu_1-\mu_{10}}$ are counted four times due to the different occurrences of q. The case $\gamma_{\mu_1-\mu_{10}} q \otimes \gamma^{\mu_1-\mu_{10}} q$ is excluded since it has $11 \otimes 11$ matrices.

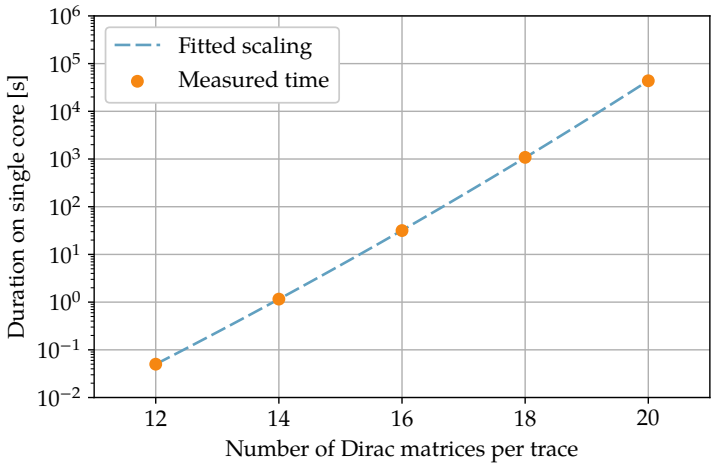

Figure 5.6: The computation of eq. (5.29) needs approximately 12 h on one core of a modern CPU. The double exponential scaling predicts for the evaluation of traces with 22×22 matrices a duration of 617 CPU Hours, or 26 days on a single core. This estimation demonstrates a lower limit for parallelized evaluation with e.g. `tform`.

The traces are computed with the consecutive use of the `tracen` command of `FORM`. For products of long traces the needed computation time rises approximately exponentially with the number of matrices, as shown in fig. 5.6.

This scaling behavior makes it increasingly difficult to project to basis elements with an increasing number Dirac matrices. With the presented techniques and current soft- and hardware, the projection on more than 10 matrices in both fermion lines is not feasible. Alternative approaches to increase this limit could be:

- Usage of a different tool than `tracen`. A promising approach based on graph coloring algorithms is presented in ref. [133]. Unfortunately, it is only formulated in four dimensions and an extension to d-dimensional Dirac matrices would be necessary.
- Usage of a different scalar product than eq. (5.20). An alternative would be, for example:

$$\mathbb{G}'_{ij} \;=\; \mathrm{Tr}_d\left(B^{(i)} B^{(j)} B^{(i)} B^{(j)} \Big|_{\gamma_5 \to 0} \right) . \tag{5.30}$$

  In our case this would result in one large trace with a maximum of 40 Dirac-matrices, but with all indices contracted.
- Usage of other tensor reduction approaches such as Passarino–Veltman reduction [134]. This ansatz is used in the cross-check calculation of this work, where we use the program `FeynCalc` [135] with additional support of `FERMAT` [136] to perform the tensor reduction. Unfortunately, this leads to other problems like a proliferation of terms for high tensor ranks.

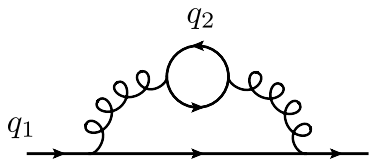

Figure 5.7: OS quark field and mass renormalization constants are sensitive to other quark masses starting at two-loop order.

5.3 RENORMALIZATION

We have seen in chapter 4 that the matrix elements on both sides of the matching have to be renormalized. In this section we summarize the used renormalization constants in addition to the ones already described in sections 2.5 and 3.3.

The external quarks of the regarded process $\bar{s}b \to \bar{b}s$ usually require a wave function renormalization. The constant Z_2 factorizes on both sides of the matching equation eq. (4.5). However, we introduce it for convenience according to eqs. (3.73) and (3.74).

Since we compute the matrix elements in arbitrary R_ξ gauge, the gauge parameter ξ has to be renormalized according to eq. (2.32) up to $\mathcal{O}(\alpha_s)$ with

$$Z_3 = 1 + \left(\frac{\alpha_s}{4\pi\epsilon}\right)\left(\frac{5}{3}C_A + \frac{\xi}{2}C_A - \frac{4}{3}n_f T_F\right), \tag{5.31}$$

defined in $\overline{\text{MS}}$.

To the same order we need the renormalization of the QCD coupling constant which is given by

$$Z_{\alpha_s} = 1 + \left(\frac{\alpha_s}{4\pi\epsilon}\right)\left(-\frac{11}{3}C_A + \frac{4}{3}n_f T_F\right). \tag{5.32}$$

Equations (5.31) and (5.32) are both directly applicable to theories with n_f active quark flavors since renormalization constants are mass-independent in $\overline{\text{MS}}$. Both renormalization constants are currently known up to five-loop order [104, 105].

We further need the renormalization of the b-quark mass to $\mathcal{O}(\alpha_s)$. In this calculation we choose the OS mass renormalization, as given in eq. (3.88). Z_{m_b} is mass dependent in this scheme and also sensitive to the masses of other quarks through diagrams shown in fig. 5.7. Since this dependence first occurs at $\mathcal{O}(\alpha_s^2)$, $Z_{m_b}^{\text{OS}}$ can be used as stated in eq. (3.88).

For a non-vanishing charm-mass, Z_{m_c} is needed to $\mathcal{O}(\alpha_s^2)$ since the leading order diagrams on the $\Delta B = 1$ side of the matching are m_c dependent. In the OS scheme this renormalization constant, expanded for $m_c \ll m_b$, is given by [117, 137]

$$\begin{aligned} Z_{m_c}^{\text{OS}} &= 1 + \left(\frac{\alpha_s}{4\pi}\right)\left\{-\frac{4}{\epsilon} - 4\ln\left(\frac{\mu^2}{m_c^2}\right) - \frac{16}{3}\right. \\ &\quad \left. + \epsilon\left[-2\ln^2\left(\frac{\mu^2}{m_c^2}\right) - \frac{16}{3}\ln\left(\frac{\mu^2}{m_c^2}\right) - \frac{\pi^2}{3} - \frac{32}{3}\right]\right\} \\ &\quad + \left(\frac{\alpha_s}{4\pi}\right)^2\left\{\frac{1}{\epsilon^2}\left(30 - \frac{4n_f}{3}\right) + \frac{1}{\epsilon}\left[16\ln\left(\frac{\mu^2}{m_c^2}\right) + \frac{10n_f}{9} - \frac{37}{3}\right]\right. \end{aligned}$$

$$
\begin{aligned}
&+ n_f \left[\frac{4}{3} \ln^2\left(\frac{\mu^2}{m_c^2}\right) + \frac{52}{9} \ln\left(\frac{\mu^2}{m_c^2}\right) + \frac{8\pi^2}{9} + \frac{71}{9} \right] \\
&+ n_h \left[\frac{463 z^2}{2450} - \frac{2}{315}\left(27z^2 + 112z - 910\right) \ln(z) + \frac{304z}{225} \right. \\
&\left. - \frac{4\ln^2(z)}{3} - \frac{8\pi^2}{9} - \frac{302}{27} \right] + n_v \left(8 - \frac{8\pi^2}{3}\right) \\
&+ \frac{8\zeta(3)}{3} - \frac{20\pi^2}{9} - \frac{2537}{18} - 6\ln^2\left(\frac{\mu^2}{m_c^2}\right) - \frac{250}{3} \ln\left(\frac{\mu^2}{m_c^2}\right) \\
&\left. - \frac{16\pi^2 \ln(2)}{9} \right\} + \mathcal{O}(z^3) \,,
\end{aligned}
\tag{5.33}
$$

where we set $n_c = 3$. The variables n_h and n_v denote the numbers of active flavors with the masses m_b and m_c, respectively. We also use the abbreviation

$$
z = \frac{m_c^2}{m_b^2} \,. \tag{5.34}
$$

All masses in eq. (5.33) are defined in the OS scheme.

6

ANALYTIC RESULTS

In this chapter we present the results for Γ_{12}, and thus for the physical matching coefficients in the $\Delta B = 2$ basis. Our results are stated in the form of

$$\Gamma_{12} = \frac{G_F m_b^2}{24\pi M_B}\left[H(z)\,\langle B|\,Q\,|\overline{B}\rangle\,(\mu_2) + \widetilde{H}_S(z)\,\langle B|\,\widetilde{Q}_S\,|\overline{B}\rangle\,(\mu_2)\right] + \mathcal{O}\left(\frac{\Lambda}{m_b}\right), \tag{6.1}$$

with m_b defined in the OS scheme. The coefficients H and $\widetilde{H}_S$ are reformulated in comparison to eq. (4.16) to describe the physical basis of $\{Q, \widetilde{Q}_S, R_0\}$. The Wilson coefficients contain the primary results of this work. They are decomposed as

$$H(z) \equiv -\lambda_c^2 H^{cc}(z) - 2\lambda_c\lambda_u H^{uc}(z) - \lambda_u^2 H^{uu}(z)\,, \tag{6.2}$$

and similarly for $\widetilde{H}_S$.

In our calculation we expand "naively" up to linear order in the small parameter

$$z = \left(\frac{m_c}{m_b}\right)^2 \equiv \left(\frac{m_c^{\text{OS}}}{m_b^{\text{OS}}}\right)^2. \tag{6.3}$$

A naive expansion is defined as a Laurent series of the integrand of a Feynman integral. A priori this leads to wrong results in comparison to the asymptotic expansion described in section 3.5. We explicitly checked that the naive expansion up to $\mathcal{O}(z)$ differs from the asymptotic expansion only for diagrams in which a charm-quark loop arises from a gluon propagator correction. Thus, up to $\mathcal{O}(\alpha_s)$ the naive expansion is sufficient to the linear order in z. At order $\mathcal{O}(\alpha_s^2)$ and beyond diagrams as shown in fig. 6.1 cannot be treated with the naive expansion. Fortunately, the leading z-contributions for three-loop diagrams such as figs. 6.1i and 6.1ii are known in the literature [68, 69]. For one-loop and two-loop diagrams with insertions of the chromomagnetic operator P_8, we find agreement of the naive and the asymptotic expansion up to $\mathcal{O}(z)$. Sample diagrams of the latter are presented in figs. 6.1iii and 6.1iv.

In the following sections we present the results in different orders in α_s. They are further distinguished according to their contributions of CMM Wilson coefficients:

$$\begin{aligned} H^{ab}(z) &\equiv \sum_{\substack{i,j\in\{1,\dots,6,8\},\\ j\geq i}} C_i C_j\; p_{ij}^{ab}(z)\,, \\ \widetilde{H}_S^{ab}(z) &\equiv \sum_{\substack{i,j\in\{1,\dots,6,8\},\\ j\geq i}} C_i C_j\; p_{ij}^{S,ab}(z)\,, \qquad ab \in \{cc, uc, uu\}\,. \end{aligned} \tag{6.4}$$

As shown in table 2.2, the $\Delta B = 1$ Wilson coefficients of the current-current operators are numerically more significant. Hence, the inclusion of penguin operators are numerically subleading. For this reason we consider penguin operator contributions

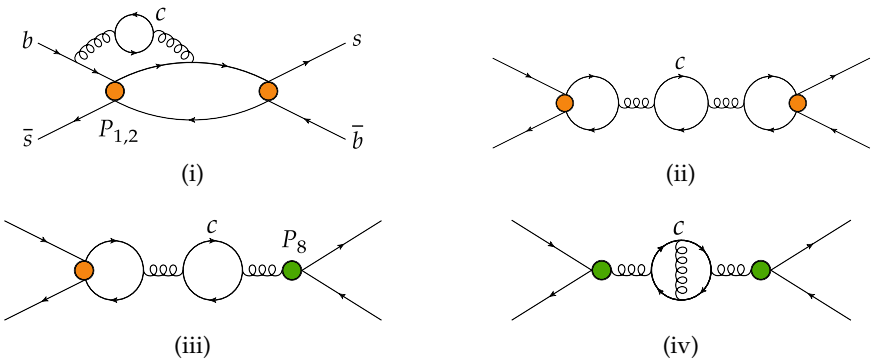

Figure 6.1: A priori these diagrams lead to wrong results when a Laurent expansion around $z \to 0$ under the integral sign is applied instead of using an asymptotic expansion. For diagrams (iii) and (iv) the naive and asymptotic expansion agree up to $\mathcal{O}(z)$.

Operator contributions	Publications 1-loop	2-loop	3-loop
$P_{12} \times P_{12}$	[63] (LO)	[65–67] (NLO)	[68, 69] (NNLO)
$P_{12} \times P_{3-6}$	[63] (LO)	[69, 70] (NLO)	
$P_{3-6} \times P_{3-6}$	[63] (LO)	[71] (NLO)	
$P_{12} \times P_8$	[65, 66] (NLO)	[68, 69, 71] (NNLO)	
$P_{3-6} \times P_8$	[69, 71] (NLO)	[71] (NNLO)	
$P_8 \times P_8$	[69, 71] (NNLO)	[71] (N^3LO)	
$1/m_b$	[47, 63, 67] (LO)		

Table 6.1: The appearances of the different Γ_{12} contributions are summarized according to their operator insertions. The entry for $1/m_b$ denotes higher order contributions in the Λ/m_b expansion. In refs. [68, 69] only partial results are given.

only up to two-loop order. For the more involved three-loop calculation we focus solely on the numerically dominant current-current insertions.

Not all results presented in this chapter are new. Some of them are known for more than 20 years. Table 6.1 summarizes the individual contributions and their, also partial, appearances in publications.

The coefficients p_{ij}^{ab} are given as an expansion in the strong coupling constant and in z:

$$\begin{aligned} p_{ij}^{ab}(z) &\equiv \sum_{n=0}^{3} \left(\frac{\alpha_s^{(5)}(\mu_1)}{4\pi}\right)^n p_{ij}^{ab,(n)}(z)\,, \\ p_{ij}^{S,ab}(z) &\equiv \sum_{n=0}^{3} \left(\frac{\alpha_s^{(5)}(\mu_1)}{4\pi}\right)^n p_{ij}^{S,ab,(n)}(z)\,, \end{aligned} \tag{6.5}$$

where terms of $\mathcal{O}(z^{3/2})$ and beyond are discarded. All results are presented with $n_c = 3$, but in the ancillary files given for arbitrary n_c.

LO contributions			Number of diagrams	Number of loops
$P_{1,2}$	$\times$	$P_{1,2}$	32	1
$P_{1,2}$	$\times$	P_{3-6}	64	1
P_{3-6}	$\times$	P_{3-6}	1312	1
$P_{1,2}$	$\times$	E	320	1
P_{3-6}	$\times$	E	2352	1
E	$\times$	E	192	1

Table 6.2: The number of evaluated $\mathcal{O}(\alpha_s^0)$ diagrams in the $\Delta B = 1$ theory are shown. The entry for E also includes evanescent operators which do not directly contribute to the $\mathcal{O}(\alpha_s^0)$ results but are either needed for the renormalization of higher order results or for consistency checks discussed in section 6.5. The stated numbers are the amount of diagrams generated by `qgraf`.

6.1 LEADING ORDER RESULTS

At leading order in α_s, the $\Delta B = 1$ side of the matching consists of one-loop diagrams, whereas there are only tree-level diagrams on the $\Delta B = 2$ side. Sample diagrams are shown in fig. 6.2. To this order all results are fully known in the literature. We present them here for completeness.

By including evanescent operators the number of diagrams are shown in table 6.2. There, also combinations of evanescent operators like $E_1^{(1)} \times E_1^{(2)}$ are included which are not directly needed for the results of this work. We include them as well to analyze their possible contributions in the matching. Which evanescent operators must necessarily be regarded can be seen from their contributions in the renormalization, as presented in appendix A.

All diagrams with two current-current operator insertions ($P_{1/2}$) have the structure of fig. 6.2i with u- and c-quark propagators in the loop. From them, we get

$$\begin{aligned}
p_{11}^{cc,(0)}(z) &= \frac{23}{72} - \frac{11z}{6}, & p_{11}^{S,cc,(0)}(z) &= -\frac{5}{9}, \\
p_{12}^{cc,(0)}(z) &= \frac{1}{6} - 2z, & p_{12}^{S,cc,(0)}(z) &= -\frac{4}{3}, \\
p_{22}^{cc,(0)}(z) &= 1 - 3z, & p_{22}^{S,cc,(0)}(z) &= 1.
\end{aligned} \tag{6.6}$$

Taking also penguin contributions into account leads to three new diagram classes as shown in figs. 6.2ii to 6.2vi. The diagrams (v) and (vi) allow only cuts through b-propagators and thus have no imaginary (absorptive) part.

The mixed current-current and penguin contributions read

$$\begin{aligned}
p_{13}^{cc,(0)}(z) &= \frac{4}{3}, & p_{13}^{S,cc,(0)}(z) &= -\frac{8}{3}, \\
p_{14}^{cc,(0)}(z) &= -\frac{5}{36}, & p_{14}^{S,cc,(0)}(z) &= -\frac{2}{9}, \\
p_{15}^{cc,(0)}(z) &= \frac{64}{3} - 96z, & p_{15}^{S,cc,(0)}(z) &= -\frac{128}{3},
\end{aligned}$$

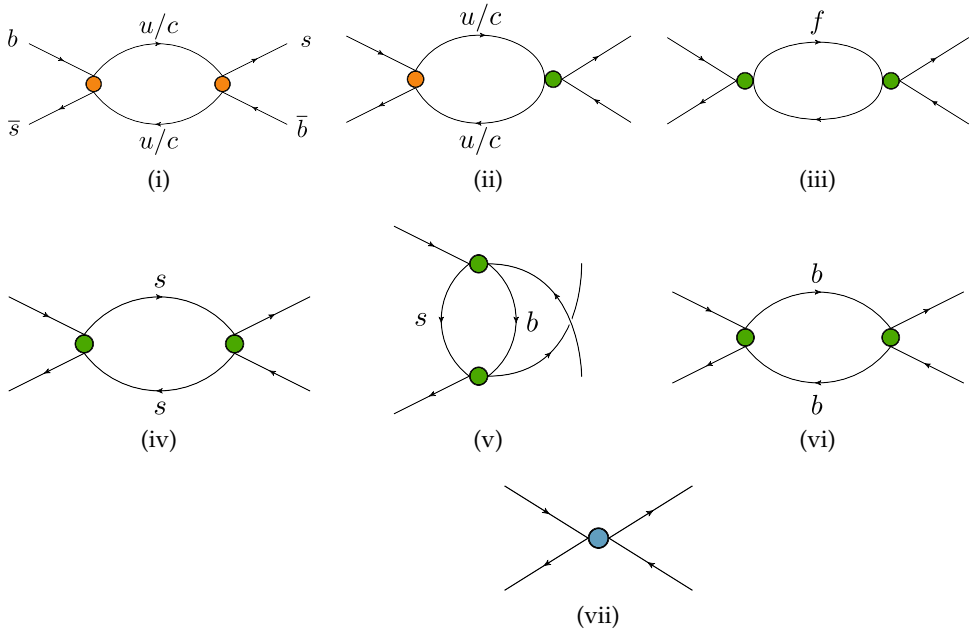

Figure 6.2: Diagrams of the leading order contribution to Γ_{12} are at one-loop order on the $\Delta B = 1$ side and at tree-level for $\Delta B = 2$. Orange dots depict current-current operators, green ones penguins, and blue ones $\Delta B = 2$ operators.

$$
\begin{aligned}
p_{16}^{cc,(0)}(z) &= 4z - \frac{20}{9}\,, & p_{16}^{S,cc,(0)}(z) &= -\frac{32}{9}\,, \\
p_{23}^{cc,(0)}(z) &= 1\,, & p_{23}^{S,cc,(0)}(z) &= -2\,, \\
p_{24}^{cc,(0)}(z) &= \frac{5}{6}\,, & p_{24}^{S,cc,(0)}(z) &= \frac{4}{3}\,, \\
p_{25}^{cc,(0)}(z) &= 16 - 72z\,, & p_{25}^{S,cc,(0)}(z) &= -32\,, \\
p_{26}^{cc,(0)}(z) &= \frac{40}{3} - 24z\,, & p_{26}^{S,cc,(0)}(z) &= \frac{64}{3}\,.
\end{aligned}
\tag{6.7}
$$

For the penguin-penguin diagrams the closed fermion loop introduces a summation over all active quark flavors. This is evident from the appearance of the factors $n_l = 3$ describing a sum over all massless flavors, and $n_v = 1$ which is the number of flavors with the mass m_c. Note that n_l and n_c only count flavors that appear in closed fermion loops in which no flavor changes occur. The results are given by

$$
\begin{aligned}
p_{33}^{cc,(0)}(z) &= 3(n_l + n_v) + 2\,, & p_{33}^{S,cc,(0)}(z) &= -6(n_l + n_v) - 1\,, \\
p_{34}^{cc,(0)}(z) &= \frac{7}{3}\,, & p_{34}^{S,cc,(0)}(z) &= -\frac{8}{3}\,, \\
p_{35}^{cc,(0)}(z) &= 60(n_l + n_v) + 64\,, & p_{35}^{S,cc,(0)}(z) &= -120(n_l + n_v) - 32\,, \\
p_{36}^{cc,(0)}(z) &= \frac{112}{3}\,, & p_{36}^{S,cc,(0)}(z) &= -\frac{128}{3}\,, \\
p_{44}^{cc,(0)}(z) &= \frac{5(n_l + n_v)}{12} + \frac{13}{72}\,, & p_{44}^{S,cc,(0)}(z) &= \frac{2(n_l + n_v)}{3} - \frac{7}{9}\,, \\
p_{45}^{cc,(0)}(z) &= \frac{112}{3}\,, & p_{45}^{S,cc,(0)}(z) &= -\frac{128}{3}\,,
\end{aligned}
$$

$$p_{46}^{cc,(0)}(z) = \frac{25(n_l+n_v)}{3} + \frac{52}{9}, \qquad p_{46}^{S,cc,(0)}(z) = \frac{40(n_l+n_v)}{3} - \frac{224}{9}, \tag{6.8}$$

$$\begin{aligned}
p_{55}^{cc,(0)}(z) &= -1296 n_v z + 408(n_l+n_v) + 512, \\
p_{55}^{S,cc,(0)}(z) &= -816(n_l+n_v) - 256, \\
p_{56}^{cc,(0)}(z) &= \frac{1792}{3}, \\
p_{56}^{S,cc,(0)}(z) &= -\frac{2048}{3}, \\
p_{66}^{cc,(0)}(z) &= -72 n_v z + \frac{170(n_l+n_v)}{3} + \frac{416}{9}, \\
p_{66}^{S,cc,(0)}(z) &= \frac{272(n_l+n_v)}{3} - \frac{1792}{9}.
\end{aligned}$$

The coefficients for "uu" can be constructed from the "cc" ones:

$$\begin{aligned}
p_{ij}^{uu,(0)}(z) &= p_{ij}^{cc,(0)}(0) \quad \text{for} \quad i \in \{1,2\} \text{ and } j \in \{1,\dots,6\}, \\
p_{ij}^{uu,(0)}(z) &= p_{ij}^{cc,(0)}(z) \quad \text{for} \quad i,j \in \{3,\dots,6\}.
\end{aligned} \tag{6.9}$$

The "uc" coefficients are given by

$$p_{ij}^{uc,(0)}(z) = \frac{p_{ij}^{cc,(0)}(z) + p_{ij}^{uu,(0)}(z)}{2} \quad \text{for} \quad i,j \in \{1,\dots,6\}. \tag{6.10}$$

Equations (6.9) and (6.10) hold similarly for p^S. They can be explained from the fact that the penguin operators introduce a factor $(\lambda_c + \lambda_u)$, whereas current-current operators multiply λ_i according to their flavors.

The results of eqs. (6.6) to (6.10) agree with [63, 65] after applying a transformation into the traditional basis according to eq. (2.49). In the referenced publications the full z-dependence is considered.

6.2 NLO RESULTS

At order α_s the number of diagrams which have to be evaluated increases substantially which can be seen from table 6.3. Furthermore, one-loop diagrams occur on the $\Delta B = 2$ theory side of the matching. According to table 6.4, their amount is small in comparison to the $\Delta B = 1$ side, but the real part of the matrix element have to be computed as well. Sample diagrams in the $\Delta B = 2$ effective theory are shown in fig. 6.3.

We give the results for the full $\mathcal{O}(\alpha_s)$ corrections to Γ_{12} in the leading order of the Λ/m_b expansion. This includes four-fermion penguin operators P_{3-6} as well as chromomagnetic P_8 contributions.

In the following sections we show a shortened version of the results using the replacements of eq. (3.103) and

$$n_l = 3, \qquad n_h = 1, \qquad n_v = 1,$$

NLO contributions			Number of diagrams	Number of loops
$P_{1,2}$	$\times$	$P_{1,2}$	832 (960)	2
$P_{1,2}$	$\times$	P_{3-6}	7296 (8064)	2
P_{3-6}	$\times$	P_{3-6}	36416 (41664)	2
$P_{1,2}$	$\times$	E	6976 (7872)	2
P_{3-6}	$\times$	E	29152 (32928)	2
E	$\times$	E	832 (960)	2
$P_{1,2}$	$\times$	P_8	48	1
P_{3-6}	$\times$	P_8	528	1
P_8	$\times$	E	624	1

Table 6.3: The number of evaluated two-loop, as well as one-loop diagrams in the $\Delta B = 1$ theory at $\mathcal{O}(\alpha_s)$ are shown. Additional evanescent operator insertions are included here as well. The numbers represent the diagrams which are left after the `tapir external_self_energy_bridge_mixing` filter is applied. The numbers in brackets are the amount of diagrams originating from `qgraf`.

NLO contributions	Number of diagrams	Number of loops
$Q^{\Delta B=2}$	48	1
$E^{\Delta B=2}$	144	1

Table 6.4: At $\mathcal{O}(\alpha_s)$ the shown number of one-loop diagrams for the $\Delta B = 2$ theory are computed. We split the contributions into physical ($Q^{\Delta B=2}$) and evanescent ($E^{\Delta B=2}$) operator insertions. Note that $\widetilde{Q}$ is included in the physical counting, although it is only needed to construct $E_1^{(1)}$.

where n_h is the number of flavors with the mass m_b. The extended results with these terms and the $e_x^{(i)}$ kept unspecified are given in the ancillary files.

In the following we discuss the contributions of different CMM operator combinations in their respective sections.

6.2.1 *Current-Current Double-Insertion*

At two-loop order most diagrams with two current-current operators are constructed from the LO ones by attaching a gluon line in all possible combinations, as shown in figs. 6.4i and 6.4ii. The additional diagram class of fig. 6.4iii consists of One-Particle Reducible (1PR) diagrams which connects two separated fermion loops by a gluon bridge.

The results proportional to λ_c^2 are given by

$$p_{11}^{cc,(1)}(z) = z\left(-\frac{14L_1}{3} - \frac{11L_2}{3} - \frac{44\ln(z)}{3} + \frac{\pi^2}{54} - \frac{4133}{216}\right) + \frac{337L_1}{324} + \frac{149L_2}{108} - \frac{5\pi^2}{108} + \frac{1789}{486},$$

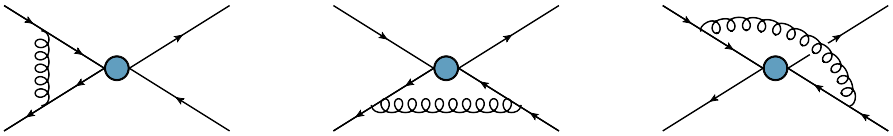

(i) (ii) (iii)

Figure 6.3: Feynman diagrams of the $\Delta B = 2$ theory at NLO are given by the tree-level contributions with additional gluon lines.

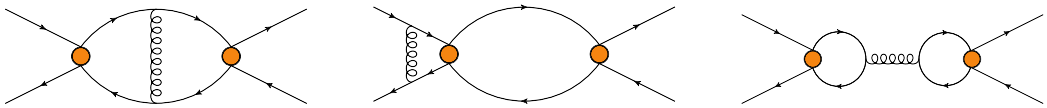

(i) (ii) (iii)

Figure 6.4: At NLO, double insertions of current-current operators include 1PI and 1PR diagrams.

$$
\begin{aligned}
p_{12}^{cc,(1)}(z) &= z\left(26L_1 - 4L_2 - 16\ln(z) - \frac{2\pi^2}{9} + \frac{1199}{18}\right) \\
&\quad - \frac{323L_1}{54} + \frac{19L_2}{9} + \frac{5\pi^2}{9} - \frac{1346}{81}, \\
p_{22}^{cc,(1)}(z) &= z\left(12L_1 - 6L_2 - 24\ln(z) + \frac{2\pi^2}{3} + \frac{115}{6}\right) \\
&\quad - \frac{14L_1}{9} + \frac{2L_2}{3} - \frac{5\pi^2}{3} + \frac{91}{54},
\end{aligned}
\tag{6.11}
$$

$$
\begin{aligned}
p_{11}^{S,cc,(1)}(z) &= -\frac{38L_1}{81} - \frac{40L_2}{27} + \left(-\frac{1159}{27} - \frac{4\pi^2}{27}\right) z - \frac{2\pi^2}{27} + \frac{2}{243}, \\
p_{12}^{S,cc,(1)}(z) &= \frac{44L_1}{27} - \frac{32L_2}{9} + \left(\frac{16\pi^2}{9} - \frac{656}{9}\right) z + \frac{8\pi^2}{9} + \frac{280}{81}, \\
p_{22}^{S,cc,(1)}(z) &= \frac{64L_1}{9} + \frac{8L_2}{3} + \left(\frac{116}{3} - \frac{16\pi^2}{3}\right) z - \frac{8\pi^2}{3} + \frac{728}{27},
\end{aligned}
$$

with $L_{1/2} = \ln(\mu_{1/2}^2/m_b^2)$. Note that the $z\ln(z)$ terms originate from the c-quark mass renormalization in the OS scheme. In fact, if z is expressed through $\overline{\text{MS}}$ masses, i.e.

$$
z \;\to\; \bar{z} \;=\; \frac{\overline{m}_c^2(\mu_c)}{\overline{m}_b^2(\mu_b)}, \tag{6.12}
$$

large logarithms like $\bar{z}\ln(\bar{z})$ vanish when choosing the newly introduced scales at the matching scale $\mu_c = \mu_b = \mu_1$ [67, 138].

As before the "uu" and "uc" contributions are obtained from the "cc" ones:

$$
\begin{aligned}
p_{ij}^{uu,(1)} &= p_{ij}^{cc,(1)}(0), \\
p_{ij}^{uc,(1)}(z) &= \frac{p_{ij}^{cc,(1)}(z) + p_{ij}^{uu,(1)}}{2} \quad \text{for} \quad i,j \in \{1,2\},
\end{aligned}
\tag{6.13}
$$

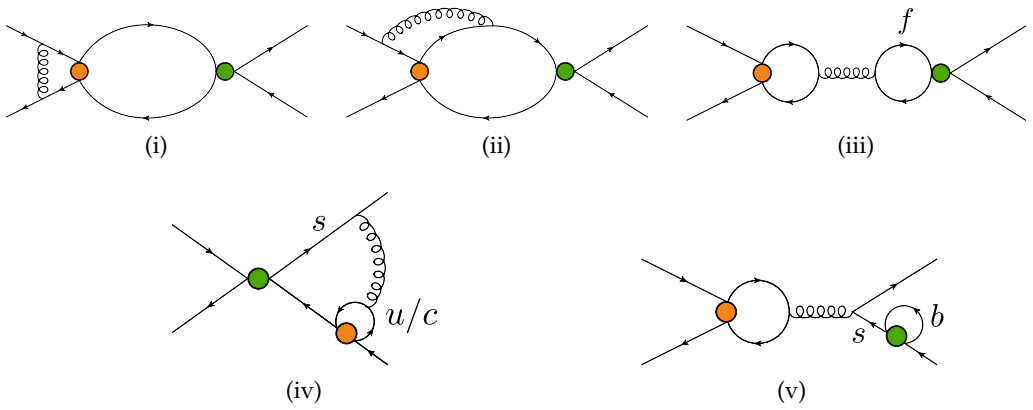

Figure 6.5: Several new diagram classes appear for simultaneous current-current and penguin insertions at NLO.

where again analogous relations hold for p^S. Equations (6.11) and (6.13) are in agreement with [65–67], where the full z dependence is given.

6.2.2 *Current-Current-Penguin Contribution*

If a penguin operator is inserted together with a current-current operator, new diagram classes as shown in fig. 6.5 occur. For example, diagrams such as fig. 6.5v appear which have a non-amputated leg. They cannot be discarded because the self-energy correction changes the quark flavor due to an FCNC. They have to be added to render the result gauge-parameter independent.

The $\mathcal{O}(\alpha_s)$ results proportional to $C_{1,2} \times C_{3-6}$ are given by

$$
\begin{aligned}
p_{13}^{cc,(1)}(z) &= \left(\frac{320}{9} - 4L_1\right) z + \frac{47L_1}{18} + \frac{56L_2}{9} - \frac{5\pi}{18\sqrt{3}} + \frac{1523}{108}\,, \\
p_{14}^{cc,(1)}(z) &= \left(\frac{59L_1}{3} + \frac{5\pi^2}{9} + \frac{4565}{108}\right) z - \frac{281L_1}{108} + \frac{L_2}{54} + \frac{5\pi^2}{18} \\
&\quad - \frac{25\pi}{108\sqrt{3}} - \frac{712}{81}\,, \\
p_{15}^{cc,(1)}(z) &= z\left(-136L_1 - 192L_2 - 768\ln(z) - \frac{16408}{9}\right) \\
&\quad + \frac{376L_1}{9} + \frac{896L_2}{9} - \frac{40\pi}{9\sqrt{3}} + 318\,, \\
p_{16}^{cc,(1)}(z) &= z\left(\frac{764L_1}{3} + 8L_2 + 32\ln(z) + \frac{8\pi^2}{9} + \frac{22850}{27}\right) \\
&\quad - \frac{1259L_1}{27} + \frac{8L_2}{27} + \frac{40\pi^2}{9} - \frac{55\pi}{27\sqrt{3}} - \frac{4243}{27}\,, \\
p_{23}^{cc,(1)}(z) &= \left(24L_1 + \frac{170}{3}\right) z - \frac{47L_1}{3} + \frac{14L_2}{3} + \frac{5\pi}{3\sqrt{3}} - \frac{677}{18}\,, \\
p_{24}^{cc,(1)}(z) &= \left(26L_1 - \frac{10\pi^2}{3} + \frac{1429}{18}\right) z - \frac{35L_1}{9} - \frac{L_2}{9} - \frac{5\pi^2}{3}
\end{aligned}
$$

$$
\begin{aligned}
&+\frac{25\pi}{18\sqrt{3}}-\frac{88}{27}\,,\\
p_{25}^{cc,(1)}(z) &= z\left(816L_1-144L_2-576\ln(z)+\frac{3656}{3}\right)\\
&-\frac{752L_1}{3}+\frac{224L_2}{3}+\frac{80\pi}{3\sqrt{3}}-580\,,\\
p_{26}^{cc,(1)}(z) &= z\left(128L_1-48L_2-192\ln(z)-\frac{16\pi^2}{3}+\frac{6140}{9}\right)\\
&-\frac{290L_1}{9}-\frac{16L_2}{9}-\frac{80\pi^2}{3}+\frac{110\pi}{9\sqrt{3}}-\frac{442}{9}\,,
\end{aligned}
\tag{6.14}
$$

$$
\begin{aligned}
p_{13}^{S,cc,(1)}(z) &= -\frac{4L_1}{3}-\frac{64L_2}{9}-\frac{1720z}{9}-\frac{4\pi}{9\sqrt{3}}-\frac{130}{27}\,,\\
p_{14}^{S,cc,(1)}(z) &= 2L_1-\frac{16L_2}{27}+\left(\frac{80}{27}+\frac{8\pi^2}{9}\right)z+\frac{4\pi^2}{9}-\frac{10\pi}{27\sqrt{3}}+\frac{404}{81}\,,\\
p_{15}^{S,cc,(1)}(z) &= -\frac{64L_1}{3}-\frac{1024L_2}{9}-\frac{27952z}{9}-\frac{64\pi}{9\sqrt{3}}-\frac{2128}{9}\,,\\
p_{16}^{S,cc,(1)}(z) &= 24L_1-\frac{256L_2}{27}+\left(\frac{128\pi^2}{9}-\frac{520}{27}\right)z+\frac{64\pi^2}{9}\\
&-\frac{88\pi}{27\sqrt{3}}+\frac{2824}{27}\,,\\
p_{23}^{S,cc,(1)}(z) &= 8L_1-\frac{16L_2}{3}-\frac{448z}{3}+\frac{8\pi}{3\sqrt{3}}+\frac{116}{9}\,,\\
p_{24}^{S,cc,(1)}(z) &= \frac{32L_2}{9}+\left(\frac{488}{9}-\frac{16\pi^2}{3}\right)z-\frac{8\pi^2}{3}+\frac{20\pi}{9\sqrt{3}}+\frac{272}{27}\,,\\
p_{25}^{S,cc,(1)}(z) &= 128L_1-\frac{256L_2}{3}-\frac{6304z}{3}+\frac{128\pi}{3\sqrt{3}}+\frac{32}{3}\,,\\
p_{26}^{S,cc,(1)}(z) &= 48L_1+\frac{512L_2}{9}+\left(\frac{7520}{9}-\frac{256\pi^2}{3}\right)z\\
&-\frac{128\pi^2}{3}+\frac{176\pi}{9\sqrt{3}}+\frac{1840}{9}\,.
\end{aligned}
$$

The "uu" contributions incorporate a z-dependence due to diagrams like in fig. 6.5iii, where a c-quark loop appears independently of the current-current operator. Hence, we get

$$
\begin{aligned}
p_{13}^{uu,(1)}(z) &= p_{13}^{cc,(1)}(0)\,, & p_{13}^{S,uu,(1)}(z) &= p_{13}^{S,cc,(1)}(0)\,,\\
p_{14}^{uu,(1)}(z) &= p_{14}^{cc,(1)}(0)+\frac{5z}{9}\,, & p_{14}^{S,uu,(1)}(z) &= p_{14}^{S,cc,(1)}(0)+\frac{8z}{9}\,,\\
p_{15}^{uu,(1)}(z) &= p_{15}^{cc,(1)}(0)\,, & p_{15}^{S,uu,(1)}(z) &= p_{15}^{S,cc,(1)}(0)\,,\\
p_{16}^{uu,(1)}(z) &= p_{16}^{cc,(1)}(0)+\frac{50z}{9}\,, & p_{16}^{S,uu,(1)}(z) &= p_{16}^{S,cc,(1)}(0)+\frac{80z}{9}\,,\\
p_{23}^{uu,(1)}(z) &= p_{23}^{cc,(1)}(0)\,, & p_{23}^{S,uu,(1)}(z) &= p_{23}^{S,cc,(1)}(0)\,,\\
p_{24}^{uu,(1)}(z) &= p_{24}^{cc,(1)}(0)-\frac{10z}{3}\,, & p_{24}^{S,uu,(1)}(z) &= p_{24}^{S,cc,(1)}(0)-\frac{16z}{3}\,,
\end{aligned}
\tag{6.15}
$$

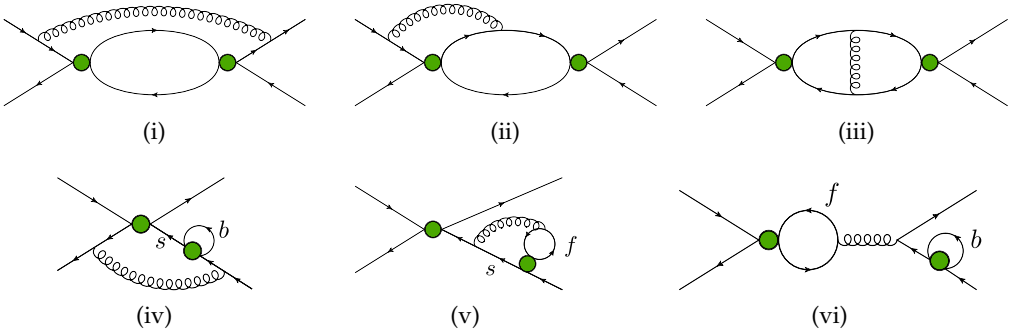

Figure 6.6: With two penguin insertions at NLO, a large variety of different diagram classes have to be taken into account.

$$p_{25}^{uu,(1)}(z) = p_{25}^{cc,(1)}(0)\,, \qquad p_{25}^{S,uu,(1)}(z) = p_{25}^{S,cc,(1)}(0)\,,$$
$$p_{26}^{uu,(1)}(z) = p_{26}^{cc,(1)}(0) - \frac{100z}{3}\,, \qquad p_{26}^{S,uu,(1)}(z) = p_{26}^{S,cc,(1)}(0) - \frac{160z}{3}\,.$$

The "uc" contributions are again given by

$$p_{ij}^{uc,(1)}(z) = \frac{p_{ij}^{cc,(1)}(z) + p_{ij}^{uu,(1)}(z)}{2} \quad \text{for } i \in \{1,2\} \text{ and } j \in \{3,\ldots,6\}\,. \tag{6.16}$$

The n_h, n_l and n_v dependent terms of eqs. (6.14) to (6.16) agree with ref. [69]. The remaining terms have been computed for the first time in the framework of this thesis [70].

6.2.3 *Penguin Double-Insertion*

In this section we consider the contributions involving $C_{3-6} \times C_{3-6}$. Sample Feynman diagrams which have to be calculated in this context are shown in fig. 6.6. The corresponding two-loop diagrams are the majority of all evaluated diagrams in this work. Since in the Hamiltonian the penguin operators are proportional to $(\lambda_c + \lambda_u)$, we have

$$p_{ij}^{cc,(1)}(z) = p_{ij}^{cu,(1)}(z) = p_{ij}^{uu,(1)}(z)\,, \tag{6.17}$$

which holds similarly for p_{ij}^{S}.

The matching coefficients read

$$p_{33}^{cc,(1)}(z) = -\frac{154L_1}{9} + \frac{184L_2}{3} + 90z - \frac{5\pi^2}{3} + \frac{5\pi}{3\sqrt{3}} + \frac{1390}{27}\,,$$
$$p_{34}^{cc,(1)}(z) = -\frac{811L_1}{54} + \frac{74L_2}{9} - \frac{10z}{3} - \frac{10\pi^2}{9} + \frac{70\pi}{9\sqrt{3}} - \frac{27991}{324}\,,$$
$$p_{35}^{cc,(1)}(z) = -\frac{4928L_1}{9} + \frac{3872L_2}{3} + 1800z - \frac{160\pi^2}{3} + \frac{160\pi}{3\sqrt{3}}$$

$$
\begin{aligned}
&+\frac{16880}{27}\,,\\
p_{36}^{cc,(1)}(z) &= \left(144L_1+\frac{440}{3}\right)z-\frac{12932L_1}{27}+\frac{1184L_2}{9}-\frac{160\pi^2}{9}\\
&+\frac{670\pi}{9\sqrt{3}}-\frac{131410}{81}\,,\\
p_{44}^{cc,(1)}(z) &= \frac{181L_1}{162}+\frac{127L_2}{108}+\left(\frac{323}{36}-\frac{5\pi^2}{3}\right)z-\frac{335\pi^2}{108}\\
&+\frac{575\pi}{108\sqrt{3}}+\frac{779}{486}\,,\\
p_{45}^{cc,(1)}(z) &= \left(576L_1+\frac{3836}{3}\right)z-\frac{14912L_1}{27}+\frac{1184L_2}{9}-\frac{160\pi^2}{9}\\
&+\frac{1120\pi}{9\sqrt{3}}-\frac{127990}{81}\,,\\
p_{46}^{cc,(1)}(z) &= \left(60L_1-\frac{100\pi^2}{3}+\frac{2455}{9}\right)z-\frac{8759L_1}{81}+\frac{1088L_2}{27}\\
&-\frac{1600\pi^2}{27}+\frac{2665\pi}{27\sqrt{3}}-\frac{50083}{243}\,,\\
p_{55}^{cc,(1)}(z) &= z\left(-2592L_2-10368\ln(z)-33120\right)-\frac{39424L_1}{9}\\
&+\frac{26944L_2}{3}-\frac{1280\pi^2}{3}+\frac{1280\pi}{3\sqrt{3}}+\frac{347104}{27}\,,\\
p_{56}^{cc,(1)}(z) &= \left(7200L_1+\frac{74000}{3}\right)z-\frac{240608L_1}{27}+\frac{18944L_2}{9}\\
&-\frac{2560\pi^2}{9}+\frac{10720\pi}{9\sqrt{3}}-\frac{2253568}{81}\,,\\
p_{66}^{cc,(1)}(z) &= z\left(-48L_1-144L_2-576\ln(z)-\frac{248\pi^2}{3}+\frac{12290}{9}\right)\\
&-\frac{59632L_1}{81}+\frac{8848L_2}{27}-\frac{10640\pi^2}{27}+\frac{12320\pi}{27\sqrt{3}}-\frac{662144}{243}\,,
\end{aligned}
\tag{6.18}
$$

$$
\begin{aligned}
p_{33}^{S,cc,(1)}(z) &= \frac{176L_1}{9}-\frac{200L_2}{3}-432z-\frac{8\pi^2}{3}+\frac{8\pi}{3\sqrt{3}}-\frac{620}{27}\,,\\
p_{34}^{S,cc,(1)}(z) &= \frac{268L_1}{27}-\frac{64L_2}{9}-\frac{16z}{3}-\frac{16\pi^2}{9}+\frac{112\pi}{9\sqrt{3}}+\frac{3506}{81}\,,\\
p_{35}^{S,cc,(1)}(z) &= \frac{5632L_1}{9}-\frac{4096L_2}{3}-8640z-\frac{256\pi^2}{3}+\frac{256\pi}{3\sqrt{3}}+\frac{9728}{27}\,,\\
p_{36}^{S,cc,(1)}(z) &= \frac{9184L_1}{27}-\frac{1024L_2}{9}-\frac{160z}{3}-\frac{256\pi^2}{9}+\frac{1072\pi}{9\sqrt{3}}+\frac{88688}{81}\,,\\
p_{44}^{S,cc,(1)}(z) &= \frac{1028L_1}{81}+\frac{136L_2}{27}-\frac{8\pi^2 z}{3}+\frac{230z}{9}-\frac{134\pi^2}{27}+\frac{230\pi}{27\sqrt{3}}\\
&+\frac{6214}{243}\,,
\end{aligned}
$$

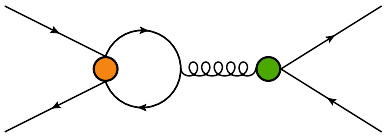

Figure 6.7: Only a single diagram type contributes to $P_{1,2} \times P_8$ at one-loop order. In the loop are either c- or a u-quark propagators.

$$
\begin{aligned}
p_{45}^{S,cc,(1)}(z) &= \frac{9472L_1}{27} - \frac{1024L_2}{9} + \frac{608z}{3} - \frac{256\pi^2}{9} + \frac{1792\pi}{9\sqrt{3}} + \frac{64784}{81}, \\
p_{46}^{S,cc,(1)}(z) &= \frac{10792L_1}{81} + \frac{2048L_2}{27} - \frac{160\pi^2 z}{3} + \frac{3568z}{9} - \frac{2560\pi^2}{27} \\
&\quad + \frac{4264\pi}{27\sqrt{3}} + \frac{123080}{243}, \\
p_{55}^{S,cc,(1)}(z) &= \frac{45056L_1}{9} - \frac{28160L_2}{3} - 58752z - \frac{2048\pi^2}{3} + \frac{2048\pi}{3\sqrt{3}} \\
&\quad - \frac{349184}{27}, \\
p_{56}^{S,cc,(1)}(z) &= \frac{167680L_1}{27} - \frac{16384L_2}{9} + \frac{6080z}{3} - \frac{4096\pi^2}{9} + \frac{17152\pi}{9\sqrt{3}} \\
&\quad + \frac{1502720}{81}, \\
p_{66}^{S,cc,(1)}(z) &= \frac{75392L_1}{81} + \frac{11776L_2}{27} - \frac{1088\pi^2 z}{3} + \frac{23696z}{9} - \frac{17024\pi^2}{27} \\
&\quad + \frac{19712\pi}{27\sqrt{3}} + \frac{717184}{243}.
\end{aligned}
$$

These results are published in ref. [71].

6.2.4 *Current-Current-Chromomagnetic Contribution*

The contribution of P_8 appears for the first time at $\mathcal{O}(\alpha_s)$ since its Feynman rule introduces a factor $g_s/(4\pi)$. For matching coefficients proportional to $C_{1,2} \times C_8$ the one-loop diagrams of fig. 6.7 have to be evaluated. They are UV-finite and necessary for the renormalization of $C_{1,2} \times C_{1,2}$ at $\mathcal{O}(\alpha_s^2)$. The matching coefficients $p_{i8}^{(1)}$ have no terms of linear order in z.

These contributions are calculated in ref. [65], and are in agreement with our results. We obtain

$$
\begin{aligned}
p_{18}^{cc,(1)}(z) &= \frac{5}{18}, & p_{18}^{S,cc,(1)}(z) &= \frac{4}{9}, \\
p_{28}^{cc,(1)}(z) &= -\frac{5}{3}, & p_{28}^{S,cc,(1)}(z) &= -\frac{8}{3},
\end{aligned}
\tag{6.19}
$$

with

$$
\begin{aligned}
p_{i8}^{uu,(1)} &= p_{i8}^{cc,(1)}(0), & p_{i8}^{S,uu,(1)} &= p_{i8}^{S,cc,(1)}(0), \\
p_{i8}^{uc,(1)} &= \frac{p_{i8}^{cc,(1)}(z) + p_{i8}^{uu,(1)}(z)}{2}, & p_{i8}^{S,uc,(1)} &= \frac{p_{i8}^{cc,(1)}(z) + p_{i8}^{S,uu,(1)}(z)}{2},
\end{aligned}
\tag{6.20}
$$

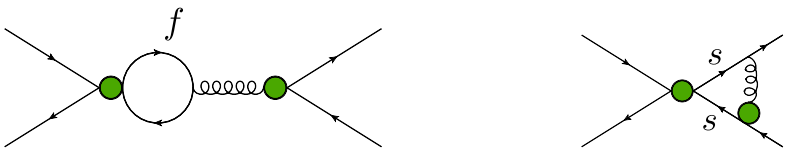

(i) (ii)

Figure 6.8: In addition to the 1PR diagrams in (i), a class of 1PI diagrams (ii) with two virtual s-quarks appear in the $P_{3-6} \times P_8$ contribution at one-loop order.

for $i \in \{1, 2\}$.

6.2.5 *Penguin-Chromomagnetic Contribution*

As for the previous matching coefficients, no $\mathcal{O}(z)$ terms appear in the results proportional to $C_{3-6} \times C_8$. Note that in comparison to the $C_{1,2} \times C_8$ case, there is an additional class of Feynman diagrams which is One-Particle Irreducible (1PI), as illustrated in fig. 6.8ii. The matching coefficients are given by

$$\begin{aligned}
p_{38}^{cc,(1)}(z) &= -\frac{32}{3}, & p_{38}^{S,cc,(1)}(z) &= \frac{64}{3}, \\
p_{48}^{cc,(1)}(z) &= -\frac{169}{18}, & p_{48}^{S,cc,(1)}(z) &= -\frac{20}{9}, \\
p_{58}^{cc,(1)}(z) &= -\frac{512}{3}, & p_{58}^{S,cc,(1)}(z) &= \frac{1024}{3}, \\
p_{68}^{cc,(1)}(z) &= -\frac{992}{9}, & p_{68}^{S,cc,(1)}(z) &= \frac{256}{9}.
\end{aligned} \tag{6.21}$$

Equation (6.20) holds also here. The results of eqs. (6.19) to (6.21) are needed to renormalize the NNLO contributions of $C_{1-6} \times C_8$. This result is published in [71] and the n_f dependent terms of it are in agreement with ref. [69].

6.3 NNLO RESULTS

At NNLO only partial results are known. The primary aim of this thesis is the determination of $\mathcal{O}(\alpha_s^2)$ corrections to Γ_{12} proportional to $C_{1,2} \times C_{1,2}$. Furthermore, all NNLO one-loop and two-loop contributions including P_8 have been computed. The number of diagrams at this order are shown in table 6.5 for the $\Delta B = 1$ side, and in table 6.6 for $\Delta B = 2$. For the latter two-loop corrections are considered including evanescent operators of the first and second generation. Sample diagrams are shown in fig. 6.9.

6.3.1 *Current-Current Double-Insertion*

The numerically dominant NNLO contribution originates from $\mathcal{O}(\alpha_s^2)$ terms proportional to $C_{1,2} \times C_{1,2}$. Sample diagrams are shown in fig. 6.10. The flavor changing self-energy corrections, which we know from NLO penguin contributions, occur

NNLO contributions			Number of diagrams	Number of loops
$P_{1,2}$	$\times$	$P_{1,2}$	26560 (31744)	3
$P_{1,2}$	$\times$	P_8	2064 (2256)	2
P_{3-6}	$\times$	P_8	20368 (22480)	2
P_8	$\times$	P_8	100 (108)	1

Table 6.5: The numbers of diagrams are shown which are needed for the $\Delta B = 1$ part of the NNLO contributions up to three loops. The presented format is similar to table 6.3. Note that no evanescent operator contributions are considered at this order.

NNLO contributions	Number of diagrams	Number of loops
$Q^{\Delta B=2}$	1016	2
$E^{\Delta B=2}$	2032	2

Table 6.6: The numbers of $\Delta B = 2$ diagrams at NNLO are shown. Corrections to evanescent operator insertions of the first two generation are also considered. Note that $\widetilde{Q}$ is counted here as a physical operator in addition to Q, Q_S and $\widetilde{Q}_S$.

for two current-current operator insertions for the first time at three-loop order, as shown in fig. 6.10ix.

Also, diagrams such as figs. 6.10i and 6.10ii appear which have a gluon self-energy correction with a c-quark loop. Since they contribute to terms of $\mathcal{O}(\sqrt{z})$, we cannot apply the naive z-expansion for these diagrams. Fortunately, the terms of the expansion stemming from only gluon propagator corrections are known in the literature [68, 69].

To construct a complete $\mathcal{O}(z)$ result, we proceed as follows:

- Computation of all NNLO $C_{1,2} \times C_{1,2}$ corrections with naive expansion in z.
- Discarding all terms which are proportional to n_v.
- Shifting $n_l \to n_l + n_v$ to recover the correct terms proportional to n_v up to $\mathcal{O}(z)$ excluding only the z-dependence stemming from gluon propagator corrections.
- Transformation of the results from ref. [68] into the CMM basis using eq. (2.50) and adding the z-dependent terms proportional to n_v to our result.

The separate treatment of the gluon propagator corrections is allowed since the simultaneous corrections of gluon propagator sub-diagrams and c-propagators from the remaining diagram are $\mathcal{O}(z^{3/2})$.

The terms taken from [68] are highlighted in orange and indicated by the prefactor n_v below. The so constructed results are given by

$$\begin{aligned} p_{11}^{cc,(2)}(z) \;= z\Bigg[& -\frac{1348}{9}L_1\ln(z) - \frac{88}{3}L_2\ln(z) - \frac{2347L_1^2}{54} + \frac{187L_2^2}{18} \\ & + \frac{31\pi^2 L_1}{54} - \frac{722039L_1}{1944} - \frac{337L_1L_2}{9} + \frac{19\pi^2 L_2}{81} + \frac{1891L_2}{81} \end{aligned}$$

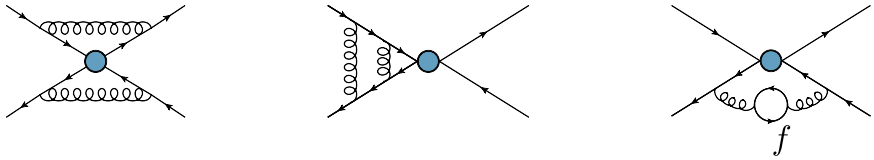

(i) (ii) (iii)

Figure 6.9: Sample NNLO diagrams on the $\Delta B = 2$ side are shown. The first dependence on m_c comes at two-loop order from corrections to the gluon propagator.

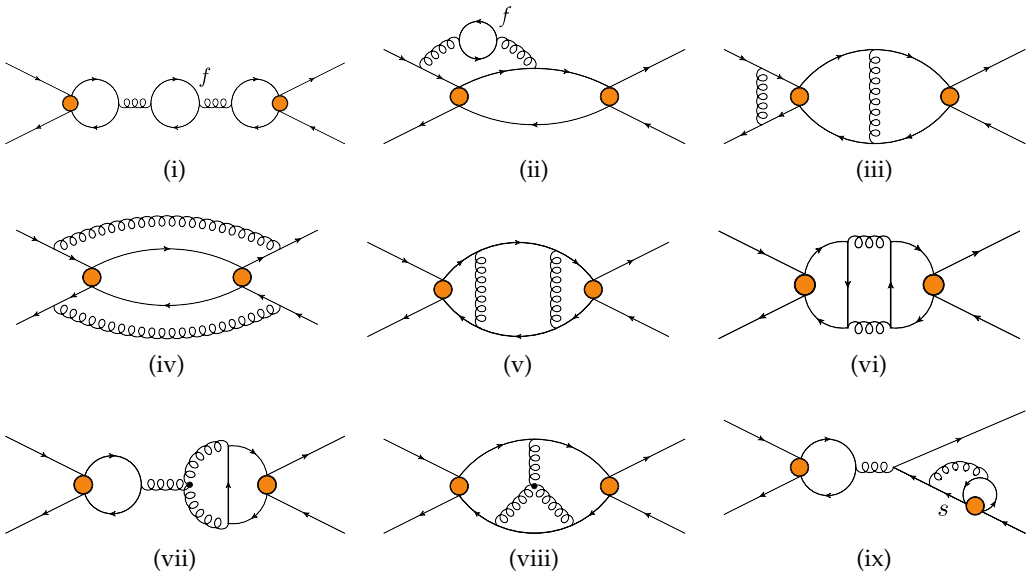

(i) (ii) (iii)
(iv) (v) (vi)
(vii) (viii) (ix)

Figure 6.10: These three-loop diagrams contribute to current-current double insertions at NNLO.

$$
\begin{aligned}
&+\frac{22\ln(z)^2}{9}+\frac{4}{27}\pi^2\ln(z)-\frac{1591\ln(z)}{3}+\frac{128581\zeta(3)}{216}\\
&-\frac{13637\pi^4}{116640}+\frac{203\sqrt{5}\pi^2}{81}+\frac{235469\pi^2}{3888}-\frac{25\pi}{162\sqrt{3}}\\
&-\frac{601385353}{583200}+\frac{176}{27}\pi^2\ln(2)-\frac{4321}{324}\pi^2\ln(2)\\
&-\frac{68}{27}\pi^2\ln\left(\frac{1}{2}+\frac{\sqrt{5}}{2}\right)\Bigg]+\frac{3211L_1^2}{324}+\frac{12911L_2L_1}{972}-\frac{5\pi^2L_1}{4}\\
&-\frac{25\pi L_1}{972\sqrt{3}}+\frac{1320817L_1}{17496}-\frac{311L_2^2}{216}+\frac{\pi^2L_2}{162}+\frac{259603L_2}{11664}\\
&+\frac{5t_2}{162\sqrt{3}}-\frac{28333\zeta(3)}{486}+\frac{23\pi^4}{4860}-\frac{2197\sqrt{5}\pi^2}{972}-\frac{216641\pi^2}{69984}\\
&-\frac{25\pi}{1458\sqrt{3}}+\frac{814589597}{4199040}-\frac{71}{972}\pi^2\ln(2)-\frac{5\pi\ln(3)}{1944\sqrt{3}}\\
&-\frac{169}{81}\pi^2\ln\left(\frac{1}{2}+\frac{\sqrt{5}}{2}\right)+\frac{56\mathrm{Cl}_2\left(\frac{\pi}{3}\right)}{243\sqrt{3}}
\end{aligned}
$$

$$
\begin{aligned}
&+n_v\Big(0.0617284\,L_1 z + 4.60031\,z + 4.75206\,\sqrt{z}\\
&-5.55556\,z\ln(z)\Big)\,,\\
p_{12}^{cc,(2)}(z) &= z\Bigg[\frac{256}{3}L_1\ln(z) - 32L_2\ln(z) + \frac{1193L_1^2}{9} + \frac{34L_2^2}{3}\\
&- \frac{44\pi^2 L_1}{9} + \frac{117563L_1}{162} + \frac{64L_1L_2}{3} - \frac{76\pi^2 L_2}{27} + \frac{6350L_2}{27}\\
&+ \frac{8\ln(z)^2}{3} - \frac{16}{9}\pi^2\ln(z) + \frac{364\ln(z)}{3} + \frac{85027\zeta(3)}{90}\\
&+ \frac{20833\pi^4}{4860} + \frac{548\pi^2}{27\sqrt{5}} - \frac{11245\pi^2}{162} + \frac{50\pi}{27\sqrt{3}} + \frac{12685151}{9720}\\
&+ \frac{64}{9}\pi^2\ln(2) - \frac{1361}{27}\pi^2\ln(2) - \frac{176}{45}\pi^2\ln\left(\frac{1}{2}+\frac{\sqrt{5}}{2}\right)\Bigg]\\
&- \frac{1751L_1^2}{54} + \frac{166L_2L_1}{81} + 10\pi^2 L_1 + \frac{25\pi L_1}{81\sqrt{3}} - \frac{1026907L_1}{5832}\\
&- \frac{L_2^2}{18} - \frac{2\pi^2 L_2}{27} - \frac{619L_2}{972} - \frac{10t_2}{27\sqrt{3}} - \frac{10573\zeta(3)}{324} - \frac{799\pi^4}{810}\\
&- \frac{299\sqrt{5}\pi^2}{81} + \frac{497221\pi^2}{11664} + \frac{50\pi}{243\sqrt{3}} - \frac{95740679}{349920}\\
&+ \frac{596}{81}\pi^2\ln(2) + \frac{5\pi\ln(3)}{162\sqrt{3}} - \frac{92}{27}\pi^2\ln\left(\frac{1}{2}+\frac{\sqrt{5}}{2}\right)\\
&- \frac{224\mathrm{Cl}_2\left(\frac{\pi}{3}\right)}{81\sqrt{3}} + n_v\Big(-0.740741\,L_1 z - 85.8705\,z\\
&+48.2515\,\sqrt{z} + 2.66667\,z\ln(z)\Big)\,,\\
p_{22}^{cc,(2)}(z) &= z\Bigg[-88L_1\ln(z) - 48L_2\ln(z) - \frac{122L_1^2}{3} + 17L_2^2 + \frac{26\pi^2 L_1}{3}\\
&- \frac{16583L_1}{54} - 22L_1L_2 + \frac{76\pi^2 L_2}{9} - \frac{109L_2}{18} + 4\ln(z)^2\\
&+ \frac{16}{3}\pi^2\ln(z) - 464\ln(z) + \frac{2521\zeta(3)}{15} + \frac{5203\pi^4}{3240}\\
&+ \frac{28\pi^2}{9\sqrt{5}} + \frac{7097\pi^2}{108} - \frac{50\pi}{9\sqrt{3}} - \frac{12332857}{16200} + \frac{32}{3}\pi^2\ln(2)\\
&- \frac{274}{9}\pi^2\ln(2) - \frac{16}{15}\pi^2\ln\left(\frac{1}{2}+\frac{\sqrt{5}}{2}\right)\Bigg] + \frac{239L_1^2}{18}\\
&- \frac{202L_2L_1}{27} - 15\pi^2 L_1 - \frac{25\pi L_1}{27\sqrt{3}} + \frac{106199L_1}{972} - \frac{19L_2^2}{3}\\
&+ \frac{2\pi^2 L_2}{9} - \frac{5117L_2}{81} + \frac{10t_2}{9\sqrt{3}} - \frac{3157\zeta(3)}{54} + \frac{971\pi^4}{540}\\
&- \frac{13\sqrt{5}\pi^2}{27} - \frac{177247\pi^2}{3888} - \frac{50\pi}{81\sqrt{3}} + \frac{74041}{14580} + \frac{148}{27}\pi^2\ln(2)
\end{aligned}
\tag{6.22}
$$

$$
\begin{aligned}
&- \frac{5\pi \ln(3)}{54\sqrt{3}} - \frac{4}{9}\pi^2 \ln\left(\frac{1}{2} + \frac{\sqrt{5}}{2}\right) + \frac{224\mathrm{Cl}_2\left(\frac{\pi}{3}\right)}{27\sqrt{3}} \\
&+ n_v \left(2.22222\, L_1 z + 70.6121\, z - 105.276\, \sqrt{z} - 32. z \ln(z)\right),
\end{aligned}
$$

$$
\begin{aligned}
p_{11}^{S,cc,(2)}(z) &= z\Bigg[-4\pi^2 L_1 - \frac{98023 L_1}{243} - \frac{32\pi^2 L_2}{81} - \frac{9272 L_2}{81} \\
&- \frac{32}{27}\pi^2 \ln(z) - \frac{9272 \ln(z)}{27} + \frac{29\zeta(3)}{3} - \frac{27529\pi^4}{14580} \\
&- \frac{344\sqrt{5}\pi^2}{81} - \frac{7103\pi^2}{486} - \frac{20\pi}{81\sqrt{3}} - \frac{33198263}{36450} \\
&+ \frac{1826}{81}\pi^2 \ln(2)\Bigg] - \frac{902 L_1^2}{243} - \frac{3064 L_2 L_1}{243} - 2\pi^2 L_1 \\
&- \frac{10\pi L_1}{243\sqrt{3}} - \frac{77617 L_1}{2187} + \frac{260 L_2^2}{27} - \frac{16\pi^2 L_2}{81} - \frac{5504 L_2}{729} \\
&+ \frac{4 t_2}{81\sqrt{3}} + \frac{28528\zeta(3)}{243} + \frac{449\pi^4}{1215} + \frac{1118\sqrt{5}\pi^2}{243} - \frac{44209\pi^2}{8748} \\
&- \frac{20\pi}{729\sqrt{3}} - \frac{67489177}{262440} - \frac{3506}{243}\pi^2 \ln(2) - \frac{\pi \ln(3)}{243\sqrt{3}} \\
&+ \frac{344}{81}\pi^2 \ln\left(\frac{1}{2} + \frac{\sqrt{5}}{2}\right) + \frac{104\mathrm{Cl}_2\left(\frac{\pi}{3}\right)}{243\sqrt{3}} \\
&+ n_v \left(0.0987654\, L_1 z - 26.8617\, z + 27.7812\, \sqrt{z}\right),
\end{aligned}
$$

$$
\begin{aligned}
p_{12}^{S,cc,(2)}(z) &= z\Bigg[32\pi^2 L_1 - \frac{23276 L_1}{81} + \frac{128\pi^2 L_2}{27} - \frac{5248 L_2}{27} \\
&+ \frac{128}{9}\pi^2 \ln(z) - \frac{5248 \ln(z)}{9} - 244\zeta(3) + \frac{5692\pi^4}{1215} \\
&- \frac{160\sqrt{5}\pi^2}{27} + \frac{3238\pi^2}{81} + \frac{80\pi}{27\sqrt{3}} + \frac{5060009}{12150} \\
&+ \frac{208}{27}\pi^2 \ln(2)\Bigg] + \frac{44 L_1^2}{81} - \frac{1856 L_2 L_1}{81} + 16\pi^2 L_1 + \frac{40\pi L_1}{81\sqrt{3}} \\
&- \frac{28733 L_1}{729} + \frac{208 L_2^2}{9} + \frac{64\pi^2 L_2}{27} - \frac{2176 L_2}{243} - \frac{16 t_2}{27\sqrt{3}} \\
&+ \frac{13934\zeta(3)}{81} + \frac{226\pi^4}{405} + \frac{520\sqrt{5}\pi^2}{81} + \frac{39995\pi^2}{1458} + \frac{80\pi}{243\sqrt{3}} \\
&- \frac{1336127}{2187} - \frac{1624}{81}\pi^2 \ln(2) + \frac{4\pi \ln(3)}{81\sqrt{3}} \\
&+ \frac{160}{27}\pi^2 \ln\left(\frac{1}{2} + \frac{\sqrt{5}}{2}\right) - \frac{416\mathrm{Cl}_2\left(\frac{\pi}{3}\right)}{81\sqrt{3}} \\
&+ n_v \left(-1.18519\, L_1 z - 72.3265\, z + 87.73\, \sqrt{z}\right),
\end{aligned}
$$

$$
\begin{aligned}
p_{22}^{S,cc,(2)}(z) \;=\; & z\Bigg[-48\pi^2 L_1 + \frac{18740 L_1}{27} - \frac{128\pi^2 L_2}{9} + \frac{928 L_2}{9} \\
& - \frac{128}{3}\pi^2 \ln(z) + \frac{928\ln(z)}{3} - 600\zeta(3) + \frac{7991\pi^4}{405} \\
& - \frac{32\sqrt{5}\pi^2}{9} - \frac{8038\pi^2}{27} - \frac{80\pi}{9\sqrt{3}} + \frac{6836747}{2025} \\
& + \frac{272}{9}\pi^2 \ln(2)\Bigg] + \frac{604 L_1^2}{27} + \frac{1064 L_2 L_1}{27} - 24\pi^2 L_1 - \frac{40\pi L_1}{27\sqrt{3}} \\
& + \frac{40370 L_1}{243} - \frac{52 L_2^2}{3} - \frac{64\pi^2 L_2}{9} + \frac{6928 L_2}{81} + \frac{16 t_2}{9\sqrt{3}} \\
& - \frac{4388\zeta(3)}{27} + \frac{398\pi^4}{135} + \frac{104\sqrt{5}\pi^2}{27} - \frac{41279\pi^2}{486} - \frac{80\pi}{81\sqrt{3}} \\
& + \frac{27476329}{58320} - \frac{656}{27}\pi^2 \ln(2) - \frac{4\pi\ln(3)}{27\sqrt{3}} \\
& + \frac{32}{9}\pi^2 \ln\left(\frac{1}{2} + \frac{\sqrt{5}}{2}\right) + \frac{416\,\mathrm{Cl}_2\left(\frac{\pi}{3}\right)}{27\sqrt{3}} \\
& + n_v\left(3.55556\, L_1 z + 176.979\, z - 105.276\,\sqrt{z}\right),
\end{aligned}
$$

We use the following abbreviation:

$$
t_2 \;\equiv\; \mathrm{Im}\left[\mathrm{Li}_2\left(\frac{3 - i\sqrt{3}}{6}\right)\right] \;\approx\; -0.389012\,, \tag{6.23}
$$

which stems from the one-loop master integral in fig. 5.2ii.

$\mathrm{Cl}_2(z)$ is the *Clausen function*, defined as (see e.g. ref. [139])

$$
\mathrm{Cl}_2(\theta) \;\equiv\; \sum_{n=1}^{\infty} \frac{\sin(n\theta)}{n^2} \;=\; -\int_0^\theta \mathrm{d}x \ln\left[2\sin\left(\frac{x}{2}\right)\right], \tag{6.24}
$$

with a function value of

$$
\mathrm{Cl}_2\left(\frac{\pi}{3}\right) \;\approx\; 1.014941\,, \tag{6.25}
$$

which occurs in the two-loop master integral shown in fig. 5.3viii and the three-loop master integral in fig. 5.4i.

The terms adapted from ref. [68] are the only part of our result which is not known analytically.

The difference between the "cc" and "uu" contributions is again proportional to powers of z:

$$
\begin{aligned}
p_{11}^{uu,(2)}(z) \;=\; & p_{11}^{cc,(2)}(0) + n_v\Big(-5.55556\, z\ln(z) + 0.0617284\, L_1 z \\
& + 4.60031\, z + 4.75206\,\sqrt{z}\Big)\,, \\
p_{12}^{uu,(2)}(z) \;=\; & p_{12}^{cc,(2)}(0) + n_v\Big(2.66667\, z\ln(z) - 0.740741\, L_1 z - 85.8705\, z
\end{aligned}
$$

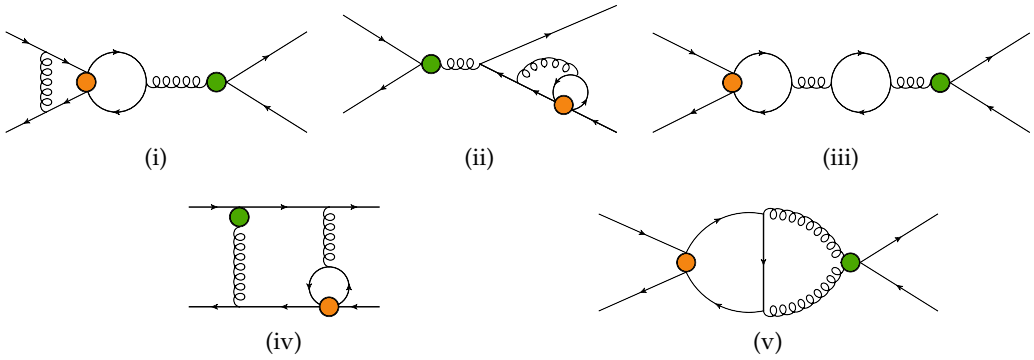

Figure 6.11: The two-loop corrections to $P_{1,2} \times P_8$ include additional 1PI diagrams and the Feynman rule of P_8 with two gluons contributes.

$$\begin{aligned} & +48.2515\sqrt{z}\Big)\,, \\ p_{22}^{uu,(2)}(z) &= p_{22}^{cc,(2)}(0) + n_v\Big(-32\,z\ln(z) + 2.22222\,L_1 z + 70.6121\,z \\ & -105.276\sqrt{z}\Big)\,, \end{aligned} \tag{6.26}$$

$$\begin{aligned} p_{11}^{S,uu,(2)}(z) &= p_{11}^{S,cc,(2)}(0) + n_v\Big(0.0987654\,L_1 z - 26.8617\,z + 27.7812\sqrt{z}\Big)\,, \\ p_{12}^{S,uu,(2)}(z) &= p_{12}^{S,cc,(2)}(0) + n_v\Big(-1.18519\,L_1 z - 72.3265\,z + 87.73\sqrt{z}\Big)\,, \\ p_{22}^{S,uu,(2)}(z) &= p_{22}^{S,cc,(2)}(0) + n_v\Big(3.55556\,L_1 z + 176.979\,z - 105.276\sqrt{z}\Big)\,. \end{aligned}$$

The z-dependence of the "uu" terms is due to charm propagators which are not connected to the spinor lines of $P_{1,2}$. The only occurrences are diagrams such as figs. 6.10i and 6.10ii which match the terms taken from ref. [68].

The "uc" terms can be obtained via

$$\begin{aligned} p_{ij}^{uc,(n)} &= \frac{p_{ij}^{cc,(n)}(z) + p_{ij}^{uu,(n)}(z)}{2}\,, \\ p_{ij}^{S,uc,(n)} &= \frac{p_{ij}^{S,cc,(n)}(z) + p_{ij}^{S,uu,(n)}(z)}{2}\,. \end{aligned} \tag{6.27}$$

The n_f dependent parts of eqs. (6.22) and (6.26) agree with ref. [68] in the limit $z \to 0$ but only for $\mu_1 = \mu_2$.

6.3.2 *Current-Current-Chromomagnetic Contribution*

The two-loop corrections to $P_{1,2} \times P_8$ contribute first at order α_s^2. For this, diagrams as shown in fig. 6.11 have to be evaluated. The Feynman rule of the chromomagnetic operator with two gluons attached appears for the first time at this order.

The corresponding matching coefficients are given by

$$p_{18}^{cc,(2)}(z) = \frac{208 L_1}{81} - \frac{L_2}{27} + \left(\frac{2615}{54} - \frac{10\pi^2}{9}\right) z - \frac{5\pi^2}{9} + \frac{25\pi}{54\sqrt{3}}$$

$$
\begin{aligned}
& - \frac{115}{486}, \\
p_{28}^{cc,(2)}(z) &= -\frac{11L_1}{27} + \frac{2L_2}{9} + \left(\frac{20\pi^2}{3} - \frac{833}{9}\right) z + \frac{10\pi^2}{3} - \frac{25\pi}{9\sqrt{3}} \\
& - \frac{3125}{81}, \\
p_{18}^{S,cc,(2)}(z) &= \frac{448L_1}{81} + \frac{32L_2}{27} + \left(\frac{1192}{27} - \frac{16\pi^2}{9}\right) z - \frac{8\pi^2}{9} + \frac{20\pi}{27\sqrt{3}} \\
& + \frac{3580}{243}, \\
p_{28}^{S,cc,(2)}(z) &= -\frac{248L_1}{27} - \frac{64L_2}{9} + \left(\frac{32\pi^2}{3} - \frac{1088}{9}\right) z + \frac{16\pi^2}{3} - \frac{40\pi}{9\sqrt{3}} \\
& - \frac{4568}{81}.
\end{aligned}
\tag{6.28}
$$

For the "uu" results we get

$$
\begin{aligned}
p_{18}^{uu,(2)}(z) &= p_{18}^{cc,(2)}(0) - \frac{10z}{9}, \\
p_{28}^{uu,(2)}(z) &= p_{28}^{cc,(2)}(0) + \frac{20z}{3}, \\
p_{18}^{S,uu,(2)}(z) &= p_{18}^{S,cc,(2)}(0) - \frac{16z}{9}, \\
p_{28}^{S,uu,(2)}(z) &= p_{28}^{S,cc,(2)}(0) + \frac{32z}{3},
\end{aligned}
\tag{6.29}
$$

and "uc" is again determined by eq. (6.20).

The n_f-parts of these results are in agreement with [68, 69].

6.3.3 *Penguin-Chromomagnetic Contribution*

For the two-loop contributions of $P_{3-6} \times P_8$ similar diagrams as in the previous section occur. In addition, graphs with closed fermion loops have to be taken into account, as shown in fig. 6.12.

The corresponding matching results at $\mathcal{O}(\alpha_s^2)$ read

$$
\begin{aligned}
p_{38}^{cc,(2)}(z) &= -\frac{85L_1}{27} - \frac{448L_2}{9} - \frac{196z}{3} + \frac{25\pi^2}{6} - \frac{107\pi}{18\sqrt{3}} - \frac{17201}{81}, \\
p_{48}^{cc,(2)}(z) &= -\frac{3269L_1}{162} - \frac{427L_2}{27} + \left(\frac{20\pi^2}{3} - \frac{404}{3}\right) z + \frac{169\pi^2}{12} \\
& - \frac{514\pi}{27\sqrt{3}} - \frac{43016}{243}, \\
p_{58}^{cc,(2)}(z) &= \frac{5120L_1}{27} - \frac{7168L_2}{9} - \frac{760z}{3} + \frac{770\pi^2}{9} - \frac{28\pi}{9\sqrt{3}} - \frac{430238}{81}, \\
p_{68}^{cc,(2)}(z) &= -\frac{8962L_1}{81} - \frac{6976L_2}{27} + \left(\frac{200\pi^2}{3} - \frac{4222}{3}\right) z + \frac{3761\pi^2}{27} \\
& - \frac{3220\pi}{27\sqrt{3}} - \frac{474656}{243},
\end{aligned}
\tag{6.30}
$$

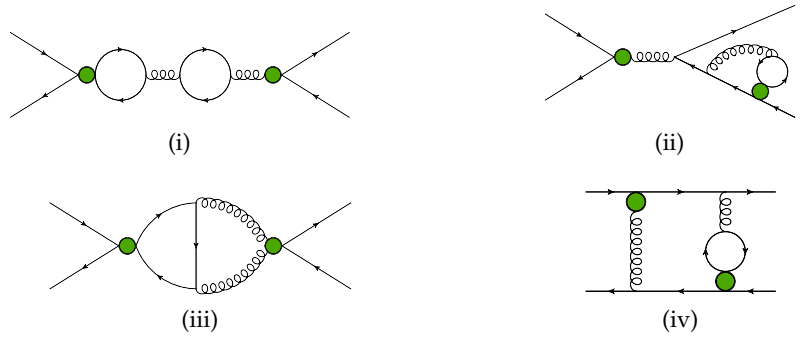

Figure 6.12: Most diagrams of the $P_{3-6} \times P_8$ contribution at two-loop order include closed fermion loops. An exception looks similar to the diagram of fig. 6.11v with internal s-quark lines.

$$
\begin{aligned}
p_{38}^{S,cc,(2)}(z) &= \frac{440L_1}{27} + \frac{512L_2}{9} + \frac{608z}{3} - \frac{596\pi^2}{27} - \frac{52\pi}{9\sqrt{3}} + \frac{22504}{81}, \\
p_{48}^{S,cc,(2)}(z) &= -\frac{4804L_1}{81} - \frac{160L_2}{27} + \left(\frac{32\pi^2}{3} - \frac{128}{3}\right) z + \frac{1090\pi^2}{81} \\
&\quad - \frac{1120\pi}{27\sqrt{3}} - \frac{46988}{243}, \\
p_{58}^{S,cc,(2)}(z) &= \frac{17408L_1}{27} + \frac{8192L_2}{9} + \frac{11456z}{3} - \frac{8912\pi^2}{27} - \frac{1984\pi}{9\sqrt{3}} \\
&\quad + \frac{420304}{81}, \\
p_{68}^{S,cc,(2)}(z) &= -\frac{28624L_1}{81} + \frac{2048L_2}{27} + \left(\frac{320\pi^2}{3} - \frac{160}{3}\right) z + \frac{5608\pi^2}{81} \\
&\quad - \frac{8416\pi}{27\sqrt{3}} - \frac{423440}{243},
\end{aligned}
$$

For the "uu" contributions we get

$$
\begin{aligned}
p_{38}^{uu,(2)}(z) &= p_{38}^{cc,(2)}(0) - \frac{196z}{3}, \\
p_{48}^{uu,(2)}(z) &= p_{48}^{cc,(2)}(0) + \left(-\frac{404}{3} + \frac{20\pi^2}{3}\right) z, \\
p_{58}^{uu,(2)}(z) &= p_{58}^{cc,(2)}(0) - \frac{760z}{3}, \\
p_{68}^{uu,(2)}(z) &= p_{68}^{cc,(2)}(0) + \left(-\frac{4222}{3} + \frac{200\pi^2}{3}\right) z, \\
p_{38}^{S,uu,(2)}(z) &= p_{38}^{S,cc,(2)}(0) + \frac{608z}{3}, \\
p_{48}^{S,uu,(2)}(z) &= p_{48}^{S,cc,(2)}(0) + \left(-\frac{128}{3} + \frac{32\pi^2}{3}\right) z, \\
p_{58}^{S,uu,(2)}(z) &= p_{58}^{S,cc,(2)}(0) + \frac{11456z}{3}, \\
p_{68}^{S,uu,(2)}(z) &= p_{68}^{S,cc,(2)}(0) + \left(-\frac{160}{3} + \frac{320\pi^2}{3}\right) z.
\end{aligned}
\tag{6.31}
$$

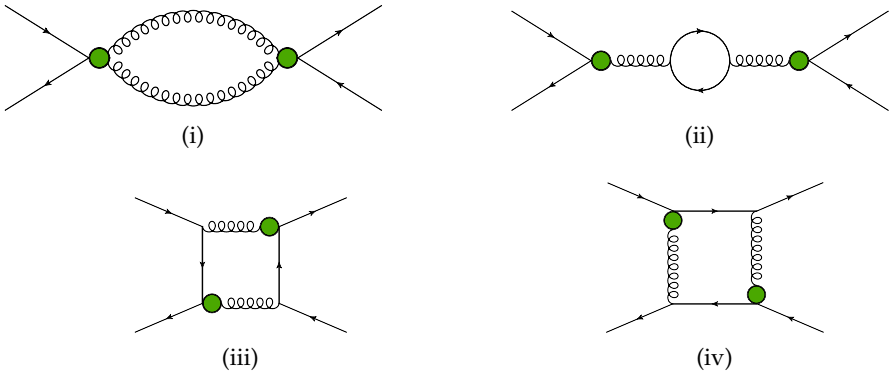

Figure 6.13: Sample one-loop order diagrams with two P_8 insertions are presented. The box diagrams (iii) and (iv) only have allowed cuts through at least one gluon line.

Equation (6.20) can be used to extract the "uc" terms. These results are published in [71].

6.3.4 *Chromomagnetic Double-insertions*

The leading order diagram with two P_8 operator insertions to the process $b\bar{s} \to \bar{b}s$ is a simple tree-level graph with a gluon bridge. Since this diagram has no loop corrections, it has no absorptive part as well and does not contribute to Γ_{12}. The matter changes at NNLO where one-loop diagrams shown in fig. 6.13 are considered. The matching coefficients proportional to $C_8 \times C_8$ are only known up to their n_f dependence [68, 69]. Our results agree with them and are given by

$$\begin{aligned} p_{88}^{cc,(2)}(z) &= p_{88}^{uu,(2)}(z) = p_{88}^{uc,(2)}(z) = -\frac{13}{18}, \\ p_{88}^{S,cc,(2)}(z) &= p_{88}^{S,uu,(2)}(z) = p_{88}^{S,uc,(2)}(z) = -\frac{68}{9}, \end{aligned} \tag{6.32}$$

as shown in ref. [71]. These contributions have manifestly no linear z dependence.

6.4 N^{3}LO RESULTS

In addition to the contributions to Γ_{12} we computed in the previous sections, the question arises how large the effect of the last missing two-loop correction to $P_8 \times P_8$ is. The latter is formally N^{3}LO, i.e. of order α_s^3. It is reasonable to expect that the contributions could be large due to the manifold interaction possibilities of QCD, especially when the two gluon vertex of P_8 is considered. The occurring Feynman diagrams are counted in table 6.7 and illustrated in fig. 6.14. For their renormalization only the finite diagrams from section 6.3.4 have to be evaluated.

Our resulting matching coefficients are given by

$$\begin{aligned} p_{88}^{cc,(3)}(z) &= p_{88}^{uu,(3)}(z) = p_{88}^{uc,(3)}(z), \\ p_{88}^{S,cc,(3)}(z) &= p_{88}^{S,uu,(3)}(z) = p_{88}^{S,uc,(3)}(z). \end{aligned} \tag{6.33}$$

N^{3}LO contributions	Number of diagrams	Number of loops
$P_8 \times P_8$	4174 (4690)	2

Table 6.7: The regarded subset of N^{3}LO diagrams involves only a moderate amount of two-loop diagrams in comparison to other contributions at NNLO or potentially N^{3}LO. The shown numbers are presented similarly as in table 6.3.

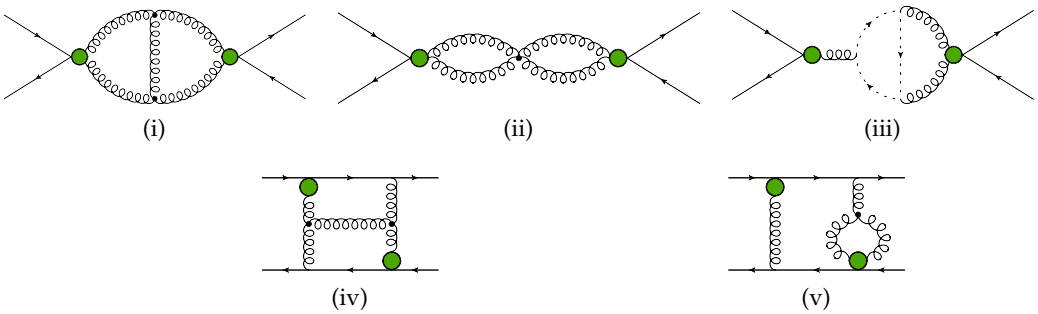

Figure 6.14: Sample diagrams for $P_8 \times P_8$ at two-loop order are shown.

with

$$\begin{aligned} p_{88}^{cc,(3)}(z) &= -\frac{13L_1}{3} + \frac{233L_2}{27} + \left(\frac{373}{9} - \frac{20\pi^2}{3}\right) z - \frac{208\pi^2}{27} \\ &\quad + \frac{151\pi}{9\sqrt{3}} + \frac{18743}{486}, \\ p_{88}^{S,cc,(3)}(z) &= -\frac{136L_1}{3} - \frac{544L_2}{27} + \left(-\frac{152}{9} - \frac{32\pi^2}{3}\right) z + \frac{28\pi^2}{81} \\ &\quad + \frac{440\pi}{9\sqrt{3}} - \frac{57632}{243}. \end{aligned} \tag{6.34}$$

Most likely the dominant N^{3}LO contributions arise from $P_{1,2} \times P_{1,2}$ which would require the calculation of corresponding four-loop integrals. Additionally, three-loop corrections with evanescent and penguin operators would be necessary for the renormalization of the latter. However, all this is beyond the scope of this thesis.

6.5 DISCUSSION OF THE RESULTS

The presented results of the previous chapter are in accordance with prior calculations, except for the μ_2 dependence of ref. [68]. To test the consistency of the new contributions to Γ_{12} we include several consistency checks.

Contribution			Order
P_{1-6}	$\times$	$E^{(1)}_{1-4}$	α_s^0
P_{1-6}	$\times$	$E^{(2)}_{1,2}$	α_s^0
$P_{1,2}$	$\times$	$E^{(2)}_{3,4}$	α_s^0
$E^{(1)}_{1,2}$	$\times$	$E^{(1)}_{1-4}$	α_s^0
$E^{(1)}_{1,2}$	$\times$	$E^{(2)}_{1,2}$	α_s^0
P_8	$\times$	$E^{(2)}_{1,2}$	α_s
P_{1-6}	$\times$	$E^{(1)}_{1,2}$	α_s
$P_{1,2}$	$\times$	$E^{(1)}_{3,4}$	α_s
$E^{(1)}_{1,2}$	$\times$	$E^{(1)}_{1,2}$	α_s

Table 6.8: In the matching we keep the evanescent $\Delta B = 1$ Wilson coefficients of the operators stated in the left column up to the specified order.

Gauge parameter dependence

Throughout the calculation everything was computed within a general R_ξ gauge.[1] For physical quantities we expect that they are free from the gauge parameter ξ, and hence manifestly gauge invariant. We observe that this is indeed the case for Γ_{12}.

Evanescent Wilson coefficient dependence

We further traced the behavior of the evanescent operators during the whole calculation. This implies keeping the renormalized evanescent Wilson coefficients on the $\Delta B = 1$ as well as on the $\Delta B = 2$ side of the matching. The contributions of table 6.8 were taken into account for the former. Not all combinations of the in section 2.4 introduced operators could be analyzed since evanescent operators contribute with large Dirac matrix chains. For example, the matrix element of $E^{(2)}_3 \times E^{(2)}_3$ would involve a projection on up to $14 \otimes 14$ Dirac matrices. This exceeds the limit of $10 \otimes 10$ γ-matrices we encountered in section 5.2.

For the matrix elements of the $\Delta B = 2$ theory we keep the Wilson coefficients of all four generations of evanescent operators at LO, the first three at $\mathcal{O}(\alpha_s)$ and the first two at $\mathcal{O}(\alpha_s^2)$. We observe that the $\Delta B = 1$ evanescent Wilson coefficients contribute after the matching only to the evanescent coefficients of the $\Delta B = 2$ side. Although it is required in dimensional regularization to match also evanescent coefficients, the dependence on the evanescent $\Delta B = 1$ Wilson coefficients drops out for the physical matching results, as it was expected in chapter 4.

1 With exception of the scaling parameters α_Q and $\alpha_{\widetilde{Q}_S}$ which were obtained in Feynman-'t Hooft gauge.

Renormalization scale dependence

In chapter 4 we describe the matching of the matrix elements at a common scale μ_1. Afterwards, we use RGE techniques of the $\Delta B = 2$ theory to relate the matching coefficients H and $\widetilde{H}_S$ to the hadronic matrix elements defined at an a priori different scale μ_2. Hence, the μ_1 dependence of H and $\widetilde{H}_S$ should be of higher order in α_s. This can be tested from following requirement:

$$\begin{aligned}
\mu_1 \frac{\mathrm{d}}{\mathrm{d}\mu_1} H &= \left[\left(\mu_1 \frac{\mathrm{d}}{\mathrm{d}\mu_1} \alpha_s(\mu_1) \right) \frac{\partial}{\partial \alpha_s(\mu_1)} + \sum_i \left(\mu_1 \frac{\mathrm{d}}{\mathrm{d}\mu_1} C_i \right) \frac{\partial}{\partial C_i} + \mu_1 \frac{\partial}{\partial \mu_1} \right] H \\
&= \left[\beta\left(\alpha_s(\mu_1)\right) \frac{\partial}{\partial \alpha_s(\mu_1)} + \sum_{i,j} \gamma_{ji} C_j \frac{\partial}{\partial C_i} + \mu_1 \frac{\partial}{\partial \mu_1} \right] H \\
&\overset{!}{=} \text{higher order in } \alpha_s \,,
\end{aligned} \tag{6.35}$$

and similarly for $\widetilde{H}_S$. The matrix γ is the ADM of the $\Delta B = 1$ theory. It is currently known up to three-loop order [79, 140], and it can be constructed from the effective renormalization constants presented in appendix A.

For the results proportional to the $\Delta B = 1$ Wilson coefficients and orders in α_s shown previously in this chapter, we find that the derivative of eq. (6.35) is indeed of higher orders in α_s. This means, for example, that the μ_1 dependence of the $C_{1,2} \times C_{1,2}$ contributions is $\mathcal{O}\left(\alpha_s^3\right)$.

IR-regulator dependence

To test the consistency of our matching procedure we used a finite a gluon mass to regulate IR-divergences up to $\mathcal{O}(\alpha_s)$ on both sides of the matching. We followed the same approach as in section 3.5. The corresponding master integrals which appear additionally to figs. 3.2 and 3.4 are shown in fig. 6.15 and given in the ancillary files.

For the considered subset we find the same results as with dimensional regularization.

Further Crosschecks

Every result stated in this chapter was computed by two independent calculations. As already mentioned in section 5.2, the cross-check calculation uses a different approach for tensor reduction. Furthermore, the usage of `tapir` was employed in only one calculation. The agreement of both approaches provides a non-trivial check of the used setups.

Only the results for the master integrals were used in both setups simultaneously. This is however not bothersome since their results are checked numerically. This check also includes the asymptotic expansion of the integrals of section 3.5, which can be tested with the programs `FIESTA` [141] and `pySecDec` [142]. Furthermore, the

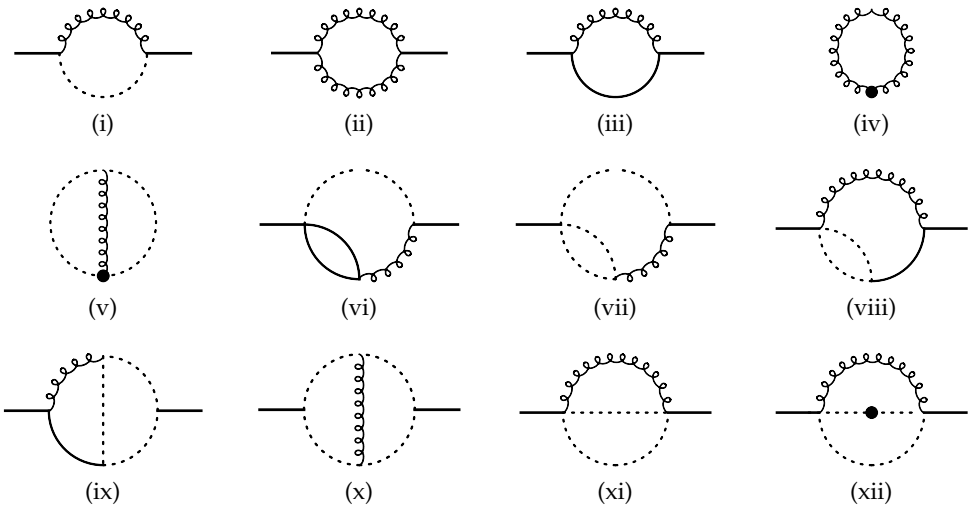

Figure 6.15: These master integrals occur additionally to the ones of figs. 5.2 and 5.3 if the IR divergences are regulated with a non-zero gluon mass (curly lines). With this alternative regularization we find the same result for Γ_{12} as with dimensional regularization up to NLO.

master integrals are additionally checked by expanding in $q^2 \ll m_b^2$ and afterwards taking the limit $q^2 \to m_b^2$.

7

PHENOMENOLOGY

In the following we analyze the results of the previous chapter and their numerical effects on physical observables. We begin with a discussion of Γ_{12}. From eq. (6.1) the following relation is evident:

$$\Gamma_{12} \propto m_b^2 . \tag{7.1}$$

Since this prefactor stems from $q^2 = m_b^2$, we choose $m_b \equiv m_b^{\text{OS}}$ and express the Wilson coefficients according to this choice. From this starting point, we could alternatively express the prefactor of Γ_{12} with a different mass definition. From the perturbation theory point of view, different renormalization conditions are equivalent and can be translated into each other. The differences between observables expressed in various mass definitions are of higher order in α_s. Taking these orders into account should lead to a reduction of the scheme dependence. For comparison, we hence define three different renormalization schemes which we distinguish by their prefactor mass definitions:

- pole: m_b^{OS},
- $\overline{\text{MS}}$: $\overline{m}_b(\mu_b)$,
- Potential Subtracted (PS): m_b^{PS}.

The latter definition subtracts contributions of the heavy quark potential from the OS mass [143]. It is assumed that quantities expressed in terms of m_b^{PS} have a better convergence behavior when taking higher orders in α_s into account in comparison to the OS mass. The subtraction term is currently known up to $\mathcal{O}(\alpha_s^4)$ [144, 145].

Except for the prefactor mass, the remaining terms of Γ_{12} are expressed in terms of $\overline{\text{MS}}$ variables using the relation which transforms the OS mass to $\overline{\text{MS}}$ mass at $\mathcal{O}(\alpha_s^2)$ [117]. For example, at $\mathcal{O}(\alpha_s)$ these relations for $q = b, c$ are given by

$$\begin{aligned} m_q^{\text{OS}} &= \overline{m}_q(\mu_q)\left[1 + C_F\left(\frac{\alpha_s}{4\pi}\right)\left(3\ln\left(\frac{\mu_q^2}{\overline{m}_q^2(\mu_q)}\right) + 4\right)\right] + \mathcal{O}(\alpha_s^2) , \\ z &= \bar{z}\left[1 - 6C_F\left(\frac{\alpha_s}{4\pi}\right)\left(\ln\left(\frac{\mu_b^2}{\mu_c^2}\right) + \ln(\bar{z})\right)\right] + \mathcal{O}(\alpha_s^2) , \end{aligned} \tag{7.2}$$

with

$$\bar{z} = \left(\frac{\overline{m}_c(\mu_c)}{\overline{m}_b(\mu_b)}\right)^2 . \tag{7.3}$$

Together with the $\overline{\text{MS}}$ masses $\overline{m}_c$ and $\overline{m}_b$, new renormalization scales μ_c and μ_b are introduced. Using $\bar{z}$ in favor of z has the advantage of a better convergence behavior. Instead of measuring m_c^{OS} directly, it is determined from its relation to $\overline{m}_c$ [146]. This relation suffers from large corrections in the α_s expansion since the OS mass

$\overline{m}_c(3\,\text{GeV})$	=	$0.993 \pm 0.008\,\text{GeV}$	[148]	$\alpha_s(m_Z)$	=	0.1179 ± 0.001	[149]
$\overline{m}_b(\overline{m}_b)$	=	$4.163 \pm 0.016\,\text{GeV}$	[150]	$\overline{m}_t^{\text{OS}}$	=	$172.9 \pm 0.4\,\text{GeV}$	[149]
M_B^s	=	$5.36688 \pm 0.00014\,\text{GeV}$	[149]	M_B^d	=	$5.27963 \pm 0.00012\,\text{GeV}$	[149]
f_B^s	=	0.2307 ± 0.0013	[151]	f_B^d	=	0.1905 ± 0.0013	[151]
ΔM_s^{exp}	=	$17.7656 \pm 0.0057\,\text{ps}^{-1}$	[152]	ΔM_d^{exp}	=	$0.5065 \pm 0.0019\,\text{ps}^{-1}$	[153]
B_Q^s	=	0.813 ± 0.034	[41]	B_Q^d	=	0.806 ± 0.041	[41]
$B_{\widetilde{Q}_S}^s$	=	1.31 ± 0.09	[41]	$B_{\widetilde{Q}_S}^d$	=	1.20 ± 0.09	[41]
$B'^s_{R_0}$	=	-0.43 ± 0.17	[41]	$B'^d_{R_0}$	=	-0.35 ± 0.19	[41]
$B'^s_{R_1}$	=	0.07	[154]	$B'^d_{R_1}$	$\approx$	0	
$B'^s_{\widetilde{R}_1}$	=	0.04	[154]	$B'^d_{\widetilde{R}_1}$	$\approx$	0	
$B'^s_{R_2}$	=	-0.18 ± 0.07	[154]	$B'^d_{R_2}$	=	$B'^s_{R_2}$	[69]
$B'^s_{R_3}$	=	0.38 ± 0.13	[154]	$B'^d_{R_3}$	=	$B'^s_{R_3}$	[69]
$\lvert V_{cb}\rvert^{\text{incl}}$	=	0.04216 ± 0.00051	[155]	$\lvert V_{cb}\rvert^{\text{excl}}$	=	0.03936 ± 0.00068	[156]
δ	=	$1.196^{+0.045}_{-0.043}$	[149]	$\lvert V_{ub}\rvert/\lvert V_{cb}\rvert$	=	0.083 ± 0.006	[157]
G_F	=	$1.1663787 \times 10^{-5}\,\text{GeV}^{-2}$	[149]				
λ_u^s/λ_t^s	=	$-(0.00865 \pm 0.00042) + (0.01832 \pm 0.00039)i$					[69, 158]
λ_u^d/λ_t^d	=	$(0.0122 \pm 0.0097) - (0.4203 \pm 0.0090)i$					[69, 158]

Table 7.1: Summary of numeric values needed for the determination of $\Delta\Gamma$ and a_{fs} for $B_s/\overline{B}_s$ and $B_d/\overline{B}_d$. The values for $B'^d_{R_1}$ and $B'^d_{\widetilde{R}_1}$ are neglectable since they are suppressed by m_d/m_b [154]. Also, the uncertainties for G_F, $B'^s_{R_1}$ and $B'^s_{\widetilde{R}_1}$ are negligible due to their marginal contribution. We use the abbreviation $\lambda_x^q \equiv V_{xq}^* V_{xb}$. For $\lvert V_{cb}\rvert^{\text{incl}}$ we use an updated value instead of ref. [159].

definition is affected by the renormalon ambiguity (see e.g. ref. [147]). Hence, using $\overline{m}_c$ and $\overline{m}_b$ prevents this issue. For the numeric evaluation of Γ_{12}, we use the exact $\bar{z}$-dependence for the contributions for which it is known in the literature. The remainder is expanded to leading order in $\bar{z}$ after transforming the results to the CMM basis and expanding the $\Delta B = 1$ matching coefficients in α_s.

According to eqs. (1.15) and (1.17), the real and imaginary part of Γ_{12}/M_{12} has to be considered for the determination of $\Delta\Gamma/\Delta M$ and a_{fs}. $\Delta\Gamma$ can be extracted from the approximate formula:

$$\Delta\Gamma \;\approx\; 2|\Gamma_{12}|\,, \tag{7.4}$$

which is affected from the large uncertainty of the prefactor λ_t. If we use instead the ratio Γ_{12}/M_{12} to extract $\Delta\Gamma$, λ_t cancels from eqs. (1.40) and (1.48). Additionally, the bag parameter of the dominant matrix element $\langle Q\rangle$ drops out from Γ_{12}/M_{12} and only the relative size of the remaining bag parameters according to B_Q is considered.

The next-to-leading order corrections to Γ_{12} in the Λ/m_b expansion are known at tree-level and added to our result [47, 63, 67]. For these terms the same mass definition is used for all schemes. We choose m_b^{PS} determined from the N^{3}LO $\overline{\text{MS}}$-PS relation [64].

For the numerical analysis we use the input parameters from table 7.1. Furthermore, the hadronic $\Delta B = 2$ matrix elements are parametrized according to

$$\begin{aligned} \langle B_q | \, Q(\mu_2) \, | \overline{B}_q \rangle &= \frac{8}{3} \left(M_B^q f_B^q \right)^2 B_Q^q(\mu_2) \,, \\ \langle B_q | \, \widetilde{Q}_S(\mu_2) \, | \overline{B}_q \rangle &= \frac{1}{3} \left(M_B^q f_B^q \right)^2 B_{\widetilde{Q}_S}^q(\mu_2) \,, \\ \langle B_q | \, R_i \, | \overline{B}_q \rangle &= \left(M_B^q f_B^q \right)^2 B'^q_{R_i} \,. \end{aligned} \tag{7.5}$$

From eq. (3.5) we see that not all bag parameters B'_{R_i} are independent:

$$\begin{aligned} B'^q_{\widetilde{R}_2} &= -\, B'^q_{R_2} \\ B'^q_{\widetilde{R}_3} &= B'^q_{R_3} + \frac{1}{2} B'^q_{R_2} \,. \end{aligned} \tag{7.6}$$

Additionally, we use the program `RunDec` [64] for the QCD running and flavor-decoupling of quark masses and α_s. For a better comparison, we set the renormalization scales, as defined in chapter 4, to the same values for all schemes. We choose

$$\mu_0 = 165\,\text{GeV} \,, \qquad \mu_b = \mu_c = \mu_1 = 4.2\,\text{GeV} \,, \qquad \mu_2 = m_b^{\text{OS}} \,. \tag{7.7}$$

With table 7.1 we get $m_b^{\text{OS}} = 4.757\,\text{GeV}$ from the two-loop $\overline{\text{MS}}$-OS relation, $\overline{m}_b(4.2\,\text{GeV}) = 4.156\,\text{GeV}$ and $m_b^{\text{PS}} = 4.479\,\text{GeV}$ from the four-loop definition of the PS mass at $\mu = \overline{m}_b(\overline{m}_b)$. We employ $m_b^{\text{PS}} \equiv m_b^{\text{PS}}(\mu_f)$ at the infrared scale $\mu_f = 2\,\text{GeV}$.

Since μ_1 is the matching scale for the HQE of Γ_{12}, we utilize it as a measure to express our restricted knowledge of higher orders in α_s. According to the RGE improved perturbation theory we employ for the $\Delta B = 2$ matching coefficients, the dependence of Γ_{12} on μ_1 is expected to decrease with higher orders in α_s.

7.1 $B_s / \overline{B}_s$

With the NLO result of M_{12} [49], we get the following for $B_s / \overline{B}_s$:

$$\left(\frac{\Delta\Gamma_s}{\Delta M_s} \right)^{\text{pole}} = \left(3.79^{+0.76}_{-0.81\,\text{scale}} \pm 0.11_B \pm 0.78_{1/m_b} \pm 0.05_{\text{input}} \right) \times 10^{-3} \,, \tag{7.8a}$$

$$\left(\frac{\Delta\Gamma_s}{\Delta M_s} \right)^{\overline{\text{MS}}} = \left(4.33^{+0.29}_{-0.44\,\text{scale}} \pm 0.12_B \pm 0.78_{1/m_b} \pm 0.05_{\text{input}} \right) \times 10^{-3} \,, \tag{7.8b}$$

$$\left(\frac{\Delta\Gamma_s}{\Delta M_s} \right)^{\text{PS}} = \left(4.20^{+0.50}_{-0.60\,\text{scale}} \pm 0.12_B \pm 0.78_{1/m_b} \pm 0.05_{\text{input}} \right) \times 10^{-3} \,. \tag{7.8c}$$

The uncertainties indicated by "scale" are given by the minimal and maximal values for the variation of μ_1 in the range between 2.5 and 10 GeV. The "B" uncertainty is propagated from the leading order bag parameters B_Q and $B_{\widetilde{Q}_S}$. "$1/m_b$" are the uncertainties stemming from the bag parameters of the power suppressed hadronic matrix elements. The numbers denoted by "input" include the uncertainties of the remaining input parameters of table 7.1.

A non-negligible part of the scaling uncertainty is accounted to the μ_1 variation of the power suppressed Λ/m_b terms. Numerically, the shift of the central value and the effect on the scale uncertainty stemming from Γ_{12}^{1/m_b} are given by

$$\left(\frac{\Delta\Gamma_s}{\Delta M_s}\right)^{1/m_b} = \left(-1.53^{+0.11}_{-0.13\text{scale}}\right) \times 10^{-3}\,. \tag{7.9}$$

By multiplying the experimental value of ΔM_s to eq. (7.8), the following results are obtained for the width differences:

$$(\Delta\Gamma_s)^{\text{pole}} = \left(6.73^{+1.34}_{-1.43\text{scale}} \pm 0.20_B \pm 1.38_{1/m_b} \pm 0.10_{\text{input}}\right) \times 10^{-2}\,\text{ps}^{-1}\,, \tag{7.10a}$$

$$(\Delta\Gamma_s)^{\overline{\text{MS}}} = \left(7.69^{+0.52}_{-0.78\text{scale}} \pm 0.21_B \pm 1.38_{1/m_b} \pm 0.08_{\text{input}}\right) \times 10^{-2}\,\text{ps}^{-1}\,, \tag{7.10b}$$

$$(\Delta\Gamma_s)^{\text{PS}} = \left(7.46^{+0.89}_{-1.07\text{scale}} \pm 0.21_B \pm 1.38_{1/m_b} \pm 0.08_{\text{input}}\right) \times 10^{-2}\,\text{ps}^{-1}\,. \tag{7.10c}$$

For the combination of the results in the $\overline{\text{MS}}$ and PS schemes, we obtain

$$(\Delta\Gamma_s)^{\text{comb}} = (7.57 \pm 1.63) \times 10^{-2}\,\text{ps}^{-1}\,, \tag{7.11}$$

where the uncertainties of the individual schemes are symmetrized, averaged and finally combined with the standard deviation from both mean values. The reason not to consider the pole scheme in eq. (7.11) is explained below.

This result is compared with the experimental determination [153]:

$$(\Delta\Gamma_s)^{\text{exp}} = (8.2 \pm 0.5) \times 10^{-2}\,\text{ps}^{-1}\,. \tag{7.12}$$

Within the theoretical uncertainties this is in agreement with eq. (7.11).

Similarly, we obtain for the CP asymmetry:

$$(a_{\text{fs}}^s)^{\text{pole}} = \left(2.20^{+0.01}_{-0.07\text{scale}} \pm 0.01_B \pm 0.06_{1/m_b} \pm 0.07_{\text{input}}\right) \times 10^{-5}\,, \tag{7.13a}$$

$$(a_{\text{fs}}^s)^{\overline{\text{MS}}} = \left(2.16^{+0.09}_{-0.16\text{scale}} \pm 0.01_B \pm 0.06_{1/m_b} \pm 0.06_{\text{input}}\right) \times 10^{-5}\,, \tag{7.13b}$$

$$(a_{\text{fs}}^s)^{\text{PS}} = \left(2.22^{+0.05}_{-0.12\text{scale}} \pm 0.01_B \pm 0.06_{1/m_b} \pm 0.07_{\text{input}}\right) \times 10^{-5}\,, \tag{7.13c}$$

with the combined result of the $\overline{\text{MS}}$ and PS scheme:

$$(a_{\text{fs}}^s)^{\text{comb}} = (2.19 \pm 0.14) \times 10^{-5}\,. \tag{7.14}$$

For comparison, at the time of writing the experimental world average is given by [153]

$$(a_{\text{fs}}^s)^{\text{exp}} = (-60 \pm 280) \times 10^{-5}\,. \tag{7.15}$$

Our determined results lie in all schemes within this error bar.

From eq. (7.8) we see a relatively large difference between the scale uncertainties in the different schemes. The μ_1 dependence of $\Delta\Gamma_s/\Delta M_s$ and a_{fs}^s are depicted in

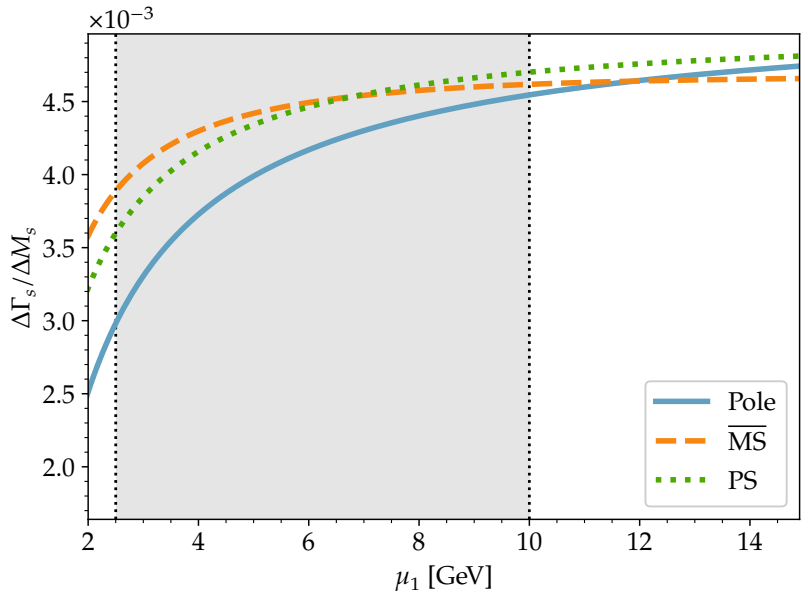

(i)

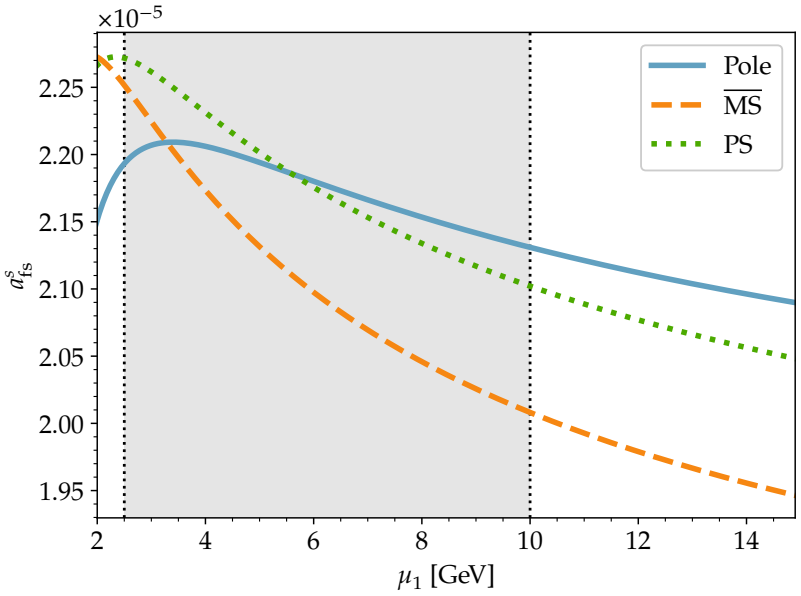

(ii)

Figure 7.1: The μ_1 dependence of $\Delta\Gamma_s/\Delta M_s$ (i) and a_{fs}^s (ii) is shown in all three schemes. The gray band marks the region of μ_1 which is used to quantify the scale uncertainties. The scales μ_b and μ_c are fixed to 4.2 GeV.

fig. 7.1. For $\Delta\Gamma_s/\Delta M_s$, all three curves of fig. 7.1i show a monotonous behavior and the function value bands overlap mostly for μ_1 between 2.5 GeV and 10 GeV. The curves for a_{fs}^s in fig. 7.1ii also show an overlap, but the curves have a local maximum which lies for the pole scheme inside the regarded μ_1 variation range.

To further analyze the scheme differences, the different $\Delta B = 1$ contributions to $\Delta\Gamma_s/\Delta M_s$ are presented in tables 7.2 to 7.4. The splitting between the orders in α_s shows that for $P_{1,2} \times P_{1,2}$ the NLO contribution is of comparable size as the NNLO contribution for the $\overline{\text{MS}}$ and PS scheme. Furthermore, we see a clear suppression of the penguin contributions in comparison to the current-current ones. Also, the higher order corrections in the Λ/m_b expansion have an effect which is of similar size as the leading Λ/m_b terms at NLO.

The μ_1-dependence of $\Delta\Gamma_s/\Delta M_s$ according to the different perturbative corrections with Γ_{12}^{1/m_b}, μ_b and μ_c held fixed are shown in fig. 7.2. In these illustrations one can see no flattening in the curves when comparing $\mathcal{O}(\alpha_s)$ and $\mathcal{O}(\alpha_s^2)$ effects. This can also be observed in figs. 7.2i, 7.2iii and 7.2iii where only the contributions of current-current operators to different orders in α_s are considered.

However, varying instead the renormalization scales $\mu_1 = \mu_b = \mu_c$ simultaneously, shows the expected flattening in the scale dependence of $\Delta\Gamma_s/\Delta M_s$ in the comparison of NLO and NNLO for the case with penguin contributions in figs. 7.3i, 7.3iii and 7.3v, as well as if only $P_{1,2} \times P_{1,2}$ are taken into account in figs. 7.3ii, 7.3iv and 7.3vi.

Concerning the different schemes in which we define the prefactor of Γ_{12}, we see from figs. 7.2 and 7.3 that the $\overline{\text{MS}}$ scheme leads to the most overlap between the values of $\Delta\Gamma_s/\Delta M_s$ according to different orders in α_s. In the PS scheme the bands are further separated but still closer together than in the pole scheme, where the bands barely overlap. Especially when estimating the uncertainty due to unknown corrections in α_s with a variation of only μ_1, as in fig. 7.2, the pole scheme leads to a clear underestimation. This is related to the fact that the corrections of the OS-$\overline{\text{MS}}$ mass relation are large due to the renormalon ambiguity. Thus, the bands separate further when taking higher orders in α_s into account in comparison to other schemes. We conclude that the pole scheme should be replaced in favor of other physically motivated mass schemes, such as the PS scheme which is renormalon free [160]. The differences between the PS and $\overline{\text{MS}}$ schemes are additionally depicted in fig. 7.4, where the simultaneous $\mu_1 = \mu_b = \mu_c$ variation is illustrated. In the latter one can see a clear convergence between both schemes towards the NNLO corrections.

The numerical values of the evanescent factors $e_x^{(i)}$ which are not given in the literature, i.e. the ones that are not stated in eq. (3.7), have only a small effect on the NNLO corrections of $\Delta\Gamma_s/\Delta M_s$. For example, if we vary all of them simultaneously between 0 and 100 the central values of Γ_{12}/M_{12} change by $\mathcal{O}(1)$ percent. For our analysis we use the choice of eq. (3.103).

Another point of interest is the validity of the $\bar{z}$ expansion. In table 7.5 we compare the expansion to $\mathcal{O}(\bar{z}^0)$ and up to $\mathcal{O}(\bar{z})$ according to their effects on the relative size of $P_{1,2} \times P_{1,2}$ contributions to $\Delta\Gamma_s/\Delta M_s$. One can see that the linear order in $\bar{z}$ has an overall effect which is not negligible. For the $\mathcal{O}(\alpha_s^2)$ corrections which are

not known with exact z dependence, the $\bar{z}$ corrections have a moderate size which shows that the expansion in $\bar{z}$ is a useful approximation. For a_{fs} this expansion is more significant since it depends strongly on m_c due to the GIM mechanism.

Contribution	Combined	α_s^0	α_s	α_s^2	α_s^3
$P_{1,2} \times P_{1,2}$	151.%	259.%	−70.2%	−37.7%	–
$P_{1,2} \times P_{3-6}$	−13.9%	−16.1%	2.17%	–	–
$P_{3-6} \times P_{3-6}$	2.52%	2.34%	0.187%	–	–
$P_{1,2} \times P_8$	1.52%	–	1.38%	0.139%	–
$P_{3-6} \times P_8$	−0.513%	–	−0.381%	−0.132%	–
$P_8 \times P_8$	−0.00508%	–	–	−0.00357%	−0.00151%
$1/m_b$	−40.3%	−40.3%	–	–	–

Table 7.2: Relative sizes of individual $\Delta\Gamma_s/\Delta M_s$ contributions to central value in the pole scheme.

Contribution	Combined	α_s^0	α_s	α_s^2	α_s^3
$P_{1,2} \times P_{1,2}$	144.%	173.%	−13.6%	−15.3%	–
$P_{1,2} \times P_{3-6}$	−11.4%	−10.7%	−0.66%	–	–
$P_{3-6} \times P_{3-6}$	1.99%	1.56%	0.427%	–	–
$P_{1,2} \times P_8$	1.2%	–	0.923%	0.274%	–
$P_{3-6} \times P_8$	−0.392%	–	−0.255%	−0.138%	–
$P_8 \times P_8$	−0.00385%	–	–	−0.00238%	−0.00147%
$1/m_b$	−35.3%	−35.3%	–	–	–

Table 7.3: Relative sizes of individual $\Delta\Gamma_s/\Delta M_s$ contributions to central value in the $\overline{\text{MS}}$ scheme.

Contribution	Combined	α_s^0	α_s	α_s^2	α_s^3
$P_{1,2} \times P_{1,2}$	146.%	207.%	−37.2%	−23.9%	–
$P_{1,2} \times P_{3-6}$	−12.3%	−12.8%	0.54%	–	–
$P_{3-6} \times P_{3-6}$	2.19%	1.87%	0.321%	–	–
$P_{1,2} \times P_8$	1.32%	–	1.1%	0.214%	–
$P_{3-6} \times P_8$	−0.438%	–	−0.304%	−0.134%	–
$P_8 \times P_8$	−0.00432%	–	–	−0.00285%	−0.00147%
$1/m_b$	−36.3%	−36.3%	–	–	–

Table 7.4: Relative sizes of individual $\Delta\Gamma_s/\Delta M_s$ contributions to central value in the PS scheme.

In fig. 7.5 we compare in the $\overline{\text{MS}}$ scheme the determination of $\Delta\Gamma_s$ from eq. (7.4) with the ratio $\Delta\Gamma_s/\Delta M_s$. The SM prediction for ΔM_s is shown as well which is given by the approximate formula

$$\Delta M_s \approx 2|M_{12}|\,. \tag{7.16}$$

	α_s^0		α_s		α_s^2	
Scheme	$\bar{z}^0$	$\bar{z}$	$\bar{z}^0$	$\bar{z}$	$\bar{z}^0$	$\bar{z}$
Pole	286.%	260.%	−68.%	−69.8%	−36.6%	−37.7%
$\overline{\text{MS}}$	191.%	174.%	−8.56%	−13.1%	−13.2%	−15.3%
PS	229.%	208.%	−33.5%	−36.8%	−21.8%	−23.9%

Table 7.5: The relative contributions of $P_{1,2} \times P_{1,2}$ to $\Delta\Gamma_s/\Delta M_s$ are shown in different schemes and orders in α_s. The contributions are shown either to $\mathcal{O}(\bar{z}^0)$ or up to $\mathcal{O}(\bar{z})$. Contributions from Γ_{1/m_b} are not considered.

Since M_{12} does not depend on the Γ_{12} matching scale μ_1, and has only a neglectable dependence on μ_0 according to ref. [49], no μ-variation is considered for ΔM_s. The main uncertainty of ΔM_s stems from the input parameter λ_t, for which the CKM matrix elements V_{ts} and V_{tb} have to be inserted. Since only absolute values are needed, we can assume for the former:

$$|V_{ts}| \;=\; |V_{cb}| \;+\; \mathcal{O}\left(\lambda^4\right) , \tag{7.17}$$

which holds according to the Wolfenstein parameterization of eq. (1.30). The precise values for $|V_{tb}|$ and $|V_{ts}|$ are determined using a program by ref. [161] with the CKM parameters δ and $|V_{ub}|/|V_{cb}|$ as input as given in table 7.1. Another problem arises from the tension between different determinations of $|V_{cb}|$ from either inclusive or exclusive B-decays. Both are shown for comparison in fig. 7.5. In table 7.1 we use an updated result for $|V_{cb}|^{\text{incl}}$. The standard input is referenced as $|V_{cb}|^{\text{incl}} = 0.042 \pm 0.0064$ [159]. An alternative approach for the determination from inclusive decays is provided in ref. [162]. We conclude from fig. 7.5 that the determination of $\Delta\Gamma_s$ from $\Delta\Gamma_s/\Delta M_s$ leads to a more reliable result due the ambivalent V_{cb} input. Additionally, the positions of the measured results in this plot show that they agree the most with the inclusive determination of V_{cb}.

7.2 $B_d/\overline{B}_d$

For the $B_d/\overline{B}_d$ system the same arguments hold that we discussed for $B_s/\overline{B}_s$. The only differences between both predictions are the input values for λ_u/λ_t, the bag parameter B_i, the decay constant f_B and the averaged meson mass M_B. Since some Λ/m_b suppressed matrix elements are proportional to m_q/m_b, where q is the spectator quark flavor, they can be neglected for B_d. With the input of table 7.1 we obtain from Γ_{12}^d/M_{12}^d the width difference

$$(\Delta\Gamma_d)^{\text{pole}} \;=\; \left(1.92^{+0.40}_{-0.41\,\text{scale}} \pm 0.06_B \pm 0.40_{1/m_b} \pm 0.03_{\text{input}}\right) \times 10^{-3}\,\text{ps}^{-1} , \tag{7.18a}$$

$$(\Delta\Gamma_d)^{\overline{\text{MS}}} \;=\; \left(2.19^{+0.17}_{-0.23\,\text{scale}} \pm 0.06_B \pm 0.40_{1/m_b} \pm 0.02_{\text{input}}\right) \times 10^{-3}\,\text{ps}^{-1} , \tag{7.18b}$$

$$(\Delta\Gamma_d)^{\text{PS}} \;=\; \left(2.13^{+0.27}_{-0.31\,\text{scale}} \pm 0.06_B \pm 0.40_{1/m_b} \pm 0.03_{\text{input}}\right) \times 10^{-3}\,\text{ps}^{-1} , \tag{7.18c}$$

and the CP asymmetry

$$\left(a_{\text{fs}}^d\right)^{\text{pole}} = \left(-5.06^{+0.17}_{-0.01\,\text{scale}} \pm 0.02_B \pm 0.14_{1/m_b} \pm 0.15_{\text{input}}\right) \times 10^{-4}\,, \tag{7.19a}$$

$$\left(a_{\text{fs}}^d\right)^{\overline{\text{MS}}} = \left(-4.97^{+0.36}_{-0.2\,\text{scale}} \pm 0.02_B \pm 0.14_{1/m_b} \pm 0.15_{\text{input}}\right) \times 10^{-4}\,, \tag{7.19b}$$

$$\left(a_{\text{fs}}^d\right)^{\text{PS}} = \left(-5.11^{+0.28}_{-0.11\,\text{scale}} \pm 0.02_B \pm 0.14_{1/m_b} \pm 0.16_{\text{input}}\right) \times 10^{-4}\,. \tag{7.19c}$$

Since the mentioned differences to B_s are either GIM suppressed or cancel substantially in the ratio $\Delta\Gamma/\Delta M$, we can alternatively use the following to estimate $\Delta\Gamma_d$:

$$\frac{\Delta\Gamma_d}{\Delta M_d} \approx \frac{\Delta\Gamma_s}{\Delta M_s}\,. \tag{7.20}$$

From this assumption, we get

$$(\Delta\Gamma_d)_{\text{alt}}^{\text{pole}} = \left(1.92^{+0.38}_{-0.41\,\text{scale}} \pm 0.06_B \pm 0.39_{1/m_b} \pm 0.03_{\text{input}}\right) \times 10^{-3}\,\text{ps}^{-1}\,, \tag{7.21a}$$

$$(\Delta\Gamma_d)_{\text{alt}}^{\overline{\text{MS}}} = \left(2.19^{+0.15}_{-0.22\,\text{scale}} \pm 0.06_B \pm 0.39_{1/m_b} \pm 0.02_{\text{input}}\right) \times 10^{-3}\,\text{ps}^{-1}\,, \tag{7.21b}$$

$$(\Delta\Gamma_d)_{\text{alt}}^{\text{PS}} = \left(2.13^{+0.25}_{-0.31\,\text{scale}} \pm 0.06_B \pm 0.39_{1/m_b} \pm 0.03_{\text{input}}\right) \times 10^{-3}\,\text{ps}^{-1}\,, \tag{7.21c}$$

where the mean values as well as the uncertainties are comparable to eq. (7.18).

For the combination of the results of eqs. (7.18) and (7.19) in the $\overline{\text{MS}}$ and PS schemes, we obtain

$$(\Delta\Gamma_d)^{\text{comb}} = (2.16 \pm 0.47) \times 10^{-3}\,\text{ps}^{-1}\,, \tag{7.22}$$

$$\left(a_{\text{fs}}^d\right)^{\text{comb}} = (-5.04 \pm 0.33) \times 10^{-4}\,. \tag{7.23}$$

The according determinations from experiment are given by [69, 153]

$$(\Delta\Gamma_d)^{\text{exp}} = (-1.32 \pm 6.58) \times 10^{-3}\,\text{ps}^{-1}\,, \tag{7.24}$$

$$(a_{\text{fs}}^d)^{\text{exp}} = (-21 \pm 17) \times 10^{-4}\,. \tag{7.25}$$

Due to large experimental error, no qualitative statement for $\Delta\Gamma_d$ in comparison to the SM prediction can be made except that they agree within the uncertainty. The same holds for a_{fs}^d.

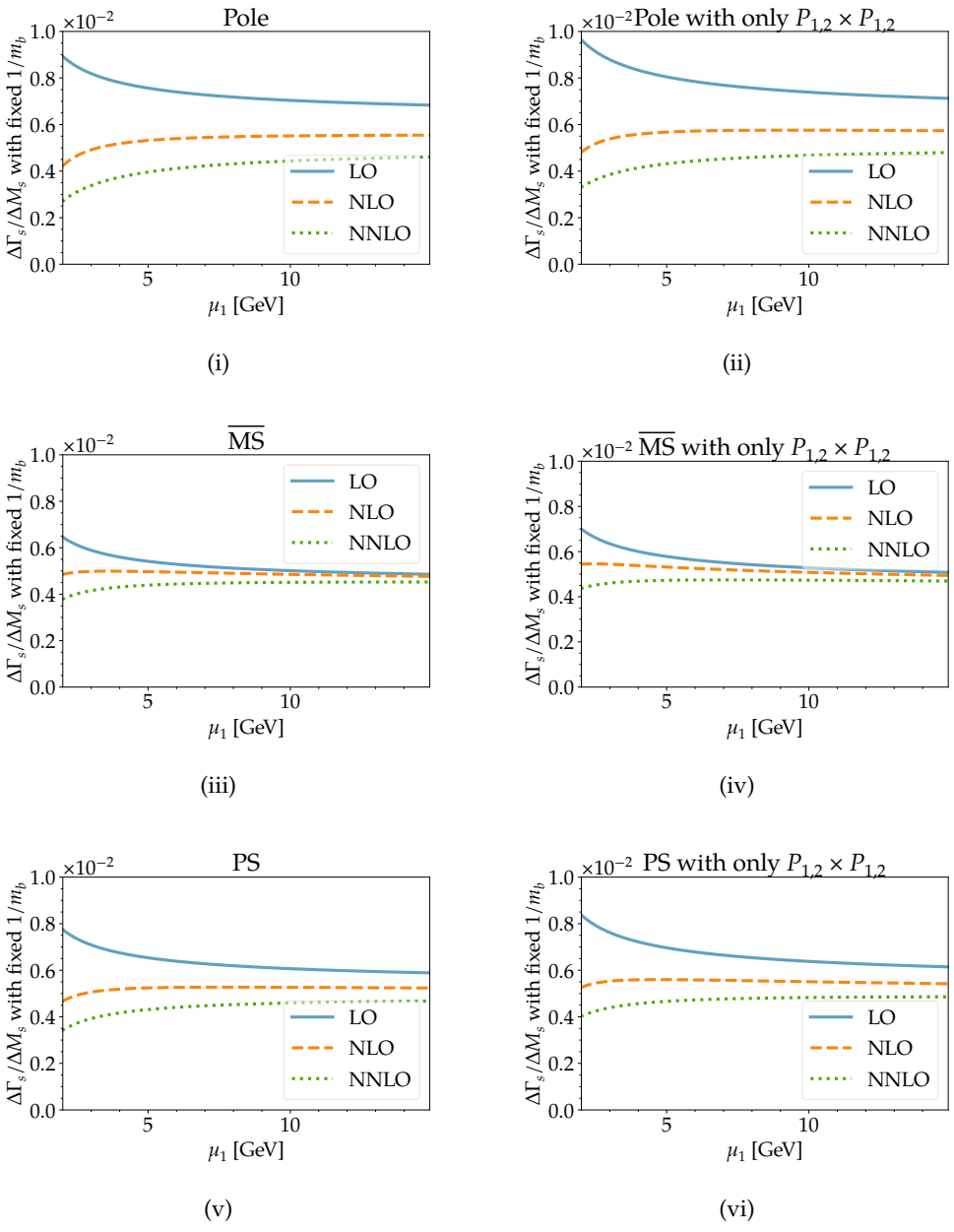

Figure 7.2: The μ_1 dependence of $\Delta\Gamma_s/\Delta M_s$ is presented with the different corrections in α_s for the pole, $\overline{\text{MS}}$ and PS scheme. For the left-hand side all CMM operators are considered, whereas on the right-hand side the penguins contributions are neglected. For these plots the CMM Wilson coefficients are expanded in α_s and only the terms up to α_s^0 are kept for LO, α_s^1 for NLO and α_s^2 for NNLO. The Λ/m_b terms are not varied and equal in each scheme. The scales μ_b and μ_c are fixed to 4.2 GeV.

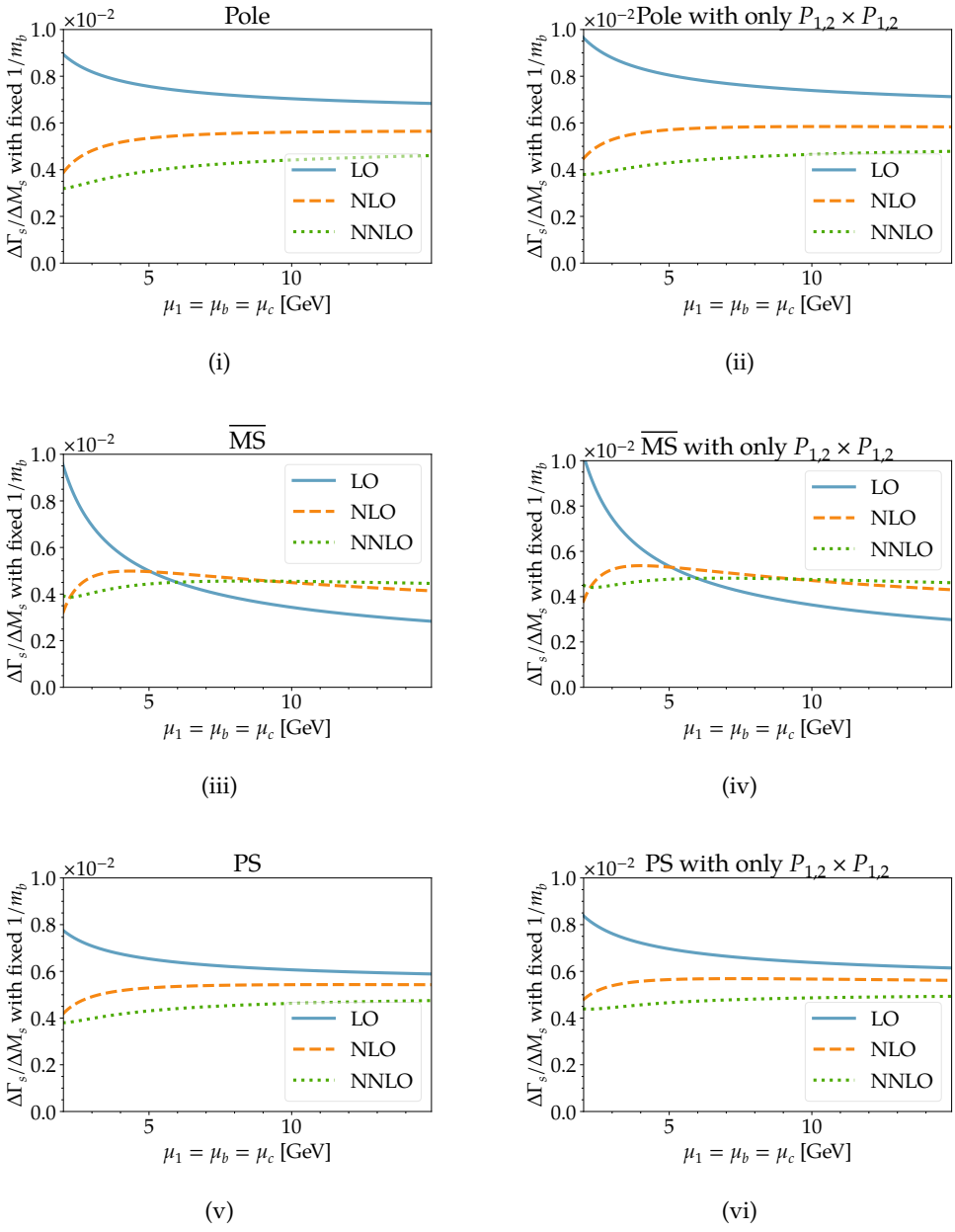

Figure 7.3: The scale variations between the different orders in α_s show a significant difference when the scales $\mu_1 = \mu_b = \mu_c$ are varied simultaneously in comparison to fig. 7.2.

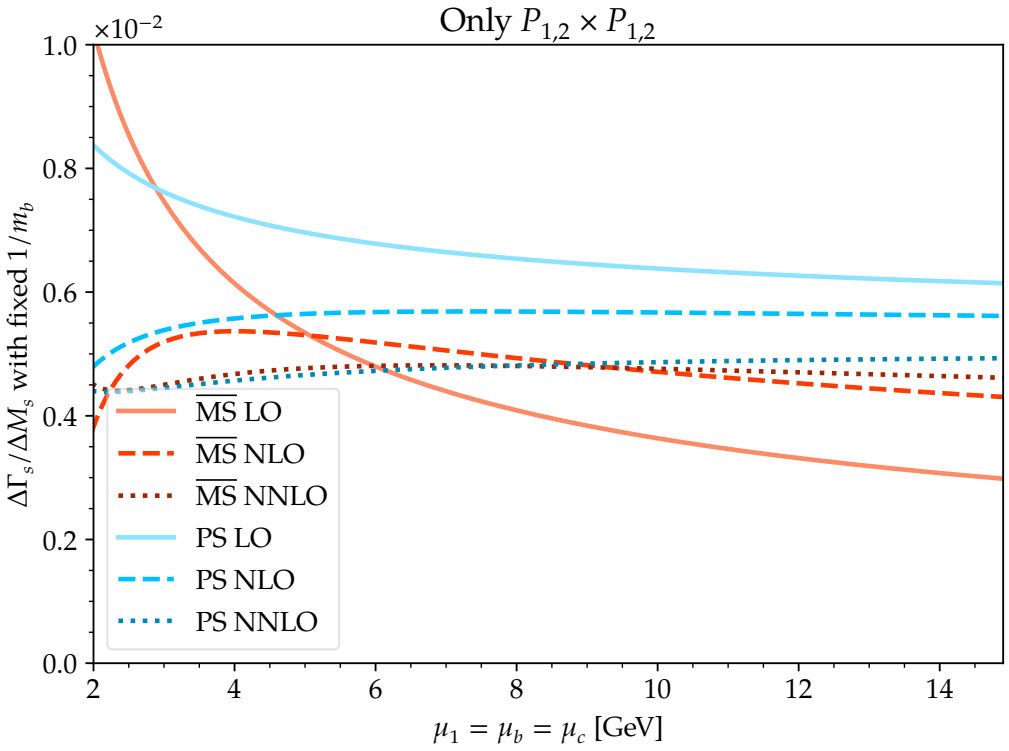

Figure 7.4: The scheme differences between $\overline{\text{MS}}$ and PS are depicted for $\Delta\Gamma_s/\Delta M_s$ for different orders in α_s. For the simultaneous $\mu_1 = \mu_b = \mu_c$ variation, only the contributions of two current-current insertions are considered, and Γ_{1/m_b} is held fixed.

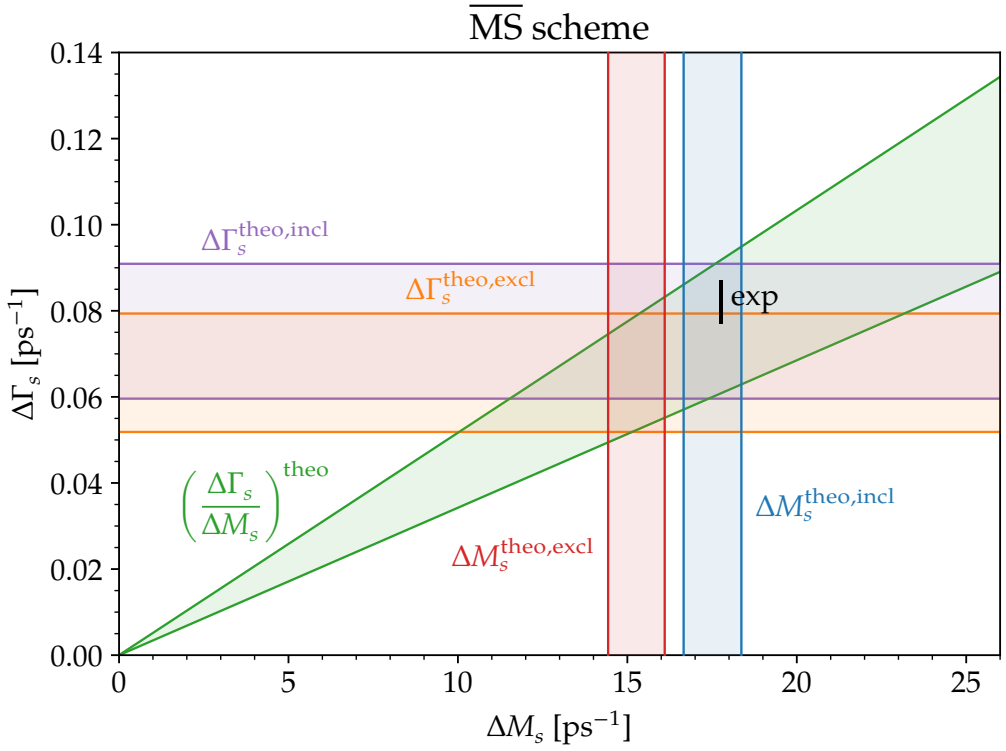

Figure 7.5: In this plot the determinations of $\Delta\Gamma_s$ and ΔM_s from eqs. (7.4) and (7.16) is compared to the ratio $\Delta\Gamma_s/\Delta M_s$ in the $\overline{\text{MS}}$ scheme. We depict two different values for $\Delta\Gamma_s$ and ΔM_s, respectively, with $|V_{cb}|$ determined from exclusive and inclusive B-decays. The experimental results are shown as a box within their 1σ deviation. The experimental error for ΔM_s is bloated by factor of 10 for a better visualization.

8

CONCLUSION AND OUTLOOK

In this work, we computed new predictions for the width difference $\Delta\Gamma$ and the flavor-specific CP-asymmetry a_{fs} of neutral B_s- and B_d-mesons. For the $\Delta B = 1$ side of the matching calculation we used the CMM basis which is a novelty in the determination of $\Delta\Gamma$ and a_{fs}. Furthermore, the $\Delta B = 2$ basis was extended by several new evanescent operators. We computed the corresponding $\Delta B = 2$ renormalization matrix and specified the RGE running of the effective operators or Wilson coefficients together with the two-loop ADM. All results were computed with unspecified evanescent parameters $e_x^{(i)}$ which could provide a future crosscheck for non-perturbative calculations of the hadronic $\Delta B = 2$ operator matrix elements. Other novel results of this work are the finite renormalization factors α_i which give the two-loop matrix element of R_0 the correct power scaling of Λ/m_b. These factors are a necessary input for the determination of the bag parameter of R_0 in lattice or sum rule computations.

For the calculation of $\Delta\Gamma$ and a_{fs} we took contributions of penguin operators $P_{1-6,8}$ into account which describe subleading effects due to their numerically suppressed Wilson coefficients. With them, we completed the calculation of the order α_s corrections at leading order in the HQE. Furthermore, contributions at NNLO were computed including two insertions of current-current operators $P_{1,2}$ which are expected to be the numerically dominant terms of that order. Additionally, further one-loop and two-loop corrections including the chromomagnetic penguin operator P_8 are presented which are formally NNLO and N^{3}LO. Our results were computed up to the second power in m_c using a naive integrand expansion where it is applicable and gives the same result as the asymptotic expansion. Although this expansion leads to small corrections, they are needed for a_{fs} which is sensitive to m_c due to the GIM suppression. Consecutive calculations may include higher orders in m_c to improve the predictions of $\Delta\Gamma$ and especially a_{fs}. We also showed that the NNLO corrections to $\Delta\Gamma$ are of comparable size as the NLO ones which is due to the small size of the latter. This leads to the conclusion that further contributions should be considered, including penguin effects at NNLO and the presumably dominant current-current effects at N^{3}LO. We have also seen that the power suppressed Λ/m_b corrections are of the same magnitude as NLO contributions of the leading powers in Λ/m_b. Thus, future calculations should consider α_s corrections to Γ_{1/m_b} as well.

We employed a plethora of tools to handle the $\mathcal{O}(10^5)$ Feynman diagrams which occurred in the framework of this work. One of them is `tapir` which was developed in the light of the problems that emerged during the presented calculations. We also encountered the problem of tensor reduction and explained the general idea behind the projection ansatz. During the calculation of Γ_{12} we reached the limitations of this approach and encountered them with technical finesse. However, future projects

have to invest more work in pushing these limits further or using a different tensor reduction method.

Our ambition to reduce the theory uncertainties of $\Delta\Gamma_s$ down to the size of the experimental one has not yet succeeded. However, we improved on the current phenomenological results and laid the groundwork for further calculations. For the observables $\Delta\Gamma_d$, a_{fs}^s and a_{fs}^d the uncertainties of the SM predictions are below the ones of experimental determinations. This provides further motivation for more precise experimental results.

Part III

APPENDIX

A

RENORMALIZATION MATRIX OF THE CMM BASIS

In this appendix, we describe the renormalization of the CMM basis of eqs. (2.26), (2.27) and (2.16) according to the results of refs. [75, 140], and extend it to the current-current operators $P_{1,2}^{uu}$, $P_{1,2}^{uc}$ and $P_{1,2}^{cu}$ which are not stated in the literature. However, their renormalization constants can be reconstructed from the known ones if the renormalization matrix is extended, and the requirement that only operators can mix which describe interactions of the same particles. This means that $P_{1,2}^{cu}$ and $P_{1,2}^{uc}$ operators do not mix with $P_{1,2}^{cc}$, $P_{1,2}^{uu}$ or any penguin operator. For simplicity, we refer here to the renormalization of the Wilson coefficients according to

$$\vec{C}_i^0 \;=\; \vec{C}_j Z_{ji}\,, \qquad \text{with} \qquad Z \;=\; \begin{pmatrix} Z_{QQ} & Z_{QE} \\ Z_{EQ} & Z_{EE} \end{pmatrix}. \tag{A.1}$$

The indices i and j can describe either a physical operator,

$$P \;\equiv\; \{P_1^{cc}, P_2^{cc}, P_1^{cu}, P_2^{cu}, P_1^{uc}, P_2^{uc}, P_1^{uu}, P_2^{uu}, P_3, P_4, P_5, P_6, P_8\}\,, \tag{A.2}$$

or an evanescent operator

$$\begin{aligned} E \;\equiv\; \{&E_1^{(1),cc}, E_2^{(1),cc}, E_1^{(1),cu}, E_2^{(1),cu}, E_1^{(1),uc}, E_2^{(1),uc}, E_1^{(1),uu}, \\ &E_2^{(1),uu}, E_3^{(1)}, E_4^{(1)}, E_1^{(2),cc}, E_2^{(2),cc}, E_1^{(2),cu}, E_2^{(2),cu}, E_1^{(2),uc}, \\ &E_2^{(2),uc}, E_1^{(2),uu}, E_2^{(2),uu}, E_3^{(2)}, E_4^{(2)}\}\,, \end{aligned} \tag{A.3}$$

in the given order. Note that we introduce additional evanescent "uu", "uc" and "cu" operators which are in accordance to the "cc" operators. We use the same parameterization as eq. (2.40).

The renormalization among Wilson coefficients of physical operators up to $\mathcal{O}(\alpha_s^2)$ is given by

$$Z_{QQ}^{(1,1)} \;=\; \begin{pmatrix} -2 & \frac{4}{3} & 0 & 0 & 0 & 0 & 0 & 0 & 0 & -\frac{1}{9} & 0 & 0 & \frac{167}{648} \\ 6 & 0 & 0 & 0 & 0 & 0 & 0 & 0 & 0 & \frac{2}{3} & 0 & 0 & \frac{19}{27} \\ 0 & 0 & -2 & \frac{4}{3} & 0 & 0 & 0 & 0 & 0 & 0 & 0 & 0 & 0 \\ 0 & 0 & 6 & 0 & 0 & 0 & 0 & 0 & 0 & 0 & 0 & 0 & 0 \\ 0 & 0 & 0 & 0 & -2 & \frac{4}{3} & 0 & 0 & 0 & 0 & 0 & 0 & 0 \\ 0 & 0 & 0 & 0 & 6 & 0 & 0 & 0 & 0 & 0 & 0 & 0 & 0 \\ 0 & 0 & 0 & 0 & 0 & 0 & -2 & \frac{4}{3} & 0 & -\frac{1}{9} & 0 & 0 & \frac{167}{648} \\ 0 & 0 & 0 & 0 & 0 & 0 & 6 & 0 & 0 & \frac{2}{3} & 0 & 0 & \frac{19}{27} \\ 0 & 0 & 0 & 0 & 0 & 0 & 0 & 0 & 0 & -\frac{26}{3} & 0 & 1 & \frac{92}{27} \\ 0 & 0 & 0 & 0 & 0 & 0 & 0 & 0 & -\frac{20}{9} & \frac{2n_f}{3} - \frac{80}{9} & \frac{2}{9} & \frac{5}{12} & -\frac{37n_f}{216} - \frac{427}{324} \\ 0 & 0 & 0 & 0 & 0 & 0 & 0 & 0 & 0 & -\frac{128}{3} & 0 & 10 & 9n_f + \frac{2192}{27} \\ 0 & 0 & 0 & 0 & 0 & 0 & 0 & 0 & -\frac{128}{9} & \frac{20n_f}{3} - \frac{272}{9} & \frac{20}{9} & -\frac{1}{3} & \frac{55n_f}{27} - \frac{1906}{81} \\ 0 & 0 & 0 & 0 & 0 & 0 & 0 & 0 & 0 & 0 & 0 & 0 & \frac{2n_f}{3} - \frac{19}{3} \end{pmatrix}, \tag{A.4}$$

$$
Z_{QQ}^{(2,2)} = \begin{pmatrix}
17-\frac{2n_f}{3} & \frac{4n_f}{9}-\frac{26}{3} & 0 & 0 & 0 & 0 & 0 & 0 & \frac{10}{81} & \frac{269}{162}-\frac{2n_f}{27} & -\frac{1}{81} & -\frac{5}{216} & * \\
2n_f-39 & 4 & 0 & 0 & 0 & 0 & 0 & 0 & -\frac{20}{27} & \frac{4n_f}{9}-\frac{188}{27} & \frac{2}{27} & \frac{5}{36} & * \\
0 & 0 & 17-\frac{2n_f}{3} & \frac{4n_f}{9}-\frac{26}{3} & 0 & 0 & 0 & 0 & 0 & 0 & 0 & 0 & * \\
0 & 0 & 2n_f-39 & 4 & 0 & 0 & 0 & 0 & 0 & 0 & 0 & 0 & * \\
0 & 0 & 0 & 0 & 17-\frac{2n_f}{3} & \frac{4n_f}{9}-\frac{26}{3} & 0 & 0 & 0 & 0 & 0 & 0 & * \\
0 & 0 & 0 & 0 & 2n_f-39 & 4 & 0 & 0 & 0 & 0 & 0 & 0 & * \\
0 & 0 & 0 & 0 & 0 & 0 & 17-\frac{2n_f}{3} & \frac{4n_f}{9}-\frac{26}{3} & \frac{10}{81} & \frac{269}{162}-\frac{2n_f}{27} & -\frac{1}{81} & -\frac{5}{216} & * \\
0 & 0 & 0 & 0 & 0 & 0 & 2n_f-39 & 4 & -\frac{20}{27} & \frac{4n_f}{9}-\frac{188}{27} & \frac{2}{27} & \frac{5}{36} & * \\
0 & 0 & 0 & 0 & 0 & 0 & 0 & 0 & \frac{68}{27} & \frac{1919}{27}-\frac{22n_f}{9} & \frac{4}{27} & \frac{n_f}{3}-\frac{269}{36} & * \\
0 & 0 & 0 & 0 & 0 & 0 & 0 & 0 & \frac{1550}{81}-\frac{40n_f}{27} & \frac{4n_f^2}{9}-\frac{67n_f}{6}+\frac{7046}{81} & \frac{4n_f}{27}-\frac{283}{162} & \frac{5n_f}{18}-\frac{455}{108} & * \\
0 & 0 & 0 & 0 & 0 & 0 & 0 & 0 & -\frac{640}{27} & \frac{44n_f}{9}+\frac{7376}{27} & \frac{172}{27} & \frac{10n_f}{3}-\frac{590}{9} & * \\
0 & 0 & 0 & 0 & 0 & 0 & 0 & 0 & \frac{9248}{81}-\frac{328n_f}{27} & \frac{40n_f^2}{9}-\frac{788n_f}{9}+\frac{25904}{81} & \frac{40n_f}{27}-\frac{1292}{81} & \frac{23n_f}{18}-\frac{11}{27} & * \\
0 & 0 & 0 & 0 & 0 & 0 & 0 & 0 & 0 & 0 & 0 & 0 & \frac{4n_f^2}{9}-10n_f+\frac{494}{9}
\end{pmatrix},
\tag{A.5}
$$

$$
Z_{QQ}^{(2,1)} = \begin{pmatrix}
\frac{4n_f}{9}+\frac{79}{12} & \frac{10n_f}{27}-\frac{205}{18} & 0 & 0 & 0 & 0 & 0 & 0 & -\frac{353}{243} & -\frac{1567}{972} & \frac{67}{486} & -\frac{35}{648} & * \\
\frac{5n_f}{3}+\frac{83}{4} & 3 & 0 & 0 & 0 & 0 & 0 & 0 & -\frac{104}{81} & \frac{338}{81} & \frac{14}{81} & \frac{35}{108} & * \\
0 & 0 & \frac{4n_f}{9}+\frac{79}{12} & \frac{10n_f}{27}-\frac{205}{18} & 0 & 0 & 0 & 0 & 0 & 0 & 0 & 0 & * \\
0 & 0 & \frac{5n_f}{3}+\frac{83}{4} & 3 & 0 & 0 & 0 & 0 & 0 & 0 & 0 & 0 & * \\
0 & 0 & 0 & 0 & \frac{4n_f}{9}+\frac{79}{12} & \frac{10n_f}{27}-\frac{205}{18} & 0 & 0 & 0 & 0 & 0 & 0 & * \\
0 & 0 & 0 & 0 & \frac{5n_f}{3}+\frac{83}{4} & 3 & 0 & 0 & 0 & 0 & 0 & 0 & * \\
0 & 0 & 0 & 0 & 0 & 0 & \frac{4n_f}{9}+\frac{79}{12} & \frac{10n_f}{27}-\frac{205}{18} & -\frac{353}{243} & -\frac{1567}{972} & \frac{67}{486} & -\frac{35}{648} & * \\
0 & 0 & 0 & 0 & 0 & 0 & \frac{5n_f}{3}+\frac{83}{4} & 3 & -\frac{104}{81} & \frac{338}{81} & \frac{14}{81} & \frac{35}{108} & * \\
0 & 0 & 0 & 0 & 0 & 0 & 0 & 0 & -\frac{1117}{81} & -\frac{13n_f}{9}-\frac{29129}{324} & \frac{100}{81} & \frac{3493}{432}-\frac{n_f}{18} & * \\
0 & 0 & 0 & 0 & 0 & 0 & 0 & 0 & \frac{92n_f}{81}-\frac{6839}{486} & \frac{667n_f}{9}-\frac{79409}{972} & \frac{509}{81}-\frac{2n_f}{81} & \frac{13499}{2592}-\frac{5n_f}{108} & * \\
0 & 0 & 0 & 0 & 0 & 0 & 0 & 0 & \frac{40n_f}{81}-\frac{81280}{81} & \frac{730n_f}{9}-\frac{127076}{81} & \frac{1944}{4n_f}+\frac{8659}{81} & \frac{37n_f}{9}+\frac{13463}{54} & * \\
0 & 0 & 0 & 0 & 0 & 0 & 0 & 0 & -\frac{40n_f}{9}-\frac{81280}{81} & -\frac{634n_f}{9}-\frac{222446}{243} & \frac{100n_f}{81}-\frac{13001}{243} & \frac{311n_f}{54}+\frac{59429}{648} & * \\
0 & 0 & 0 & 0 & 0 & 0 & 0 & 0 & 0 & 0 & 0 & 0 & \frac{623n_f}{108}-\frac{95}{9}
\end{pmatrix}.
\tag{A.6}
$$

The variable n_f denotes the number of active quark flavors. The asterisk "$*$" indicates unknown entries. In the case of eqs. (A.5) and (A.6) the only unspecified renormalization constants are the ones which mix the bare C_8 into other coefficients at $\mathcal{O}\left(\alpha_s^2\right)$. Due to our definition of P_8 this effect is $\mathcal{O}\left(\alpha_s^3\right)$. Note that our P_8 definition is different from the one in ref. [140].

The renormalization contribution of evanescent to physical Wilson coefficients is given by

$$Z_{QE}^{(1,1)} = \begin{pmatrix}
\frac{5}{12} & \frac{2}{9} & 0 & 0 & 0 & 0 & 0 & 0 & 0 & 0 & 0 & 0 & 0 & 0 & 0 & 0 & 0 & 0 & 0 & 0 \\
1 & 0 & 0 & 0 & 0 & 0 & 0 & 0 & 0 & 0 & 0 & 0 & 0 & 0 & 0 & 0 & 0 & 0 & 0 & 0 \\
0 & 0 & \frac{5}{12} & \frac{2}{9} & 0 & 0 & 0 & 0 & 0 & 0 & 0 & 0 & 0 & 0 & 0 & 0 & 0 & 0 & 0 & 0 \\
0 & 0 & 1 & 0 & 0 & 0 & 0 & 0 & 0 & 0 & 0 & 0 & 0 & 0 & 0 & 0 & 0 & 0 & 0 & 0 \\
0 & 0 & 0 & 0 & \frac{5}{12} & \frac{2}{9} & 0 & 0 & 0 & 0 & 0 & 0 & 0 & 0 & 0 & 0 & 0 & 0 & 0 & 0 \\
0 & 0 & 0 & 0 & 1 & 0 & 0 & 0 & 0 & 0 & 0 & 0 & 0 & 0 & 0 & 0 & 0 & 0 & 0 & 0 \\
0 & 0 & 0 & 0 & 0 & 0 & \frac{5}{12} & \frac{2}{9} & 0 & 0 & 0 & 0 & 0 & 0 & 0 & 0 & 0 & 0 & 0 & 0 \\
0 & 0 & 0 & 0 & 0 & 0 & 1 & 0 & 0 & 0 & 0 & 0 & 0 & 0 & 0 & 0 & 0 & 0 & 0 & 0 \\
0 & 0 & 0 & 0 & 0 & 0 & 0 & 0 & 0 & 0 & 0 & 0 & 0 & 0 & 0 & 0 & 0 & 0 & 0 & 0 \\
0 & 0 & 0 & 0 & 0 & 0 & 0 & 0 & 0 & 0 & 0 & 0 & 0 & 0 & 0 & 0 & 0 & 0 & 0 & 0 \\
0 & 0 & 0 & 0 & 0 & 0 & 0 & 0 & 0 & 1 & 0 & 0 & 0 & 0 & 0 & 0 & 0 & 0 & 0 & 0 \\
0 & 0 & 0 & 0 & 0 & 0 & 0 & 0 & \frac{2}{9} & \frac{5}{12} & 0 & 0 & 0 & 0 & 0 & 0 & 0 & 0 & 0 & 0 \\
0 & 0 & 0 & 0 & 0 & 0 & 0 & 0 & 0 & 0 & 0 & 0 & 0 & 0 & 0 & 0 & 0 & 0 & 0 & 0
\end{pmatrix}, \tag{A.7}$$

$$
Z_{QE}^{(2,2)} = \begin{pmatrix}
\frac{5n_f}{36} - \frac{25}{6} & \frac{2n_f}{27} - \frac{31}{18} & 0 & 0 & 0 & 0 & 0 & 0 & 0 & 0 & \frac{19}{96} & \frac{5}{108} & 0 & 0 & 0 & 0 & 0 & 0 & 0 & 0 \\
\frac{n_f}{3} - \frac{31}{4} & 0 & 0 & 0 & 0 & 0 & 0 & 0 & 0 & 0 & \frac{5}{24} & \frac{1}{9} & 0 & 0 & 0 & 0 & 0 & 0 & 0 & 0 \\
0 & 0 & \frac{5n_f}{36} - \frac{25}{6} & \frac{2n_f}{27} - \frac{31}{18} & 0 & 0 & 0 & 0 & 0 & 0 & 0 & 0 & \frac{19}{96} & \frac{5}{108} & 0 & 0 & 0 & 0 & 0 & 0 \\
0 & 0 & \frac{n_f}{3} - \frac{31}{4} & 0 & 0 & 0 & 0 & 0 & 0 & 0 & 0 & 0 & \frac{5}{24} & \frac{1}{9} & 0 & 0 & 0 & 0 & 0 & 0 \\
0 & 0 & 0 & 0 & \frac{5n_f}{36} - \frac{25}{6} & \frac{2n_f}{27} - \frac{31}{18} & 0 & 0 & 0 & 0 & 0 & 0 & 0 & 0 & \frac{19}{96} & \frac{5}{108} & 0 & 0 & 0 & 0 \\
0 & 0 & 0 & 0 & \frac{n_f}{3} - \frac{31}{4} & 0 & 0 & 0 & 0 & 0 & 0 & 0 & 0 & 0 & \frac{5}{24} & \frac{1}{9} & 0 & 0 & 0 & 0 \\
0 & 0 & 0 & 0 & 0 & 0 & \frac{5n_f}{36} - \frac{25}{6} & \frac{2n_f}{27} - \frac{31}{18} & 0 & 0 & 0 & 0 & 0 & 0 & 0 & 0 & \frac{19}{96} & \frac{5}{108} & 0 & 0 \\
0 & 0 & 0 & 0 & 0 & 0 & \frac{n_f}{3} - \frac{31}{4} & 0 & 0 & 0 & 0 & 0 & 0 & 0 & 0 & 0 & \frac{5}{24} & \frac{1}{9} & 0 & 0 \\
0 & 0 & 0 & 0 & 0 & 0 & 0 & 0 & \frac{1}{9} & 0 & 0 & 0 & 0 & 0 & 0 & 0 & 0 & 0 & \frac{1}{9} & \frac{5}{24} \\
0 & 0 & 0 & 0 & 0 & 0 & 0 & 0 & \frac{5}{108} & 0 & 0 & 0 & 0 & 0 & 0 & 0 & 0 & 0 & \frac{5}{108} & \frac{19}{96} \\
0 & 0 & 0 & 0 & 0 & 0 & 0 & 0 & -\frac{4}{9} & \frac{2n_f}{27} - \frac{77}{18} & 0 & 0 & 0 & 0 & 0 & 0 & 0 & 0 & 0 & 0 \\
0 & 0 & 0 & 0 & 0 & 0 & 0 & 0 & 0 & 0 & \frac{n_f}{3} - \frac{5}{4} & \frac{5n_f}{36} - \frac{137}{72} & 0 & 0 & 0 & 0 & 0 & 0 & 0 & 0
\end{pmatrix}, \tag{A.8}
$$

$$
Z_{QE}^{(2,1)} = \begin{pmatrix}
\frac{1531}{288} - \frac{5n_f}{216} & -\frac{n_f}{81} - \frac{1}{72} & 0 & 0 & 0 & 0 & 0 & 0 & 0 & 0 & \frac{1}{384} & -\frac{35}{864} & 0 & 0 & 0 & 0 & 0 & 0 & 0 & 0 \\
\frac{119}{16} - \frac{n_f}{18} & \frac{8}{9} & 0 & 0 & 0 & 0 & 0 & 0 & 0 & 0 & -\frac{35}{192} & -\frac{7}{72} & 0 & 0 & 0 & 0 & 0 & 0 & 0 & 0 \\
0 & 0 & \frac{1531}{288} - \frac{5n_f}{216} & -\frac{n_f}{81} - \frac{1}{72} & 0 & 0 & 0 & 0 & 0 & 0 & 0 & 0 & \frac{1}{384} & -\frac{35}{864} & 0 & 0 & 0 & 0 & 0 & 0 \\
0 & 0 & \frac{119}{16} - \frac{n_f}{18} & \frac{8}{9} & 0 & 0 & 0 & 0 & 0 & 0 & 0 & 0 & -\frac{35}{192} & -\frac{7}{72} & 0 & 0 & 0 & 0 & 0 & 0 \\
0 & 0 & 0 & 0 & \frac{1531}{288} - \frac{5n_f}{216} & -\frac{n_f}{81} - \frac{1}{72} & 0 & 0 & 0 & 0 & 0 & 0 & 0 & 0 & \frac{1}{384} & -\frac{35}{864} & 0 & 0 & 0 & 0 \\
0 & 0 & 0 & 0 & \frac{119}{16} - \frac{n_f}{18} & \frac{8}{9} & 0 & 0 & 0 & 0 & 0 & 0 & 0 & 0 & -\frac{35}{192} & -\frac{7}{72} & 0 & 0 & 0 & 0 \\
0 & 0 & 0 & 0 & 0 & 0 & \frac{1531}{288} - \frac{5n_f}{216} & -\frac{n_f}{81} - \frac{1}{72} & 0 & 0 & 0 & 0 & 0 & 0 & 0 & 0 & \frac{1}{384} & -\frac{35}{864} & 0 & 0 \\
0 & 0 & 0 & 0 & 0 & 0 & \frac{119}{16} - \frac{n_f}{18} & \frac{8}{9} & 0 & 0 & 0 & 0 & 0 & 0 & 0 & 0 & -\frac{35}{192} & -\frac{7}{72} & 0 & 0 \\
0 & 0 & 0 & 0 & 0 & 0 & 0 & 0 & -\frac{7}{72} & -\frac{35}{192} & 0 & 0 & 0 & 0 & 0 & 0 & 0 & 0 & 0 & 0 \\
0 & 0 & 0 & 0 & 0 & 0 & 0 & 0 & -\frac{35}{864} & \frac{1}{384} & 0 & 0 & 0 & 0 & 0 & 0 & 0 & 0 & -\frac{7}{72} & -\frac{35}{192} \\
0 & 0 & 0 & 0 & 0 & 0 & 0 & 0 & \frac{23}{18} & \frac{51}{4} - \frac{n_f}{18} & 0 & 0 & 0 & 0 & 0 & 0 & 0 & 0 & -\frac{35}{864} & \frac{1}{384} \\
0 & 0 & 0 & 0 & 0 & 0 & 0 & 0 & \frac{7}{6} - \frac{n_f}{81} & \frac{317}{72} - \frac{5n_f}{216} & 0 & 0 & 0 & 0 & 0 & 0 & 0 & 0 & 0 & 0 \\
0 & 0 & 0 & 0 & 0 & 0 & 0 & 0 & 0 & 0 & 0 & 0 & 0 & 0 & 0 & 0 & 0 & 0 & 0 & 0
\end{pmatrix}. \tag{A.9}
$$

The renormalization matrix Z_{EQ} includes finite terms which are already present at $\mathcal{O}(\alpha_s^0)$, but describe $\mathcal{O}(\alpha_s)$ effects due to P_8. The only non-vanishing contributions are given by

$$\begin{aligned} Z^{(0,0)}_{E_3^{(1)}P_8} &= -64\,, & Z^{(0,0)}_{E_4^{(1)}P_8} &= \frac{32}{3}\,, \\ Z^{(0,0)}_{E_3^{(2)}P_8} &= -512\,, & Z^{(0,0)}_{E_4^{(2)}P_8} &= \frac{256}{3}\,. \end{aligned} \tag{A.10}$$

The contributions at $\mathcal{O}(\alpha_s)$ are partially unknown. They are given by

$$Z^{(1,0)}_{EQ} = \begin{pmatrix} 64 & \frac{32}{3} & 0 & 0 & 0 & 0 & 0 & 0 & 0 & \frac{4}{9} & 0 & 0 & -\frac{761}{162} \\ 48 & -64 & 0 & 0 & 0 & 0 & 0 & 0 & 0 & -\frac{8}{3} & 0 & 0 & -\frac{454}{27} \\ 0 & 0 & 64 & \frac{32}{3} & 0 & 0 & 0 & 0 & 0 & 0 & 0 & 0 & 0 \\ 0 & 0 & 48 & -64 & 0 & 0 & 0 & 0 & 0 & 0 & 0 & 0 & 0 \\ 0 & 0 & 0 & 0 & 64 & \frac{32}{3} & 0 & 0 & 0 & 0 & 0 & 0 & 0 \\ 0 & 0 & 0 & 0 & 48 & -64 & 0 & 0 & 0 & 0 & 0 & 0 & 0 \\ 0 & 0 & 0 & 0 & 0 & 0 & 64 & \frac{32}{3} & 0 & \frac{4}{9} & 0 & 0 & -\frac{761}{162} \\ 0 & 0 & 0 & 0 & 0 & 0 & 48 & -64 & 0 & -\frac{8}{3} & 0 & 0 & -\frac{454}{27} \\ 0 & 0 & 0 & 0 & 0 & 0 & 0 & 0 & \frac{8960}{3} & -2432 & -\frac{1280}{3} & 320 & -180n_f - \frac{15824}{3} \\ 0 & 0 & 0 & 0 & 0 & 0 & 0 & 0 & -\frac{4480}{9} & -40n_f - \frac{8864}{3} & \frac{640}{9} & \frac{1280}{3} & \frac{2116}{9} - \frac{1165n_f}{18} \\ * & * & 0 & 0 & 0 & 0 & 0 & 0 & 0 & 16 & 0 & 0 & * \\ * & * & 0 & 0 & 0 & 0 & 0 & 0 & 0 & -96 & 0 & 0 & * \\ 0 & 0 & * & * & 0 & 0 & 0 & 0 & 0 & 0 & 0 & 0 & 0 \\ 0 & 0 & * & * & 0 & 0 & 0 & 0 & 0 & 0 & 0 & 0 & 0 \\ 0 & 0 & 0 & 0 & * & * & 0 & 0 & 0 & 0 & 0 & 0 & 0 \\ 0 & 0 & 0 & 0 & * & * & 0 & 0 & 0 & 0 & 0 & 0 & 0 \\ 0 & 0 & 0 & 0 & 0 & 0 & * & * & 0 & 16 & 0 & 0 & * \\ 0 & 0 & 0 & 0 & 0 & 0 & * & * & 0 & -96 & 0 & 0 & * \\ 0 & 0 & 0 & 0 & 0 & 0 & 0 & 0 & * & * & * & * & * \\ 0 & 0 & 0 & 0 & 0 & 0 & 0 & 0 & * & * & * & * & * \end{pmatrix}. \tag{A.11}$$

All entries of $Z^{(1,1)}_{EQ}$ are either zero or unknown, except for

$$Z^{(1,1)}_{E_3^{(1)}P_8} = \frac{3616}{3} - \frac{128n_f}{3}\,, \quad Z^{(1,1)}_{E_4^{(1)}P_8} = \frac{64n_f}{9} - \frac{80}{9}\,. \tag{A.12}$$

The $\mathcal{O}(\alpha_s^2)$ terms of Z_{EQ} are not known as well.

The renormalization matrix which mixes the Wilson coefficients of evanescent operators among themselves is also only partially known. The $\mathcal{O}(\alpha_s)$ terms read

$$Z_{EE}^{(1,1)} = \begin{pmatrix}
-7 & -\frac{4}{3} & 0 & 0 & 0 & 0 & 0 & 0 & 0 & 0 & \frac{5}{12} & \frac{2}{9} & 0 & 0 & 0 & 0 & 0 & 0 & 0 & 0 \\
-6 & 0 & 0 & 0 & 0 & 0 & 0 & 0 & 0 & 0 & 1 & 0 & 0 & 0 & 0 & 0 & 0 & 0 & 0 & 0 \\
0 & 0 & -7 & -\frac{4}{3} & 0 & 0 & 0 & 0 & 0 & 0 & 0 & 0 & \frac{5}{12} & \frac{2}{9} & 0 & 0 & 0 & 0 & 0 & 0 \\
0 & 0 & -6 & 0 & 0 & 0 & 0 & 0 & 0 & 0 & 0 & 0 & 1 & 0 & 0 & 0 & 0 & 0 & 0 & 0 \\
0 & 0 & 0 & 0 & -7 & -\frac{4}{3} & 0 & 0 & 0 & 0 & 0 & 0 & 0 & 0 & \frac{5}{12} & \frac{2}{9} & 0 & 0 & 0 & 0 \\
0 & 0 & 0 & 0 & -6 & 0 & 0 & 0 & 0 & 0 & 0 & 0 & 0 & 0 & 1 & 0 & 0 & 0 & 0 & 0 \\
0 & 0 & 0 & 0 & 0 & 0 & -7 & -\frac{4}{3} & 0 & 0 & 0 & 0 & 0 & 0 & 0 & 0 & \frac{5}{12} & \frac{2}{9} & 0 & 0 \\
0 & 0 & 0 & 0 & 0 & 0 & -6 & 0 & 0 & 0 & 0 & 0 & 0 & 0 & 0 & 0 & 1 & 0 & 0 & 0 \\
0 & 0 & 0 & 0 & 0 & 0 & 0 & 0 & -\frac{64}{3} & -14 & 0 & 0 & 0 & 0 & 0 & 0 & 0 & 0 & 0 & 1 \\
0 & 0 & 0 & 0 & 0 & 0 & 0 & 0 & -\frac{28}{9} & \frac{13}{3} & 0 & 0 & 0 & 0 & 0 & 0 & 0 & 0 & \frac{2}{9} & \frac{5}{12} \\
* & * & 0 & 0 & 0 & 0 & 0 & 0 & 0 & 0 & * & * & 0 & 0 & 0 & 0 & 0 & 0 & 0 & 0 \\
* & * & 0 & 0 & 0 & 0 & 0 & 0 & 0 & 0 & * & * & 0 & 0 & 0 & 0 & 0 & 0 & 0 & 0 \\
0 & 0 & * & * & 0 & 0 & 0 & 0 & 0 & 0 & 0 & 0 & * & * & 0 & 0 & 0 & 0 & 0 & 0 \\
0 & 0 & * & * & 0 & 0 & 0 & 0 & 0 & 0 & 0 & 0 & * & * & 0 & 0 & 0 & 0 & 0 & 0 \\
0 & 0 & 0 & 0 & * & * & 0 & 0 & 0 & 0 & 0 & 0 & 0 & 0 & * & * & 0 & 0 & 0 & 0 \\
0 & 0 & 0 & 0 & * & * & 0 & 0 & 0 & 0 & 0 & 0 & 0 & 0 & * & * & 0 & 0 & 0 & 0 \\
0 & 0 & 0 & 0 & 0 & 0 & * & * & 0 & 0 & 0 & 0 & 0 & 0 & 0 & 0 & * & * & 0 & 0 \\
0 & 0 & 0 & 0 & 0 & 0 & * & * & 0 & 0 & 0 & 0 & 0 & 0 & 0 & 0 & * & * & 0 & 0 \\
0 & 0 & 0 & 0 & 0 & 0 & 0 & 0 & * & * & 0 & 0 & 0 & 0 & 0 & 0 & 0 & 0 & * & * \\
0 & 0 & 0 & 0 & 0 & 0 & 0 & 0 & * & * & 0 & 0 & 0 & 0 & 0 & 0 & 0 & 0 & * & *
\end{pmatrix}. \tag{A.13}$$

The entries of $Z_{EE}^{(2,i)}$ are throughout unknown.

B

FIERZ IDENTITIES

In this appendix, we recall a simple way to derive Fierz identities in four space-time dimensions as it is stated in ref. [163]. The bilinear covariants basis can be stated by several combinations of independent basis vectors. Instead of using the ones of eq. (2.21), we could as well choose the following 16 basis vectors:

$$\Gamma^A \in \left\{ P_R,\ P_L,\ P_R\gamma^\mu,\ P_L\gamma^\mu,\ \sigma^{\mu\nu} \right\}, \tag{B.1}$$

with $P_{R/L} = (1 \pm \gamma_5)/2$ and $\sigma^{\mu\nu} = i[\gamma^\mu, \gamma^\nu]/2$.

The fact that eq. (B.1) is a closed basis can be used to reduce any spinor space tensor build out of Dirac matrices. First, one has to define a scalar product between the Γ^A. The necessary dual vectors Γ_A for the scalar product are in general different from the Γ^A, and have to fulfill the orthogonality relation of

$$\mathrm{Tr}_4\left(\Gamma^A\Gamma_B\right) \stackrel{!}{=} 2\delta_{AB}\,. \tag{B.2}$$

Note that in eq. (B.2) no sum over Lorentz indices is applied. Thus, the dual basis of eq. (B.1) is given by

$$\Gamma_A \in \left\{ P_R,\ P_L,\ P_L\gamma_\mu,\ P_R\gamma_\mu,\ \frac{1}{2}\sigma_{\mu\nu} \right\}. \tag{B.3}$$

Using the completeness of eq. (B.1), we can write a general bilinear term as

$$X = x_A\Gamma^A, \qquad \text{with} \quad x_A = \frac{1}{2}\mathrm{Tr}_4(X\Gamma_A)\,, \tag{B.4}$$

where we assume Einstein's summation convention.

By inserting eq. (B.2) into eq. (B.4), a completeness relation can be found according to

$$\begin{aligned} X_{ij} &= \frac{1}{2}\sum_{k,l} X_{kl}\Gamma_{A,lk}\Gamma^A_{ij} \\ \Leftrightarrow \quad \sum_{\alpha,\beta} X_{\alpha\beta}\delta_{\alpha i}\delta_{\beta j} &= \frac{1}{2}\sum_{\alpha,\beta} X_{\alpha\beta}\sum_{k,l}\delta_{\alpha k}\delta_{\beta l}\Gamma_{A,lk}\Gamma^A_{ij} \\ \Rightarrow \quad \delta_{\alpha i}\delta_{\beta j} &= \frac{1}{2}\Gamma_{A,\beta\alpha}\Gamma^A_{ij}\,. \end{aligned} \tag{B.5}$$

The last line follows by comparing the coefficients of every matrix element $X_{\alpha\beta}$.

Thus, for a combination of two Dirac chains we get

$$\begin{aligned} \left(X\right)_{ij}\left(Y\right)_{kl} &= \eta\frac{1}{2}\left(X\Gamma_A Y\right)_{il}\left(\Gamma^A\right)_{kj} \\ &= \eta\frac{1}{4}\mathrm{Tr}_4[X\Gamma_A Y\Gamma_B]\ \left(\Gamma^B\right)_{il}\left(\Gamma^A\right)_{kj}\,. \end{aligned} \tag{B.6}$$

We introduce the parameter η to account for a different treatment of fermion operators as anti-commuting Graßmann numbers ($\eta = -1$), and commuting spinors which originate from Feynman rules ($\eta = 1$).

As an example, we prove eqs. (3.2b) and (3.2c):

$$\begin{aligned} 4\,(\sigma^{\mu\nu}P_L)_{ij}\,(\sigma_{\mu\nu}P_L)_{kl} \;&=\; -\,\mathrm{Tr}_4\big[\sigma^{\mu\nu}\sigma_{\mu\nu}P_L\big]\,(P_L)_{il}\,(P_L)_{kj} \\ &\quad -\frac{1}{2}\mathrm{Tr}_4\big[\sigma^{\mu\nu}\sigma_{\rho\sigma}\sigma_{\mu\nu}P_L\big]\,(P_L)_{il}(\sigma^{\rho\sigma})_{kj} \\ &\quad -\frac{1}{2}\mathrm{Tr}_4\big[\sigma^{\mu\nu}\sigma_{\mu\nu}\sigma_{\rho\sigma}P_L\big]\,(\sigma^{\rho\sigma})_{il}(P_L)_{kj} \\ &\quad -\frac{1}{4}\mathrm{Tr}_4\big[\sigma^{\mu\nu}\sigma_{\alpha\beta}\sigma_{\mu\nu}\sigma_{\rho\sigma}P_L\big]\,(\sigma^{\rho\sigma})_{il}(\sigma^{\alpha\beta})_{kj} \\ &=\; -\,24\,(P_L)_{il}\,(P_L)_{kj} - 2(-\delta_{\rho\alpha}\delta_{\sigma\beta} \\ &\quad +\delta_{\rho\beta}\delta_{\sigma\alpha} - \epsilon_{\rho\sigma\alpha\beta})(\sigma^{\rho\sigma})_{il}(\sigma^{\alpha\beta})_{kj}\,. \end{aligned} \tag{B.7}$$

To reduce this further, let us examine the terms on the right-hand side of eqs. (3.2b) and (3.2c):

$$\begin{aligned} 4\,(P_L)_{ij}\,(P_L)_{kl} \;&=\; -\,\mathrm{Tr}_4[P_L]\,(P_L)_{il}\,(P_L)_{kj} \\ &\quad -\frac{1}{4}\mathrm{Tr}_4\big[\sigma_{\alpha\beta}\sigma_{\rho\sigma}P_L\big]\,(\sigma^{\rho\sigma})_{il}(\sigma^{\alpha\beta})_{kj} \\ &=\; -\,2\,(P_L)_{il}\,(P_L)_{kj} + \frac{1}{2}(-\delta_{\rho\alpha}\delta_{\sigma\beta} \\ &\quad -\delta_{\rho\beta}\delta_{\sigma\alpha} - \epsilon_{\rho\sigma\alpha\beta})(\sigma^{\rho\sigma})_{il}(\sigma^{\alpha\beta})_{kj}\,. \end{aligned} \tag{B.8}$$

Combining eqs. (B.7) and (B.8) and putting the expressions between the corresponding fermion operators gives

$$\begin{aligned} 4\,(\sigma^{\mu\nu}P_L)_{ij}\,(\sigma_{\mu\nu}P_L)_{kl} + 16\,(P_L)_{ij}\,(P_L)_{kl} \;&=\; 32\,(P_L)_{il}\,(P_L)_{kj} \\ \Rightarrow \qquad Q_T + 4Q_S \;&=\; -8\tilde{Q}_S\,. \end{aligned} \tag{B.9}$$

For spinors, the right-hand side would have a different sign.

C

EVANESCENCE OF R_0

As stated in eq. (3.4), a certain combination of the operators Q, Q_S and $\widetilde{Q}_S$ is of higher order in the Λ/m_b expansion. In this section, we prove the following four-dimensional identity with respect to possible implications in dimensional regularization:

$$\langle R_0 \rangle^{\text{tree}} \;=\; \frac{1}{2}\langle Q \rangle^{\text{tree}} + \langle Q_S \rangle^{\text{tree}} + \langle \widetilde{Q}_S \rangle^{\text{tree}} \;=\; \mathcal{O}\left(\frac{\Lambda}{m_b}\right), \tag{C.1}$$

which holds up to corrections of order α_s.

Equation (C.1) can only be proven with the usage of explicit four-dimensional relations. In dimensional regularization the power suppression only applies to the $\mathcal{O}(\epsilon^0)$ term. The $\mathcal{O}(\epsilon)$ remainder is still defined at the leading order in the Λ/m_b. Thus, the usage of four-dimensional identities is only allowed by introducing evanescent operators in order to define the scaling of R_0 appropriately.

We start with a four-dimensional Fierz identity and resolve it with the relations derived in appendix B. It is given by

$$\begin{aligned}
(\gamma^\mu P_L)_{ij}\,(\gamma^\nu P_L)_{kl} \;&\overset{d=4}{=}\; -\frac{1}{4}\mathrm{Tr}_4(\gamma^\mu P_L \gamma^\rho P_R \gamma^\nu P_L \gamma^\tau P_R)\,(\gamma_\tau P_L)_{il}\,(\gamma_\rho P_L)_{kj} \\
&=\; -\frac{1}{8}\Big[\mathrm{Tr}_4(\gamma^\mu\gamma^\rho\gamma^\nu\gamma^\tau) + \mathrm{Tr}_4(\gamma^\mu\gamma^\rho\gamma^\nu\gamma^\tau\gamma_5)\Big] \\
&\quad\times (\gamma_\tau P_L)_{il}\,(\gamma_\rho P_L)_{kj} \\
&=\; -\frac{1}{2}(\gamma^\nu P_L)_{il}\,(\gamma^\mu P_L)_{kj} - \frac{1}{2}(\gamma^\mu P_L)_{il}\,(\gamma^\nu P_L)_{kj} \\
&\quad+\frac{1}{2}g^{\mu\nu}\,(\gamma^\rho P_L)_{il}\,(\gamma_\rho P_L)_{kj} \\
&\quad+\frac{i}{2}\epsilon^{\mu\rho\nu\tau}\,(\gamma_\tau P_L)_{il}\,(\gamma_\rho P_L)_{kj}\,.
\end{aligned} \tag{C.2}$$

Furthermore, the equations of motion are needed which hold exactly in d dimensions. Since we discard terms of higher orders in Λ/m_b and assume $m_s \ll m_b$, we can use the Dirac equation in the $\Delta B = 2$ Hamiltonian as

$$\begin{aligned}
i\bar{b}\overleftarrow{\not{\partial}} \;&=\; i\bar{b}\overleftarrow{\not{D}} + \mathcal{O}(m_b^0) \;=\; -m_b\bar{b} + \mathcal{O}(m_b^0)\,, \\
i\not{\partial}s \;&=\; \mathcal{O}(m_b^0)\,.
\end{aligned} \tag{C.3}$$

Thus, only the leading kinematic term of the b-quark is considered.

By neglecting total derivatives we find the following relations:

$$(\bar{b}\overleftarrow{\not{\partial}}P_L s)(\bar{b}\overleftarrow{\not{\partial}}P_L s) \;=\; -m_b^2(\bar{b}P_L s)(\bar{b}P_L s) + \mathcal{O}(m_b) \tag{C.4a}$$

$$\big((\partial^\mu\bar{b})\gamma^\nu P_L s\big)\,\big((\partial_\nu\bar{b})\gamma_\mu P_L s\big) \;=\; -m_b^2\,(\bar{b}P_L s)\,(\bar{b}P_L s) + \mathcal{O}(m_b) \tag{C.4b}$$

$$\begin{aligned}\left((\partial^\mu \bar{b})\gamma^\nu P_L s\right)\left((\partial_\mu \bar{b})\gamma_\nu P_L s\right) &= -\left(\bar{b}\gamma^\nu P_L s\right)\left((\Box \bar{b})\gamma_\nu P_L s\right) \\ &= m_b^2\left(\bar{b}\gamma^\nu P_L s\right)\left(\bar{b}\gamma_\nu P_L s\right) + \mathcal{O}(m_b)\,.\end{aligned} \tag{C.4c}$$

In eq. (C.4c) the analogy of eq. (C.3) for the Klein-Gordon equation has been used.

It is now possible to rewrite Q_S in d dimensions according to

$$\begin{aligned}Q_S &= \left(\bar{b}_i P_L s_i\right)\left(\bar{b}_j P_L s_j\right) \\ &= -\frac{1}{m_b^2}\left(\bar{b}_i \overleftarrow{\not\partial} P_L s_i\right)\left(\bar{b}_j \overleftarrow{\not\partial} P_L s_j\right) + \mathcal{O}(1/m_b) \\ &\overset{(C.2)}{=} \frac{1}{2m_b^2}\Big[\left(\bar{b}_i \overleftarrow{\not\partial} P_L s_j\right)\left(\bar{b}_j \overleftarrow{\not\partial} P_L s_i\right) \\ &\quad + \left((\partial^\mu \bar{b}_i)\gamma^\nu P_L s_j\right)\left((\partial_\nu \bar{b}_j)\gamma_\mu P_L s_i\right) \\ &\quad - \left((\partial^\mu \bar{b}_i)\gamma^\nu P_L s_j\right)\left((\partial_\mu \bar{b}_j)\gamma_\nu P_L s_i\right) \\ &\quad - i\widetilde{\epsilon}^{\mu\rho\nu\tau}\left((\partial_\mu \bar{b}_i)\gamma_\tau P_L s_j\right)\left((\partial_\nu \bar{b}_j)\gamma_\rho P_L s_i\right)\Big] \\ &\quad + E_0 + \mathcal{O}(1/m_b) \\ &\overset{(C.4)}{=} -\widetilde{Q}_S - \frac{1}{2}\widetilde{Q} - \frac{i}{2m_b^2}\widetilde{\epsilon}^{\mu\rho\nu\tau}\left((\partial_\mu \bar{b}_i)\gamma_\tau P_L s_j\right)\left((\partial_\nu \bar{b}_j)\gamma_\rho P_L s_i\right) \\ &\quad + E_0 + \mathcal{O}(\frac{1}{m_b})\,.\end{aligned} \tag{C.5}$$

In eq. (C.5) we introduce the evanescent operator E_0. It is defined as the difference between the relation which is derived by the four-dimensional eq. (C.2).

The object $\widetilde{\epsilon}^{\mu\rho\nu\tau}$ is formally defined in dimensional regularization as

$$\widetilde{\epsilon}^{\mu\rho\nu\tau} \equiv \frac{i}{4}\mathrm{Tr}_d(\gamma^\mu\gamma^\rho\gamma^\nu\gamma^\tau\gamma_5)\,, \tag{C.6}$$

which is total antisymmetric. In our employed NDR scheme, this term must not be evaluated since it leads to ambiguous results. Nevertheless, if only its antisymmetric property is taken into account, the usage of eq. (C.6) is of no concern. The factor of $\widetilde{\epsilon}^{\mu\rho\nu\tau}$ in eq. (C.5) is symmetric under the exchange of the Lorentz indices μ and ν. This can be seen from integration by parts relation and using Schwarz's theorem to allow a symmetric interchange of the derivatives. Hence, the term vanishes, and we are left with the evanescent operator E_0 which is given by

$$E_0 = \frac{1}{2}\widetilde{Q} + Q_S + \widetilde{Q}_S\,. \tag{C.7}$$

However, this does not provide any further information. The only difference between E_0 and e.g. $E_1^{(1)}$ of eq. (3.6a) arises from the fact that E_0 is only evanescent in the leading order in $1/m_b$, whereas the evanescence of $E_1^{(1)}$ follows solely from Fierz symmetry.

For eq. (C.1) it follows,

$$\begin{aligned}\langle R_0\rangle^{\text{tree}} &= \frac{1}{2}\langle Q\rangle^{\text{tree}} + \langle Q_S\rangle^{\text{tree}} + \langle\widetilde{Q}_S\rangle^{\text{tree}} \\ &= \langle E_0\rangle - \frac{1}{2}\langle E_1^{(1)}\rangle + \mathcal{O}\left(\frac{\Lambda}{m_b}\right)\,,\end{aligned} \tag{C.8}$$

where leading term in Λ/m_b manifestly vanishes in four dimensions.

D

CALCULATION SETUP

In this appendix, we summarize the software and the employed methods for the evaluation of Feynman diagrams which is used in the context of this work. In fig. D.1 a flowchart is presented which contains the various programs used for this purpose.

D.1 PROGRAM TOOLCHAIN

The diagram generation according to the allowed Feynman rules is performed with the program `qgraf` [127]. For this, we specify which particles are present in our theory and if they are fermions or bosons. It is also necessary to state the interactions of the particles, such that `qgraf` can build Feynman graph representations of the regarded amplitude. A graph consists of edges, corresponding to the particle propagators, and vertices for particle interactions. `qgraf` also offers filter options to restrain diagram classes. With the option `onshell`, for example, it is possible to generate only diagrams without self-energy corrections on external legs, so-called amputated diagrams. In addition to the graph representation, the program provides the symmetry factor and the relative sign for each diagram.

The next program takes the generated graphs of `qgraf` and inserts the corresponding Feynman rules to build an amplitude. This task is accomplished with `tapir` [121] which is further described in appendix D.2. The output is provided as processable `FORM` [128] code.

The next program is `exp` [118, 119] which is used to map momenta of a Feynman graph onto a set of predefined topologies. The result is a `makefile` which is the entry point for the evaluation setup for all individual graphs, called "`calc`". In the `calc` setup the programs `MATAD` [102] and `MINCER` [120] are included to compute massive tadpole- and massless propagator integrals up to three-loop order. If other integral classes are considered, one can use `tapir` to generate `FORM` scripts which combine the scalar factors of the integral to an *integral family* function of the form

$$I\left(a_1,\ldots,a_n\right) \;=\; \int\ldots\int \frac{\mathrm{d}^d k_1 \ldots \mathrm{d}^d k_l}{(2\pi)^{ld}} \prod_{i=1}^{n} \frac{1}{D_i^{a_i}} \,. \tag{D.1}$$

The set $\{a_i\}$ are denoted as *indices* to describe different members of the family I. The D_i are denominator functions which depend on the masses, external- and loop momenta.

We also use the `FORM` program `color` [164] in `calc`. It enables the computation of group theory factors in various gauge groups. With the help of calc, it is possible to express our results in terms of Casimir operators of the QCD gauge group $\mathrm{SU_c}(n_c)$. However, the $\Delta B = 2$ operators of chapter 3 are not defined in a distinct group

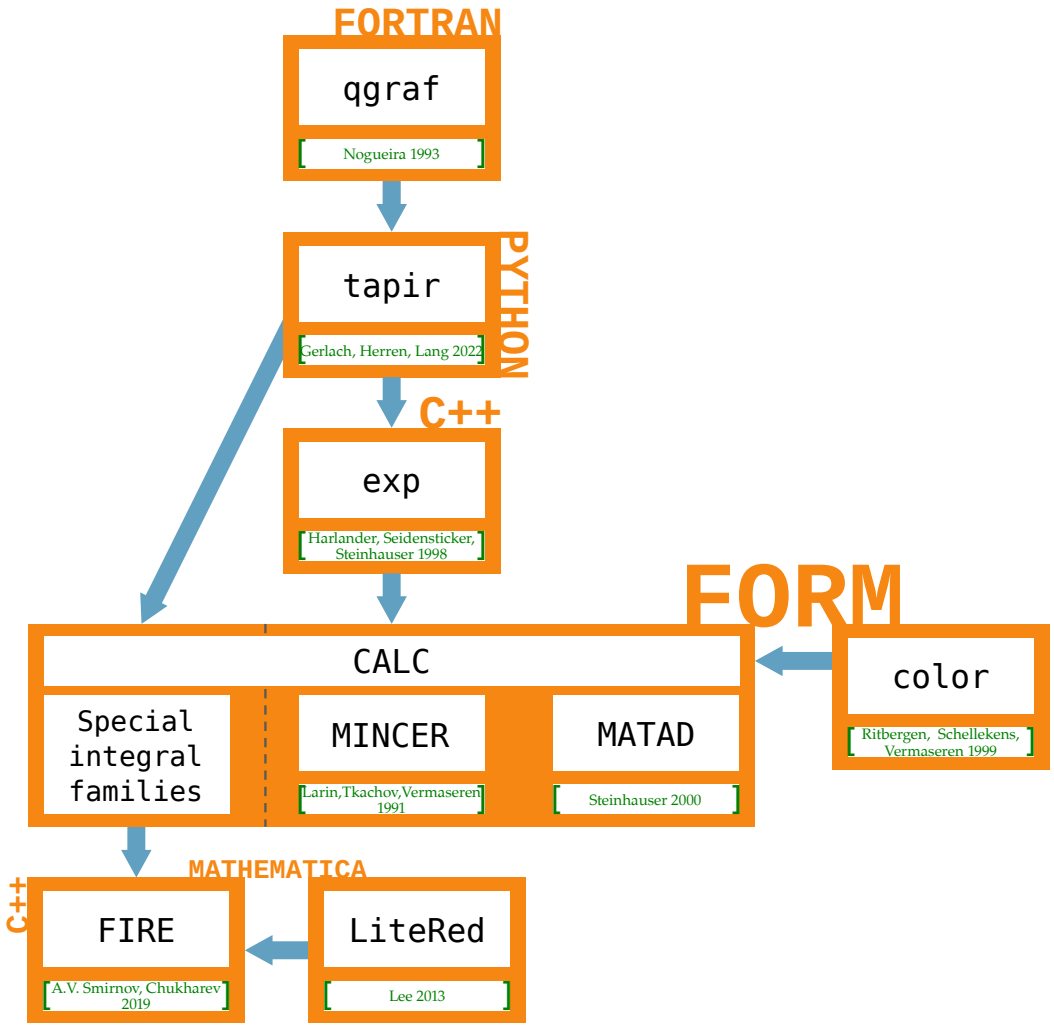

Figure D.1: Our toolchain uses a variety of different programs. Additionally, there are several unmentioned auxiliary scripts which connect the main programs.

representation, like the $\Delta B = 1$ operators. Hence, the matching results can only be stated in terms of the number of colors, n_c.

D.2 THE PROGRAM tapir

As described in appendix D.1, qgraf is the first program we use to generate all Feynman diagrams of the according process. For several subsequent steps we use the program tapir [121] which stands for Topologies, Amplitudes, Partial fraction decomposition and Input for Reduction. tapir is build on the main functionalities of the program q2e [118, 119] but extends them in many ways. To explain all features and to set it in context for future applications, we describe the procedure for the computation of the numerically dominating three-loop contributions to Γ_{12} with a non-vanishing c-quark mass. Thus, we consider the process $b(q_1)\bar{s}(q_2) \to s(q_3)\bar{b}(q_4)$ with $q_1 = q_4 = (m_b, \vec{0})^T$ and $q_2 = q_3 = 0$ in the $\Delta B = 1$ theory of chapter 2 with two current-current operator insertions.

The first problem arises from the fact that diagrams such as shown in fig. D.2i contribute which have self-energy corrections on external legs. To account for these diagrams, tapir provides diagram filters to complement the ones of qgraf. The latter generates with the option offshell only diagrams with self-energy corrections on the external legs, but also including the ones which do not change the flavor of the particle. With respect of the LSZ reduction formula [115], such diagrams must not be taken into account for the calculation of Γ_{12}. The option self_energy_bridge_mixing of tapir searches in the topological structure of the diagram for so-called *bridges*, which denote edges of a graph which do not belong to a loop. If two or more bridges are found, it is checked if all lines between two bridges are 1PI. If this is the case, then a self-energy sub-diagram is found. Additionally, when the two regarded bridges belong to different particle types the filter applies. The same is done for the option external_self_energy_bridge_mixing with the additional restriction that one of the bridges must be an external line. Applying this filter to the output of qgraf reduces the number of three-loop diagrams from $\mathcal{O}(32000)$ to $\mathcal{O}(27000)$.

After filtering the diagrams, it is often advantageous to combine different diagrams according to their topological structure. Thus, the problem size reduces substantially and scalar integral families can be expressed more easily. For this purpose, tapir includes routines to analyze and manipulate the topology of a diagram as well. As a *graph topology* we denote the general graph information, i.e. the set of edges e_i which are given by the set of vertices they connect, and the according edge *colors* which corresponds to the masses of the propagators. In Feynman graphs there are also external edges which carry the external momenta.

One way to express a Feynman graph is given by the so-called *Nickel notation* [165, 166] which consists of two parts. For the example topology of fig. D.2ii, it is given by

```
11ee|2|e3|554|5e|| : Mc_Mc_q1_q2||q3_|Mc_Mc_Mb|_q4||.
```

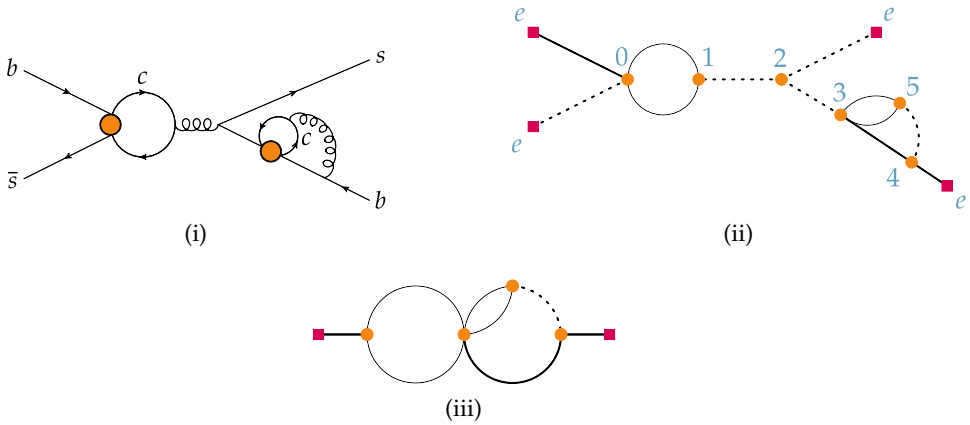

Figure D.2: The example three-loop diagram (i) has a self-energy correction on an external line. Its graph topology is shown in (ii), whereas in (iii) we have applied the topology simplifications of `tapir`. Dashed lines denoted massless edges, solid bold ones have the mass m_b and solid thin lines stand for m_c.

The first part specifies the topological structure of the graph in which each entry describes a vertex and its connection to other vertices. The different entries are separated by a vertical line "|" and describe the vertex of the number at which position it is stated in the notation. For example, the first entry describes the vertex which is labeled as "0". It is connected to vertex "1" via two edges and to two external vertices which are denoted by "e" in the notation. For the subsequent entries the already mentioned connections must not be repeated. Thus, it is sufficient for the entry of vertex "1" to describe only its connection to vertex "2" et cetera. The second part of the Nickel notation defines the coloring of the edges of the first entry. Massive lines are represented by the name of their mass, massless lines are kept empty, and external lines are distinguished by their momenta. The colorings are separated by an underscore "_".

Since the vertices can be numbered in different ways, this notation is not unique. To compare topologies of different graphs, we iterate though all possible enumerations and extract the Nickel notation with the least lexicographic order. This unique label is called *Nickel index*. For the topology of fig. D.2ii, the Nickel index is given by

```
1123|2|e|e4|55|ee| : Mc_Mc_Mb_||q4|q3_|Mc_Mc|q1_q2|.
```

As mentioned, `tapir` includes additional topology manipulation routines which simplify the topological structure without changing the according integral family. For example, since bridges are not part of a loop, their corresponding propagators are loop-momentum independent, and we can remove them from the graph topology. The same is true for auxiliary particles which are used to express complex vertices, e.g. the four-gluon vertex, in way which is better suited for automatized computations. Also, the external s-lines can be removed since their momenta are set to zero. With these simplifications, the topology of our example diagram becomes as shown in fig. D.2iii.

By computing all Nickel indices of the considered three-loop diagrams with the mentioned simplifications, we conclude with $\mathcal{O}(1000)$ different topologies. `tapir`

is capable of generating so-called "topology files" which combine scalar integral expressions in the `calc` setup to scalar integral family functions. In general these families have linear dependent denominators. To apply an IBP reduction we have to perform a partial fraction decomposition first. `tapir` does this step according to the procedure described in appendix D.3. In our three-loop example, this step is not necessary if the option `topo_remove_duplicate_lines` is used which removes duplicate lines with the same momentum and mass.

After applying partial fraction decomposition, several smaller integral families emerge which have in general no graph representation. To be able to reduce the number of these analytic objects, the strategy according ref. [167] is employed. It starts by computing the Symanzik polynomials $\mathcal{U}$ and $\mathcal{F}$ of the family which is described in more detail in appendix D.5. Then, a renaming of the Feynman parameters is applied in such a way that the polynomial $\mathcal{U} \times \mathcal{F}$ is lexicographically minimal. The so found polynomial uniquely characterizes an integral family such that it can be used to identify a priori different families. However, symmetries in an integral family lead to equal lexicographic Feynman parameter labels without an equal $\mathcal{U} \times \mathcal{F}$. Thus, when comparing different polynomials, one has to iterate over all found symmetries. This symmetry handling is characteristic for the *Light Pak algorithm* [142]. The algebraic minimization routine of `tapir` utilizes the algebra system `sympy` [168]. Unfortunately, the reduction of the $\mathcal{O}(1000)$ integral families is too involved for the current implementation of the minimization algorithm. Nevertheless, the output for these families can be used as a direct input for subsequent programs such as `FIRE` [122].

To build amplitudes from the `qgraf` output, `tapir` also provides the insertion of Feynman rules to a `FORM` readable expression. The according rules can either be build manually or by using `FeynRules` [169] with the according `UFO` [170] format. The latter can be processed by `tapir` to get proper `FORM` expressions.

To make use of all these routines, `tapir` supports several output formats. For example, the diagram and topology information is provided in such a way that it serves as an input for `exp`.

D.3 PARTIAL FRACTION DECOMPOSITION

After expressing the Feynman diagrams in terms of integral families, several reduction steps follow to simplify the problem. In general, the denominators D_i are linear dependent which can be reduced using partial fraction decomposition. Diagram families with linear independent denominators are required to apply the reduction step described in appendix D.4. We illustrate the procedure with a simple example which is given by the integral family

$$I\left(a_1, a_2\right) \;=\; \int \frac{\mathrm{d}^d k}{(2\pi)^d} \frac{1}{[k^2 - m_1^2]^{a_1} [k^2 - m_2^2]^{a_2}}\,, \tag{D.2}$$

with $a_1, a_2 \in \mathbb{Z}^+$. Obviously, the following relation between the denominators holds:

$$m_2^2 - m_1^2 \;=\; (k^2 - m_1^2) - (k^2 - m_2^2)\,. \tag{D.3}$$

Since the left-hand side does not dependent on the loop momentum, eq. (D.3) can be used to gradually decrease the indices of $I_1(a_1, a_2)$ by multiplying the ratio of the right- and the left-hand side. We get

$$\begin{aligned} I\left(a_1, a_2\right) &= \frac{1}{m_2^2 - m_1^2} \int \frac{\mathrm{d}^d k}{(2\pi)^d} \left(\frac{1}{[k^2 - m_1^2]^{a_1 - 1} [k^2 - m_2^2]^{a_2}} \right. \\ &\quad \left. - \frac{1}{[k^2 - m_1^2]^{a_1} [k^2 - m_2^2]^{a_2 - 1}} \right) \\ &= \frac{1}{m_2^2 - m_1^2} \Big[I(a_1 - 1, a_2) - I(a_1, a_2 - 1) \Big] . \end{aligned} \tag{D.4}$$

A subsequent application of this rule leads to a reduction into two new integral families:

$$\begin{aligned} I_1\left(a_1\right) &= \int \frac{\mathrm{d}^d k}{(2\pi)^d} \frac{1}{[k^2 - m_1^2]^{a_1}} , \\ I_2\left(a_1\right) &= \int \frac{\mathrm{d}^d k}{(2\pi)^d} \frac{1}{[k^2 - m_2^2]^{a_1}} . \end{aligned} \tag{D.5}$$

Additionally, the reduction is also applicable for $a_1 < 0 < a_2$ or $a_1 > 0 > a_2$. In these cases, eq. (D.4) can be restated to increase the appropriate index.

If more than one relation can be found between the denominator functions, one has to find a way to subsequently remove the denominators without re-inserting another one that was already canceled out. For this purpose, we employ the idea of ref. [167] in `tapir` which states the usage of Gröbner bases [171] for partial fraction decomposition. In principle, the Gröbner basis of the denominator relations directly gives the symbolic substitutions in the correct order to reduce any member of the integral family to subsequent families.

Let us exemplify this idea with the following integral family:

$$\begin{aligned} I\left(a_1, a_2, a_3\right) &= \int \frac{\mathrm{d}^d k}{(2\pi)^d} \frac{1}{[k^2]^{a_1} [k^2 - m_1^2]^{a_2} [k^2 - m_2^2]^{a_3}} \\ &= \int \frac{\mathrm{d}^d k}{(2\pi)^d} \frac{1}{D_1^{a_1} D_2^{a_2} D_3^{a_3}} , \end{aligned} \tag{D.6}$$

where we have $a_1, a_2, a_3 \in \mathbb{Z}$. As an input we need a complete basis of polynomials with the denominator functions D_i as algebraic variables. To also account for numerators, we treat the reciprocal of the denominator function $\widetilde{D}_i \equiv 1/D_i$ as an independent variable as well. As polynomial functions, we construct algebraic relations which are equal to zero, such as

$$K = \{D_1 \widetilde{D}_1 - 1,\, D_2 \widetilde{D}_2 - 1,\, D_3 \widetilde{D}_3 - 1,\, D_1 - D_2 - m_1^2,\, D_1 - D_3 - m_2^2\} . \tag{D.7}$$

The Gröbner basis of K can be determined with the *Buchberger algorithm* [171]. In `tapir` we utilize an improved version of this algorithm which is implemented in `sympy` [172]. The result is given by a reduced polynomial basis expressed in a similar

form one would get from Gaussian elimination. This basis can be then restated as substitution rules. For K we get

$$\begin{aligned}
D_1 &= D_3 + m_2^2\,, \\
D_2 &= D_3 - m_1^2 + m_2^2\,, \\
\frac{D_3}{D_1} &= 1 - \frac{m_2^2}{D_1}\,, \\
\frac{D_3}{D_2} &= 1 + \frac{m_1^2 - m_2^2}{D_2}\,, \\
\frac{1}{D_1 D_2} &= \frac{1}{m_1^2}\left(\frac{1}{D_2} - \frac{1}{D_1}\right)\,, \\
\frac{1}{D_2 D_3} &= \frac{1}{m_1^2 - m_2^2}\left(\frac{1}{D_2} - \frac{1}{D_3}\right)\,, \\
\frac{1}{D_1 D_3} &= \frac{1}{m_2^2}\left(\frac{1}{D_3} - \frac{1}{D_1}\right)\,.
\end{aligned} \tag{D.8}$$

By repeated application of eq. (D.8), every member of I can be reduced to subfamilies with only one remaining denominator function.

D.4 INTEGRATION BY PARTS

If all diagrams are expressed in terms of integral families with linear independent denominators, the commonly used next step is to apply an IBP reduction. The general idea to use this kind relations for Feynman integrals dates back to ref. [173].

A simple example is provided if we take the following integral family into account:

$$I(a_1, a_2) = \int \frac{\mathrm{d}^d k}{(2\pi)^d} \frac{1}{[k^2]^{a_1}[k^2 - 2k\cdot q]^{a_2}}\,. \tag{D.9}$$

An IBP relation can be derived from the requirement that the integrand evaluates to zero at the boundary. Hence, also a total derivative under the integral leads to zero, as in

$$\begin{aligned}
0 &= \int \frac{\mathrm{d}^d k}{(2\pi)^d} \frac{\partial}{\partial k_\mu}\cdot k_\mu \frac{1}{[k^2]^{a_1}[k^2 - 2k\cdot q]^{a_2}} \\
&= (-2a_1 - a_2 + d) I(a_1, a_2) - a_2 I(a_1 - 1, a_2 + 1)\,.
\end{aligned} \tag{D.10}$$

A second relation can be found by changing the differentiation according to

$$\begin{aligned}
0 &= \int \frac{\mathrm{d}^d k}{(2\pi)^d} q_\mu \cdot \frac{\partial}{\partial k_\mu} \frac{1}{[k^2]^{a_1}[k^2 - 2k\cdot q]^{a_2}} \\
&= 2a_2 q^2 I(a_1, a_2 + 1) - a_2 I(a_1 - 1, a_2 + 1) \\
&\quad + (a_2 - a_1) I(a_1, a_2) + a_1 I(a_1 + 1, a_2 - 1)\,.
\end{aligned} \tag{D.11}$$

If we combine eqs. (D.10) and (D.11) and shift the indices, we get

$$I(a_1, a_2) = -\frac{(a_1 + a_2 - d)(2(a_1 + a_2 - 1) - d)}{2(a_2 - 1)q^2(2a_1 + a_2 - d)} I(a_1, a_2 - 1)\,. \tag{D.12}$$

This can be used to iteratively move the second index to $a_2 = 1$, except for $a_2 \leq 1$ in which the integral vanishes. Inserting this result in eq. (D.10) gives

$$I(a_1, 1) = \frac{a_1 - d + 1}{2q^2(2a_1 - d + 1)} I(a_1 - 1, 1)\,, \tag{D.13}$$

which can be used to move the first index to $a_1 = 0$. Thus, every member of the family I can be expressed in terms of the *master integral* $I(0, 1)$.

In multi-loop calculations IBP relations are in general more complicated, and solving the difference equations in a closed form is very time-consuming. A solution to this problem is provided by *Laporta's algorithm* [174]. It became the standard to reduce scalar Feynman integrals to a linear combination of a finite set of master integrals.

For our purposes we use the program `FIRE` [122], which makes use of `LiteRed` [175] to identify and utilize symmetries of integral families. `FIRE` also offers a function to find identical master integrals of different families.

After applying the IBP reduction we are left with a small amount of master integrals in comparison to the original size of the problem. The further treatment of master integrals is the topic of the next section.

D.5 COMPUTATION OF MASTER INTEGRALS

Over the past decades, the evaluation of Feynman integrals became an art form in itself, leading to a vast spectrum of ideas and computer programs (see e.g. ref. [176] for an extensive overview). Here, we focus only on the methods used in the context of this work.

An important representation of a scalar Feynman integral I is via Feynman parameters x_i. We get (see e.g. ref. [110])

$$\begin{aligned} I(a_1, \ldots, a_n) = {} & \frac{i^l}{(4\pi)^{dl/2}} \frac{\Gamma\left(a - \frac{ld}{2}\right)}{\prod_i \Gamma(a_i)} \int_0^\infty \ldots \int_0^\infty \left(\prod_{i=1}^n \mathrm{d}x_i \; x_i^{a_i - 1} \right) \\ & \times \delta\left(\sum_{i=1}^n x_i - 1 \right) \frac{\mathcal{U}^{a - \frac{(l+1)d}{2}}}{\mathcal{F}^{a - \frac{ld}{2}}}\,, \end{aligned} \tag{D.14}$$

with l denoting the number of loops, and

$$a = \sum_{i=1}^n a_i\,. \tag{D.15}$$

$\mathcal{U}$ and $\mathcal{F}$ are the so-called graph- or Symanzik-polynomials. They can be computed in various ways from the momentum representation (see e.g. ref. [177] for an overview).

A straightforward way to compute $\mathcal{U}$ and $\mathcal{F}$ is given by the *forest formula*. For this, all spanning forests of the Feynman graph must be taken into account. We differentiate between one-forests $\mathcal{T}_1$, also called spanning trees, and two-forests $\mathcal{T}_2$. A spanning tree is a set of edges (propagators) $\{e_i\}$ which connects all vertices

without forming a loop. A two-forest is defined as a spanning tree with two disjoint connected components. The Symanzik polynomials are then given by [177]

$$\begin{aligned}\mathcal{U} &= \sum_{T\in\mathcal{T}_1}\prod_{e_i\notin T} x_i\,,\\ \mathcal{F} &= \sum_{(T_1,T_2)\in\mathcal{T}_2}\left(\prod_{e_i\notin(T_1,T_2)} x_i\right)\left(\sum_{q_i\in\{q(T_1)\}}\sum_{q_j\in\{q(T_2)\}} q_i.q_j\right)+\mathcal{U}\sum_i x_i m_i^2\,.\end{aligned} \tag{D.16}$$

The set $\{q(T_i)\}$ consists of the external momenta whose corresponding legs are attached to the tree T_i. m_i denotes the mass of edge e_i.

Equation (D.14) is useful to reveal some features of the regarded integral. Here we follow ref. [178].

For two disjoint sets of Feynman parameters $X, Y \subset \{x_i\}$ with $\emptyset \neq X \cup Y \neq \{x_i\}$, we describe the scaling behavior at the integration boundaries of an integrand F with

$$\omega_{X,Y}(F) \;=\; |X| - |Y| + \deg_{X,Y}(F)\,. \tag{D.17}$$

$|X|$ is defined as the number of elements in set X. $\deg_{X,Y}(F)$ is the scaling degree of F for $\lambda \to 0$ with the replacements $x_i \to \lambda x_i$ for $x_i \in X$, and $x_j \to \lambda^{-1} x_j$ for $x_j \in Y$. Thus, $\deg_{X,Y}(F)$ is defined such that

$$\lim_{\lambda\to 0}\left(\lambda^{-\deg_{X,Y}(F)} F\,\middle|\,\begin{array}{l} x_i \to \lambda x_i \text{ for } x_i \in X \\ x_j \to \lambda^{-1} x_j \text{ for } x_j \in Y\end{array}\right) \tag{D.18}$$

is finite and non-zero. Therefore, $\omega_{X,Y}$ describes the degree of divergence at the integration boundaries, i.e. it is not sensitive to divergences that occur inside the integration region. If $\omega_{X,Y} \leq 0$ for any X and Y, the integral is divergent. It is finite if $\min(\omega_{X,Y}) > 0$ holds for all X and Y.

It can be shown [178] that the integrand F can be replaced by $\widetilde{F} = \mathcal{D}_{X,Y} F$ without changing the value of the integral, but with

$$\omega_{X,Y}(\widetilde{F}) \;>\; \omega_{X,Y}(F)\,, \tag{D.19}$$

and

$$\omega_{X',Y'}(\widetilde{F}) \;\geq\; \omega_{X',Y'}(\widetilde{F}) \qquad \forall X', Y' \subset \{x_i\}\,. \tag{D.20}$$

Thus, $\mathcal{D}_{X,Y}$ describes an analytic regularization operator that can be used to extract poles from a Feynman integral. It is given by

$$\mathcal{D}_{X,Y} \;=\; \frac{1}{\omega_{X,Y}}\left(\deg_{X,Y} - \sum_{x_i\in X} x_i\frac{\partial}{\partial x_i} - \sum_{x_j\in Y} x_j\frac{\partial}{\partial x_j}\right)\,. \tag{D.21}$$

Hence, only those $\omega_{X,Y}$ must be regarded for which holds

$$\lim_{\epsilon\to 0}(\omega_{X,Y}) \;=\; 0\,. \tag{D.22}$$

Sometimes, the form of eq. (D.14) is already sufficient to be evaluated with the integration functionality of a computer algebra system such as `Mathematica` [179]. For more complicated integrals additional tools have to be used.

For example, the idea of ref. [180] is to use *Multiple Polylogarithms* (MPLs) and their relations in the context of Feynman integrals. These special functions are defined by the recursive relation (see e.g. ref. [176])

$$G(a_1, \ldots, a_n; z) \;=\; \int_0^z \frac{\mathrm{d}z'}{z' - a_1} G(a_2, \ldots, a_n; z')\,, \tag{D.23}$$

with the initial condition $G(;z) = 1$. The arguments $\{a_i\}$ are called *letters*. A special notation of G concerns arguments with zeros:

$$G_{m_1,\ldots,m_n}(a_1, \ldots, a_n; z) \;=\; G(\underbrace{0, \ldots, 0}_{m_1-1}, a_1, \underbrace{0, \ldots, 0}_{m_2-1}, a_2, \ldots, \underbrace{0, \ldots, 0}_{m_n-1}, a_n; z)\,. \tag{D.24}$$

It is used to express MPLs in a sum representation:

$$G_{m_1,\ldots,m_n}(a_1, \ldots, a_n; z) \;=\; (-1)^n \mathrm{Li}_{m_1,\ldots,m_n}\left(\frac{z}{a_1}, \frac{a_1}{a_2}, \ldots, \frac{a_{n-1}}{a_n}\right)\,, \tag{D.25}$$

with the nested sum defined by

$$\mathrm{Li}_{m_1,\ldots,m_n}(a_1, \ldots, a_n) \;=\; \sum_{\infty > i_1 > i_2 > \cdots > i_n > 0} \frac{a_1^{i_1}}{i_1^{m_1}} \cdots \frac{a_n^{i_n}}{i_n^{m_n}}\,. \tag{D.26}$$

A special subclass of MPLs are the *multiple Zeta values*. They are given by

$$\zeta_{m_1,\ldots,m_n} \;=\; \mathrm{Li}_{m_1,\ldots,m_n}(1, \ldots, 1)\,. \tag{D.27}$$

Another related function class are *Harmonic Polylogarithms* (HPLs) [181], they are defined as

$$H_{m_1,\ldots,m_n}(z) \;=\; \mathrm{Li}_{m_1,\ldots,m_n}(z, 1, \ldots, 1)\,. \tag{D.28}$$

A Feynman integral can be expressed as an MPL if it is regularized and linearly reducible. The latter condition states that for an integration order of Feynman parameters $\{x_1, x_2, \ldots, x_n\}$ the integrand is given as a product of a rational function, which is only linear in the integration variable, and an MPL. Not all Feynman integrals fulfill the condition of linear reducibility. For those, an expansion in ϵ leads to a closed analytic form which benefits from several transformation identities. In our case, all master integrals that occur at three-loop order are linearly reducible after proper variable transformations and integration orders.

The translation to MPLs and the subsequent simplifications are performed with the program `HyperInt` [125]. Also, the arising two-loop master integrals are either known in the literature or can be evaluated with `HyperInt` as well.

In the following, we illustrate the integration procedure described in this section by two simple examples.

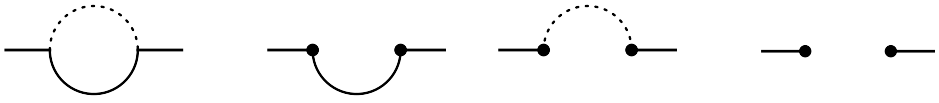

Figure D.3: The integral of eq. (D.29) is shown pictorially (i), as well as its spanning trees (ii) and the two-forest (iii). Note that the latter does not contain any internal edges.

One-loop example

We begin with the following one-loop integral:

$$I_1 = \int \frac{\mathrm{d}^d k}{k^2(k^2 - 2k\cdot q)}\,, \tag{D.29}$$

with $q^2 = m^2$.

The Symanzik polynomials can be computed with the help of eq. (D.16) and the spanning forests as shown in figs. D.3ii and D.3iii. We get

$$\begin{aligned} \mathcal{U} &= x_1 + x_2\,, \\ \mathcal{F} &= x_1 x_2\, q\cdot(-q) + \mathcal{U} x_2 m^2 \;=\; x_2^2 m^2\,. \end{aligned} \tag{D.30}$$

Thus, I_2 in Feynman parameter representation according to eq. (D.14) is given by

$$I_1 = i\pi^{d/2}\Gamma(\epsilon) \int_0^\infty \mathrm{d}x_1 \int_0^\infty \mathrm{d}x_2\, \delta(x_2 - 1)\, \frac{(x_1 + x_2)^{-2+2\epsilon}}{\left(m^2 x_2^2\right)^\epsilon}\,. \tag{D.31}$$

Here we used the *Cheng-Wu theorem* [182] which states that the argument in the δ-function can be replaced by a subset of Feynman parameters. Whereas, the integration region of the remaining parameters is extended to infinity.

Equation (D.29) is easily evaluated in terms of Γ-functions:

$$I_1 = i\pi^{d/2} \left(m^2\right)^{-\epsilon} \Gamma(\epsilon)\, \frac{1}{1-2\epsilon}\,. \tag{D.32}$$

Two-loop example

As an example at two-loops, we take the following integral into account:

$$I_2 = \iint \frac{\mathrm{d}^d k\, \mathrm{d}^d l}{(k^2 - 2k\cdot q)\, l^2\, (k+l)^2}\,, \tag{D.33}$$

which is shown in fig. D.4 together with its one- and two-forests. The Symanzik polynomials of I_2 are given by

$$\begin{aligned} \mathcal{U} &= x_1 x_2 + x_1 x_3 + x_2 x_3\,, \\ \mathcal{F} &= m^2 \left(x_1^2 x_2 + x_1^2 x_3\right)\,. \end{aligned} \tag{D.34}$$

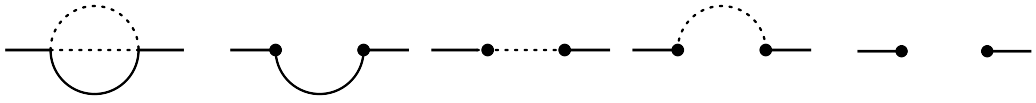

Figure D.4: The two-loop example of eq. (D.33) has three possible spanning trees. The two-forest is the same as for eq. (D.29).

After applying the Cheng-Wu theorem and evaluating the δ-function to remove x_1, the Feynman parameter integral is given by

$$I_2 \;=\; -\pi^d \Gamma\left(-1+2\epsilon\right)\left(m^2\right)^{1-2\epsilon} \int_0^\infty \mathrm{d}x_2 \int_0^\infty \mathrm{d}x_3 \, \frac{\left(x_2+x_3+x_2x_3\right)^{-3+3\epsilon}}{\left(x_2+x_3\right)^{-1+2\epsilon}} \,. \tag{D.35}$$

Since every term in $\mathcal{U}$ and $\mathcal{F}$ is individually non-negative, the degree of divergence $\omega_{X,Y}$ as given in eq. (D.17) represents the actual divergence behavior of the integral. We find a minimum value of

$$\omega_{\{x_2,x_3\},\emptyset} \;=\; \epsilon \,. \tag{D.36}$$

According to eq. (D.21), we can thus replace the integrand of eq. (D.35) by

$$\mathcal{D}_{\{x_2,x_3\},\emptyset} \frac{\left(x_2+x_3+x_2x_3\right)^{-3+3\epsilon}}{\left(x_2+x_3\right)^{-1+2\epsilon}} \;=\; -\frac{3(\epsilon-1)x_2x_3\left(x_2+x_3+x_2x_3\right)^{-4+3\epsilon}}{\epsilon\left(x_2+x_3\right)^{-1+2\epsilon}} \,. \tag{D.37}$$

By analyzing the degree of divergence of this new integral, we find that it is $\min(\omega_{X,Y}) > 0$, and hence finite. Since all divergences are now separated from the integral, we can safely expand it in ϵ. The different orders in ϵ are stated by

$$I_2 \;=\; \sum_{i=-2}^{\infty} I_2^{(i)} \quad \text{with} \quad I_2^{(n)} \;=\; \mathcal{O}(\epsilon^n) \,. \tag{D.38}$$

For the leading term we get

$$\frac{1}{\mathcal{N}^2} I_2^{(-2)} \;=\; -\frac{3m^2}{2\epsilon^2} \int_0^\infty \mathrm{d}x_2 \int_0^\infty \mathrm{d}x_3 \, \frac{x_2x_3\left(x_2+x_3\right)}{\left(x_2+x_3+x_2x_3\right)^4} \,, \tag{D.39}$$

with the usual prefactor $\mathcal{N} = i\pi^{d/2}\mu^{-\epsilon}e^{-\epsilon\gamma_E}$. Both integrals are straightforward to evaluate using the Euler beta function. We arrive at

$$\frac{1}{\mathcal{N}^2} I_2^{(-2)} \;=\; -\frac{m^2}{2\epsilon^2} \,. \tag{D.40}$$

The $\mathcal{O}\left(\epsilon^{-1}\right)$ term is given by

$$\begin{aligned} \frac{1}{\mathcal{N}^2} I_2^{(-1)} \;=\; & \frac{3m^2}{2\epsilon} \int_0^\infty dx_2 \int_0^\infty \mathrm{d}x_3 \, \frac{x_2x_3\left(x_2+x_3\right)}{\left(x_3x_2+x_2+x_3\right)^4} \\ & \cdot \left[-1-2\ln\left(\frac{\mu^2}{m^2}\right)+2\ln(x_2+x_3)-3\ln(x_2+x_3+x_2x_3)\right] . \end{aligned} \tag{D.41}$$

`HyperInt` can solve these integrals by iteratively identifying the linear reducible integrands in terms of MPLs and linear rational functions. Then, the integrals are iteratively solved using eq. (D.23):

$$\int_0^\infty \mathrm{d}x \frac{1}{x-a_1} G(a_2,\ldots,a_n;x) \;\equiv\; \operatorname*{Reg}_{z\to\infty} G(a_1,\ldots,a_n;z)\,, \tag{D.42}$$

where we defined a regularized limit of an MPL whose expansion around $z_0 \to \infty$ is uniquely given by [183]

$$G(a_1,\ldots,a_n;z) \;=\; \sum_{i=0}^{n} c_i(z)\ln^i(z)\,, \tag{D.43}$$

with

$$\operatorname*{Reg}_{z\to\infty} G(a_1,\ldots,a_n;z) \;\equiv\; c_0(\infty)\,. \tag{D.44}$$

If the resulting term, after taking the limit, is again an MPL multiplying a linear rational function, the procedure can be repeated for the next integration step.

With `HyperInt` we find:

$$\begin{aligned}\frac{1}{\mathcal{N}^2} I_2^{(-1)} \;&=\; -\frac{m^2}{\epsilon}\left[\frac{5}{4} + \operatorname*{Reg}_{z\to\infty} G\left(-\frac{m^2}{\mu^2};z\right)\right] \\ &=\; -\frac{m^2}{\epsilon}\left[\frac{5}{4} + \ln\left(\frac{\mu^2}{m^2}\right)\right]\,.\end{aligned} \tag{D.45}$$

The last step is evident from the splitting of the MPL:

$$G\left(-a;z\right) \;=\; \ln\left(\frac{a+z}{a}\right) \;=\; \ln\left(z\right) + \ln\left(\frac{1}{a}+\frac{1}{z}\right)\,. \tag{D.46}$$

The latter term is $c_0(z)$ which evaluates to

$$\operatorname*{Reg}_{z\to\infty} G\left(-a;z\right) \;=\; -\ln(a)\,. \tag{D.47}$$

Finally, we regard the finite part of I_2:

$$\begin{aligned}\frac{1}{\mathcal{N}^2} I_2^{(0)} \;=\; &\frac{m^2}{4}\int_0^\infty \mathrm{d}x_2 \int_0^\infty \mathrm{d}x_3\, \frac{x_2x_3(x_2+x_3)}{(x_3x_2+x_2+x_3)^4}\Bigg\{2\pi^2+12 \\ &+12\ln\left(\frac{\mu^2}{m^2}\right)^2 + 12\ln\left(\frac{\mu^2}{m^2}\right) + 12\ln^2(x_2+x_3) \\ &+18\left[2\ln\left(\frac{\mu^2}{m^2}\right)+1\right]\ln(x_3x_2+x_2+x_3) \\ &-12\ln(x_2+x_3)\left[2\ln\left(\frac{\mu^2}{m^2}\right)+3\ln(x_3x_2+x_2+x_3)+1\right] \\ &+27\ln^2(x_3x_2+x_2+x_3)\Bigg\}\,.\end{aligned} \tag{D.48}$$

`HyperInt` evaluates these integrals to

$$\begin{aligned}\frac{1}{\mathcal{N}^2} I_2^{(0)} &= -m^2 \operatorname*{Reg}_{z\to\infty} \left[\frac{3}{2} G\left(0,-1;z\right) + \frac{5}{2} G\left(-\frac{m^2}{\mu^2};z\right)\right. \\ &\quad \left. + \frac{11}{8} + \frac{\pi^2}{6} + 2G\left(-\frac{m^2}{\mu^2},-\frac{m^2}{\mu^2};z\right)\right].\end{aligned} \tag{D.49}$$

The following new objects occur [139, 181]:

$$\begin{aligned} G\left(0,-1;z\right) &\overset{(D.25)}{=} -\mathrm{Li}_2(-z) = \zeta(2) + \frac{1}{2}\ln^2(z) + \mathrm{Li}_2\left(-\frac{1}{z}\right), \\ G\left(-a,-a;z\right) &= \mathrm{Li}_{1,1}(-\frac{z}{a},1) \overset{(D.28)}{=} H_{1,1}(-\frac{z}{a}) = \frac{1}{2}\ln^2\left(1+\frac{z}{a}\right) \\ &= \frac{1}{2}\left[\ln\left(\frac{1}{a}+\frac{1}{z}\right)+\ln(z)\right]^2. \end{aligned} \tag{D.50}$$

Thus, the finite part of the integral becomes

$$\frac{1}{\mathcal{N}^2} I_2^{(0)} = -m^2\left[\ln^2\left(\frac{\mu^2}{m^2}\right) + \frac{5}{2}\ln\left(\frac{\mu^2}{m^2}\right) + \frac{5\pi^2}{12} + \frac{11}{8}\right]. \tag{D.51}$$

Note that both described example integrals can be computed more easily with other methods. They were only taken into account for illustration purposes. The described methods can be used to evaluate e.g. massless four-loop four-point integrals [178]

BIBLIOGRAPHY

[1] P. A. M. Dirac. "The Quantum Theory of the Emission and Absorption of Radiation." In: *Proceedings of the Royal Society of London Series A* 114.767 (Mar. 1927), pp. 243–265. DOI: 10.1098/rspa.1927.0039.

[2] A. Einstein. "Zur Elektrodynamik bewegter Körper." In: *Annalen der Physik* 322.10 (1905), pp. 891–921. DOI: https://doi.org/10.1002/andp.19053221004.

[3] R. P. Feynman. "Space-time approach to nonrelativistic quantum mechanics." In: *Rev. Mod. Phys.* 20 (1948), pp. 367–387. DOI: 10.1103/RevModPhys.20.367.

[4] R. P. Feynman. "The Theory of positrons." In: *Phys. Rev.* 76 (1949). Ed. by L. M. Brown, pp. 749–759. DOI: 10.1103/PhysRev.76.749.

[5] R. P. Feynman. "Mathematical formulation of the quantum theory of electromagnetic interaction." In: *Phys. Rev.* 80 (1950). Ed. by L. M. Brown, pp. 440–457. DOI: 10.1103/PhysRev.80.440.

[6] S. Tomonaga. "On a relativistically invariant formulation of the quantum theory of wave fields." In: *Prog. Theor. Phys.* 1 (1946), pp. 27–42. DOI: 10.1143/PTP.1.27.

[7] Julian S. Schwinger. "On Quantum electrodynamics and the magnetic moment of the electron." In: *Phys. Rev.* 73 (1948), pp. 416–417. DOI: 10.1103/PhysRev.73.416.

[8] Julian S. Schwinger. "Quantum electrodynamics. I A covariant formulation." In: *Phys. Rev.* 74 (1948). Ed. by K. A. Milton, p. 1439. DOI: 10.1103/PhysRev.74.1439.

[9] S. L. Glashow. "Partial Symmetries of Weak Interactions." In: *Nucl. Phys.* 22 (1961), pp. 579–588. DOI: 10.1016/0029-5582(61)90469-2.

[10] Abdus Salam. "Weak and Electromagnetic Interactions." In: *Conf. Proc. C* 680519 (1968), pp. 367–377. DOI: 10.1142/9789812795915_0034.

[11] Steven Weinberg. "A Model of Leptons." In: *Phys. Rev. Lett.* 19 (1967), pp. 1264–1266. DOI: 10.1103/PhysRevLett.19.1264.

[12] A. Einstein. "Die Grundlage der allgemeinen Relativitätstheorie." In: *Annalen der Physik* 354.7 (1916), pp. 769–822. DOI: https://doi.org/10.1002/andp.19163540702.

[13] Albert Einstein. "Erklärung der Perihelbewegung des Merkur aus der allgemeinen Relativitätstheorie." In: *Sitzungsberichte der Königlich Preußischen Akademie der Wissenschaften (Berlin* (Jan. 1915), pp. 831–839.

[14] Frank Watson Dyson, Arthur Stanley Eddington, and C. Davidson. "IX. A determination of the deflection of light by the sun's gravitational field, from observations made at the total eclipse of May 29, 1919." In: *Philosophical Transactions of the Royal Society of London. Series A, Containing Papers of a Mathematical or Physical Character* 220.571-581 (1920), pp. 291–333. DOI: 10.1098/rsta.1920.0009.

[15] B. P. Abbott et al. "Observation of Gravitational Waves from a Binary Black Hole Merger." In: *Phys. Rev. Lett.* 116.6 (2016), p. 061102. DOI: 10.1103/PhysRevLett.116.061102. arXiv: 1602.03837 [gr-qc].

[16] A. D. Sakharov. "Violation of CP Invariance, C asymmetry, and baryon asymmetry of the universe." In: *Pisma Zh. Eksp. Teor. Fiz.* 5 (1967), pp. 32–35. DOI: 10.1070/PU1991v034n05ABEH002497.

[17] J. H. Christenson, J. W. Cronin, V. L. Fitch, and R. Turlay. "Evidence for the 2π Decay of the K_2^0 Meson." In: *Phys. Rev. Lett.* 13 (1964), pp. 138–140. DOI: 10.1103/PhysRevLett.13.138.

[18] Antonio Riotto and Mark Trodden. "Recent progress in baryogenesis." In: *Ann. Rev. Nucl. Part. Sci.* 49 (1999), pp. 35–75. DOI: 10.1146/annurev.nucl.49.1.35. arXiv: hep-ph/9901362.

[19] Roel Aaij et al. "Test of lepton universality in beauty-quark decays." In: *Nature Phys.* 18.3 (2022), pp. 277–282. DOI: 10.1038/s41567-021-01478-8. arXiv: 2103.11769 [hep-ex].

[20] B. Abi et al. "Measurement of the Positive Muon Anomalous Magnetic Moment to 0.46 ppm." In: *Phys. Rev. Lett.* 126.14 (2021), p. 141801. DOI: 10.1103/PhysRevLett.126.141801. arXiv: 2104.03281 [hep-ex].

[21] Andrzej J. Buras. *Gauge Theory of Weak Decays: The Standard Model and the Expedition to New Physics Summits*. Cambridge University Press, 2020. DOI: 10.1017/9781139524100.

[22] Ulrich Nierste. "Three Lectures on Meson Mixing and CKM phenomenology." In: *Helmholz International Summer School on Heavy Quark Physics*. Mar. 2009, pp. 1–38. arXiv: 0904.1869 [hep-ph].

[23] Marina Artuso, Guennadi Borissov, and Alexander Lenz. "CP violation in the B_s^0 system." In: *Rev. Mod. Phys.* 88.4 (2016). [Addendum: Rev.Mod.Phys. 91, 049901 (2019)], p. 045002. DOI: 10.1103/RevModPhys.88.045002. arXiv: 1511.09466 [hep-ph].

[24] V. Weisskopf and Eugene P. Wigner. "Calculation of the natural brightness of spectral lines on the basis of Dirac's theory." In: *Z. Phys.* 63 (1930), pp. 54–73. DOI: 10.1007/BF01336768.

[25] V. Weisskopf and E. Wigner. "Over the natural line width in the radiation of the harmonius oscillator." In: *Z. Phys.* 65 (1930), pp. 18–29. DOI: 10.1007/BF01397406.

[26] *B physics at the Tevatron: Run II and beyond*. Dec. 2001. arXiv: hep-ph/0201071.

[27] S. L. Glashow, J. Iliopoulos, and L. Maiani. "Weak Interactions with Lepton-Hadron Symmetry." In: *Phys. Rev. D* 2 (1970), pp. 1285–1292. DOI: 10.1103/PhysRevD.2.1285.

[28] Nicola Cabibbo. "Unitary Symmetry and Leptonic Decays." In: *Phys. Rev. Lett.* 10 (1963), pp. 531–533. DOI: 10.1103/PhysRevLett.10.531.

[29] Makoto Kobayashi and Toshihide Maskawa. "CP Violation in the Renormalizable Theory of Weak Interaction." In: *Prog. Theor. Phys.* 49 (1973), pp. 652–657. DOI: 10.1143/PTP.49.652.

[30] Lincoln Wolfenstein. "Parametrization of the Kobayashi-Maskawa Matrix." In: *Phys. Rev. Lett.* 51 (1983), p. 1945. DOI: 10.1103/PhysRevLett.51.1945.

[31] *CKMFitter*. http://ckmfitter.in2p3.fr. Accessed: 2022-03-16.

[32] Kenneth G. Wilson. "Nonlagrangian models of current algebra." In: *Phys. Rev.* 179 (1969), pp. 1499–1512. DOI: 10.1103/PhysRev.179.1499.

[33] K. G. Wilson and W. Zimmermann. "Operator product expansions and composite field operators in the general framework of quantum field theory." In: *Commun. Math. Phys.* 24 (1972), pp. 87–106. DOI: 10.1007/BF01878448.

[34] Wolfhart Zimmermann. "Normal products and the short distance expansion in the perturbation theory of renormalizable interactions." In: *Annals Phys.* 77 (1973), pp. 570–601. DOI: 10.1016/0003-4916(73)90430-2.

[35] Edward Witten. "Short Distance Analysis of Weak Interactions." In: *Nucl. Phys. B* 122 (1977), pp. 109–143. DOI: 10.1016/0550-3213(77)90428-X.

[36] Thomas Jubb, Matthew Kirk, Alexander Lenz, and Gilberto Tetlalmatzi-Xolocotzi. "On the ultimate precision of meson mixing observables." In: *Nucl. Phys. B* 915 (2017), pp. 431–453. DOI: 10.1016/j.nuclphysb.2016.12.020. arXiv: 1603.07770 [hep-ph].

[37] Emel Dalgic, Alan Gray, Elvira Gamiz, Christine T. H. Davies, G. Peter Lepage, Junko Shigemitsu, Howard Trottier, and Matthew Wingate. "$B_s^0 - \bar{B}_s^0$ mixing parameters from unquenched lattice QCD." In: *Phys. Rev. D* 76 (2007), p. 011501. DOI: 10.1103/PhysRevD.76.011501. arXiv: hep-lat/0610104.

[38] Elvira Gamiz, Christine T. H. Davies, G. Peter Lepage, Junko Shigemitsu, and Matthew Wingate. "Neutral B Meson Mixing in Unquenched Lattice QCD." In: *Phys. Rev. D* 80 (2009), p. 014503. DOI: 10.1103/PhysRevD.80.014503. arXiv: 0902.1815 [hep-lat].

[39] N. Carrasco et al. "B-physics from $N_f = 2$ tmQCD: the Standard Model and beyond." In: *JHEP* 03 (2014), p. 016. DOI: 10.1007/JHEP03(2014)016. arXiv: 1308.1851 [hep-lat].

[40] A. Bazavov et al. "$B^0_{(s)}$-mixing matrix elements from lattice QCD for the Standard Model and beyond." In: *Phys. Rev. D* 93.11 (2016), p. 113016. DOI: 10.1103/PhysRevD.93.113016. arXiv: 1602.03560 [hep-lat].

[41] R. J. Dowdall, C. T. H. Davies, R. R. Horgan, G. P. Lepage, C. J. Monahan, J. Shigemitsu, and M. Wingate. "Neutral B-meson mixing from full lattice QCD at the physical point." In: *Phys. Rev. D* 100.9 (2019), p. 094508. DOI: 10.1103/PhysRevD.100.094508. arXiv: 1907.01025 [hep-lat].

[42] C. S. Huang, Ailin Zhang, and Shi-Lin Zhu. "Matrix elements of four quark operators relevant to lifetime difference Delta Gamma (B(s)) from QCD sum rules." In: *Eur. Phys. J. C* 21 (2001), pp. 313–318. DOI: 10.1007/s100520100724. arXiv: hep-ph/0011145.

[43] Matthias Jamin and Bjorn O. Lange. "f(B) and f(B(s)) from QCD sum rules." In: *Phys. Rev. D* 65 (2002), p. 056005. DOI: 10.1103/PhysRevD.65.056005. arXiv: hep-ph/0108135.

[44] J. G. Korner, A. I. Onishchenko, Alexey A. Petrov, and A. A. Pivovarov. "Bo anti-Bo mixing beyond factorization." In: *Phys. Rev. Lett.* 91 (2003), p. 192002. DOI: 10.1103/PhysRevLett.91.192002. arXiv: hep-ph/0306032.

[45] Andrey G. Grozin, Thomas Mannel, and Alexei A. Pivovarov. "Towards a Next-to-Next-to-Leading Order analysis of matching in B^0-$\bar{B}^0$ mixing." In: *Phys. Rev. D* 96.7 (2017), p. 074032. DOI: 10.1103/PhysRevD.96.074032. arXiv: 1706.05910 [hep-ph].

[46] Daniel King, Alexander Lenz, and Thomas Rauh. "B_s mixing observables and $|V_{td}/V_{ts}|$ from sum rules." In: *JHEP* 05 (2019), p. 034. DOI: 10.1007/JHEP05(2019)034. arXiv: 1904.00940 [hep-ph].

[47] Alexander Lenz and Ulrich Nierste. "Theoretical update of $B_s - \bar{B}_s$ mixing." In: *JHEP* 06 (2007), p. 072. DOI: 10.1088/1126-6708/2007/06/072. arXiv: hep-ph/0612167.

[48] T. Inami and C. S. Lim. "Effects of Superheavy Quarks and Leptons in Low-Energy Weak Processes k(L) —> mu anti-mu, K+ —> pi+ Neutrino anti-neutrino and Ko <—> anti-Ko." In: *Prog. Theor. Phys.* 65 (1981). [Erratum: Prog.Theor.Phys. 65, 1772 (1981)], p. 297. DOI: 10.1143/PTP.65.297.

[49] Andrzej J. Buras, Matthias Jamin, and Peter H. Weisz. "Leading and Next-to-leading QCD Corrections to ϵ Parameter and $B^0 - \bar{B}^0$ Mixing in the Presence of a Heavy Top Quark." In: *Nucl. Phys. B* 347 (1990), pp. 491–536. DOI: 10.1016/0550-3213(90)90373-L.

[50] R. E. Cutkosky. "Singularities and Discontinuities of Feynman Amplitudes." In: *Journal of Mathematical Physics* 1.5 (Sept. 1960), pp. 429–433. DOI: 10.1063/1.1703676.

[51] Valery A. Khoze and Mikhail A. Shifman. "HEAVY QUARKS." In: *Sov. Phys. Usp.* 26 (1983), p. 387. DOI: 10.1070/PU1983v026n05ABEH004398.

[52] Mikhail A. Shifman and M. B. Voloshin. "Preasymptotic Effects in Inclusive Weak Decays of Charmed Particles." In: *Sov. J. Nucl. Phys.* 41 (1985), p. 120.

[53] Ikaros I. Y. Bigi and N. G. Uraltsev. "Gluonic enhancements in non-spectator beauty decays: An Inclusive mirage though an exclusive possibility." In: *Phys. Lett. B* 280 (1992), pp. 271–280. DOI: 10.1016/0370-2693(92)90066-D.

[54] B. Blok and Mikhail A. Shifman. "The Rule of discarding 1/N(c) in inclusive weak decays. 1." In: *Nucl. Phys. B* 399 (1993), pp. 441–458. DOI: 10.1016/0550-3213(93)90504-I. arXiv: hep-ph/9207236.

[55] Ikaros I. Y. Bigi, N. G. Uraltsev, and A. I. Vainshtein. "Nonperturbative corrections to inclusive beauty and charm decays: QCD versus phenomenological models." In: *Phys. Lett. B* 293 (1992). [Erratum: Phys.Lett.B 297, 477–477 (1992)], pp. 430–436. DOI: 10.1016/0370-2693(92)90908-M. arXiv: hep-ph/9207214.

[56] B. Blok and Mikhail A. Shifman. "The Rule of discarding 1/N(c) in inclusive weak decays. 2." In: *Nucl. Phys. B* 399 (1993), pp. 459–476. DOI: 10.1016/0550-3213(93)90505-J. arXiv: hep-ph/9209289.

[57] John R. Ellis, M. K. Gaillard, Dimitri V. Nanopoulos, and S. Rudaz. "The Phenomenology of the Next Left-Handed Quarks." In: *Nucl. Phys. B* 131 (1977). [Erratum: Nucl.Phys.B 132, 541 (1978)], p. 285. DOI: 10.1016/0550-3213(77)90374-1.

[58] J. S. Hagelin. "Mass Mixing and CP Violation in the $B^0 - \bar{B}^0$ system." In: *Nucl. Phys. B* 193 (1981), pp. 123–149. DOI: 10.1016/0550-3213(81)90521-6.

[59] E. Franco, Maurizio Lusignoli, and A. Pugliese. "Strong Interaction Corrections to CP Violation in Bo Anti-bo Mixing." In: *Nucl. Phys. B* 194 (1982), p. 403. DOI: 10.1016/0550-3213(82)90018-9.

[60] Ling-Lie Chau. "Quark Mixing in Weak Interactions." In: *Phys. Rept.* 95 (1983), pp. 1–94. DOI: 10.1016/0370-1573(83)90043-1.

[61] A. J. Buras, W. Slominski, and H. Steger. "Bo anti-Bo Mixing, CP Violation and the B Meson Decay." In: *Nucl. Phys. B* 245 (1984), pp. 369–398. DOI: 10.1016/0550-3213(84)90437-1.

[62] Valery A. Khoze, Mikhail A. Shifman, N. G. Uraltsev, and M. B. Voloshin. "On Inclusive Hadronic Widths of Beautiful Particles." In: *Sov. J. Nucl. Phys.* 46 (1987), p. 112.

[63] M. Beneke, G. Buchalla, and I. Dunietz. "Width Difference in the $B_s - \bar{B}_s$ System." In: *Phys. Rev. D* 54 (1996). [Erratum: Phys.Rev.D 83, 119902 (2011)], pp. 4419–4431. DOI: 10.1103/PhysRevD.54.4419. arXiv: hep-ph/9605259.

[64] Florian Herren and Matthias Steinhauser. "Version 3 of RunDec and CRunDec." In: *Comput. Phys. Commun.* 224 (2018), pp. 333–345. DOI: 10.1016/j.cpc.2017.11.014. arXiv: 1703.03751 [hep-ph].

[65] M. Beneke, G. Buchalla, C. Greub, A. Lenz, and U. Nierste. "Next-to-leading order QCD corrections to the lifetime difference of B(s) mesons." In: *Phys. Lett. B* 459 (1999), pp. 631–640. DOI: 10.1016/S0370-2693(99)00684-X. arXiv: hep-ph/9808385.

[66] M. Ciuchini, E. Franco, V. Lubicz, F. Mescia, and C. Tarantino. "Lifetime differences and CP violation parameters of neutral B mesons at the next-to-leading order in QCD." In: *JHEP* 08 (2003), p. 031. DOI: 10.1088/1126-6708/2003/08/031. arXiv: hep-ph/0308029.

[67] Martin Beneke, Gerhard Buchalla, Alexander Lenz, and Ulrich Nierste. "CP asymmetry in flavor specific B decays beyond leading logarithms." In: *Phys. Lett. B* 576 (2003), pp. 173–183. DOI: 10.1016/j.physletb.2003.09.089. arXiv: hep-ph/0307344.

[68] H. M. Asatrian, Artyom Hovhannisyan, Ulrich Nierste, and Arsen Yeghiazaryan. "Towards next-to-next-to-leading-log accuracy for the width difference in the $B_s - \bar{B}_s$ system: fermionic contributions to order $(m_c/m_b)^0$ and $(m_c/m_b)^1$." In: *JHEP* 10 (2017), p. 191. DOI: 10.1007/JHEP10(2017)191. arXiv: 1709.02160 [hep-ph].

[69] Hrachia M. Asatrian, Hrachya H. Asatryan, Artyom Hovhannisyan, Ulrich Nierste, Sergey Tumasyan, and Arsen Yeghiazaryan. "Penguin contribution to the width difference and CP asymmetry in B_q-$\bar{B}_q$ mixing at order $\alpha_s^2 N_f$." In: *Phys. Rev. D* 102.3 (2020), p. 033007. DOI: 10.1103/PhysRevD.102.033007. arXiv: 2006.13227 [hep-ph].

[70] Marvin Gerlach, Ulrich Nierste, Vladyslav Shtabovenko, and Matthias Steinhauser. "Two-loop QCD penguin contribution to the width difference in $B_s - \overline{B}_s$ mixing." In: *JHEP* 07 (2021), p. 043. DOI: 10.1007/JHEP07(2021)043. arXiv: 2106.05979 [hep-ph].

[71] Marvin Gerlach, Ulrich Nierste, Vladyslav Shtabovenko, and Matthias Steinhauser. *The width difference in $B - \overline{B}$ mixing at order α_s and beyond*. Accepted for publication in JHEP. Feb. 2022. arXiv: 2202.12305 [hep-ph].

[72] Mikhail A. Shifman, A. I. Vainshtein, and Valentin I. Zakharov. "Nonleptonic Decays of K Mesons and Hyperons." In: *Sov. Phys. JETP* 45 (1977), p. 670.

[73] Matthew D. Schwartz. *Quantum Field Theory and the Standard Model*. Cambridge University Press, Mar. 2014. ISBN: 978-1-107-03473-0, 978-1-107-03473-0.

[74] John C. Collins. *Renormalization: An Introduction to Renormalization, The Renormalization Group, and the Operator Product Expansion*. Vol. 26. Cambridge Monographs on Mathematical Physics. Cambridge: Cambridge University Press, 1986. ISBN: 978-0-521-31177-9, 978-0-511-86739-2. DOI: 10.1017/CBO9780511622656.

[75] Konstantin G. Chetyrkin, Mikolaj Misiak, and Manfred Munz. "$|\Delta F| = 1$ nonleptonic effective Hamiltonian in a simpler scheme." In: *Nucl. Phys. B* 520 (1998), pp. 279–297. DOI: 10.1016/S0550-3213(98)00131-X. arXiv: hep-ph/9711280.

[76] Christoph Bobeth, Mikolaj Misiak, and Jorg Urban. "Photonic penguins at two loops and m_t dependence of $BR[B \to X_s l^+ l^-]$." In: *Nucl. Phys. B* 574 (2000), pp. 291–330. DOI: 10.1016/S0550-3213(00)00007-9. arXiv: hep-ph/9910220.

[77] Martin Gorbahn and Ulrich Haisch. "Effective Hamiltonian for non-leptonic $|\Delta F| = 1$ decays at NNLO in QCD." In: *Nucl. Phys. B* 713 (2005), pp. 291–332. DOI: 10.1016/j.nuclphysb.2005.01.047. arXiv: hep-ph/0411071.

[78] Mikolaj Misiak and Matthias Steinhauser. "Three loop matching of the dipole operators for $b \to s\gamma$ and $b \to sg$." In: *Nucl. Phys. B* 683 (2004), pp. 277–305. DOI: 10.1016/j.nuclphysb.2004.02.006. arXiv: hep-ph/0401041.

[79] Martin Gorbahn, Ulrich Haisch, and Mikolaj Misiak. "Three-loop mixing of dipole operators." In: *Phys. Rev. Lett.* 95 (2005), p. 102004. DOI: 10.1103/PhysRevLett.95.102004. arXiv: hep-ph/0504194.

[80] Gerard 't Hooft and M. J. G. Veltman. "Regularization and Renormalization of Gauge Fields." In: *Nucl. Phys. B* 44 (1972), pp. 189–213. DOI: 10.1016/0550-3213(72)90279-9.

[81] Warren Siegel. "Supersymmetric Dimensional Regularization via Dimensional Reduction." In: *Phys. Lett. B* 84 (1979), pp. 193–196. DOI: 10.1016/0370-2693(79)90282-X.

[82] Andrzej J. Buras and Peter H. Weisz. "QCD Nonleading Corrections to Weak Decays in Dimensional Regularization and 't Hooft-Veltman Schemes." In: *Nucl. Phys. B* 333 (1990), pp. 66–99. DOI: 10.1016/0550-3213(90)90223-Z.

[83] P. Breitenlohner and D. Maison. "Dimensionally Renormalized Green's Functions for Theories with Massless Particles. 1." In: *Commun. Math. Phys.* 52 (1977), p. 39. DOI: 10.1007/BF01609070.

[84] P. Breitenlohner and D. Maison. "Dimensionally Renormalized Green's Functions for Theories with Massless Particles. 2." In: *Commun. Math. Phys.* 52 (1977), p. 55. DOI: 10.1007/BF01609071.

[85] P. Breitenlohner and D. Maison. "Dimensional Renormalization and the Action Principle." In: *Commun. Math. Phys.* 52 (1977), pp. 11–38. DOI: 10.1007/BF01609069.

[86] Guy Bonneau. "Consistency in Dimensional Regularization With γ_5." In: *Phys. Lett. B* 96 (1980), pp. 147–150. DOI: 10.1016/0370-2693(80)90232-4.

[87] Guy Bonneau. "Preserving Canonical Ward Identities in Dimensional Regularization With a Nonanticommuting γ_5." In: *Nucl. Phys. B* 177 (1981), pp. 523–527. DOI: 10.1016/0550-3213(81)90185-1.

[88] J. S. R. Chisholm. "Relativistic scalar products of γ matrices." In: *Il Nuovo Cimento (1955-1965)* 30.1 (1963), pp. 426–428. ISSN: 1827-6121. DOI: 10.1007/BF02750778.

[89] Michael J. Dugan and Benjamin Grinstein. "On the vanishing of evanescent operators." In: *Phys. Lett. B* 256 (1991), pp. 239–244. DOI: 10.1016/0370-2693(91)90680-O.

[90] Stefan Herrlich and Ulrich Nierste. "Evanescent operators, scheme dependences and double insertions." In: *Nucl. Phys. B* 455 (1995), pp. 39–58. DOI: 10.1016/0550-3213(95)00474-7. arXiv: hep-ph/9412375.

[91] Mikolaj Misiak and Jorg Urban. "QCD corrections to FCNC decays mediated by Z penguins and W boxes." In: *Phys. Lett. B* 451 (1999), pp. 161–169. DOI: 10.1016/S0370-2693(99)00150-1. arXiv: hep-ph/9901278.

[92] Andrzej J. Buras, Matthias Jamin, Markus E. Lautenbacher, and Peter H. Weisz. "Two loop anomalous dimension matrix for $\Delta S = 1$ weak nonleptonic decays I: $\mathcal{O}(\alpha_s^2)$." In: *Nucl. Phys. B* 400 (1993), pp. 37–74. DOI: 10.1016/0550-3213(93)90397-8. arXiv: hep-ph/9211304.

[93] Andrzej J. Buras, Martin Gorbahn, Ulrich Haisch, and Ulrich Nierste. "Charm quark contribution to K+ —> pi+ nu anti-nu at next-to-next-to-leading order." In: *JHEP* 11 (2006). [Erratum: JHEP 11, 167 (2012)], p. 002. DOI: 10.1007/JHEP11(2012)167. arXiv: hep-ph/0603079.

[94] F. Gabbiani, E. Gabrielli, A. Masiero, and L. Silvestrini. "A Complete analysis of FCNC and CP constraints in general SUSY extensions of the standard model." In: *Nucl. Phys. B* 477 (1996), pp. 321–352. DOI: 10.1016/0550-3213(96)00390-2. arXiv: hep-ph/9604387.

[95] Jonathan A. Bagger, Konstantin T. Matchev, and Ren-Jie Zhang. "QCD corrections to flavor changing neutral currents in the supersymmetric standard model." In: *Phys. Lett. B* 412 (1997), pp. 77–85. DOI: 10.1016/S0370-2693(97)00920-9. arXiv: hep-ph/9707225.

[96] John S. Hagelin, S. Kelley, and Toshiaki Tanaka. "Supersymmetric flavor changing neutral currents: Exact amplitudes and phenomenological analysis." In: *Nucl. Phys. B* 415 (1994), pp. 293–331. DOI: 10.1016/0550-3213(94)90113-9.

[97] Stefan Herrlich and Ulrich Nierste. "The Complete |delta S| = 2 - Hamiltonian in the next-to-leading order." In: *Nucl. Phys. B* 476 (1996), pp. 27–88. DOI: 10.1016/0550-3213(96)00324-0. arXiv: hep-ph/9604330.

[98] Marco Ciuchini, E. Franco, V. Lubicz, G. Martinelli, I. Scimemi, and L. Silvestrini. "Next-to-leading order QCD corrections to Delta F = 2 effective Hamiltonians." In: *Nucl. Phys. B* 523 (1998), pp. 501–525. DOI: 10.1016/S0550-3213(98)00161-8. arXiv: hep-ph/9711402.

[99] Andrzej J. Buras, Mikolaj Misiak, and Jorg Urban. "Two loop QCD anomalous dimensions of flavor changing four quark operators within and beyond the standard model." In: *Nucl. Phys. B* 586 (2000), pp. 397–426. DOI: 10.1016/S0550-3213(00)00437-5. arXiv: hep-ph/0005183.

[100] Martin Gorbahn, Sebastian Jager, Ulrich Nierste, and Stephanie Trine. "The supersymmetric Higgs sector and $B - \bar{B}$ mixing for large tan β." In: *Phys. Rev. D* 84 (2011), p. 034030. DOI: 10.1103/PhysRevD.84.034030. arXiv: 0901.2065 [hep-ph].

[101] Markus Fierz. "Zur Fermischen Theorie des β-Zerfalls." In: *Zeitschrift fur Physik* 104.7-8 (July 1937), pp. 553–565. DOI: 10.1007/BF01330070.

[102] Matthias Steinhauser. "MATAD: A Program package for the computation of MAssive TADpoles." In: *Comput. Phys. Commun.* 134 (2001), pp. 335–364. DOI: 10.1016/S0010-4655(00)00204-6. arXiv: hep-ph/0009029.

[103] P. A. Baikov, K. G. Chetyrkin, and J. H. Kühn. "Five-Loop Running of the QCD coupling constant." In: *Phys. Rev. Lett.* 118.8 (2017), p. 082002. DOI: 10.1103/PhysRevLett.118.082002. arXiv: 1606.08659 [hep-ph].

[104] F. Herzog, B. Ruijl, T. Ueda, J. A. M. Vermaseren, and A. Vogt. "The five-loop beta function of Yang-Mills theory with fermions." In: *JHEP* 02 (2017), p. 090. DOI: 10.1007/JHEP02(2017)090. arXiv: 1701.01404 [hep-ph].

[105] Thomas Luthe, Andreas Maier, Peter Marquard, and York Schroder. "The five-loop Beta function for a general gauge group and anomalous dimensions beyond Feynman gauge." In: *JHEP* 10 (2017), p. 166. DOI: 10.1007/JHEP10(2017)166. arXiv: 1709.07718 [hep-ph].

[106] Gerhard Buchalla, Andrzej J. Buras, and Markus E. Lautenbacher. "Weak decays beyond leading logarithms." In: *Rev. Mod. Phys.* 68 (1996), pp. 1125–1144. DOI: 10.1103/RevModPhys.68.1125. arXiv: hep-ph/9512380.

[107] P. A. Baikov, K. G. Chetyrkin, and J. H. Kühn. "Quark Mass and Field Anomalous Dimensions to $\mathcal{O}(\alpha_s^5)$." In: *JHEP* 10 (2014), p. 076. DOI: 10.1007/JHEP10(2014)076. arXiv: 1402.6611 [hep-ph].

[108] Thomas Luthe, Andreas Maier, Peter Marquard, and York Schröder. "Five-loop quark mass and field anomalous dimensions for a general gauge group." In: *JHEP* 01 (2017), p. 081. DOI: 10.1007/JHEP01(2017)081. arXiv: 1612.05512 [hep-ph].

[109] K. G. Chetyrkin, G. Falcioni, F. Herzog, and J. A. M. Vermaseren. "Five-loop renormalisation of QCD in covariant gauges." In: *JHEP* 10 (2017). [Addendum: JHEP 12, 006 (2017)], p. 179. DOI: 10.1007/JHEP10(2017)179. arXiv: 1709.08541 [hep-ph].

[110] V. A. Smirnov. *Feynman integral calculus*. 2006.

[111] Fyodor V. Tkachov. "Towards systematic near threshold calculations in perturbative QFT." In: *Phys. Lett. B* 412 (1997), pp. 350–358. DOI: 10.1016/S0370-2693(97)01017-4. arXiv: hep-ph/9703424.

[112] M. Beneke and Vladimir A. Smirnov. "Asymptotic expansion of Feynman integrals near threshold." In: *Nucl. Phys. B* 522 (1998), pp. 321–344. DOI: 10.1016/S0550-3213(98)00138-2. arXiv: hep-ph/9711391.

[113] Vladimir A. Smirnov. "Applied asymptotic expansions in momenta and masses." In: *Springer Tracts Mod. Phys.* 177 (2002), pp. 1–262.

[114] Andrzej Czarnecki and Vladimir A. Smirnov. "Threshold behavior of Feynman diagrams: The Master two loop propagator." In: *Phys. Lett. B* 394 (1997), pp. 211–217. DOI: 10.1016/S0370-2693(96)01698-X. arXiv: hep-ph/9608407.

[115] H. Lehmann, K. Symanzik, and W. Zimmermann. "On the formulation of quantized field theories." In: *Nuovo Cim.* 1 (1955), pp. 205–225. DOI: 10.1007/BF02731765.

[116] Peter Marquard, Alexander V. Smirnov, Vladimir A. Smirnov, and Matthias Steinhauser. "Four-loop wave function renormalization in QCD and QED." In: *Phys. Rev. D* 97.5 (2018), p. 054032. DOI: 10.1103/PhysRevD.97.054032. arXiv: 1801.08292 [hep-ph].

[117] Matteo Fael, Kay Schönwald, and Matthias Steinhauser. "Exact results for Z_m^{OS} and Z_2^{OS} with two mass scales and up to three loops." In: *JHEP* 10 (2020), p. 087. DOI: 10.1007/JHEP10(2020)087. arXiv: 2008.01102 [hep-ph].

[118] R. Harlander, T. Seidensticker, and M. Steinhauser. "Complete corrections of Order alpha alpha-s to the decay of the Z boson into bottom quarks." In: *Phys. Lett. B* 426 (1998), pp. 125–132. DOI: 10.1016/S0370-2693(98)00220-2. arXiv: hep-ph/9712228.

[119] T. Seidensticker. "Automatic application of successive asymptotic expansions of Feynman diagrams." In: *6th International Workshop on New Computing Techniques in Physics Research: Software Engineering, Artificial Intelligence Neural Nets, Genetic Algorithms, Symbolic Algebra, Automatic Calculation*. May 1999. arXiv: hep-ph/9905298.

[120] S. A. Larin, F. V. Tkachov, and J. A. M. Vermaseren. "The FORM version of MINCER." In: (Sept. 1991).

[121] Marvin Gerlach, Florian Herren, and Martin Lang. *`tapir`: A tool for topologies, amplitudes, partial fraction decomposition and input for reductions*. Submitted to CPC. Jan. 2022. arXiv: 2201.05618 [hep-ph].

[122] A. V. Smirnov and F. S. Chuharev. "FIRE6: Feynman Integral REduction with Modular Arithmetic." In: *Comput. Phys. Commun.* 247 (2020), p. 106877. DOI: 10.1016/j.cpc.2019.106877. arXiv: 1901.07808 [hep-ph].

[123] Bernd Jantzen, Alexander V. Smirnov, and Vladimir A. Smirnov. "Expansion by regions: revealing potential and Glauber regions automatically." In: *Eur. Phys. J. C* 72 (2012), p. 2139. DOI: 10.1140/epjc/s10052-012-2139-2. arXiv: 1206.0546 [hep-ph].

[124] J. Fleischer, M. Yu. Kalmykov, and A. V. Kotikov. "Two loop selfenergy master integrals on-shell." In: *Phys. Lett. B* 462 (1999). [Erratum: Phys.Lett.B 467, 310–310 (1999)], pp. 169–177. DOI: 10.1016/S0370-2693(99)00892-8. arXiv: hep-ph/9905249.

[125] Erik Panzer. "Algorithms for the symbolic integration of hyperlogarithms with applications to Feynman integrals." In: *Comput. Phys. Commun.* 188 (2015), pp. 148–166. DOI: 10.1016/j.cpc.2014.10.019. arXiv: 1403.3385 [hep-th].

[126] Marco Ciuchini, E. Franco, V. Lubicz, and F. Mescia. "Next-to-leading order QCD corrections to spectator effects in lifetimes of beauty hadrons." In: *Nucl. Phys. B* 625 (2002), pp. 211–238. DOI: 10.1016/S0550-3213(02)00006-8. arXiv: hep-ph/0110375.

[127] Paulo Nogueira. "Automatic Feynman graph generation." In: *J. Comput. Phys.* 105 (1993), pp. 279–289. DOI: 10.1006/jcph.1993.1074.

[128] Ben Ruijl, Takahiro Ueda, and Jos Vermaseren. "FORM version 4.2." In: (July 2017). arXiv: 1707.06453 [hep-ph].

[129] Vladyslav Shtabovenko. Private communication.

[130] Roger A. Horn and Charles R. Johnson. *Matrix Analysis*. Cambridge University Press, 1990. ISBN: 0521386322.

[131] Arnold Dresden. "The fourteenth western meeting of the American Mathematical Society." In: *Bulletin of the American Mathematical Society* 26.9 (1920), pp. 385 –396. DOI: bams/1183425340. URL: https://doi.org/.

[132] R. Penrose. "A generalized inverse for matrices." In: *Mathematical Proceedings of the Cambridge Philosophical Society* 51 (1955). DOI: 10.1017/S0305004100030401.

[133] Marcel Golz. "Contraction of Dirac matrices via chord diagrams." In: (Oct. 2017). arXiv: 1710.05164 [math-ph].

[134] G. Passarino and M. J. G. Veltman. "One Loop Corrections for e+ e- Annihilation Into mu+ mu- in the Weinberg Model." In: *Nucl. Phys. B* 160 (1979), pp. 151–207. DOI: 10.1016/0550-3213(79)90234-7.

[135] Vladyslav Shtabovenko, Rolf Mertig, and Frederik Orellana. "FeynCalc 9.3: New features and improvements." In: *Comput. Phys. Commun.* 256 (2020), p. 107478. DOI: 10.1016/j.cpc.2020.107478. arXiv: 2001.04407 [hep-ph].

[136] Robert H. Lewis. *Computer Algebra System Fermat*, http://home.bway.net/lewis.

[137] N. Gray, David J. Broadhurst, W. Grafe, and K. Schilcher. "Three Loop Relation of Quark (Modified) Ms and Pole Masses." In: *Z. Phys. C* 48 (1990), pp. 673–680. DOI: 10.1007/BF01614703.

[138] Martin Beneke, Gerhard Buchalla, Christoph Greub, Alexander Lenz, and Ulrich Nierste. "The $B^+ - B_d^0$ Lifetime Difference Beyond Leading Logarithms." In: *Nucl. Phys. B* 639 (2002), pp. 389–407. DOI: 10.1016/S0550-3213(02)00561-8. arXiv: hep-ph/0202106.

[139] *NIST Digital Library of Mathematical Functions*. http://dlmf.nist.gov/, Release 1.1.4 of 2022-01-15. F. W. J. Olver, A. B. Olde Daalhuis, D. W. Lozier, B. I. Schneider, R. F. Boisvert, C. W. Clark, B. R. Miller, B. V. Saunders, H. S. Cohl, and M. A. McClain, eds. URL: http://dlmf.nist.gov/.

[140] Paolo Gambino, Martin Gorbahn, and Ulrich Haisch. "Anomalous dimension matrix for radiative and rare semileptonic B decays up to three loops." In: *Nucl. Phys. B* 673 (2003), pp. 238–262. DOI: 10.1016/j.nuclphysb.2003.09.024. arXiv: hep-ph/0306079.

[141] A. V. Smirnov, N. D. Shapurov, and L. I. Vysotsky. "FIESTA5: numerical high-performance Feynman integral evaluation." In: (Oct. 2021). arXiv: 2110.11660 [hep-ph].

[142] G. Heinrich, S. Jahn, S. P. Jones, M. Kerner, F. Langer, V. Magerya, A. Pöldaru, J. Schlenk, and E. Villa. "Expansion by regions with pySecDec." In: *Comput. Phys. Commun.* 273 (2022), p. 108267. DOI: 10.1016/j.cpc.2021.108267. arXiv: 2108.10807 [hep-ph].

[143] M. Beneke. "A Quark mass definition adequate for threshold problems." In: *Phys. Lett. B* 434 (1998), pp. 115–125. DOI: 10.1016/S0370-2693(98)00741-2. arXiv: hep-ph/9804241.

[144] Peter Marquard, Alexander V. Smirnov, Vladimir A. Smirnov, Matthias Steinhauser, and David Wellmann. "$\overline{\text{MS}}$-on-shell quark mass relation up to four loops in QCD and a general SU(N) gauge group." In: *Phys. Rev. D* 94.7 (2016), p. 074025. DOI: 10.1103/PhysRevD.94.074025. arXiv: 1606.06754 [hep-ph].

[145] Peter Marquard, Alexander V. Smirnov, Vladimir A. Smirnov, and Matthias Steinhauser. "Quark Mass Relations to Four-Loop Order in Perturbative QCD." In: *Phys. Rev. Lett.* 114.14 (2015), p. 142002. DOI: 10.1103/PhysRevLett.114.142002. arXiv: 1502.01030 [hep-ph].

[146] Johann H. Kuhn, Matthias Steinhauser, and Christian Sturm. "Heavy Quark Masses from Sum Rules in Four-Loop Approximation." In: *Nucl. Phys. B* 778 (2007), pp. 192–215. DOI: 10.1016/j.nuclphysb.2007.04.036. arXiv: hep-ph/0702103.

[147] M. Beneke. "Renormalons." In: *Phys. Rept.* 317 (1999), pp. 1–142. DOI: 10.1016/S0370-1573(98)00130-6. arXiv: hep-ph/9807443.

[148] Konstantin G. Chetyrkin, Johann H. Kuhn, Andreas Maier, Philipp Maierhofer, Peter Marquard, Matthias Steinhauser, and Christian Sturm. "Addendum to "Charm and bottom quark masses: An update"." In: (Oct. 2017). [Addendum: Phys.Rev.D 96, 116007 (2017)]. DOI: 10.1103/PhysRevD.96.116007. arXiv: 1710.04249 [hep-ph].

[149] P.A. Zyla et al. "Review of Particle Physics." In: *PTEP* 2020.8 (2020), p. 083C01. DOI: 10.1093/ptep/ptaa104.

[150] K. G. Chetyrkin, J. H. Kuhn, A. Maier, P. Maierhofer, P. Marquard, M. Steinhauser, and C. Sturm. "Charm and Bottom Quark Masses: An Update." In: *Phys. Rev. D* 80 (2009), p. 074010. DOI: 10.1103/PhysRevD.80.074010. arXiv: 0907.2110 [hep-ph].

[151] A. Bazavov et al. "B- and D-meson leptonic decay constants from four-flavor lattice QCD." In: *Phys. Rev. D* 98.7 (2018), p. 074512. DOI: 10.1103/PhysRevD.98.074512. arXiv: 1712.09262 [hep-lat].

[152] R. Aaij et al. "Precise determination of the B_s^0–$\overline{B}_s^0$ oscillation frequency." In: *Nature Phys.* 18.1 (2022), pp. 1–5. DOI: 10.1038/s41567-021-01394-x. arXiv: 2104.04421 [hep-ex].

[153] Yasmine Sara Amhis et al. "Averages of b-hadron, c-hadron, and τ-lepton properties as of 2018." In: *Eur. Phys. J. C* 81.3 (2021), p. 226. DOI: 10.1140/epjc/s10052-020-8156-7. arXiv: 1909.12524 [hep-ex].

[154] Christine T. H. Davies, Judd Harrison, G. Peter Lepage, Christopher J. Monahan, Junko Shigemitsu, and Matthew Wingate. "Lattice QCD matrix elements for the $B_s^0 - \bar{B}_s^0$ width difference beyond leading order." In: *Phys. Rev. Lett.* 124.8 (2020), p. 082001. DOI: 10.1103/PhysRevLett.124.082001. arXiv: 1910.00970 [hep-lat].

[155] Marzia Bordone, Bernat Capdevila, and Paolo Gambino. "Three loop calculations and inclusive Vcb." In: *Phys. Lett. B* 822 (2021), p. 136679. DOI: 10.1016/j.physletb.2021.136679. arXiv: 2107.00604 [hep-ph].

[156] Y. Aoki et al. "FLAG Review 2021." In: (Nov. 2021). arXiv: 2111.09849 [hep-lat].

[157] Roel Aaij et al. "Determination of the quark coupling strength $|V_{ub}|$ using baryonic decays." In: *Nature Phys.* 11 (2015), pp. 743–747. DOI: 10.1038/nphys3415. arXiv: 1504.01568 [hep-ex].

[158] J. Charles, Andreas Hocker, H. Lacker, S. Laplace, F. R. Le Diberder, J. Malcles, J. Ocariz, M. Pivk, and L. Roos. "CP violation and the CKM matrix: Assessing the impact of the asymmetric B factories." In: *Eur. Phys. J. C* 41.1 (2005), pp. 1–131. DOI: 10.1140/epjc/s2005-02169-1. arXiv: hep-ph/0406184.

[159] Paolo Gambino, Kristopher J. Healey, and Sascha Turczyk. "Taming the higher power corrections in semileptonic B decays." In: *Phys. Lett. B* 763 (2016), pp. 60–65. DOI: 10.1016/j.physletb.2016.10.023. arXiv: 1606.06174 [hep-ph].

[160] Martin Beneke. "Pole mass renormalon and its ramifications." In: *Eur. Phys. J. ST* 230.12-13 (2021), pp. 2565–2579. DOI: 10.1140/epjs/s11734-021-00268-w. arXiv: 2108.04861 [hep-ph].

[161] Ulrich Nierste. Private communication.

[162] Yuuki Hayashi, Yukinari Sumino, and Hiromasa Takaura. "Determination of $|V_{cb}|$ using N^{3}LO perturbative corrections to $\Gamma(B \to X_c \ell \nu)$ and 1S masses." In: (Feb. 2022). arXiv: 2202.01434 [hep-ph].

[163] C. C. Nishi. "Simple derivation of general Fierz-like identities." In: *Am. J. Phys.* 73 (2005), pp. 1160–1163. DOI: 10.1119/1.2074087. arXiv: hep-ph/0412245.

[164] T. van Ritbergen, A. N. Schellekens, and J. A. M. Vermaseren. "Group theory factors for Feynman diagrams." In: *Int. J. Mod. Phys. A* 14 (1999), pp. 41–96. DOI: 10.1142/S0217751X99000038. arXiv: hep-ph/9802376.

[165] Bernhard Nickel, Daniel Meiron, and George A. Jr. Baker. "Compilation of 2-pt and 4-pt graphs for continuous spin model." In: *University of Guelph Report* (1977).

[166] D. Batkovich, Yu. Kirienko, M. Kompaniets, and S. Novikov. "GraphState - a tool for graph identification and labelling." In: (Sept. 2014). arXiv: 1409.8227 [hep-ph].

[167] Alexey Pak. "The Toolbox of modern multi-loop calculations: novel analytic and semi-analytic techniques." In: *J. Phys. Conf. Ser.* 368 (2012). Ed. by Liliana Teodorescu, David Britton, Nigel Glover, Gudrun Heinrich, Jerome Lauret, Axel Naumann, Thomas Speer, and Pedro Teixeira-Dias, p. 012049. DOI: 10.1088/1742-6596/368/1/012049. arXiv: 1111.0868 [hep-ph].

[168] Aaron Meurer et al. "SymPy: symbolic computing in Python." In: *PeerJ Computer Science* 3 (Jan. 2017), e103. ISSN: 2376-5992. DOI: 10.7717/peerj-cs.103.

[169] Adam Alloul, Neil D. Christensen, Céline Degrande, Claude Duhr, and Benjamin Fuks. "FeynRules 2.0 - A complete toolbox for tree-level phenomenology." In: *Comput. Phys. Commun.* 185 (2014), pp. 2250–2300. DOI: 10.1016/j.cpc.2014.04.012. arXiv: 1310.1921 [hep-ph].

[170] Celine Degrande, Claude Duhr, Benjamin Fuks, David Grellscheid, Olivier Mattelaer, and Thomas Reiter. "UFO - The Universal FeynRules Output." In: *Comput. Phys. Commun.* 183 (2012), pp. 1201–1214. DOI: 10.1016/j.cpc.2012.01.022. arXiv: 1108.2040 [hep-ph].

[171] B. Buchberger. "A Theoretical Basis for the Reduction of Polynomials to Canonical Forms." In: 10.3 (1976). ISSN: 0163-5824. DOI: 10.1145/1088216.1088219.

[172] Bernd Sturmfels. "Grobner Bases—a Computational Approach to Commutative Algebra (Thomas Becker and Volker Weispfenning)." In: *SIAM Review* 36.2 (1994), pp. 323–323. DOI: 10.1137/1036089.

[173] K. G. Chetyrkin and F. V. Tkachov. "Integration by Parts: The Algorithm to Calculate beta Functions in 4 Loops." In: *Nucl. Phys. B* 192 (1981), pp. 159–204. DOI: 10.1016/0550-3213(81)90199-1.

[174] S. Laporta. "High precision calculation of multiloop Feynman integrals by difference equations." In: *Int. J. Mod. Phys. A* 15 (2000), pp. 5087–5159. DOI: 10.1142/S0217751X00002159. arXiv: hep-ph/0102033.

[175] Roman N. Lee. "LiteRed 1.4: a powerful tool for reduction of multiloop integrals." In: *J. Phys. Conf. Ser.* 523 (2014). Ed. by Jianxiong Wang, p. 012059. DOI: 10.1088/1742-6596/523/1/012059. arXiv: 1310.1145 [hep-ph].

[176] Stefan Weinzierl. "Feynman Integrals." In: (Jan. 2022). arXiv: 2201.03593 [hep-th].

[177] Christian Bogner and Stefan Weinzierl. "Feynman graph polynomials." In: *Int. J. Mod. Phys. A* 25 (2010), pp. 2585–2618. DOI: 10.1142/S0217751X10049438. arXiv: 1002.3458 [hep-ph].

[178] Erik Panzer. "On hyperlogarithms and Feynman integrals with divergences and many scales." In: *JHEP* 03 (2014), p. 071. DOI: 10.1007/JHEP03(2014)071. arXiv: 1401.4361 [hep-th].

[179] Wolfram Research, Inc. *Mathematica, Version 13.0.0*. Champaign, IL, 2021. URL: https://www.wolfram.com/mathematica.

[180] Francis Brown. "The Massless higher-loop two-point function." In: *Commun. Math. Phys.* 287 (2009), pp. 925–958. DOI: 10.1007/s00220-009-0740-5. arXiv: 0804.1660 [math.AG].

[181] E. Remiddi and J. A. M. Vermaseren. "Harmonic polylogarithms." In: *Int. J. Mod. Phys. A* 15 (2000), pp. 725–754. DOI: 10.1142/S0217751X00000367. arXiv: hep-ph/9905237.

[182] Hung Cheng and T. T. Wu. *EXPANDING PROTONS: SCATTERING AT HIGH-ENERGIES*. 1987.

[183] Erik Panzer. "Feynman integrals and hyperlogarithms." PhD thesis. Humboldt U., 2015. DOI: 10.18452/17157. arXiv: 1506.07243 [math-ph].

DANKSAGUNG

Ich möchte zunächst Professor Matthias Steinhauser dafür danken, dass er es mir ermöglicht hat in seiner Arbeitsgruppe zu promovieren. Dieses Privileg ist nicht vielen vergönnt und ich schätze mich glücklich, dieses auch wahrgenommen zu haben. Zudem danke ich ihm für seine Einsicht, Diskussionsbereitschaft, sowie seiner Fähigkeit Bugs und Probleme aufzuspüren, die tief in der komplexen Maschinerie einer Rechnung verborgen sind. Außerdem danke ich Professor Ulrich Nierste, der mit seinem tiefen Verständnis über die Physik mein manchmal nur technisches Wissen ergänzen und erweitern konnte. Daneben danke ich Vladyslav Shtabovenko für die zahlreichen Diskussionen und die tolle kollaborative Arbeit, ohne die ich dieses Projekt in den drei Jahren meiner Promotion wahrscheinlich nicht derart hätte abschließen können.

Ich danke Florian Herren und Martin Lang für die Zusammenarbeit an `tapir`, welches mit ihrer Unterstützung und Beiträgen zu einem vielseitigen und nützlichen Werkzeug wurde.

Ich möchte zudem Arnd Behring, Joshua Davies, Matteo Fael, Marco Fedele, Florian Herren und Kay Schönwald für die Hilfe und Diskussionen danken. Ich danke Michelle Benzel, Florian Herren, Martin Lang, Ulrich Nierste, Vladyslav Shtabovenko und Matthias Steinhauser zum Korrekturlesen dieser Arbeit.

Außerdem danke ich dem gesamten TTP, allem voran Martina Schorn, für die tolle Atmosphäre während meinen vier Jahren, die ich dort verbringen durfte. Daniel Baranowski und Matthias Linster möchte ich für die tolle Zeit in 12/19 danken, wo wir, pandemiebedingt, leider nur begrenzte Zeit verbringen konnten.

Zudem möchte ich den IT-Admins am ITP und TTP danken, dass sie es geschafft haben, die Computer-Infrastruktur zu pflegen, (meistens) ohne dass alles im Chaos ausgebrochen ist.

Ich danke Benedikt Dennig, Johannes Eichin, Martin Heinrich, Philipp Markus, Martin Marz und Maximilian Schäfer die mir durch das gesamte Studium hinweg (und darüber hinaus) meine Zeit in Karlsruhe zu einem sehr schönen Erlebnis gemacht haben.

Des Weiteren danke ich meiner Familie, die mich stets in meinen Plänen und Vorhaben unterstützt hat. Genauso möchte ich Claudia und Michael Benzel danken, dass sie mich so herzlich aufgenommen haben und mir ihr Büro zur Verfügung gestellt haben.

Besonderen Dank gebührt Michelle Benzel, die mich seit nun mehr als zehn Jahren unterstützt und mich auf meinen bisherigen Lebenswegen begleitet und so manche Freud und Leid teilte.

COLOPHON

This document was typeset using the typographical look-and-feel `classicthesis` developed by André Miede and Ivo Pletikosić. The style was inspired by Robert Bringhurst's seminal book on typography *"The Elements of Typographic Style"*. `classicthesis` is available for both LaTeX and LyX:

https://bitbucket.org/amiede/classicthesis/

All Feynman diagrams in this work were created with `jaxodraw` and `inkscape`.
The plots of chapter 7 were created with the `python3` library `matplotlib`.
For all other graphics the program `Affinity Designer` was used.

Final Version as of May 25, 2022 (classicthesis v4.6).